FRIEDRICH MIESCHER INSTITUTE FOR BIOMEDICAL RESEARCH

# Identification and characterization of cell adhesion molecules controlling synapse stability

## Inauguraldissertation

zur Erlangung der Würde eines Doktors der Philosophie
vorgelegt der Philosophisch-Naturwissenschaftlichen Fakultät der Universität Basel

Von
**Eva-Maria Enneking**
**(aus Lahr, Schwarzwald, Deutschland)**

**Basel, September 2012**

creative commons

**Namensnennung-Keine kommerzielle Nutzung-Keine Bearbeitung 2.5 Schweiz**

---

**Sie dürfen:**

das Werk vervielfältigen, verbreiten und öffentlich zugänglich machen

**Zu den folgenden Bedingungen:**

**Namensnennung**. Sie müssen den Namen des Autors/Rechteinhabers in der von ihm festgelegten Weise nennen (wodurch aber nicht der Eindruck entstehen darf, Sie oder die Nutzung des Werkes durch Sie würden entlohnt).

**Keine kommerzielle Nutzung**. Dieses Werk darf nicht für kommerzielle Zwecke verwendet werden.

**Keine Bearbeitung**. Dieses Werk darf nicht bearbeitet oder in anderer Weise verändert werden.

- Im Falle einer Verbreitung müssen Sie anderen die Lizenzbedingungen, unter welche dieses Werk fällt, mitteilen. Am Einfachsten ist es, einen Link auf diese Seite einzubinden.
- Jede der vorgenannten Bedingungen kann aufgehoben werden, sofern Sie die Einwilligung des Rechteinhabers dazu erhalten.
- Diese Lizenz lässt die Urheberpersönlichkeitsrechte unberührt.

**Die gesetzlichen Schranken des Urheberrechts bleiben hiervon unberührt.**

Die Commons Deed ist eine Zusammenfassung des Lizenzvertrags in allgemeinverständlicher Sprache: http://creativecommons.org/licenses/by-nc-nd/2.5/ch/legalcode.de

Haftungsausschluss:
Die Commons Deed ist kein Lizenzvertrag. Sie ist lediglich ein Referenztext, der den zugrundeliegenden Lizenzvertrag übersichtlich und in allgemeinverständlicher Sprache wiedergibt. Die Deed selbst entfaltet keine juristische Wirkung und erscheint im eigentlichen Lizenzvertrag nicht. Creative Commons ist keine Rechtsanwaltsgesellschaft und leistet keine Rechtsberatung. Die Weitergabe und Verlinkung des Commons Deeds führt zu keinem Mandatsverhältnis.

Quelle: http://creativecommons.org/licenses/by-nc-nd/2.5/ch/ Datum: 3.4.2009

Genehmigt von der Philosophisch-Naturwissenschaftlichen Fakultät
auf Antrag von:

Dr. Jan Pielage
Prof. Heinrich Reichert
Prof. Peter Scheiffele
Dr. Filippo Rijli

Basel, den 18.09.2012 Prof. Dr. Jörg Schibler

Faust. Habe nun, ach! Philosophie,
Juristerei und Medizin,
Und leider auch Theologie!
Durchaus studiert, mit heißem Bemühn.
Da steh’ ich nun, ich armer Tor,
Und bin so klug als wie zuvor!
Heiße Magister, heiße Doktor gar,
Und ziehe schon an die zehen Jahr,
Herauf, herab und quer und krumm,
Meine Schüler an der Nase herum –
Und sehe, daß wir nichts wissen können!
Das will mir schier das Herz verbrennen.
Zwar bin ich gescheiter als alle die Laffen,
Doktoren, Magister, Schreiber und Pfaffen;
Mich plagen keine Skrupel noch Zweifel,
Fürchte mich weder vor Hölle noch Teufel –
Dafür ist mir auch alle Freud’ entrissen,
Bilde mir nicht einm was Rechts zu wissen,
Bilde mir nicht ein, ich könnte was lehren,
Die Menschen zu bessern und zu bekehren.
Auch hab’ ich weder Gut noch Geld,
Noch Ehr’ und Herrlichkeit der Welt;
Es möchte kein Hund so länger leben!
Drum hab’ ich mich der Magie ergeben,
Ob mir durch Geistes Kraft und Mund
Nicht manch Geheimnis würde kund;
Daß ich nicht mehr mit sauerm Schweiß,
Zu sagen brauche, was ich nicht weiß;
Daß ich erkenne, was die Welt
Im Innersten zusammenhält,
Schau’ alle Wirkenskraft und Samen,
Und tu’ nicht mehr in Worten kramen.

Johann Wolfgang von Goethe

# CONTENT

# Summary

Neuronal circuits form the basis of a functional nervous system to process and integrate information and to react to environmental cues. The formation of functional synaptic connections between neurons is essential for the establishment of these circuits. During development and in response to activity information processing within neuronal circuits is adjusted by the selective addition or elimination of individual synapses. Impairment of synapse stability can lead to the disruption of neuronal circuits and results in severe neurodegenerative diseases. Thus, it is important to understand the molecular mechanisms controlling synaptic maintenance and plasticity.

Trans-synaptic interactions mediated by cell adhesion molecules (CAMs) have the potential to provide a stable connection between two neighboring neurons. Many cell adhesion molecules have been identified controlling the initial steps of neuronal circuit formation such as axon guidance, target recognition and synaptogenesis. However detailed knowledge about the identity and regulation of cell adhesion molecules during synapse stabilization is missing to date.

In this study I used the *Drosophila melanogaster* larval neuromuscular junction (NMJ) as a model system to identify novel cell adhesion molecules controlling synaptic maintenance *in vivo*. I performed an unbiased RNAi-based screen targeting entire classes of cell adhesion molecules with potential functions during nervous system development. I identified a number of novel candidates that have the potential to control synapse stabilization and performed a detailed characterization of two genes: *neuroglian* (*nrg*) encoding the L1-type CAM and *CG31708* (*uhu*) coding for an Immunoglobulin (Ig) domain protein

The L1-type CAM Neuroglian has the capability to interact with the adaptor protein Ankyrin2 (Ank2), which is part of a molecular network underneath the cell membrane that can control synapse stability by directly coupling CAMs to the presynaptic actin and microtubule cytoskeleton. In addition to Ank2, this network consists of the scaffolding proteins α- and β-Spectrin and the actin capping molecule Hts/Adducin. By combining biochemical, biophysical and genetic assays I demonstrated that the impairment of Ankyrin binding causes an increase in Nrg mobility that correlates with increased synaptic growth but decreased stability. In summary my results provide evidence of a novel regulatory module controlling synapse stability and growth through the regulated interaction between L1-type CAMs and Ankyrins.

# 1. Introduction

The nervous system is composed of billions of neurons and glial cells that form a complex interconnected structure to process information which is transferred via electrical signals (action potentials, AP) that are propagated from one cell to the other through direct connections between neurons. The synaptic contacts are asymmetric to ensure directionality of information transfer (Bucher and Goaillard, 2011). A functional unit in the nervous system is a neuronal circuit which can consist of many different neuronal cell types that can be located in very distant locations within the brain or body. To form a functional circuit the axons of the neurons have to perform the difficult task to navigate through the body and find the right target area and cell (Maness and Schachner, 2007; Schwarting and Henion, 2011). After the first contact various changes within the pre- and postsynaptic cell have to occur to ensure the functionality of the synapse (Lu et al., 2009; Owald and Sigrist, 2009). During nervous system development in many cases exuberant synaptic contacts form that are not needed for the mature circuit (Low and Cheng, 2005). In a process called pruning these additional contacts are removed in a controlled fashion to ensure the stability of the circuit (Faulkner et al., 2007; Low and Cheng, 2005). In response to activity changes, neuronal circuits can change their wiring pattern to adapt and allow for learning and memory (Bednarek and Caroni, 2011; Ruediger et al., 2011). In contrast, most synaptic contacts remain stable during lifetime to ensure proper nervous system function (Bednarek and Caroni, 2011). Failures in synaptic maintenance can result in severe neurodegenerative disease including amyotrophic lateral sclerosis (ALS) or spinal muscular atrophy (Boillee et al., 2006; Dion et al., 2009). A brief summary of the processes important for neuronal circuit assembly is shown in Figure 1.

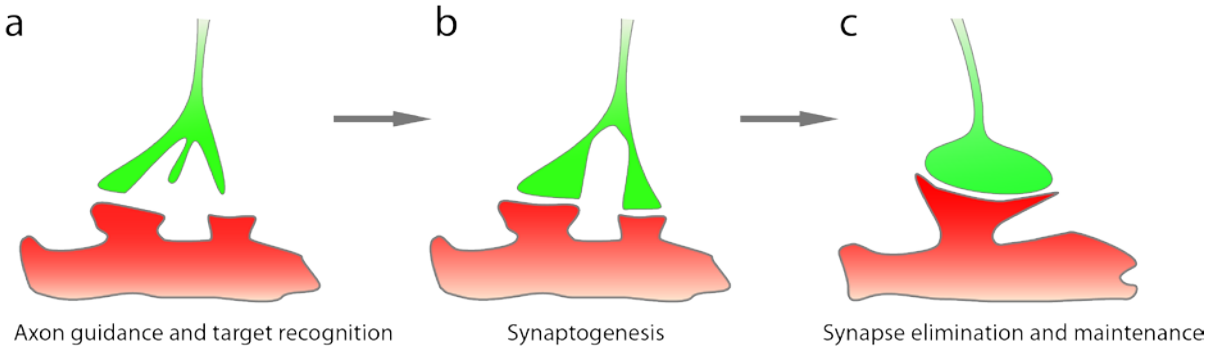


**Figure 1 - Steps of synapse development**

Neuronal circuits are the basis of a functional nervous system. They consist of multiple neurons that form specialized connections with each other called synapses. Synapses are important to process and transfer action potentials thus information about external or internal cues. Synapse formation can be divided into three distinct steps. (a) Axon guidance and target recognition: A dynamic growth cone

extends towards the target area and finds its right target cell and sub cellular department. (b) Synaptogenesis: Once the right target cell is reached an initial synaptic contact is made and pre- and postsynaptic specializations are formed. The immature synapse differentiates into a functional mature synapse. (c) Synapse elimination and maintenance: During and after development synaptic contacts need to be stable but at the same time allow dynamic changes of the wiring pattern due to pruning of excessive synapse formation during normal development or activity changes during learning and memory.

Trans-synaptic interactions mediated by CAMs have the potential to control formation, function and stability of neuronal circuits (Dalva et al., 2007; Shapiro et al., 2007). In my RNAi screen I targeted entire classes of CAMs to identify important players for synapse stabilization. Here, I would like to briefly describe key characteristics of the different classes of CAMs included in my screen and then highlight some examples during the three steps of neuronal circuit development shown in Figure 1.

## 1.1. Cell adhesion molecules in the nervous system

The classes of CAMs included in the screen were the Cadherins, Integrins, Ig-domain proteins, Semaphorins and leucine-rich repeat (LRR) proteins (Shapiro et al., 2007).

Cadherins are homophilic cell adhesion molecules that can provide adhesion between neighboring cells and can be regulated in a $Ca^{2+}$-dependent manner (Arikkath and Reichardt, 2008; Shapiro and Weis, 2009; Tanaka et al., 2000). Integrins are single pass transmembrane proteins, which consist of a large extracellular domain and a small intracellular domain. The functional unit of an Integrin is a heterodimer of α- and β-subunits (Arnaout et al., 2005; Humphries et al., 2003). Integrins have been implicated in many functions in the nervous system such as learning and memory (Grotewiel et al., 1998; McGeachie et al., 2011). Members of the class of Ig-domain proteins usually harbor multiple Ig-domains in their extracellular domain that promote homo- and heterophilic interactions (Blaess et al., 1998; Castellani et al., 2002; Hillenbrand et al., 1999; Volkmer et al., 1996). Examples for Ig-domain proteins are the NCAM family, the SynCAM family and the L1CAM family (Kriebel et al., 2012; Maness and Schachner, 2007; Schmid and Maness, 2008). The cytoplasmic domain of Ig-domain proteins is important for downstream signaling and connections to the cytoskeleton (Forni et al., 2004; Garver et al., 1997; Gil et al., 2003; Islam et al., 2004; Pollerberg et al., 1987; Tuvia et al., 1997). Semaphorins are a heterogeneous class of secreted and transmembrane proteins characterized by special Sema domains (Kolodkin et al., 1993). They interact with their receptors called Plexins and Neuropilins (Raper, 2000) but also can interact with Ig-domain proteins (Castellani et al., 2002; Godenschwege and Murphey, 2009).

The last class of CAMs I would like to describe here are the leucine-rich repeat (LRR) proteins (de Wit et al., 2011; Linhoff et al., 2009). LRR domains are generally known as protein-protein interaction domains and proteins with this domain can be either secreted or harboring a transmembrane domain (Chen et al., 2001; Linhoff et al., 2009; Owuor et al., 2009). Many LRR proteins are essential for nervous system development and function (Chen et al., 2001; Ko et al., 2009; Linhoff et al., 2009)

## 1.2. Axon guidance

The axonal growth cone of a newborn neuron navigates through the brain by using a variety of navigation cues. These include interaction with proteins presented on cells at intermediate targets or diffusible morphogens that create gradients along which the axon can grow (Vitriol and Zheng, 2012). Neurons are highly compartmentalized and the axons need to make the right decision which part of the target neuron to contact. (Figure 1 a)

Cell adhesion molecules play an important role during axon guidance and target recognition as they can mediate direct contacts between cells (Schwarting and Henion, 2011). The interaction can be either homophilic or heterophilic and can either induce repulsion or attraction from this cell (Hummel et al., 2003; Luo and Flanagan, 2007; Marquardt et al., 2005; Vitriol and Zheng, 2012). The DSCAM/Dscam family of Ig-domain CAMs mediates homophilic interactions that induce self avoidance of cells expressing the same isoform of Dscam (Hattori et al., 2008). In *Drosophila* many thousands of isoforms can be expressed from a single locus through differential splicing (Schmucker et al., 2000), which contribute to the establishment of a variety of neuronal circuits like the olfactory and the visual system (Hummel et al., 2003; Millard et al., 2007). Examples of a heterophilic interaction required for axon guidance that can be either attractive or repulsive are the family of GPI anchored Ephrins and their receptors. These are receptor tyrosine kinases and activate downstream signaling cascade upon Ephrin binding (Boulin et al., 2006; Helmbacher et al., 2000; Luo and Flanagan, 2007; Marquardt et al., 2005).

In addition, a large number of CAMs have been described that mediate axon guidance and target recognition via homo- and heterophilic interactions such as the Semaphorins, L1CAMs and Cadherins (Godenschwege and Murphey, 2009; Hall and Bieber, 1997; Hummel and Zipursky, 2004).

## 1.3. Synapse formation and differentiation

Once the axon growth cone comes in contact with the appropriate postsynaptic target cell it needs to differentiate into a presynaptic terminal. At the same time the target cell also specializes to serve as the postsynaptic site of the synapse. Pre- and postsynaptic cells accumulate components needed for neurotransmission. During later steps of development these initial contacts further differentiate to build the mature contact.

Trans-synaptic connections mediated by cell adhesion molecules are important for the appropriate formation and regulation of these processes (Chen and Cheng, 2009; Siddiqui and Craig, 2011). Cell culture studies revealed important CAMs involved in synapse formation (Linhoff et al., 2009; Scheiffele et al., 2000). The expression of Neuroligins in non-neuronal cells induced the assembly of a functional presynapse within contacting neurons (Scheiffele et al., 2000). Neuroligins interact with presynaptic expressed Neurexins (Craig and Kang, 2007) and can induce the formation of excitatory and inhibitory synapses. Neurexins, in addition, can interact with the class of LRR transmembrane (LRRTM) proteins and cooperates with N-Cadherin during vesicle accumulation (de Wit et al., 2009; Ko et al., 2009; Stan et al., 2010).

The integrin family has been described to be essential for the change from an immature synapse to a mature synapse. This is accompanied by the change in neurotransmitter subunit composition and activity. Chavis and colleagues blocked integrin β3 in an *in vitro* assay and observed proper initial formation of synaptic contacts but failures during the differentiation into a mature synapse (Chavis and Westbrook, 2001).

## 1.4. Synapse maintenance and elimination

Another unique feature of the nervous system is its ability to modulate its wiring pattern in response to external stimuli. Synapse stabilization and elimination need to be highly regulated to ensure the functionality of the system (Faulkner et al., 2007; Kantor and Kolodkin, 2003; Low and Cheng, 2005). Failures in these processes can lead to the progressive loss of neurons and subsequent neurodegenerative diseases like ALS or Huntington`s disease (Boillee et al., 2006; Luo and O'Leary, 2005).

Cell adhesion molecules have the potential to control both maintenance and elimination since they can mediate strong adhesion, which can be regulated in a number of ways (Crossin and Krushel, 2000). However, little is known regarding the identity and regulation of cell adhesion molecules during synapse stabilization. A class of cell adhesion molecules involved in the maintenance of synaptic contacts are the Cadherins (Benson and Huntley, 2012; Lefebvre et al., 2008; Wang et al., 2002). *In vivo* studies showed that gamma-Protocadherins are essential for the survival of neurons in the spinal cord, the cerebral cortex as well as in the retina. Knock down of gamma-Protocadherins *in vitro* results in apoptosis of differentiated mature synapses (Lefebvre et al., 2008; Wang et al., 2002). In humans the autosomal recessive retinal dystrophy has been associated with mutations in the *protocadherin21* gene. The onset of this disease is in late teenage years with night vision loss and progresses during adult live due to severe cone and rod degenerations (Henderson et al., 2010).

The identification of molecules that promote the stabilization of synaptic contacts is important for the understanding of the mechanisms leading to neurodegenerative diseases. All classes of cell adhesion molecules, described above, have the potential to provide a direct mechanic link between two cells via extracellular interactions and thus CAMs are likely candidates to control synapse stability. However, the complexity of the vertebrate nervous system and genome makes it more difficult to investigate the function of CAMs (Hortsch, 2000). I used the model system fruit fly *Drosophila melanogaster* to circumvent these problems.

In the following chapter I will describe and highlight the advantages of the *Drosophila* model system, especially the larval neuromuscular junction (NMJ) in comparison to more complex systems in vertebrates.

## 1.5. *Drosophila melanogaster* as a model system

The fruit fly *Drosophila melanogaster* was first described in 1830 by Johann Wilhem Meigen and has been first maintained and studied in the lab by Charles W. Woodworth. Since then, it was used to answer a wide range of biological questions. There are many advantages for using *Drosophila* as a model system in the lab in comparison to vertebrates. These include the short generation time, the easy handling, the little space need and the great variety of genetic and molecular tools developed in the last 100 years. Many genes from *Drosophila* are conserved during evolution thus studies in the fly can give answers to processes and

mechanisms in the vertebrate system (Hortsch, 2000; Zhao and Hortsch, 1998). In Figure 2 the life cycle of *Drosophila* melanogaster is shown. From a fertilized egg to the hatching of a fly it takes about 8 days at 25 °C.

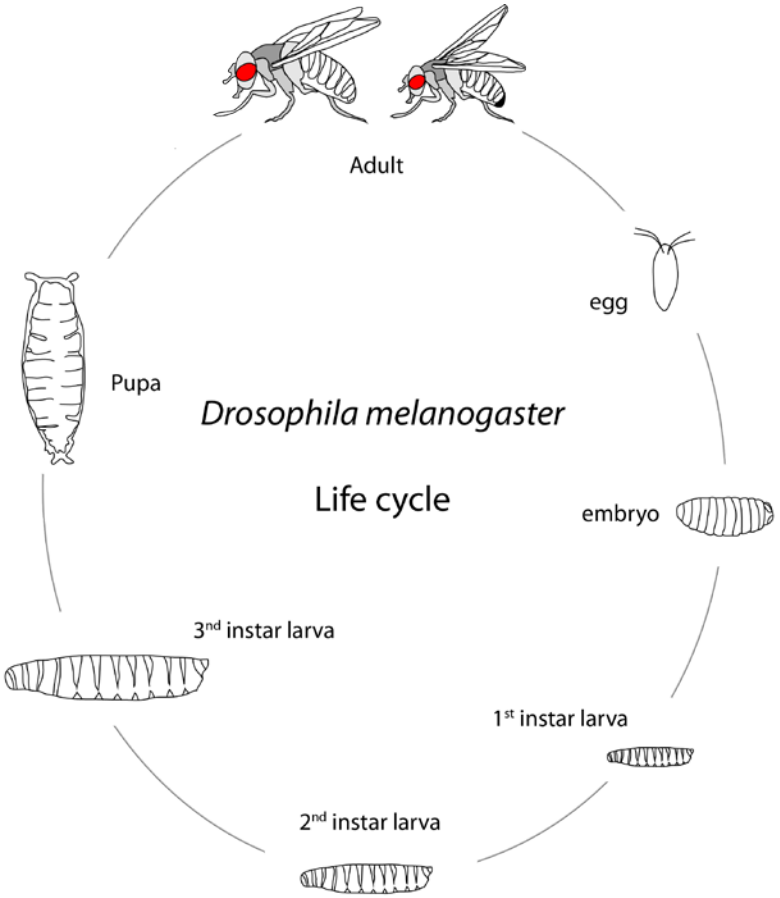


**Figure 2 - *Drosophila* life cycle and stages of development**

The life-cycle of *Drosophila melanogaster* from egg-hatching to the adult fly lasts about 8 days. After embryogenesis the larvae hatch and pass through three larval stages (1st instar larvae, 2nd instar larvae, 3rd instar larvae) and two larval molts. These larval stages can be identified based on the structure of the mouth apparatus and the appearance and structure of the anterior and posterior spiracles. 4 days after egg-hatching the puparium formation occurs and the imago emerges after another 4 days. 8 h post-hatching the adult flies become perceptive and start mating.

### 1.5.1. The *Drosophila* neuromuscular junction to study synapse development

The *Drosophila* NMJ was first used as a model system in neurobiology in the 1970s by Jan and Jan describing the basic physiological and pharmacological properties of the system (Jan and Jan, 1976a; Jan and Jan, 1976b). Since then the NMJ became an important model system to study neurodevelopmental problems such as axon guidance, target selection, synaptic function and synapse maintenance (Fouquet et al., 2009; Hall and Bieber, 1997; McCabe et al., 2004; Owald et al., 2012; Ramser et al., 2010; Schuster et al., 1996a; Schuster et al.,

1996b; Wan et al., 2000). What makes this system so attractive for scientists? The advantages of this model system are various. First, we can analyze proteins at the level of individual synapses in high resolution using different advanced imaging techniques. Second, it is possible to manipulate single motoneurons using genetic tools like the Gal4/UAS system or the MARCM technique (Brand and Perrimon, 1993; Lee and Luo, 2001). Third, each motoneuron can be identified based on the projection pattern and muscle innervation and the dendritic tree in the ventral nerve cord (VNC) of the brain (Landgraf et al., 2003). Fourth, the *Drosophila* NMJ is a glutamatergic synapse and therefore shares key features with central synapses in vertebrates (Jan and Jan, 1976a; Thomas and Sigrist, 2012).

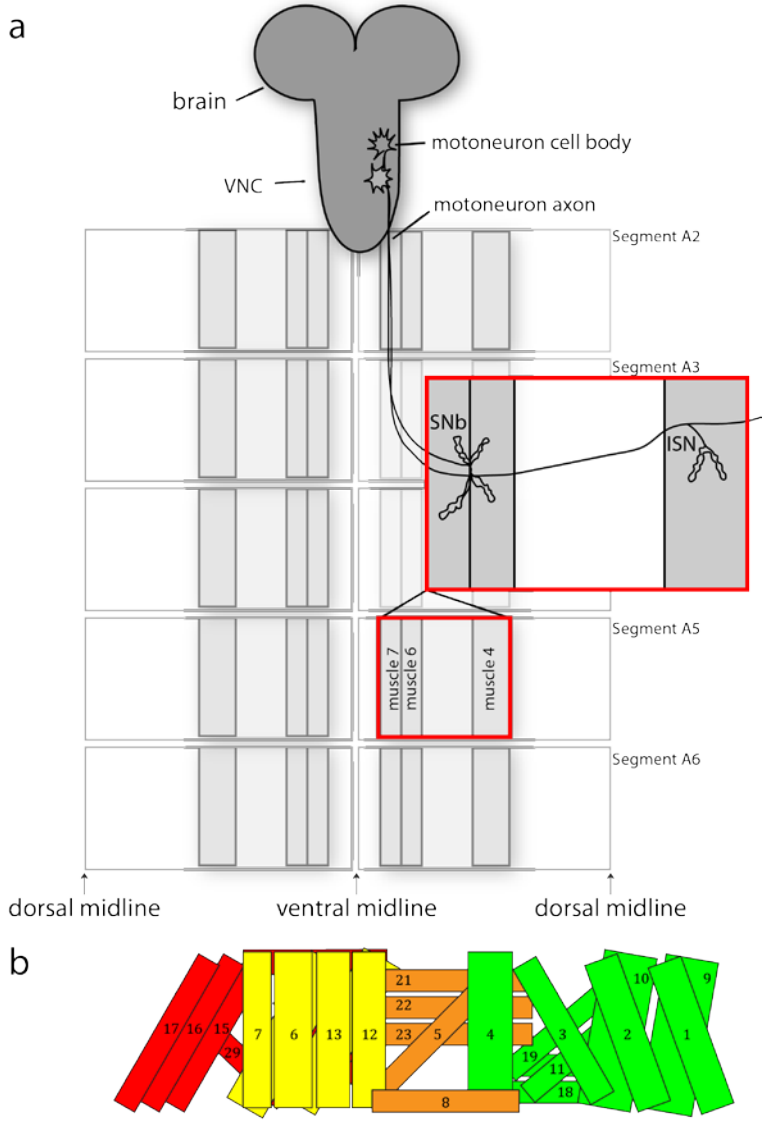


**Figure 3 - Overview of the larval motoneurons and muscles**

**(a)** Schematic view onto a larval preparation. The brain is shown in grey with the ventral nerve cord (VNC), where the motoneuron cell bodies are located. Simplified examples of two motoneurons

innervating muscle 4 and muscle 6/7 of abdominal segment A5 are shown here in the zoom-in (highlighted through the red boxes). These extend their axons towards their target muscle and form NMJ terminals. Muscle 4 is innervated by the intersegmental nerve (ISN) and muscle 6/7 by the segmental nerve b (SNb).Using our larval preparation we can analyze the abdominal segments A2-A6. The larvae are opened along the dorsal midline and each segment is separated into two equal hemisegments by the ventral midline. **(b)** Schematic scheme of the larval muscles within a hemisegment, the muscle are colored based on the nerves that innervate the muscles. The green muscles are innervated by the ISN (1, 2, 3, 4, 9, 10, 11, 18, 19, 20), the orange muscles are innervated by the SNa (5, 8, 21-24), the yellow muscles by the SNb (6, 7, 12, 13, 30, 14, 28) and the red muscles by the SNc/d (15-17, 25-27, 29).

### 1.5.2. Organization and structure of the neuromuscular circuitry

Motoneurons are characterized by their axonal trajectorys, the innervation of specific muscles and the dendritic tree in the central nervous system (CNS) (Landgraf et al., 2003). The motoneuron cellbodies are located in the outer layer of the CNS in the VNC (Figure 3). The motoneuron axons exit the VNC and extend their axons towards the target muscle. Most muscles are innervated by multiple motoneuron types described below, but there are exceptions such as muscle 4 which is only innervated by Type I motoneurons. The 30 muscles per hemisegment are innervated by three nerves, the transversal nerve (TN), the intersegmental nerve (ISN) and the segmental nerve (SN) (Figure 3 b). There are three types of motoneurons in *Drosophila* larvae. Type I motoneurons (1b and 1s) are glutamatergic motoneurons (Jan and Jan, 1976a; Jan and Jan, 1976b). At the NMJ each Type I synaptic terminal consists of multiple varicosities called boutons and within each bouton there are multiple synapses opposed by glutamate receptors in the muscle. Ultrastructurally most synapses of Type I motoneurons are characterized by an electron dense structure called T-bar. Vesicles seem to be physically attached to the T-bars, which facilitates vesicle release (Owald et al., 2012; Reiff et al., 2002; Thomas and Sigrist, 2012). T-bars are associated with $Ca^{2+}$ channels, to induce locally high $Ca^{2+}$-domains (Kittel et al., 2006; Owald et al., 2012). Type I motoneurons submerge deep into the muscle and are surrounded by the sub synaptic reticulum (SSR) which are foldings of the muscle membrane (Figure 4). Type II and III motoneurons use octopamine or peptides as neurotransmitter. They differ ultrastructually from the Type I motoneurons and remain on the muscle surface (Figure 4)

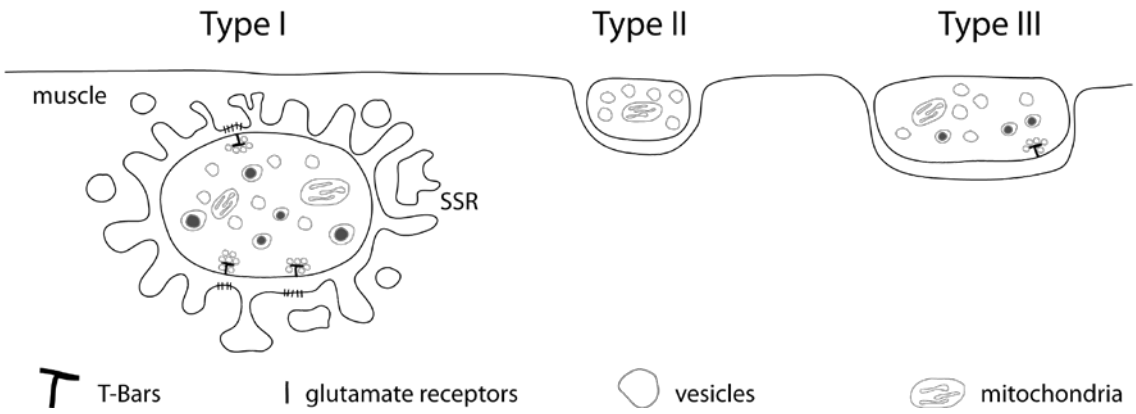


**Figure 4 - Three types of motoneurons and their characteristics**

Type I motoneurons are glutamatergic neurons. They submerge deep into the muscle and are surrounded by the sub synaptic reticulum (SSR). Ultrastructurally Type I synapses are characterized by an electron dense structure called T-bars which facilitate vesicle release. T-bars are associated with synaptic vesicles and $Ca^{2+}$-channels to induce local high $Ca^{2+}$-domains required for vesicle release thus for the propagation of action potentials. In the postsynaptic muscle, glutamate receptors cluster are opposite of T-bars. In contrast, Type II and III motoneurons are peptidergic or octopaminergic neurons that stay on top of the muscles and are not surrounded by the SSR. Both contain synaptic vesicles and mitochondria but no glutamate receptors cluster in the muscle and only in Type III motoneuron terminal T-bars can be found.

### 1.5.3. Synaptic maintenance at the *Drosophila* larval NMJ

So far a small number of proteins has been identified to be essential for synapse stability. The functions of these protein range from signaling molecules to cytoskeleton proteins. Previously an assay has been established that can be used to visualize synaptic retractions (Eaton et al., 2002; Pielage et al., 2011; Pielage et al., 2008). The pre- and postsynaptic structures are stained with specific antibodies. At stable synapses these markers are opposing each other (Figure 5 a). The elimination of the presynapse is faster than the disassembly of the postsynaptic specialization, thus unopposed postsynaptic markers indicate the presence of an instable synapse (Figure 5 b, c). The establishment of a genome wide RNAi library (Dietzl et al., 2007) allows now to screen directly any genes of interest.

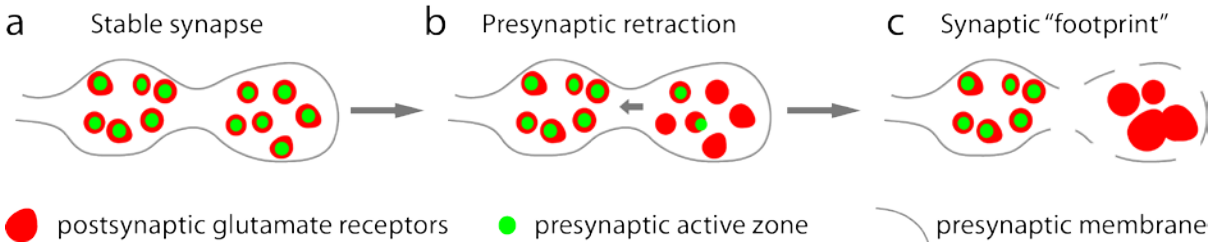


**Figure 5 - Process of synapse destabilization at the *Drosophila* NMJ**

**(a)** A stable *Drosophila* larval NMJ is characterized presynaptic markers (green) opposed by postsynaptic glutamate markers (red) and a continuously formed presynaptic membrane (grey). **(b)** Failures during synapse stabilization caused by RNAi mediated knock down or mutations of stability promoting genes the presynaptic terminal retracts. **(c)** A synaptic "footprint" is marked by the loss of presynaptic markers, a clustering of glutamate receptors and the fragmentation of the membrane.

In the RNAi-based screen of cell adhesion molecules I identified the L1-type CAM homolog Neuroglian as an important CAM for synapse maintenance. The main part of this thesis was the detailed characterization of Nrg and its function and regulation at the larval NMJ. Therefore, I will describe and discuss here the family of L1CAMs in vertebrates and *Drosophila* in more detail.

## 1.6. L1CAM and the *Drosophila* homolog Neuroglian

### 1.6.1. The L1CAM family

In vertebrates the L1CAM family consists of four members, which are Neurofascin, L1CAM, CHL1 (close homolog of L1) and NrCAM (Neuronal cell adhesion molecule). L1CAM proteins are highly conserved during evolution (Figure 7) (Zhao and Hortsch, 1998). In contrast to the vertebrate family, *Drosophila melanogaster* and the nematode *Caenorhabditis elegans* (*C. elegans*) have only one L1CAM homolog whereas in the zebrafish *Danio rerio* two homologous genes have been identified (Becker et al., 2004; Pocock et al., 2008; Sasakura et al., 2005). A series of gene duplications could be responsible for this difference in the number of genes from arthropods to mammalians (Amores et al., 1998; Pebusque et al., 1998).

Most L1CAMs family members have six Ig-domains and five Fibronectin (Fn) type III domains in the extracellular domain. Exceptions exist for Neurofascin and *C. elegans* Sax-7 due to alternative splicing (Hassel et al., 1997; Sasakura et al., 2005). Both homo- and heterophilic interactions within the L1CAM family as well as with other CAMs have been demonstrated for the extracellular domain. A summary is shown in Table 1. Homophilic binding has been reported for all L1CAM family members except CHL1 (Hillenbrand et al., 1999). Heterophilic interactions have been demonstrated e.g. for Neurofascin and NgCAM which interact *in trans* as well as for Neurofascin and NrCAM (Hillenbrand et al., 1999; Volkmer et al., 1996). The cytoplasmic domains of L1CAMs are between 85 and 148 amino acids long. A summary of interaction partners of the intracellular domains is shown in Table 1.

The neuronal isoforms of vertebrate L1CAMs can have an RSLE motif in their cytoplasmic domain which is important for the sorting of L1 proteins to growth cones of neurons and the induction of AP-2 mediated endocytosis via clathrin coated pits (Kamiguchi et al., 1998). This motif is spliced into the neuronal isoforms of most L1CAMs (Reid and Hemperly, 1992). Further conserved domains between vertebrates and invertebrates are the FERM binding domain, the FIGQY motif and a PDZ protein binding domain. The binding of FERM domain proteins is involved in neurite outgrowth and regeneration of injured hippocampal neurons (Cheng et al., 2005a; Haas et al., 2004). The FIGQY motif is an important regulatory region controlling the interactions with Ankyrins and Doublecortin (Hortsch et al., 2009;

Kizhatil et al., 2002). Taken together L1CAMs have the potential to integrate and regulated many different processes through their great variety of interaction partners.

**Table 1 - Table of L1CAM interaction partners**

| *Domain* | *Interaction partner* | *Cellular context* |
|---|---|---|
| Immunoglobulin domain 1-6[10] | Axonin-TAG1[15], Neurocan[17], Neuropilin[2], Contactin[10], L1CAM[4, 20, 26, 27], Integrin[1, 6, 16, 20], Neurofascin[21] | neurite outgrowth, synapse stability[28], axon guidance |
| Fibronectin domains type III 1-5[10] | Axonin-TAG1[15], Integrin[1, 6, 20] L1CAM[3], Contactin[10] | neurite outgrowth |
| FERM[10] | ERM proteins[5] | neurit outgrowth and branching |
| RSLE[10] | AP2[12,5] | L1CAM endocytosis[12] |
| FIGQY[10] | Ankyrin[7, 19], Doublecortin[13] | synapse function[8], synapse growth and stability[28], neurite outgrowth |
| PDZ[10] | Syntenin-1[14], MAGUK SAP102[10], SAP90[10], PSD95[10] | neurite outgrowth, axon bundling[9] |
| C-terminus[10] | CKII[18, 23], ERK2, p90rsk[24], RanBP[3], Shootin1[18] | neurite outgrowth |

A summary of intra- and extracellular interaction partners of the L1CAM family grouped by the specific domains. The cellular context if identified is noted in the last column. Direct and indirect interactions *in cis* and *trans* are included in the list. The numbers indicate the reference listed here: ((1) Blaess et al., 1998; (2) Castellani et al., 2002; (3) Cheng et al., 2005b; (4) De Angelis et al., 2002; (5) Dickson et al., 2002; (6) Felding-Habermann et al., 1997; (7) Garver et al., 1997; (8) Godenschwege et al., 2006; (9) Goossens et al., 2011; (10) Haspel and Grumet, 2003; (11) Herron et al., 2009; (12) Kamiguchi et al., 1998; (13) Kizhatil et al., 2002; (14) Koroll et al., 2001; (15) Kunz et al., 1998; (16) Montgomery et al., 1996; (17) Oleszewski et al., 1999; (18) Ramser et al., 2010; (19) Shimada et al., 2008; (20) Silletti et al., 2000; (21) Tuvia et al., 1997; (22) Volkmer et al., 1996; (23) Wong et al., 1996a; (24) Wong et al., 1996b; (25) Yip et al., 1998; (26) Zhao and Siu, 1995; (27) Zhao et al., 1998; (28) Enneking et al., this study).

Many different functions of L1CAMs have been described so far in the nervous system in vertebrates and other model systems. These include neurite outgrowth and cell body adhesion (Appel et al., 1993), axon fasciculation (Ohyama et al., 2004; Wiencken-Barger et al., 2004), myelination (Barbin et al., 2004), axonal positioning (Pocock et al., 2008; Sasakura et al., 2005) axon guidance (Ango et al., 2004; Godenschwege and Murphey, 2009; Hall and Bieber, 1997) and synapse formation (Triana-Baltzer et al., 2006). However, L1CAMs have not been implicated in the control of synapse stabilization so far.

Mouse knockout studies describe a variety of phenotypes including hydrocephalus, a smaller hippocampus and cerebellum, hyperfasciculation, corpus callosum hypoplasia and memory dysfunctions (Dahme et al., 1997; Demyanenko et al., 1999; Fransen et al., 1997; Wiencken-Barger et al., 2004). Only a weak impairment of some motor functions has been described (Pratte et al., 2003). Most of these functions are regulated via extracellular interactions since knock-in mutations of C-terminal deletions showed only weaker defects (Nakamura et al., 2010). In contrast hippocampal neurons *in vitro* displayed a decrease in branching number (Nakamura et al., 2010).

L1CAMs have been implicated to contribute and be influenced by many signaling pathways during cell survival and neurite outgrowth *in vivo* and *vitro* (Forni et al., 2004; Islam et al., 2003; Nishimune et al., 2005; Whittard et al., 2006). In cultured motoneurons L1 and CHL1 can act as survival factors. This function was completely blocked by MEK and PI3K inhibitors, which indicates a role of mitogen-activated protein (MAP) kinase and PI3 kinase signaling pathways in promoting survival of motoneurons via L1 (Nishimune et al., 2005). L1 mediated neurite outgrowth requires the phosphorylation of the FIGQY Ankyrin binding motif via MAPK signaling since inhibitors of this pathway inhibit L1 mediated neurite outgrowth (Whittard et al., 2006). *In vitro* studies in cultured *Drosophila* neurons showed that a reduction of the fibroblast growth factor receptor (FGFR) signaling pathway reduced Nrg-stimulated neurite outgrowth (Forni et al., 2004). Islam and colleagues (2004) showed *in vivo* that Neuroglian overexpression altered nerve growth and pathfinding in the wing, which can be reduced through the decrease of epidermal growth factor receptor (EGFR) signaling (Islam et al., 2004).

### 1.6.2. L1CAM in human disease

Human mutations in the L1CAM family have been first described in 1992 to be associated with a neurological disorder (X-linked hydrocephalus) (Rosenthal et al., 1992). Mutations in L1CAMs are responsible for a least four neurological diseases: X-linked hydrocephalus (HSAS), MASA-syndrome (**M**ental retardation, **A**phasia, **S**huffling gait, **A**dducted thumbs), complicated spastic paraplegia (SP-1) and X-linked agenesis of the corpus callosum. In 1995 Fransen and colleagues defined the name CRASH (**C**orpus callosum hypoplasia, **R**etardation, **A**dducted thumbs, **S**pastic paraplegia and **H**ydrocephalus) syndrome for this variety of neurological syndromes caused by mutations in L1CAMs (Fransen et al., 1995). Since then,

over 100 different L1 mutations have been reported (Fransen et al., 1997; Piccione et al., 2010; Silan et al., 2005).

Most mutations identified are private and exist only in single families. Mutations can be grouped based on the type of mutation and the domains affected. The first group affects the cytoplasmic domain, the second group affects the extracellular domain including point- and missense-mutations and the third group consists of nonsense and frame shift mutations in the extracellular domain. Mutations of the third group correlate with the most severe forms of the CRASH syndrome, whereas the first group displays mostly milder phenotypes (Yamasaki et al., 1997).

The CRASH syndrome is an X-linked disease and the clinical phenotypes can vary significant between families, but only rarely within affected families. However, the syndrome of adducted thumbs is commonly associated with patients with this syndrome. Patients with mutations in the cytoplasmic domain display this phenotype implicating the loss of either intracellular interactions with the cytoskeleton or downstream signaling activation are the cause of this specific phenotype. In more severe forms of the CRASH syndrome the presence of a severe hydrocephalus correlates often with severe mental retardation and a poor survival rate (Yamasaki et al., 1997).

Some mutations identified in patients have been studied in cell culture assays to investigate the molecular mechanism underlying the disease cause. Two missense mutations in the extracellular domain (group 2) have been shown to reduce the adhesion dependent activation of EGFR (epidermal growth factor receptor) (Islam et al., 2004). However, both mutations show normal homophilic adhesion in cell aggregation assays (Nagaraj et al., 2009). Other group 2 mutations affect homo- and heterophilic binding properties or surface expression in CHO cells (De Angelis et al., 1999; De Angelis et al., 2002). Each missense mutation can affect different aspects of protein function and could thus explain the high variability of phenotypes (De Angelis et al., 1999). In *Drosophila* a hypomorphic mutation exists that mimics a human mutation in L1. This $nrg^{849}$ mutation reduces homophilic binding of Neuroglian and leads to synapse formation defects in the giant fiber (GF) synapse in the adult fly (Godenschwege et al., 2006).

### 1.6.3. *Drosophila* L1CAM

The *Drosophila* L1CAM homolog is named based on its expression in the nervous system in neurons and glial cells. *Nrg* was identified in the late 1980$^{th}$ by Bieber and colleagues (Bieber et al., 1989). In contrast to vertebrates the *Drosophila* genome encodes one L1CAM gene from which two isoforms of Neuroglian are expressed that differ only in their cytoplasmic domain but are expressed in different tissues (Figure 6 b). Nrg167 (167 kDa) is ubiquitously expressed while Nrg180 (180 kDa) is exclusively expressed in the nervous system (Hall and Bieber, 1997; Hortsch et al., 1990). The first expression of Nrg180 can be detected 6 h after egg laying (AEL) on the surface of specific CNS and PNS neurons. In contrast, Nrg167 expression in glial cells and other tissues like trachea, salivary gland and muscles can be detected only 11 h AEL.

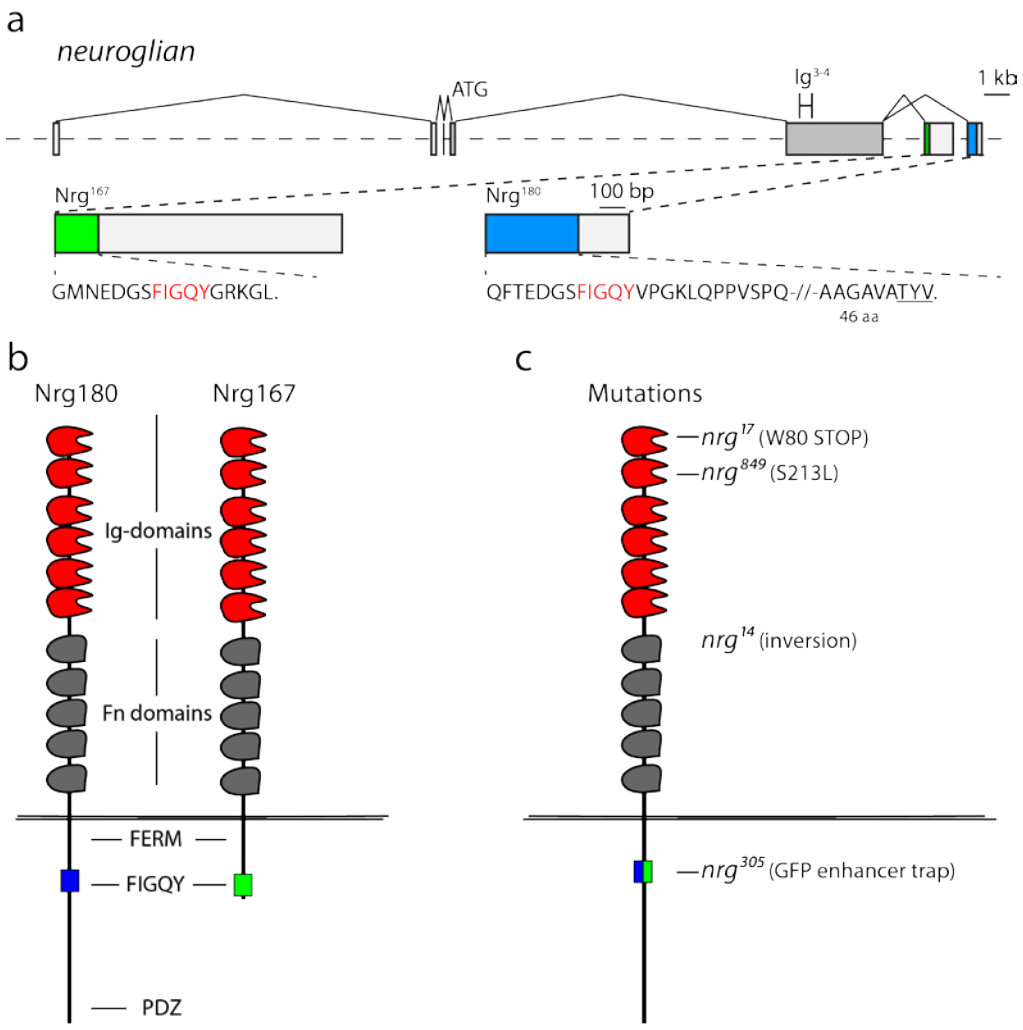


**Figure 6 - Domain structure of *Drosophila* L1CAM Neuroglian**

**(a)** Genomic locus of *neuroglian.* The intron and exon structure of the *neuroglian* locus is shown. The start codon is marked by the ATG. The two isoforms (Nrg167 and Nrg180) are generated via alternative splicing. Importantly the FIGQY Ankyrin binding motifs of the two isoform is encoded by two different exons (depicted in green for Nrg167 and blue for Nrg180). The region around the FIGQY motif is highlighted for both isoforms. The Nrg180 isoform harbors a unique C-terminus absent from the Nrg167 isoform **(b)** The *Drosophila* L1CAM homolog Neuroglian exists in two isoforms, a neuronal isoform of 180 kDa (Nrg180) and a ubiquitously expressed isoform of 167 kDa (Nrg167). Both have the same extracellular domain structure consisting of six Immunoglobulin (Ig) domains and five Fibronectin (Fn) type III domains. After the transmembrane domain a common FERM protein binding domain allows the binding of FERM domain proteins. Both isoform harbor an Ankyrin binding motif in their cytoplasmic domain. The neuronal isoform Nrg180 contains in addition an uncharacterized cytoplasmic domain of 66 amino acids, which includes a PDZ-protein binding domain in the last three amino acids. **(c)** Various mutations are available that alter the level or functions of both Nrg isoforms. $Nrg^{17}$ is a strong hypomorphic allele and characterized by a transformation of amino acid 80 into a STOP codon. $Nrg^{849}$ is a viable hypomorphic mutation (S213L). This mutation impairs homophilic binding properties of Nrg. $Nrg^{14}$ is an *nrg* null mutations caused by an uncharacterized inversion in the *nrg* gene. $Nrg^{305}$ is a viable hypomorphic mutation. A GFP enhancer trap is inserted into the intron before the exon encoding the Nrg167 FIGQY Ankyrin binding motif, decreasing the levels of both Nrg180 and Nrg167.

The domain structure of the Neuroglian isoforms is shown in Figure 6 b. Both have identical extracellular domains with six Ig-domains and five Fn type III domains like vertebrate L1CAMs. A single transmembrane domain spans the cell membrane followed by a FERM protein binding domain. The FIGQY motif is also common in both isoforms however it is encoded by two different exons (Figure 6 a). The Nrg167 isoform ends directly after the FIGQY motif (Figure 6 a, b, Figure 7). In contrast, the Nrg180 isoform has a longer unique C-terminus of 66 amino acids, which includes a PDZ protein binding domain (TYV) and a so far uncharacterized region between the FIGQY and the PDZ binding domain (Figure 6 b, Figure 7).

Many studies investigated the function of Neuroglian in the nervous system and other tissues of *Drosophila* (Garcia-Alonso et al., 2000; Godenschwege et al., 2006; Goossens et al., 2011; Hall and Bieber, 1997; Wei et al., 2004; Williams, 2009). In the following section I would like to describe the available mutations (summary in Figure 6 c). There are two embryonic lethal mutations. $Nrg^{14}$ is a mutation generated using X-ray and this induced an inversion in the *nrg* gene (Hall and Bieber, 1997; Lefevre, 1981), which is considered as a real protein null mutation. $Nrg^{17}$ is generated using ethyl methanesulfonate (EMS) and described as a mutation that leads to a premature stop (W80STOP) (Lefevre, 1981; Yamamoto et al., 2006). The mutation is considered as a strong hypomorphic mutation, as we and other demonstrated the presence of protein in mutant embryo and larvae (data not shown, Hall and Bieber, 1997). Two other viable hypomorphic mutations have been described, $nrg^{849}$ and $nrg^{305}$. The $nrg^{849}$ mutation is a point mutation within the 2$^{nd}$ Ig-domain of the extracellular domain (S213L).

Importantly, this mutation is similar to a mutation found in humans in families with CRASH syndrome (De Angelis et al., 2002). *Nrg*$^{305}$ is caused by a GFP enhancer trap insertion in the intron before the exon that encodes the Nrg167 FIGQY motif (Figure 6 c). This leads to the reduction of Nrg levels and the tagging of both isoforms with GFP (Yamamoto et al., 2006, Figure 6 c, Figure 22). *Nrg*$^{3}$ is a temperature sensitive mutation that is lethal at 29 °C but viable at 18 °C (King et al., 1986). The shift to 29°C leads to a misslocalization of the protein to the cell bodies (Hall and Bieber, 1997). Using this mutation the critical phase of Nrg for viability has been defined between embryonic mid stage 15 and late stage 16 (Hall and Bieber, 1997).

First descriptions of *nrg* null mutations observed an overall normal nervous system based on FasciclinII (FasII) staining (Hall and Bieber, 1997). But sensory neurons cell bodies were disorganized and motoneurons in embryonic stage 15-17 displayed abnormal projections and contacts (Hall and Bieber, 1997). In sensory neurons like the ocellar pioneer (OP) and the bristle mechanosensory (BM) neurons the *nrg*$^{3}$ mutations caused axon guidance defects. The defects observed could not be rescued by the expression of Nrg167, but by Nrg180. In addition expression of FasII was able to rescue the OP but not BM phenotypes (Kristiansen et al., 2005), which indicates a partial redundancy of CAMs within the nervous system. Also functions of Nrg in glial cells have been described. Simultaneous knock down of *nrg* and *ank1* in glial cells that wrap around dorsal dendritic arborization neurons E (ddaE) and the ddaE neuron led to an increase in ectopic dendritic branches of the ddaE neuron (Yamamoto et al., 2006). Godenschwege et al. (2006, 2010) described a function of Nrg in synapse formation and function within the GF system of the adult fly (Boerner and Godenschwege, 2010; Godenschwege et al., 2006). Recently a function of Nrg in the mushroom body (MB) of adult flies has been described. Mutant MB display axon bundling and stalling phenotypes (Goossens et al., 2011).

### 1.6.4. L1 and Ankyrin interaction

Ankyrins are a family of adaptor molecules that link integral membrane proteins to the submembranous Spectrin-based cytoskeleton (Jenkins and Bennett, 2001). The Ankyrin binding motif FIGQY in the cytoplasmic domain of L1CAMs binds to the N-terminus of Ankyrins (Davis and Bennett, 1994; Garver et al., 1997; Tuvia et al., 1997). This FIGQY motif is highly conserved between species from *C. elegans* to vertebrates (Figure 7). Binding of L1 and Ankyrins is highly regulated by the phosphorylation of the tyrosine residue within

the FIGQY motif (Figure 8, Garver et al., 1997). Studies showed that phosphorylation of the tyrosine within the FIGQY motif inhibits Ankyrin binding and leads to increased neurite outgrowth (Garver et al., 1997; Tuvia et al., 1997). Mutations within the FIGQY (Y1229H) motif have been identified in families with CRASH syndrome and shown to impair Ankyrin recruitment to the membrane in HEK cells. In contrast, mutation within other cytoplasmic domains did not cause any phenotype. Another interesting aspect of the regulation of protein binding to the FIGQY motif is that Ankyrins are not the only interaction partner of L1CAMs. The phosphorylation of the FIGQY motif inhibits Ankyrin binding but allows the binding of Doublecortin. A study in 2002 showed that the cytoplasmic molecule Doublecortin, which is linked to the neuronal migration disorder X-linked lissencephaly, is able bind to the phosphorylated FIGQY motif of Neurofascin (Kizhatil et al., 2002).

| | |
|---|---|
| *Homo sapiens* L1 | E D G S F I G Q Y S G K K // A L E * |
| *Mus musculus* L1 | E D G S F I G Q Y S G K K // A L E * |
| *Mus musculus* Neurofascin | E D G S F I G Q Y T V K K // S L A * |
| *Drosophila melanogaster* Nrg180 | E D G S F I G Q Y V P G K L // T Y V * |
| *Drosophila melanogaster* Nrg167 | E D G S F I G Q Y G R K G L * |
| *C. elegans* Sax-7 | E D G S F I G Q Y V P Q K S // T F V * |

**Figure 7 - Sequence alignment of the Ankyrin binding motif of L1CAM family proteins**

The Ankyrin binding motif FIGQY is highly conserved between species. Here the protein sequences from the human L1CAM to the *C. elegans* homolog Sax-7 around the FIGQY Ankyrin binding motif are shown. The STOP codon is indicate by the *. In contrast to the *Drosophila* Nrg167 isoform, which ends directly after the FIGQY motif, other L1-type CAMs have an extended C-terminus with a length between 85 and 148 amino acids (indicated by the //).

In the vertebrate genome there are three *ankyrin* (*ank1-3*) genes which encode multiple different isoforms generated through complex alternative splicing (Cunha et al., 2008; Cunha and Mohler, 2009; Hopitzan et al., 2005; van Oort et al., 2008). The splicing products are classified as Ankyrin R, B and G (Ank1-3 respectively). In *Drosophila* two Ankyrin genes exist, *Dank1* (*ank1*) and *Dank2* (*ank2*). Ank2 is only expressed in neurons whereas Ank1 is more ubiquitously expressed. In contrast in *C. elegans* only one Ankyrin homolog, *unc-44*, has been identified.

In general ,Ankyrins consist of four Ankyrin domains (formed by multiple ankyrin repeats) followed by a Spectrin binding domain and a death domain (Davis and Bennett, 1984; Michaely and Bennett, 1993). The giant isoforms of Ankyrin have individual C-termini of different length. Together with the death domain these domains are important for the regulation of Ankyrin functions. The different C-termini of the Ankyrin isoforms are

generated through alternative splicing (Zhang and Bennett, 1998; Zhou et al., 1997). In addition to L1CAMs, Ankyrins are known to bind to ion channels, anion exchangers and inositol$_{(1, 4, 5)}$-triphosphate (IP3) receptors through their Ankyrin domains (Cunha et al., 2007; Mohler et al., 2005; Mohler et al., 2004; Nelson and Veshnock, 1987). Whereas the exact binding sites within the Ankyrin domains for the voltage gated sodium channel (Lowe et al., 2008) or the IP3 receptor (Mohler et al., 2005) have been identified, it is not known which Ankyrin domains are important for L1CAM interactions. However, Neurofascin and the anion exchanger AE1 bind to different Ankyrin domains in red blood cells (Bennett and Stenbuck, 1980), indicating that Ankyrins have the potential to bind multiple CAMs at the same time to form protein complexes that are linked to the Actin/Spectrin cytoskeleton (Michaely and Bennett, 1995a; Michaely and Bennett, 1995b).

Ankyrin B deficient mice exhibit neurological phenotypes such as hypoplasia of the corpus callosum and pyramidal tracts, dilated ventricles and severe postnatal degeneration of the optic nerve. These effects are caused by abnormal neurite outgrowth, axon guidance and axon fasciculation (Scotland et al., 1998).

Ankyrin binding to L1CAM molecules enhances their homophilic adhesive properties and reduces their mobility within the plasma membrane (Garver et al., 1997). Homophilic interaction of L1CAMs can activate EGF receptor tyrosine kinase activity (Islam et al., 2004), which is important for growth cone axon guidance in sensory neurons (Garcia-Alonso et al., 2000). Whittard et al. (2006) used an *in vitro* assay to monitor the FIGQY phosphorylation status. They showed that EGFR, mitogen-activated protein kinase (MAPK) and neuronal growth factor receptor (NGFR) activation induced phosphorylation of the tyrosine and this prevents the recruitment of AnkyrinG to the cell membrane (Whittard et al., 2006).

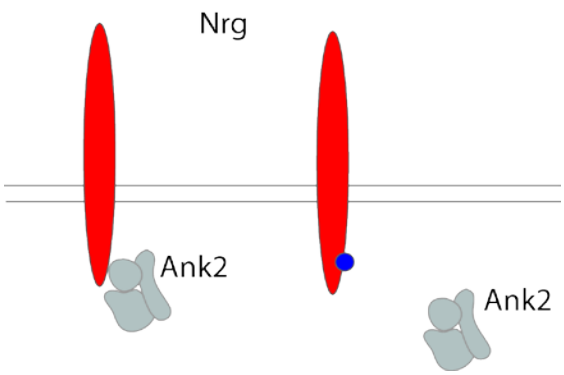


**Figure 8 - Regulation of L1-Ank interaction**

Binding of L1-type CAMs (red) to Ankyrins (grey) is mediated by the FIGQY motif in the cytoplasmic domain of L1CAMs and the N-terminal Ankyrin domains of Ankyrins. Phosphorylation (indicated here with a blue dot) of the tyrosine via an unknown kinase within the FIGQY motif prevents Ankyrin recruitment to L1CAM proteins. The phosphorylation of the FIGQY motif allows the binding of another protein called Doublecortin.

The Drosophila Ank2 protein is part of a previously identified molecular network essential for synapse stability at the *Drosophila* NMJ (Koch et al., 2008; Pielage et al., 2011; Pielage et al., 2008; Pielage et al., 2005; Pielage et al., 2006). This network consists of the adaptor molecule Ank2, α- and β-Spectrin and the actin-capping molecule Hts/Adducin and has the potential to link cell adhesion molecules to the underlying actin/microtubule cytoskeleton (Figure 9). In the screen I identified Nrg as essential for synapse stability and thus could be the cell adhesion molecule upstream of this network controlling synapse stability.

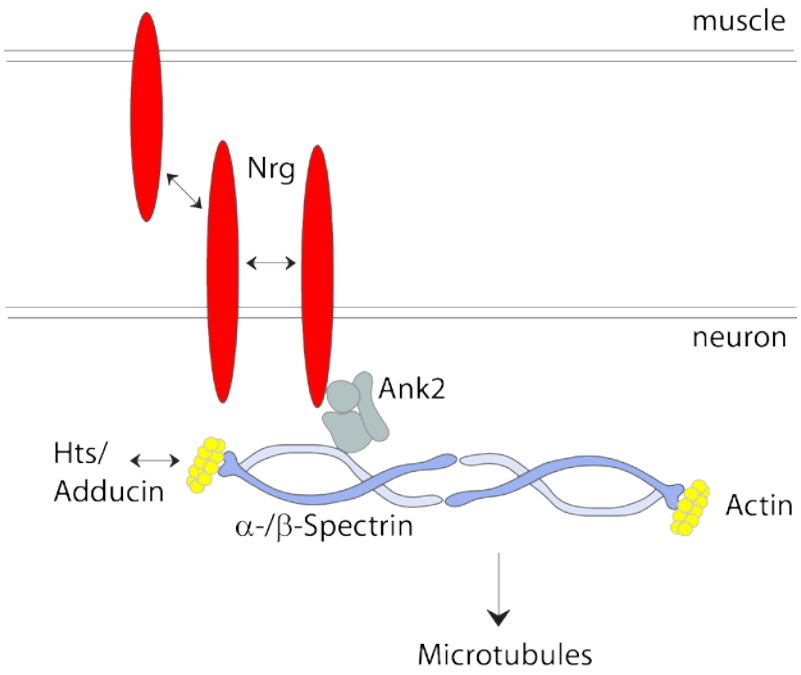


**Figure 9 - Network underlying the cell membrane important for synapse stability**

Ankyrin2 is part of a molecular network underlying the cell membrane, which has the potential to provide a link from the cell membrane to the microtubule and actin cytoskeleton, thus controlling synaptic stability. All members of this network including the anchoring molecule Ank2 (grey), the scaffolding molecules α- and β-Spectrin (blue) and the actin capping molecule Hts/Adducin have been identified to be important for synapse stability (Koch et al., 2008; Pielage et al., 2011; Pielage et al., 2008; Pielage et al., 2005; Pielage et al., 2006). Neuroglian can interact with Ank2 in a regulated fashion having the potential to be upstream of this network controlling synapse stability.

## 1.4. Aim of the Work

In the nervous system synaptic contacts between neurons are highly specialized structures essential to transfer information. During the formation of the nervous system neurons have to connect with each other and form functional circuits. Importantly these neuronal circuits need to be stable and plastic at the same time allowing changes in connectivity both during development and in response to activity e.g. during learning and memory. The inappropriate loss of synaptic contacts can lead to severe neurodegenerative diseases. Trans-synaptic interactions mediated by cell adhesion molecules have the potential to directly link two neighboring cells and provide a regulatory module controlling stability and plasticity of this contact. Many cell adhesion molecules have been described as crucial during early steps of neuronal circuit development such as axon guidance and synapse formation. In contrast, little is known about the cell adhesion molecules controlling synapse maintenance and plasticity. In this study, I aimed to identify cell adhesion molecules and the underlying regulatory mechanisms controlling synapse maintenance. As a model system I used the *Drosophila* neuromuscular junction, which allows the analysis of synapse development at the resolution of single synapses *in vivo*. I performed an unbiased RNAi screen to identify potential stabilizing cell adhesion molecules and performed a detailed analysis of two genes using advanced genetic, biochemical, biophysical and imaging techniques.

# 2. Results

## 3.1. RNAi Screen

To identify new cell adhesion molecules important for NMJ development and stability, I performed an unbiased RNAi-based screen using a high-resolution assay that combines immunohistochemistry with high resolution confocal microscopy. This assay has been used in a number of studies to identify stability and formation defects at the *Drosophila* NMJ (Eaton and Davis, 2005; Eaton et al., 2002; Pielage et al., 2011; Pielage et al., 2008; Pielage et al., 2005; Wan et al., 2000). I screened entire classes of cell adhesion molecules that were selected based on previous described functions in the nervous system (listed in Table 2). In addition, I screened a selection of potential CAM interacting proteins and included positive controls of genes with previously described functions at the NMJ. To identify important pre- as well as postsynaptic cell adhesion molecules, I used a Gal4 driver line combination that allowed the knock down of proteins in the motoneuron and the muscle simultaneously (*elav*$^{C155}$-Gal4; UAS-*dcr2*; BG57-Gal4).

**Table 2 - List of the transmembrane protein classes screened in this study**

| *Class of transmembrane protein* | *# candidates* |
|---|---|
| Ig-domain proteins | 126 |
| LRR-domain proteins | 70 |
| Cadherins | 19 |
| Laminins | 9 |
| Integrins | 8 |
| Semaphorins | 10 |
| Von willebrand factor | 5 |
| CAM interacting proteins | 40 |
| Positive controls | 26 |
| Total | 313 |

The numbers indicate the number of VDRC lines screened for each class. A total of 313 candidates have been screened, a list of all VDRC lines and CG numbers can be found in the appendix Table 17-24. Abbreviations used in the table: Ig = immunoglobulin, LRR = leucine-rich repeat, CAM = cell adhesion molecule

The assay used in the RNAi screen is based on the observation that the presence of a presynaptic motoneuron induces the formation of postsynaptic specializations. Thus, whenever postsynaptic markers are observed without opposing presynaptic markers we can conclude that the NMJ has been retracted. In wild type pre- and postsynaptic markers are always opposing each other and only in 1-2% of all NMJs unopposed postsynaptic markers can be observed. However, these are only small retractions of maximal 1-3 boutons per NMJ. In addition, the presynaptic membrane is stained using Hrp, which allows analyzing the

membrane integrity. RNAi mediated knock down or mutations of genes involved in synapse stability results in an increase in the frequency of NMJs showing unopposed postsynaptic markers and a fragmentation of the presynaptic membrane.

In the screen, I analyzed in a first step all NMJs of the abdominal segments A2-A6 in three animals to identify potential candidates affecting synapse stability. Additionally, muscle and morphology phenotypes like protrusions were noted. Using RNAi lines of genes with previously identified phenotypes at the NMJ, I ensured that the RNAi conditions enabled a significant knock down of target genes. Importantly, I was able to identify 80% of all positive controls. In the next chapter, I would like to describe some of these positive controls since this validates the RNAi method to screen for candidates important for NMJ development and stability

### 3.1.1. Validation of the screening conditions

Among the positive controls, RNAi lines were included that target the pre- and postsynaptic markers used for our screening assay: Brp and the glutamate receptor subunit GluRIIE. In *Drosophila* glutamate receptor are heteromultimeric receptors with four distinct subunits: GluRIII, GluRIIE, GluRIID and either GluRIIA or B. In Figure 10, I show exemplary images of muscle 4 NMJs after knock down of Brp and GluRIIE. Both markers are significantly decreased. Brp is knocked down completely, thus only postsynaptic markers are visible. The analysis of the presynaptic membrane demonstrates that these NMJs are still stable in accordance with previous studies using *brp* mutations (Fouquet et al., 2009; Kittel et al., 2006; Wagh et al., 2006).

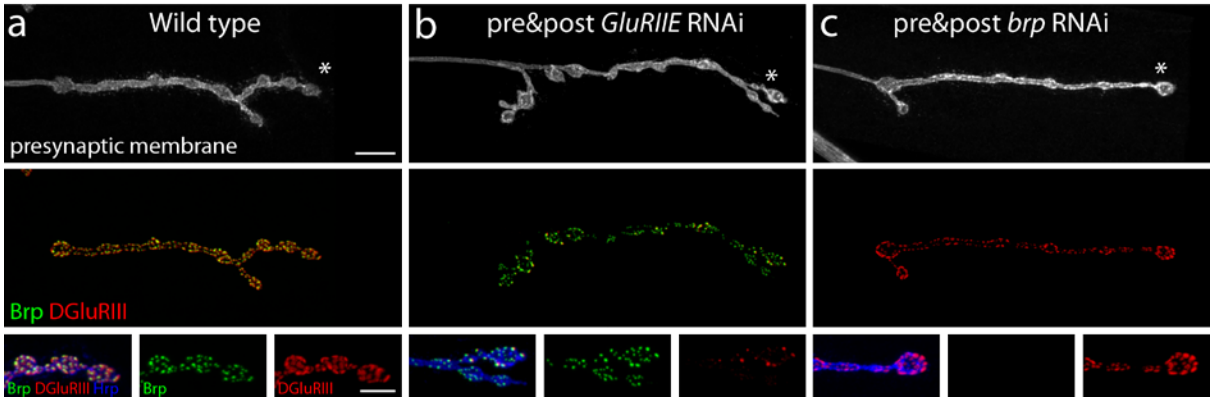


**Figure 10 - RNAi mediated knock down of Brp and GluRIIE reduced protein level without affecting synaptic stability**

**(a-c)** Muscle 4 NMJ stained for presynaptic active zone marker Brp (green), postsynaptic glutamate receptors DGluRIII (red) and the presynaptic membrane (Hrp, blue, grey). **(a)** A wild type NMJ with opposing pre- and postsynaptic markers and an intact presynaptic membrane. Terminal boutons are highlighted in the inset. **(b)** A muscle 4 NMJ after simultaneous pre- and postsynaptic knock down of DGluRIIE. In *Drosophila* glutamate receptor are heteromultimeric receptors with four distinct subunits: GluRIII, GluRIIE, GluRIID and either GluRIIA or B. Thus, the loss of GluRIIE leads to a decrease in DGluRIII staining in the muscle. However, the NMJ remains stable based on the membrane staining. Terminal boutons are highlighted in the inset. **(c)** A muscle 4 NMJ after pre- and postsynaptic knock down of Brp. This leads to the loss of Brp in the NMJ terminal. The NMJ is still stable, based on the integrity of the membrane and the normally clustered glutamate receptors. Terminal boutons are highlighted in the inset. Scalebar in **(a)** corresponds to **(a-c)**, 10 µm, insets 5 µm.

In addition, the SMADs *medea* (*med*) and *mother against decapentaplegic* (*mad*) were used as positive controls. Both genes have been previously identified as important for NMJ development. Mutants display severe growth defects and synaptic instability at the NMJ (Eaton and Davis, 2005). I was able to identify the RNAi lines targeting *med* and *mad* based on their synaptic retraction phenotypes. Presynaptic knock down of Med led to 10-20% of retractions on muscle 4 and muscle 6/7. An exemplary image of a muscle 6/7 retraction after RNAi mediated knock down of Med is shown in Figure 11. Figure 12 shows images of NMJs after presynaptic *mad* RNAi and quantifications of synaptic retraction frequencies are shown for muscle 6/7 and muscle 4. Loss of Mad in the presynaptic motoneuron led to about 40% of retractions at both NMJs (Figure 12 e, f). This phenotype has been confirmed using two different presynaptic Gal4 driver lines. Interestingly, the frequency of retractions was higher than in the *mad* mutants (Eaton and Davis, 2005). This is most likely due to the tissue specificity of our RNAi approach. *Mad* mutant animals have severe developmental problems indicating a requirement outside the nervous system.

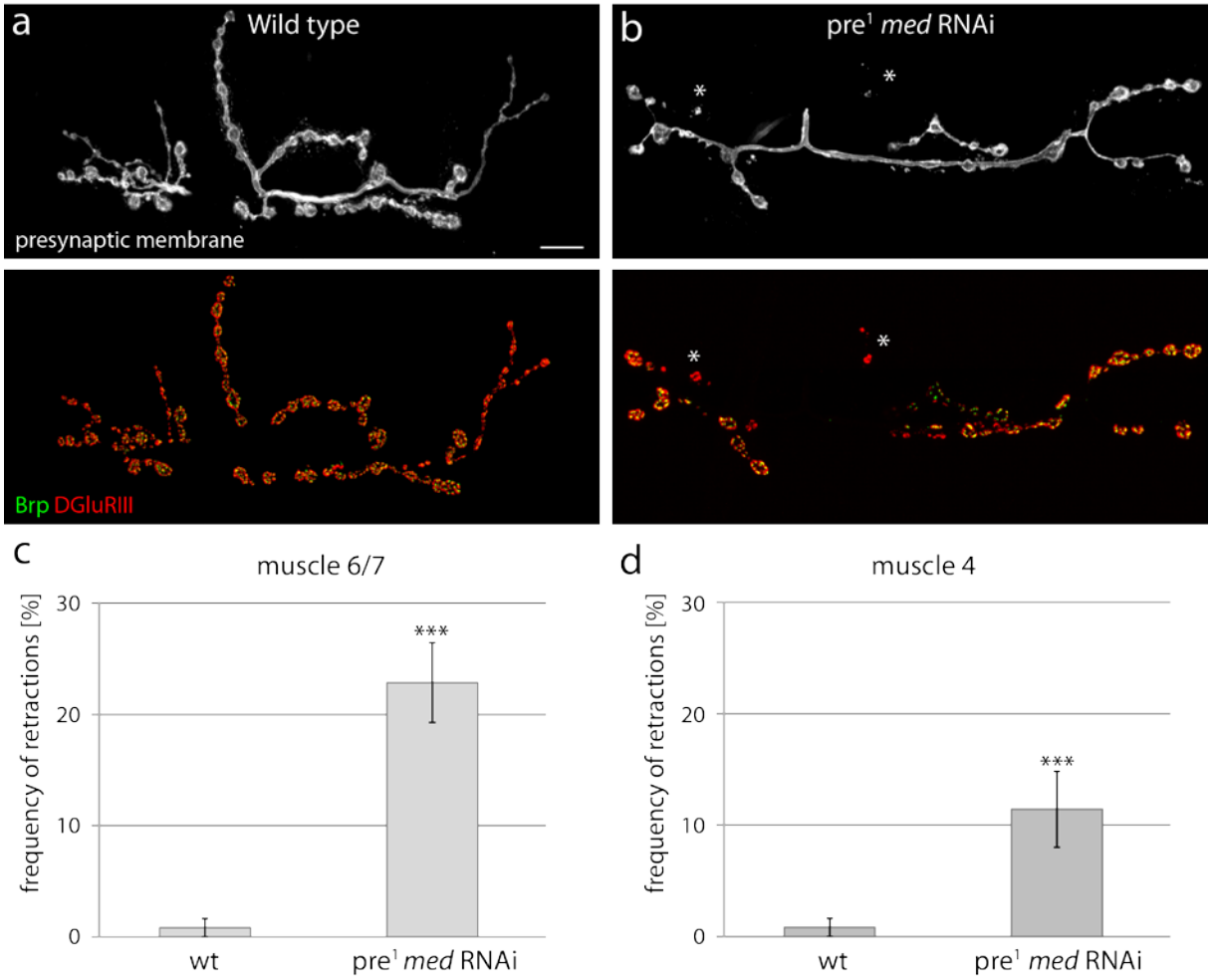


**Figure 11 - Presynaptic knock down of the SMAD Medea leads to synaptic retractions**

**(a-b)** Muscle 6/7 NMJs stained for the presynaptic active zone marker Brp (green), postsynaptic glutamate receptors (red) and the presynaptic membrane (Hrp, white). **(a)** A wild type muscle 6/7 NMJ with opposing pre- and postsynaptic markers and an intact membrane is shown. **(b)** A muscle 6/7 NMJ after presynaptic *med* RNAi. No presynaptic markers are present in the areas highlighted by the asterisk and the membrane is fragmented. **(c)** Quantification of the retraction frequency after presynaptic knock down of Med. At muscle 6/7 23% of all NMJs are affected ($P \leq 0.0001$, n = 5 -12 animals analyzed). **(d)** Quantification of retraction frequency on muscle 4. 11% of all NMJ show retractions after presynaptic *med* RNAi ($P = 0.0014$, n = 7-12 animals analyzed). Scale bar in **(a)** corresponds to **(a-b)**, 10 µm. Error bars represent SEM.

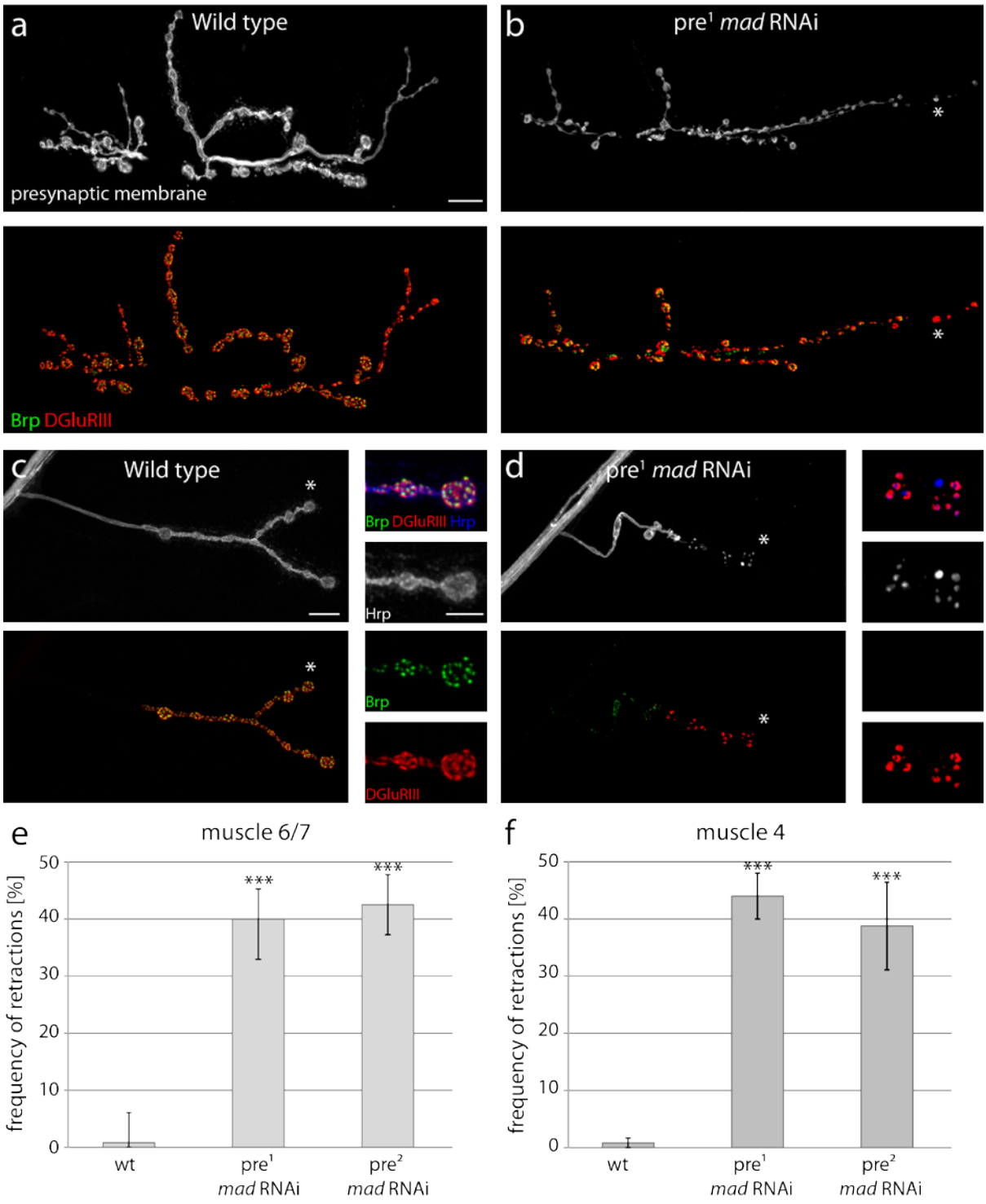


**Figure 12 - Presynaptic knock down of the SMAD Mother against dpp leads severe retractions**

**(a-d)** Larval NMJs stained for presynaptic active zone marker Brp (green) and postsynaptic glutamate receptors (red). In addition, the presynaptic membrane is stained with Hrp (blue, white). **(a)** A wild type muscle 6/7 NMJ is shown. Pre- and postsynaptic markers are opposing each other and the membrane is intact. **(b)** A muscle 6/7 NMJ after presynaptic knock down of Mad is shown. The NMJ partially lost the presynaptic marker Brp and shows a strong fragmentation of the membrane in the region indicated by the asterisk. **(c)** A wild type muscle 4 NMJ with opposing pre- and postsynaptic

markers and an intact membrane. The asterisk indicates the boutons highlighted in the insets. **(d)** A muscle 4 NMJ after presynaptic *mad* RNAi. The presynaptic membrane is highly fragmented and the presynaptic marker Brp is lost from the entire NMJ terminal. Remnants of Brp cluster are visible in the axon of the NMJ. The area indicated by the asterisk is highlighted in the insets. **(e)** Quantification of retraction frequency on muscle 6/7 using two different Gal4 driver line combinations. 40% of muscle 6/7 NMJs show a significant increase in synaptic instability independent from the Gal4 driver line combination used ($P \leq 0.0001$ for both Gal4 lines, n = 5-12 animals analyzed) **(f)** Quantification of retraction frequency on muscle 4 using two different Gal4 driver line combinations. 40% of all muscle 4 NMJs show a significant increase in synaptic instability independent from the Gal4 driver line combination used for knock down of Mad ($P \leq 0.0001$for both Gal4 lines, n = 5-12 animals analyzed). Gal4 driver line legend: pre[1]= *elav*$^{C155}$-Gal4; UAS-*dcr2* and pre[2]= *elav*$^{C155}$-Gal4; UAS-*dcr2*-*sca*-Gal4. Scale bars in **(a, c)** corresponds to **(a-d)**, 10 µm, insets 5 µm. Error bars represent SEM.

Importantly, not only retraction phenotypes can be identified using this assay. In addition, it also allows the identification of other phenotypes like morphology and growth related phenotypes. As a positive control for these phenotypes the RNAi line targeting *highwire* (*hiw*, VDRC28163) was included in the screen. *Hiw* has been shown to be essential for the restriction of NMJ growth (McCabe et al., 2004; Wan et al., 2000). As expected, I observed a significant NMJ overgrowth after presynaptic RNAi of Hiw.

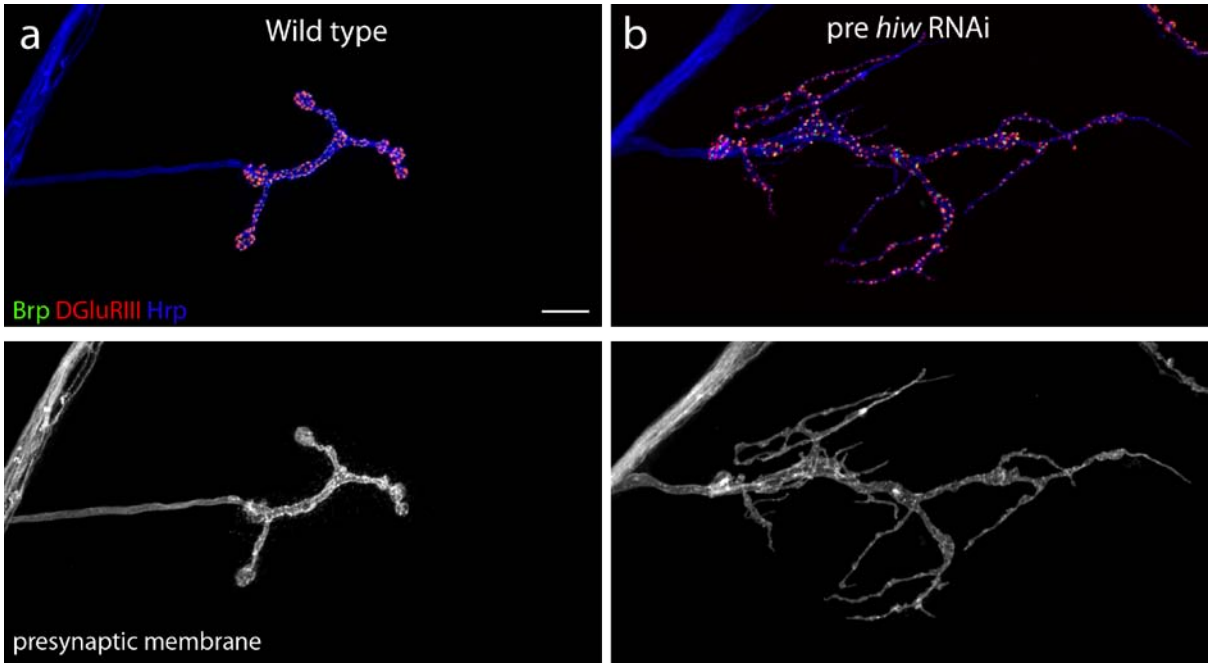


**Figure 13 - Presynaptic knock down of Highwire leads to a massive growth defects**

**(a-b)** Muscle 4 NMJs stained for presynaptic active zone marker Brp (green), postsynaptic glutamate receptors DGluRIII (red) and the presynaptic membrane (Hrp, blue, white). **(a)** A wild type muscle 4 NMJ with a normal size and morphology. **(b)** A muscle 4 NMJ after presynaptic knock down of Highwire. The size of the NMJ is massively increased through the formation of side branches and membrane protrusions. Scale bar in **(a)** corresponds to **(a, b)**, 10 µm.

Taken together, the identification of 80% of all positive controls demonstrated that the RNAi screen should allow the identification of novel genes important for synapse stability and morphology. The great advantage of the RNAi technique in comparison to the mutant analysis is the spatial and temporal control of the knock down. Thus, the overall health of an animal is in not affected by the RNAi mediated knock down and even stronger phenotypes can be observed at the NMJ in cases like *mad*.

### 3.1.2. Identification of genes important for synapse stability

In my RNAi screen, I identified 10 novel genes essential for synapse stability. The two top hits were Ig-domain proteins that are important for synapse stability in the presynaptic motoneuron: the L1CAM Neuroglian and CG31708. Neuroglian was of special interest since it has been shown to be a direct interaction partner of Ankyrins (Garver et al., 1997; Tuvia et al., 1997) and thus could be the cell adhesion molecule upstream of the molecular network controlling synapse stability at the NMJ (Koch et al., 2008; Pielage et al., 2011; Pielage et al., 2008; Pielage et al., 2005; Pielage et al., 2006, Figure 9). The main part of my thesis focused on the characterization of Neuroglian function and the interaction with Ank2 at the larval NMJ (submitted manuscript and chapter 3.3). *CG31708* is essential presynaptically for synapse stability and showed a novel retraction phenotype different from all stability genes identified so far. A phenotypic description and first characterization of this gene is described in chapter 3.4. Here, I would like to briefly describe the phenotypes of three additional hits identified in the screen. A summary of the five top hits is shown in Table 14 and a list of additional weaker hits is found in the Appendix Table 25.

**Table 3 - List of Top 10 Hits from RNAi Screen**

| *VDRC line* | *Name* | *Score* | *Class of proteins* |
|---|---|---|---|
| 6688/107991 | *nrg* | +++ | Ig |
| 38261 | *CG31708* | +++ | Ig |
| 18225 | *inc* | ++ | CAM interaction |
| 31044 | *CG5195* | ++ | LRR |
| 9788/9788 | *cora* | + | CAM interaction |

The five top hits from the RNAi screen based on the retraction frequency: +++ indicates a severe retraction phenotype, ++ a strong retraction phenotype, + mild retraction phenotype. The VDRC stock number, the gene name (CG number if uncharacterized) and the respective class of proteins are listed. Abbreviations used in this table: *nrg* = *neuroglian*, *inc* = *insomniac*, *cora* = *coracle*, Ig = immunoglobulin, CAM = cell adhesion molecule, LRR = leucine-rich repeat.

The first gene I would like to describe is *insomniac* (*inc*) which was identified using the VDRC line 18225. Presynaptic knock down of *inc* led to an increase in retraction frequency to 18% at muscle 6/7 and 16% at muscle 4 (Figure 14 d, e). Two NMJs that demonstrate the phenotype are shown in Figure 14. Importantly, I observed retractions and formation defects (Figure 14 b, c). *Insomniac* has been identified in 2011 as an important gene in the nervous system for the duration and consolidation of sleep (Stavropoulos and Young, 2011). The protein belongs to the BTB/POZ superfamily and is very small (24 kDa, 211 amino acids). Only one isoform has been identified so far. It will be interesting to relate the synaptic defect to its function in sleep control.

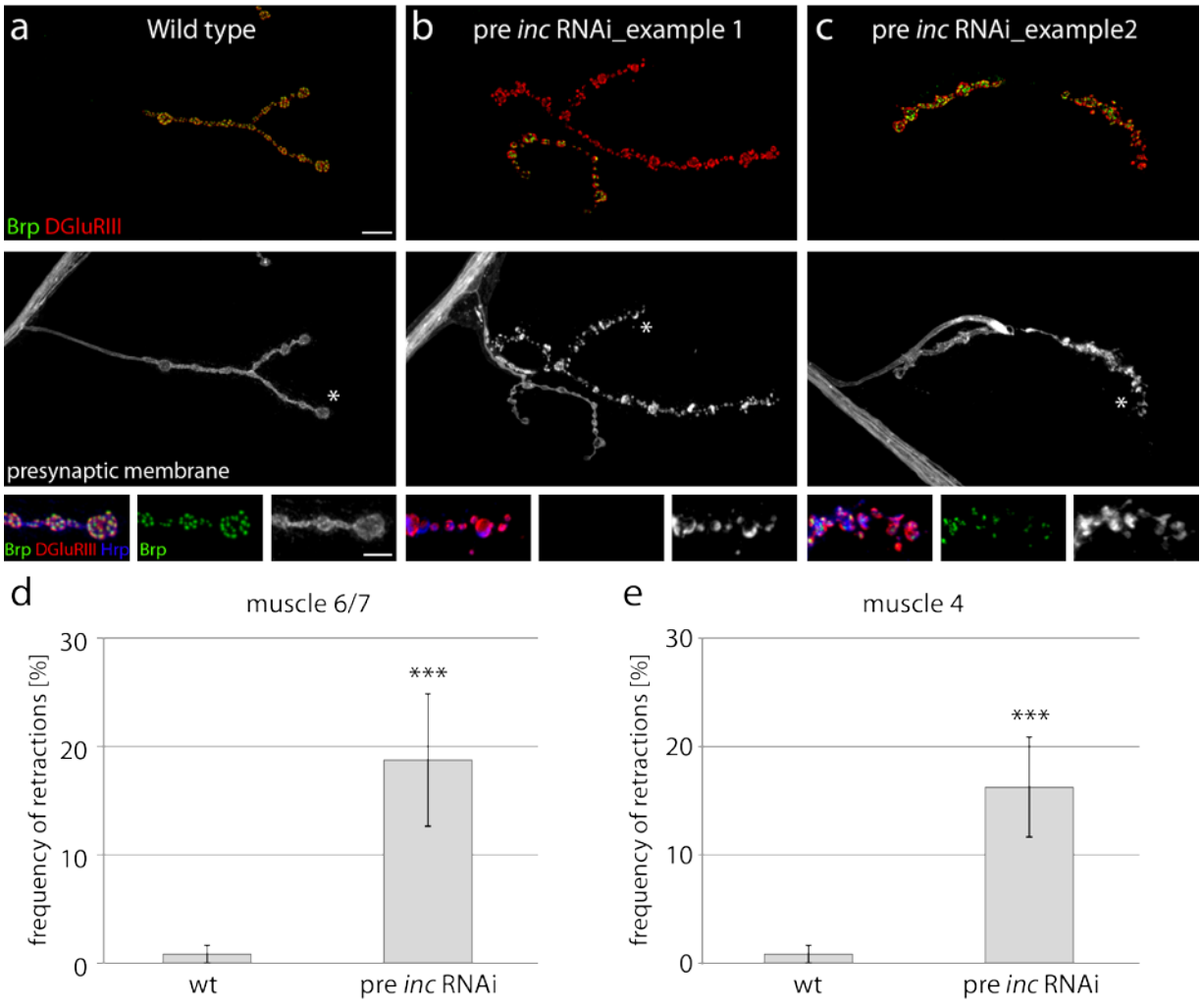


**Figure 14 - Presynaptic knock down of Insomniac leads to synaptic retractions**

**(a-c)** Larval muscle 4 NMJ stained for presynaptic active zone marker Brp (green) and postsynaptic glutamate receptors (red). In addition the presynaptic membrane is stained with Hrp (white, blue). **(a)** A wild type muscle 4 NMJ. Pre- and postsynaptic markers are opposing each other and the membrane is intact. The asterisk indicates the region highlighted in the inset below. **(b)** A muscle 4 NMJ with severe synaptic retractions. Large parts of this NMJ lost the presynaptic marker Brp, the glutamate

receptors cluster together and the membrane is highly fragmented. The region shown and highlighted in the inset below is marked by the asterisk. **(c)** A muscle 4 NMJ with formation and instability defects. The area highlighted in the inset below shows a single bouton without Brp and a fragmented membrane. The rest of the NMJ is abnormally formed based on membrane and pre- and postsynaptic staining. (d) Quantification of retraction frequency at muscle 6/7 after *inc* RNAi. 18% of all muscle 6/7 NMJs show synaptic retractions (P = 0.0022, n = 8-12) (e) Quantification of retraction frequency at muscle 4 (P = 0.0008, n = 8-12). 16% of all muscle 4 NMJ show synaptic retractions. Scale bar in **(a)** corresponds to **(a-c),** 10 µm, insets 5 µm. Error bars in **(d)** and **(e)** represent SEM.

The second hit was the 4.1 protein Coracle (Cora). Figure 15 shows that knock down of Cora led to a small but significant increase in synaptic retractions. Importantly this is caused by the presynaptic loss of Cora since the simultaneous pre- and postsynaptic knock down of Cora resulted in the identical frequency of retractions (Figure 15 c, d). *Cora* encodes a FERM-domain (**F** = 4.1 protein, **E** = ezrin, **R** = radixin, **M** = moesin) protein that has been identified as important for the selective clustering of glutamate receptors at the larval NMJ (Chen et al., 2005). Interestingly, Neuroglian has a FERM protein binding domain in the cytoplasmic domain and could therefore be a potential interaction partner of Cora.

The last hit I would like to highlight is the so far uncharacterized gene CG5195 which belongs to the family of LRR proteins. The phenotype of the RNAi knock down of CG5194 was unique in some aspects. Firstly, in contrast to all other identified candidates CG5195 was important postsynaptically to promote synapse stability (Figure 16 e, f). Secondly, postsynaptic knock down also led to severe muscle defects and corresponding changes in NMJ morphology (Figure 16 d). Presynaptic knock down resulted in synapse formation defects including the presence of satellite boutons (Figure 16 c). CG5195 is an LRR protein without a transmembrane domain but a signal peptide (Figure 16 g), thus CG5195 is likely a secreted protein controlling the coordination of pre- and postsynaptic development.

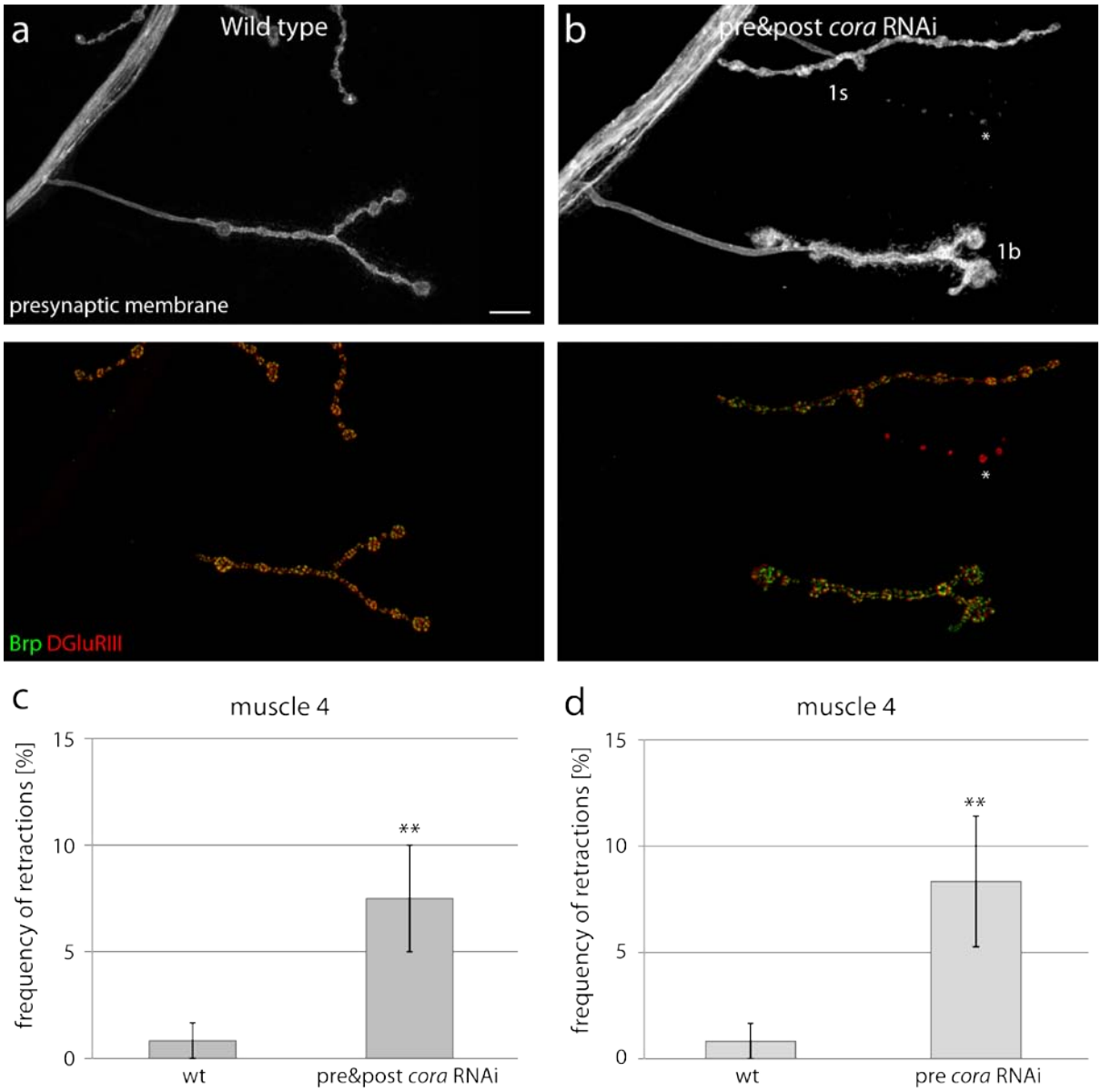


**Figure 15 - Presynaptic knock down of the 4.1.protein Cora reduces synaptic stability**

**(a-b)** Muscle 4 NMJ stained for presynaptic active zone marker Brp (green), postsynaptic glutamate receptors (red) and the presynaptic membrane (Hrp, white). **(a)** A wild type muscle 4 NMJ is shown with opposing pre- and postsynaptic markers and an intact presynaptic membrane. **(b)** A NMJ after RNAi mediated presynaptic knock down of Cora. Whereas the Type Ib NMJ is still stable, the Type 1s NMJ lost one branch where only little remnants of the membrane and the glutamate receptors are still present. Note the formation defect in the still stable Type Ib NMJ. **(c)** Quantification of the retraction frequency on muscle 6/7 after simultaneous pre- and postsynaptic *cora* RNAi. A significant increase of synaptic retractions can be observed (P = 0.0067, n = 6-12). **(d)** Quantification of the retraction frequency after presynaptic knock down of Cora. A similar number of synaptic retractions to **(c)** can be observed (P = 0.0069, n = 6-12). Scale bar in **(a)** corresponds to **(a, b)**, 10 µm. Error bars represent SEM.

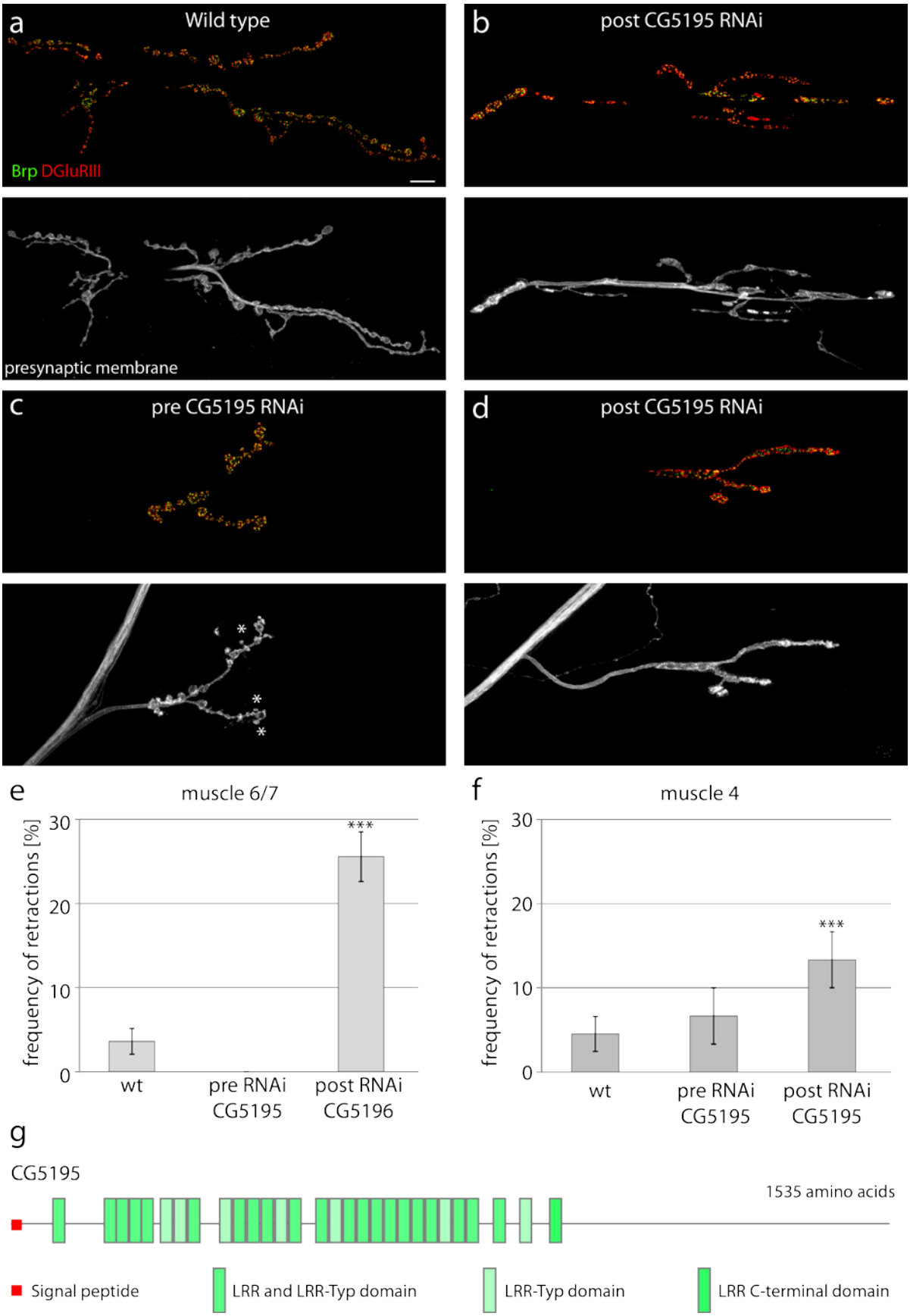


**Figure 16 - Postsynaptic knock down of CG5195 results in synaptic retractions**

**(a-d)** Larval NMJ stained for presynaptic active zone marker Brp (green) and postsynaptic glutamate receptors (red). In addition the presynaptic membrane is stained with Hrp (white). **(a)** A wild type muscle 6/7 NMJ. Pre- and postsynaptic markers are opposing each other and the membrane is intact. **(b)** A muscle 6/7 NMJ after postsynaptic knock down of CG5195. This NMJ partially lost Brp (asterisk), the glutamate receptor cluster and the presynaptic membrane is fragmented. Note the severe muscle defects caused by postsynaptic knock down of CG5195. **(c)** A muscle 4 NMJ after presynaptic knock down of CG5195 is shown. No synaptic retractions can be observed. However satellite boutons (asterisk) can be observed which are never seen in wild type. **(d)** A muscle 4 NMJ after postsynaptic knock down of CG5195. The NMJ is not retracted but lost the bouton structure of wild type NMJs. **(e)** Quantification of synaptic retraction frequency after pre- or postsynaptic knock down of CG5195 for muscle 6/7 ($P \leq 0.0001$ for postsynaptic knock down, $n = 9$ -11). **(f)** Quantification of retraction frequency after pre- or postsynaptic knock down of CG5195 for muscle 4 ($P = 0.032$ for postsynaptic knock down, $n = 9$-11). **(g)** The domain structure of CG5195 is shown based on SMART. In the N-terminus a signal peptide was identified and the protein harbors a total of 29 LRR or LRR-type domains. However no transmembrane domain has been identified. Scale bar in **(a)** corresponds to **(a-d)**, 10 µm. Error bars in **(e)** and **(f)** represent SEM.

## 3.2. Submitted manuscript

The following manuscript has been submitted to Nature Neuroscience and is still under revision:

**Trans-synaptic coordination of synaptic growth, function and stability by the L1-type CAM Neuroglian**

Eva-Maria Enneking[1,3], Sirisha R. Kudumala[2,3], Eliza Moreno[1], Raiko Stephan[1], Jana Boerner[2], Tanja A. Godenschwege[2, #] and Jan Pielage[1, #]

1. Friedrich Miescher Institute for Biomedical Research
Maulbeerstrasse 66
4058 Basel
Switzerland
Phone: +41 61 69 604 37
Fax: +41 61 69 739 76
Email: jan.pielage@fmi.ch

2. Florida Atlantic University
777 Glades Road
Boca Raton, FL 33431
U.S.A.
Phone: + 01 561 297 1390
Email: godensch@fau.edu

3. these authors contributed equally

# to whom correspondence should be addressed

## Abstract

Cell adhesion molecules mediate axon guidance and synapse formation but the mechanisms controlling synapse maintenance or plasticity *in vivo* remain largely uncharacterized. We identify the *Drosophila* L1-type CAM Neuroglian (Nrg) as a central coordinator of synapse growth, function and stability with distinct requirements in the peripheral and central nervous system. At the larval neuromuscular junction synapse stability depends on the extracellular Ig-domains and the intracellular Ankyrin interaction motif. Alterations in binding affinities to Ankyrin2 directly correlate with mobility of Nrg *in vivo* and control the balance of synapse growth and stability. At the central Giant fiber synapse Nrg coordinates pre- and postsynaptic development via a trans-synaptic signaling mechanism that depends on the dynamic regulation of the intracellular Ankyrin-binding motif. Together, our results identify the L1-type CAM Ankyrin interaction as a novel regulatory module enabling local control of synaptic connectivity and function while maintaining neuronal circuit architecture.

## Introduction

Trans-synaptic interactions mediated by cell adhesion molecules (CAMs) control the formation, function and stability of synaptic connections within neuronal circuits. While a large number of synaptogenic CAMs controlling the initial steps of synapse formation have been identified [1, 2], relatively little is known regarding the identity or regulation of CAMs selectively controlling synapse maintenance or plasticity. Information processing within neuronal circuits is adjusted by the selective addition or elimination of individual synapses both during development and in response to activity [3, 4]. These changes in connectivity can occur in very close proximity to stable synapses [5, 6] indicating the existence of mechanisms capable of local alterations of trans-synaptic adhesion. Potential mechanisms include the direct alteration of extracellular binding affinities of CAMs through binding of ligands including metal ions (e.g. $Ca^{2+}$) to extracellular domains [7]. In addition, trans-synaptic adhesion can be modulated indirectly through the selective association of CAMs with the intracellular cytoskeleton via adaptor proteins. Regulation of these interactions via posttranslational modifications can alter mobility, clustering and adhesive force of CAMs [8]. These controlled changes in biophysical properties can then induce changes in synapse morphology, strength or stability and modulate trans-synaptic signaling [9, 10].

We have previously identified a presynaptic molecular network at the *Drosophila* neuromuscular junction (NMJ) that has the potential to control synapse stability by directly

coupling CAMs to the presynaptic actin and microtubule cytoskeleton. This network consists of the adaptor molecule Ankyrin2 (Ank2), the scaffolding proteins α- and β-Spectrin and the actin-capping molecule Hts/Adducin [11-14]. Ank2 can directly interact with transmembrane proteins including ion channels, receptors and cell adhesion molecules via its N-terminal Ankyrin-repeat domain and bind to β-Spectrin or presynaptic microtubules via distinct C-terminal domains [15]. Spectrin can interact directly or via the actin-capping molecule Adducin with presynaptic actin filaments [12, 15]. Loss-of-function mutations in all of these genes severely impair synapse stability in *Drosophila* [11-14] and result in learning and memory defects as well as progressive neurodegeneration in vertebrates [16-18].

To identify cell adhesion molecules that control synapse maintenance and plasticity upstream of the Ank2/Spectrin/Adducin network, we performed an unbiased RNAi-based screen of 313 transmembrane proteins that are predicted to function as synaptic CAMs based on their domain structure [19]. These included Ig-domain containing proteins, LRRs, Cadherins, Integrins and Semaphorins. In this screen we identified the *Drosophila* L1-type CAM Nrg as an essential protein for synapse stability.

Nrg encodes the *Drosophila* ortholog of the vertebrate L1-type protein family that is composed of four closely related members: L1, CHL1 (close homolog of L1), NrCAM (neuronal CAM) and Neurofascin [20, 21]. L1-type IgCAMs usually consist of 6 Ig-domains, 3-5 fibronectin type III domains, a single transmembrane domain and an intracellular tail. The extracellular domain of L1 family proteins can mediate cell-cell adhesion via homophilic interactions and engage in a variety of heterophilic interactions with other Ig-domain proteins (e.g. NCAM, TAG-1, Contactin and others), extracellular matrix proteins and integrins [20-22]. The intracellular tail contains distinct protein-protein interaction domains controlling the localization and function of L1 proteins [23]. Most prominent is a central Ankyrin interacting motif that is highly conserved among all vertebrate L1 family proteins and *Drosophila* Neuroglian [23]. Phosphorylation of a single tyrosine within this FIGQY motif abolishes binding to Ankyrins [24-27]. The Ankyrin-binding domain is essential for mediating neuronal adhesion *in vivo* in C. elegans, however it is dispensable for L1 mediated homophilic adhesion in transfected cells in culture [28, 29].

Studies in a variety of animal models implicated all L1 family members in nervous system development [20, 21]. Human mutations in L1CAM cause a broad spectrum of neurological disorders grouped under the name L1 or CRASH syndrome. These disorders include MASA syndrome (mental retardation, aphasia, shuffling gait, adducted thumbs), agenesis of the

corpus callosum and spastic paraplegia, and additionally weak mutations in L1CAM and NrCAM have been linked to psychiatric diseases [21, 22, 30]. At the cellular level L1-type proteins are involved in neurite outgrowth, axon pathfinding and fasciculation and synapse development [21, 23]. The subcellular localization of L1-type proteins contributes to the establishment and maintenance of specialized neuronal membrane compartments including the axon initial segment (AIS) and nodes of Ranvier [31-33]. At the AIS an Ankyrin-based gradient of Neurofascin regulates the subcellular targeting of inhibitory pinceau synapses to the AIS of Purkinje cells [31, 34]. Similarly, disruption of the L1CAM - Ankyrin interaction in mice impairs inhibitory synapse function [35]. While these studies highlight essential functions of L1 family proteins, potential redundant or antagonistic functions between different L1-type proteins may mask the full extent of their importance for nervous system development. Indeed, evidence for redundant functions between L1-type proteins was provided by a double mutant analysis of L1CAM and NrCAM [36]. Together with the requirement of L1-type proteins for early nervous system development this confounds our current mechanistic understanding of L1-type protein function and regulation in synapse development and plasticity.

Nrg encodes the sole homolog of L1-type proteins in *Drosophila* with equal homology to all four vertebrate proteins. This provides a unique opportunity to unravel the contributions of L1-type proteins in synapse development and maintenance. Here, we address the specific contributions of extra- and intracellular domains of Nrg to synapse stability. We also demonstrate that binding of Nrg to Ank2 is critical for the control of mobility of Nrg *in vivo*. We use two complementary model systems, the larval neuromuscular junction and the central Giant Fiber synapse to assess the importance of this interaction for synapse development. We demonstrate that the Nrg-Ank2 interaction is essential to control the balance between synapse growth and stability. In addition, we provide evidence that regulation of the Ankyrin-binding domain of Nrg is essential to coordinate pre- and postsynaptic development via trans-synaptic signaling mechanisms.

## Results

### RNAi screen identifies the *Drosophila* L1-type CAM Neuroglian as essential for synapse stability

To identify cell adhesion molecules necessary for the maintenance of synaptic connections we performed a transgenic RNAi-based screen of 313 transmembrane proteins encoding potential cell adhesion molecules based on their domain structure and previously described

functions in axon guidance or synapse development. We knocked down candidate genes simultaneously in presynaptic neurons and postsynaptic muscles and analyzed third instar larvae for defects in synapse stability using selective pre- and postsynaptic markers (Fig. 1 a-f). In wild type animals the presynaptic active zone marker Brp is found in close opposition to postsynaptic glutamate receptor cluster at all individual synapses within the presynaptic nerve terminal demarcated by the membrane marker Hrp. In contrast, NMJs displaying postsynaptic glutamate receptor clusters without opposing presynaptic active zone markers and a fragmentation of the presynaptic membrane indicate synapse retractions [12, 13]. We identified *Drosophila* Nrg as the top hit resulting in synaptic retractions at more than 50% of all NMJs on muscle 4. We first tested whether specific knock down of Nrg either in the motoneuron or the muscle also impairs synapse stability. Presynaptic knock down of Nrg was sufficient to cause synaptic retractions equivalent to the simultaneous pre- and postsynaptic knock down (Fig. 1 b, e, g). In contrast, muscle specific *nrg* RNAi did not lead to a significant increase in synaptic retractions (Fig. 1 c, f, g). We obtained similar results when we expressed an independent *nrg* RNAi line and were able to enhance the phenotype by combining different motoneuron Gal4 drivers or by co-expressing UAS-*dcr2* to enhance RNAi efficacy (Fig. 1 g). We observed similar rates and severities of synapse retractions when using independent pre- and postsynaptic markers and when analyzing different subsets of muscles (Fig. 1 d-e; Supplementary Fig. 1; Supplementary table 1).

To monitor the efficiency of our RNAi mediated knock down we analyzed Nrg levels at larval NMJs and in brain extracts. The neuronal specific isoform Nrg180 was present throughout motoneuron axons and within the presynaptic nerve terminal (Supplementary Fig. 2 a). In contrast, Nrg167 was detected in muscles and glial cells (Supplementary Fig. 2 e). Western blots of larval brain extracts and analysis at the NMJ demonstrated that all combinations of presynaptic *nrg* RNAi efficiently knocked down Nrg180 (Figure 1 h; Supplementary Fig. 2 b). Similarly, muscle specific *nrg* RNAi knocked down Nrg167 in muscles (Supplementary Fig. 2 f). While postsynaptic *nrg* RNAi did not alter Nrg180 levels in brain extracts (Fig. 1 h), the loss of postsynaptic Nrg resulted in a significant change in presynaptic Nrg180 levels and distribution at the NMJ (Supplementary Fig. 2 f; reduced to 62.9 ± 3.7% of wild type protein within the presynaptic terminal, $P < 0.001$) indicating a requirement of postsynaptic Nrg for presynaptic Nrg localization. However, this reduction in presynaptic Nrg180 was not sufficient to impair synapse stability (Supplementary Fig. 2 c, f; Fig. 1 c, f) implicating the existence of alternative postsynaptic Nrg interaction partners essential for NMJ maintenance. To validate the specificity of our RNAi mediated knock

down we aimed to rescue the synaptic phenotypes by co-expressing wild type Nrg180. Simultaneous expression of UAS-*nrg180* but not of UAS-*mCD8-GFP* or of the homophilic cell adhesion molecule Fasciclin II (Fas II) significantly restored synapse stability and restored Nrg180 levels both in larval brains and at the NMJ (Fig. 1 g, h; Supplementary Fig. 2 d). Thus the specific loss of pre- but not postsynaptic Nrg resulted in a loss of synapse stability.

To gain insights into the molecular processes inducing synaptic retractions in animals lacking presynaptic Nrg we analyzed the distribution of two presynaptic components, Ank2 and Futsch, at early stages of synaptic retractions. The presynaptic adaptor protein Ank2 has previously been identified as an essential molecule for synapse stability and Ankyrins can directly bind to Nrg [11, 13, 15]. In addition, loss of microtubules represents an early step in synaptic retractions at the *Drosophila* NMJ that can be monitored by staining for the microtubule-associated protein Futsch [13, 14, 37]. We co-stained these NMJs either with the presynaptic active zone marker Brp or the synaptic vesicle marker DvGlut to monitor the molecular sequence of events underlying the disassembly of the presynaptic compartment. At wild type NMJs Ank2 and Futsch were present in all terminal boutons together with Brp and DvGlut. In contrast, after presynaptic knock down of Nrg we observed NMJs where Ank2 or Futsch were absent from terminal boutons that still contained presynaptic Brp or DvGlut and where the presynaptic membrane was still intact (Fig. 1 i-k). Thus loss of Ank2 and the associated microtubule cytoskeleton may represent an early step during synapse retractions caused by the loss of Nrg.

**Distinct contributions of the extra- and intracellular domain of Nrg for synapse stability**

Two domains of Nrg that may be essential for synapse maintenance are the extracellular Ig domains mediating association with postsynaptic CAMs and the intracellular Ankyrin binding domain that provides an interaction with the presynaptic cytoskeleton. To directly test for a potential role of these domains in synapse stability we generated genomic rescue constructs that allow expression of wild type and mutated *nrg* at endogenous levels using a site-directed Pacman based approach [38]. A transgenic construct encompassing the entire *nrg* locus including 25 kb upstream and 10 kb downstream regulatory sequences (P[nrg_wt]; Fig. 2a) rescued the embryonic lethal *nrg* null mutation $nrg^{14}$ (and $nrg^{17}$). We then used *galK*-mediated recombineering [39] to generate a deletion of the extracellular Ig domains 3 and 4 (P[$nrg^{\Delta Ig3\text{-}4}$]), that completely disrupts hetero- and homophilic binding capacities of Nrg [40]. In addition, we generated a specific deletion of the Ankyrin-binding domain of Nrg180

(P[*nrg180*$^{\Delta FIGQY}$]), which is possible because the domain is encoded by separate exons for the two Nrg isoforms (Fig. 2a). All constructs were inserted into the same genomic insertion site to ensure identical expression. While P[*nrg180*$^{\Delta FIGQY}$] rescued the embryonic lethality of *nrg*$^{14}$ mutants similar to the wild type construct, P[*nrg*$^{\Delta Ig3\text{-}4}$] failed to rescue the embryonic lethality. In order to analyze the larval NMJ in these embryonic lethal *nrg*$^{14}$; P[*nrg*$^{\Delta Ig3\text{-}4}$] flies, we combined the Pacman rescue approach with the MARCM technique [41]. First we analyzed motoneurons completely lacking *nrg* using the *nrg*$^{14}$ null mutation and observed two striking phenotypes. We found synapse retractions indicated by NMJs displaying remnants of the presynaptic MARCM membrane marker opposite postsynaptic glutamate receptors but lacking the presynaptic marker Brp (Fig. 2 c, d). While synapse retractions were only observed at low frequency the most common phenotype was motoneuron axons ending in "bulb-like" structures within nerve bundles, which were not connected to a postsynaptic muscle (50% of all labeled axons, Fig. 2 g-i). While the wild type *nrg* Pacman construct fully rescued these axonal and NMJ phenotypes (Fig. 2 b, f, i; Supplementary Fig. 3 a), P[*nrg*$^{\Delta Ig3\text{-}4}$] did not rescue these defects and the presence of P[*nrg180*$^{\Delta FIGQY}$] resulted only in a partial rescue. In both genotypes we observed synaptic retractions as well as axons ending in bulbs distant from a potential target muscle (Figure 2 d, e, h, i; Supplementary Fig. 3 b; Supplementary Table 1).

Prior studies showed a delay of axonal outgrowth in *nrg* mutant embryos [42-44]. Our axonal phenotypes would be consistent with such stalling of axons but, because we also observe synapse retractions in these animals, could equally be caused by a retraction of axons after initial innervation of a target muscle. Indeed, we were able to demonstrate that synaptic retractions resulted in axonal retractions. For example, Figure 2 e shows an elimination of an NMJ indicated by the complete loss of presynaptic vesicles, while fragments of the mCD8-GFP marked motoneuron membrane were still present opposite postsynaptic Dlg (Fig. 2 e$^1$). We were able to follow the tract of fragmented membrane remnants over a distance of more than 150 µm to the retraction bulb-like structure (Fig. 2 e, e$^2$). Additionally, we observed large axonal swellings in the same axon further proximal towards the cell body of the motoneuron (Figure 2 e, e$^3$). Other examples were identified as retraction bulbs because they were in close proximity to NMJs that lacked all presynaptic vesicles and the MARCM membrane marker and showed clearly reduced postsynaptic membranes when compared to a stable NMJ in close proximity (Supplemental Figure 3 b, asterisk). Rates of retraction bulbs and axonal swellings were identical in MARCM clones of *nrg*$^{14}$ and *nrg*$^{14}$; P[*nrg180*$^{\Delta Ig3\text{-}4}$] animals (Fig. 2 i). Finally, when we analyzed the innervation pattern of motoneuron axons

that still formed stable NMJs at this larval stage we could demonstrate that the lack of Nrg did not result in general axon guidance defects. We observed similar rates of innervations for all 4 major classes of motoneurons and detailed scoring revealed uniform innervation of all muscles with no obvious differences between wild type and mutant motoneurons (Fig. 2 j, Supplementary Fig. 2 c). In summary, while we cannot exclude a role for Nrg in axonal outgrowth for some cases, we provide clear evidence that Nrg is required for the maintenance of the NMJ and that this function requires both the extracellular domain and the intracellular Ankyrin-binding domain of Nrg.

**Mutations in the Nrg FIGQY motif differentially affect Ankyrin2-binding**

Based on these results we aimed to understand in detail how synaptic function of Nrg is controlled by its interaction with the Ankyrin associated cytoskeleton. Prior studies in vertebrates demonstrated that phosphorylation of the conserved tyrosine residue within the FIGQY motif has the potential to abolish the interaction of L1 type proteins with Ankyrins [24-27]. Similarly, Yeast-2-Hybrid assays showed that Nrg directly binds to *Drosophila* Ankyrin1 and Ankyrin2 and that replacing the tyrosine with a phenylalanine (Y-F) alters binding capacities [45]. We used protein immunoprecipitation (IP) assays to further characterize the interaction between Nrg and Ank2. We generated tagged Nrg180 and Ank2 UAS constructs (Ank2-S: short isoform of Ank2 containing all potential Nrg interacting domains) and co-expressed the constructs in *Drosophila* S2 cells. We were able to efficiently pull down Nrg using Ank2-S and vice versa demonstrating a biochemical interaction between the two proteins (Fig. 3 a; and data not shown). Next, we generated a series of mutations that are likely to differentially impair the binding capacities between Nrg and Ank2 by mutating the tyrosine to a phenylalanine (Y-F), aspartate (Y-D) or alanine (Y-A) or by deleting the entire FIGQY motif (ΔFIGQY). The IP assays demonstrated quantitative differences in Ank2 binding capacities for all Nrg mutations (Fig. 3 a). Compared to wild type the quantifications demonstrated a 30% decrease in binding capacities for Y-F, a 70% decrease for Y-D and a 90% reduction for the Y-A mutation. The deletion of the FIGQY motif essentially abolished the Nrg-Ank2 interaction completely (Fig. 3 b). Thus, we have identified a series of mutations that result in defined reduction of Nrg-Ank2 binding that can be used to assess the importance of the regulation of this interaction *in vivo*.

**Loss of Ankyrin2 binding results in increased lateral mobility of Nrg**

Studies of CAMs in vertebrates and *Drosophila* demonstrated that impairing the association with the cytoskeleton leads to an increase in lateral mobility and a simultaneous reduction of adhesive properties [24, 46, 47]. To analyze if Nrg is regulated in a similar manner we tested how the selective impairment of the Ank2 association changes the biophysical behavior of Nrg *in vivo*. We generated GFP-tagged UAS-transgenes of all described *nrg* FIGQY mutations using site-specific integration to ensure equal expression levels between constructs (Fig. 3 d, h). In order to test whether these mutations affect the mobility of Nrg180 within motoneurons, we used fluorescence recovery after photobleaching (FRAP) experiments *in vivo*. At the presynaptic nerve terminal only 10% of Nrg180 wild type protein was recovered indicating a very limited lateral mobility within the 200 sec time frame (Fig. 3 c, e, f). The complete deletion of the Ank2 binding site ($Nrg180^{\Delta FIGQY}$) led to a small but not significant increase in the mobile fraction of Nrg180 within this time frame (Fig. 3 e, f; P = 0.11). These results indicate that at the presynaptic nerve terminal interactions with postsynaptic CAMs may prevent significant mobility of Nrg. This is supported by our observation of a significantly larger recovery rate for wild type Nrg180 (mobile fraction of about 40%) when we tested the mobility within axonal compartments distally of muscle 4, where extracellular interactions are likely to be less significant (Fig. 3 d, g, i, j). Importantly, the deletion of the Ank2 binding domain further increased the mobile fraction by a factor of two to about 80% of total protein. When testing the different tyrosine specific point mutations, we observed a significant increase in the mobile fraction for all alterations compared to wild type, but to a lesser extent than $Nrg180^{\Delta FIGQY}$ (Fig. 3 j). Thus, impairing the interaction between Nrg and Ank2 significantly changes the mobility of Nrg in motoneuron axons *in vivo*.

**Association of Nrg180 with Ankyrin2 balances NMJ growth and stability**

To further address the function of the Nrg180-Ank2 interaction *in vivo* we introduced all FIGQY specific mutations into the wild type *nrg* Pacman construct using *galk*-mediated recombineering. In addition, we generated a deletion of the entire C-terminus of Nrg180, a complete deletion of the FIGQY motif of Nrg167 as well as a specific deletion of the last 3 amino acids of Nrg180 as this potential PDZ-protein interacting domain has been implicated in axon outgrowth of mushroom body neurons [48] (Fig. 2 a; Supplementary table 1). All constructs were inserted into the same genomic landing site and crossed into the background of the $nrg^{14}$ null mutation to create a series of “knock-in” like mutations that express mutant Neuroglian protein under endogenous control. Interestingly, all modifications of the

intracellular cytoplasmic domains of Nrg167 and Nrg180 rescued the embryonic lethality associated with *nrg* null mutations (*nrg*$^{14}$ and *nrg*$^{17}$). To confirm the specificity, expression levels and localization of our mutations we analyzed these larvae with specific antibodies recognizing either both isoforms (Nrg$^{3c1}$) or only Nrg180 (Nrg180$^{BP104}$). Because Nrg180$^{BP104}$ recognizes only wild type non-phosphorylated Nrg180 but none of our FIGQY mutations (Supplementary Fig. 4 a, b; Fig. 3 h and data not shown) we used two newly generated antibodies: Nrg180$^{cyto}$ recognizes the cytoplasmic tail of Nrg180 C-terminal of the FIGQY motif and Nrg$^{FIGQY}$ recognizes the FIGQY motif of both isoforms. With these antibodies we were able to unambiguously identify all mutated proteins and demonstrate that all constructs are expressed at equal levels within larval brains (Supplemental Fig. 4 b, d). In addition, wild type and all mutant *nrg* constructs restored Nrg180 expression within the presynaptic nerve terminal as well as Nrg167 expression within glial cells and muscles (Supplementary Fig. 4 a, c). This data demonstrates that the FIGQY domain is not essential for presynaptic localization of Nrg180.

The series of "knock-in"-like Pacman mutations allowed us to systematically determine the requirement of the different domains for normal synapse development in third instar larvae. Our analysis of synapse stability revealed a significant increase in synaptic retractions in mutants with severely disrupted Nrg180-Ank2 interactions (*nrg180*$^{Y\text{-}D}$, *nrg180*$^{Y\text{-}A}$, *nrg180*$^{\Delta FIGQY}$) but not in animals lacking the Nrg167 FIGQY motif, deletion of the PDZ binding motif nor in mutations only slightly impairing binding capacities (*nrg180*$^{Y\text{-}F}$) (Fig. 4 a-d; Supplementary Table 1). In addition, we observed a significant increase in the severity of retractions including complete eliminations (Fig. 4 c, e) consistent with our observations of the *nrg*$^{14}$; P[*nrg180*$^{\Delta FIGQY}$] MARCM clones (Fig. 2 i; Supplementary table 1). We next asked whether the Nrg FIGQY motif is directly required for the synaptic localization of Ank2 to mediate NMJ stability. Interestingly, we did not observe obvious alterations of presynaptic Ank2-L localization or protein levels in P[*nrg_wt*, *Y-F* or *ΔFIGQY*] at stable synapses when compared to *w*$^{1118}$ (Supplementary Fig. 5 a; $P > 0.05$ for comparison of protein levels, data not shown). Thus, this suggests that while Nrg and Ank2 do not depend on each other for initial synaptic localization they display a high sensitivity towards normal levels of their interaction partner because Nrg and Ank2 are among the first proteins to be lost at *nrg* and *ank2* mutant semi-stable NMJs respectively (Fig. 1 i, j; Supplementary Fig. 5 b-d).

In addition to the synapse stability defects we observed a second striking defect in our *nrg* mutations when we analyzed NMJ growth and organization. With an increasing loss of Ank2

binding capacities of Nrg180 we found an increase in both the span of the presynaptic nerve terminal and the number of synaptic boutons. At the same time we observed a corresponding decrease in synaptic bouton area (Fig. 5 a-f). Interestingly, only very subtle alterations were observed for the Y-F mutation that still binds Ank2 efficiently (Fig. 5 b, e, f) highlighting a role for Ank2 in determining NMJ size. The finding that the phenotypes for the deletion of the Nrg180 FIGQY motif and the larger C-terminal deletion were almost identical indicates that control of NMJ growth critically depends on this motif (Fig. 5 e, f). We did not observe any growth related phenotypes in $nrg^{14}$; P[$nrg167^{\Delta FIGQY}$] or $nrg^{14}$; P[$nrg180^{\Delta PDZ}$] mutant animals (Fig. 5 e, f). Together, these data demonstrate that the loss of Ank2 binding capacities of Nrg180 correlates with a loss of NMJ growth control and an impairment of synapse stability and suggest that these two parameters are tightly coupled.

**Nrg180 FIGQY motif is essential for giant fiber synapse development**

To address synaptic functions of the Nrg180-Ank2 interaction in the central nervous system (CNS), we extended our analysis to the adult Giant Fiber (GF) circuitry. We used the GF to TTMn (Tergo-trochanteral motoneuron) connection as a model neuro-neuronal synapse as it provides precise genetic control of pre- and postsynaptic neurons [49]. Previous analysis of *nrg* mutations affecting either homophilic cell adhesion properties ($nrg^{849}$) or protein levels ($nrg^{305}$) identified both axon guidance and synaptic defects at the GF terminal [50, 51]. Our "knock-in" like mutations enabled us to directly determine a requirement for the different intracellular Nrg domains with respect to GF circuit formation and function.

We analyzed the function of the GF to TTM (Tergo-Trochanteral Muscle) pathway in all viable $nrg^{14}$; P[*nrg*-mutant] animals by intracellular recordings from the TTM using either brain or thoracic stimulation to reveal potential GF-TTMn synapse or TTMn NMJ phenotypes (Fig. 8 a). Importantly, presence of the wild type *nrg* construct in *nrg* null mutants ($nrg^{14}$; P[*nrg*_wt]) established normal function in the GF-TTMn circuit. We observed no significant differences in average response latencies or following frequencies after a train of stimulations at 100 Hz when compared to wild type control animals (Fig. 6). In contrast, all mutations within the Nrg180 FIGQY motif caused a severe impairment of GF circuit function. The average response latency, a measure for synaptic strength, was significantly increased (Fig. 6) and mutant animals were not able to follow trains of high frequency stimulations when the GF was stimulated in the brain; in some animals we observed a complete absence of responses (Fig. 6 b, d). In contrast, when we bypassed the GF and stimulated the motoneurons directly with thoracic stimulation, both response latency and

ability to follow high frequency stimulation were normal for the TTMn in all tested animals (data not shown) indicating that the observed defects were specific to the GF-TTMn synaptic connection. Interestingly, we did not observe phenotypic differences between the complete deletion of the Nrg180 FIGQY motif and single point mutations that only mildly impaired Ank2 binding (e.g. *nrg180*$^{Y\text{-}F}$) indicating that a partial constitutive Nrg180-Ank2 interaction was not sufficient for GF synapse function (Fig. 6 c, d). However, all tyrosine mutations disrupt the ability to modulate the Nrg-Ank2 interaction via posttranslational phosphorylation suggesting that dynamic temporal and spatial regulation of the Nrg180-Ank2 interaction is essential to establish a functional GF synapse. In contrast, neither the Nrg167 FIGQY motif nor the C-terminal Nrg180 PDZ protein-binding motif are critical for GF circuit function (Fig. 6 c, d).

In order to determine the morphological phenotypes and to distinguish between potential axon guidance and synaptic defects we co-injected large (Rhodamin-dextran) and small (Biotin) fluorescent dyes into the GF. In wild type animals the large dye is confined to the GF and reveals the morphology of the synaptic terminal. In contrast, the small dye is able to pass through gap-junctions that provide parts of a functional connection to the postsynaptic TTM motoneuron and thus dye-couple pre- and postsynaptic neurons. In wild type animals the GF-TTMn synapse grows to a large presynaptic terminal with mixed electrical and chemical synapses [49]. While we observed no major morphological alterations of GF terminals in *nrg*$^{14}$; P[*nrg*_wt], *nrg*$^{14}$; P[*nrg167*$^{\Delta FIGQY}$] and *nrg*$^{14}$; P[*nrg180*$^{\Delta PDZ}$] mutant flies, while mutations within the Nrg180 FIGQY motif resulted in severely disrupted GF terminals in more than 80% of analyzed animals (Fig. 7 a, b). The GFs were present within the synaptic target area, however, the entire or large parts of the synaptic terminals were either thinner or swollen to abnormal sizes and often contained large vacuole-like structures (Fig. 7a insets). Similar to the electrophysiological phenotypes, we observed no obvious qualitative or quantitative differences between different Nrg180 FIGQY mutations. Next, we directly tested for the presence of a synaptic connection between GF and the postsynaptic TTMn using the dye-coupling assay. Consistent with the electrophysiological data, we found a residual synaptic connection in more than 90% of animals carrying mutations in the Nrg 180 FIGQY motif (Fig. 7a, c). However, total injection time varied between preparations and dye-coupling was often weaker or required longer injection times in mutant animals compared to animals rescued with the wild type construct. These results indicate that at least a small number of gap junctions are established at the GF terminals of Nrg180$^{\text{FIGQY}}$ mutants. When we correlated the ability to dye-couple to electrophysiological properties of these synapses, we

observed that approximately 40% of Nrg180$^{FIGQY}$ mutant animals that were positive in the dye-coupling assay did not show any functional response (Fig. 7 c). This suggests that the synaptic strength in these animals was below the threshold to trigger an action potential in the postsynaptic TTMn. In contrast, neither the deletion of the FIGQY motif of Nrg167 nor the PDZ protein-binding domain of Nrg180 affected GF morphology or function (Fig. 7). Thus, we conclude that the Ankyrin binding motif of Nrg180 but not of Nrg167 is essential for normal GF-TTMn synapse maturation and function but is not required for axon guidance or synapse targeting.

**Trans-synaptic coordination of pre- and postsynaptic development by Nrg180**

Importantly, the Pacman-based rescue approach allows us to determine both temporal and spatial requirements of the Nrg FIGQY motif when we complement it with selective expression of wild type Nrg using the Gal4/UAS system. At the GF-TTMn synapse we can use distinct Gal4-driver lines to either drive expression simultaneously in the pre- and postsynaptic neurons or selectively only in one of the two synaptic partners. In addition, we are able to express UAS-constructs at different time points during GF development (Fig. 8 a).

Simultaneous expression of wild type Nrg180 in pre- and postsynaptic neurons throughout GF circuit development was able to completely rescue all electrophysiological and morphological defects associated with point mutations (using Y-F and Y-A as representative examples) or the deletion of the Nrg180 FIGQY motif (Fig. 8 b-d and data not shown). Thus, this assay can be used to determine specific pre- and postsynaptic requirements. To our surprise, we were able to rescue the anatomical and physiological phenotypes to a similar extent by expressing wild type *nrg180* either in the pre- or the postsynaptic neuron (Fig. 8). We did not observe any non-responding animals, the average response latency was significantly restored and only subtle defects in the ability to follow multiple stimuli at 100 Hz were seen in few animals (Figure 8 b-d). In addition, the presynaptic morphological phenotypes of Nrg180$^{FIGQY}$ mutant animals were not only rescued by presynaptic expression in the GF but also by expression in the postsynaptic TTMn (Fig. 8 e). This suggests that Nrg has the ability to control GF synapse development in a trans-synaptic manner and that Nrg180 with a wild type FIGQY motif on either side of the synapse is sufficient to enable normal GF synapse development in Nrg180$^{FIGQY}$ mutant animals.

In order to unravel potential differences in temporal requirements of the Nrg180 FIGQY motif during synapse formation, we utilized a Gal4 line that starts expression in the GF only after the initial connection between the GF and the TTMn has been established (Fig. 8 a) [49,

[52]. Despite the phenotypic similarities of the Nrg180 Y-F, Y-A and ΔFIGQY mutants in the electrophysiological and morphological assays this "late presynaptic" rescue assay revealed unique differences between these mutations. While we were not able to significantly rescue the response latencies or the ability to follow high frequency stimulations in $nrg^{14}$; P[$nrg180^{\Delta FIGQY}$] or $nrg^{14}$; P[$nrg180^{Y\text{-}A}$] mutants (Fig. 8 c, d), we did observe a significant rescue of both parameters in $nrg^{14}$; P[$nrg^{Y\text{-}F}$] mutant animals. Almost 80% of the animals now displayed wild type electrophysiological properties (Fig. 8 b). Thus, a late presynaptic rescue was only possible in animals where Nrg180 retained significant Ank2 binding properties but not in animals with a severe impairment of the Nrg-Ankyrin interaction. This suggests that Nrg association to the Ankyrin based cytoskeleton is essential during early stages of GF synapse development while synapse maturation requires a dynamic regulation of this interaction.

**Discussion**

Precise control of synaptic connectivity is essential for the formation, function and maintenance of neuronal circuits. Here we identified the L1-type CAM Neuroglian as a key regulator of synapse stability *in vivo*. By combining biochemical, biophysical and genetic assays at two complementary model synapses, we demonstrate that regulation of the Nrg-Ankyrin interaction plays a critical role in controlling synapse growth, maturation and stability. Several important findings arise from our work: (1) Control of synapse stability requires Nrg mediated cell adhesion, which can be controlled by direct coupling to the presynaptic Ankyrin-associated cytoskeleton. (2) Synapse elimination and axonal retraction display striking phenotypic similarities to developmentally controlled synapse elimination at the vertebrate NMJ suggesting common cellular mechanisms between developmental and disease processes. (3) Local regulation of Nrg-Ankyrin binding provides a mechanism to gradually control the delicate balance between synapse growth and stability. (4) Trans-synaptic Nrg signaling contributes to the coordination of pre- and postsynaptic development in the CNS.

**The L1-type CAM Neuroglian controls synapse stability**

A large number of cell adhesion molecules have been implicated as important mediators of synapse development, but the regulatory mechanisms controlling structural synapse plasticity and maintenance remain largely unknown. In an unbiased RNAi screen, we identified the *Drosophila* L1-type CAM Neuroglian as essential for synapse stability at the neuromuscular

junction. We demonstrate that knock down of presynaptic Nrg induces synapse disassembly that share all cellular hallmarks of retractions observed in *ank2, spec* or *hts* mutant animals [11-14]. By analyzing individual motoneurons lacking any Nrg expression we verified this presynaptic requirement of Nrg for synapse maintenance. In addition, this allowed us for the first time to unravel the cellular events occurring in response to loss of cell adhesion at the presynaptic nerve terminal. In *nrg* mutant motoneurons, we observed both synaptic retractions and motoneuron axons ending in "retraction bulb" like structures. Excitingly, we directly observed mutant NMJs lacking any presynaptic cytoplasmic marker that are still connected via traces of clonally marked presynaptic membrane remnants to retraction bulb-like structures at large distances from the NMJ (> 150 µm). This demonstrates that loss of synapse stability can induce a cellular program resulting in the retraction of the motoneuron axon accompanied by shedding of presynaptic membrane. This phenotype shares striking similarities with developmental synapse elimination at the vertebrate NMJ [53] and points to potential similar cellular programs underlying synapse loss in development and disease. It will be of particular interest to analyze the contribution of glial cells in this process as they are part of a pro-degenerative signaling system at the NMJ and actively clear membrane remnants of degenerating or pruning axons in both *Drosophila* and vertebrates [53-56]. It is important to note that some of the axonal phenotypes would also be consistent with a stalling of the axonal growth cone before reaching the appropriate target. Indeed, prior studies in both *Drosophila* and vertebrates demonstrated a function of Nrg and L1CAM for normal rates of neurite outgrowth [21, 23, 42-44] indicating that both defects in axon growth and loss of synapse stability may have contributed to the observed phenotypes.

Although Nrg is certainly critical for NMJ maintenance our observation that 50% of larval NMJs were still stable in *nrg* null mutants clearly indicates that redundant mechanisms control synapse stability at the level of synaptic cell adhesion molecules. A candidate to provide such redundancy would be the *Drosophila* NCAM homolog FasII, which has been previously implicated in NMJ maintenance [57] and can substitute for Nrg during axonal outgrowth of ocellar neurons [43]. However, our results demonstrate that FasII cannot compensate for the loss of presynaptic Nrg at the larval NMJ (Fig. 1 g; Supplementary Fig. 1 d). The identification of the entire combinatorial code of CAMs contributing to synapse stability will be of high interest to understand the mechanisms underlying structural synapse plasticity.

**The Nrg-Ank2 interaction functions as a molecular switch to balance synapse growth and stability**

The dynamic nature of many neuronal circuits requires controlled changes in synapse assembly and disassembly without a disruption of neuronal circuit function. While extracellular interactions of synaptic cell adhesion molecules can clearly maintain synaptic connectivity, mechanistic insights regarding the regulation of these proteins to alter trans-synaptic adhesion are limited to date. The process is probably best understood for Cadherins where adhesive properties are modulated either via binding of extracellular Calcium or by altering their association with intracellular Catenins via posttranslational phosphorylation [7, 8]. These changes alter localization, clustering and trans-synaptic signaling of Cadherins leading to modulations of synaptic connectivity and function [9, 10]. Here we identify the interaction between the L1-type CAM Nrg and the adaptor protein Ank2 as a similar control module. First, we demonstrate that Nrg directly interacts with Ank2. Second, a series of specific mutations in the Ankyrin binding motif FIGQY allowed us to differentially affect the Ankyrin-binding capacity of Nrg. We demonstrated that decreasing Ank2-binding capacities correlates with an up to 2-fold increase in lateral mobility of Nrg in motoneurons. This is consistent with studies in vertebrates demonstrating that phosphorylation of the conserved tyrosine of the FIGQY motif reduces or abolishes binding to Ankyrins and increases mobility of L1-type CAMs [24-27, 47]. Finally, "knock-in" like Nrg mutants with altered Ankyrin binding capacity resulted in two striking phenotypes. There was a significant increase in synapse retractions in mutants with severely impaired Ank2 binding but not in mutants with partial binding ($Nrg180^{Y\text{-}F}$). In addition, we observed increased NMJ growth that correlated with the decrease in Ank2 binding capacities and the increase in mobility of different Nrg mutants. Thus, impairing Ank2 binding and thereby potentially decreasing the static population as well as the adhesive force of Nrg180 decreases synaptic stability but also allows increased synaptic growth. We previously identified similar switch-like alterations of synapse growth and stability in animals lacking the Spectrin-binding and actin-capping molecule *hts/adducin* [12]. Importantly, studies of *adducin2* mutant mice demonstrated that Adducin2 provides a similar function in vertebrates and is essential to mediate changes in synaptic connectivity relevant for learning and memory [16, 58]. Finally, it should be noted that we do not observe significant alterations in presynaptic Nrg or Ank2 levels in these animals similar to previous observations for the axonal localization of these proteins [45, 59]. However, we found a clear dependence on the respective partner protein at semi-stable *nrg* and *ank2* mutant synapses that displayed first signs of synapse disassembly. Thus, while Nrg and Ank2 seem not to

depend on each other for initial synapse localization, their interaction is required to maintain synaptic localization. A similar late loss of AnkyrinG has been observed in *neurofascin* mutant Purkinje cells, demonstrating a function of the L1CAM paralog for maintenance but not for initial localization of AnkG to the AIS [31, 33] and likewise AnkG is required for the maintenance of Neurofascin [34]. Together these data indicate that modulation of the Nrg-Ank2 interaction balances synapse growth and stability without disrupting synaptic localization of both proteins. Changing the interaction via posttranslational phosphorylation could thus locally decrease synapse stability thereby allowing the formation of new synapses without impairing general neuronal circuit architecture.

**Trans-synaptic Nrg function requires dynamic regulation of the Ankyrin binding motif**

Despite our detailed knowledge regarding expression of synaptogenic and potentially stabilizing cell adhesion molecules mechanistic insights into trans-synaptic control of synapse maturation or function are only recently emerging [1, 2, 9, 10]. Here we provide evidence that trans-synaptic coordination of synapse development by Nrg is controlled via dynamic regulation of the Ankyrin-binding motif.

In contrast to the larval NMJ, all mutations in the intracellular Ankyrin binding domain of Nrg180 severely disrupted GF synapse morphology and function. The lack of significant differences in phenotypic strength between mutations differentially affecting Ank2-binding indicates that normal GF synapse development requires a dynamic temporal-spatial regulation of the Nrg-Ank2 interaction via phosphorylation. To address the importance of this regulation for trans-synaptic development we selectively reintroduced wild type Nrg180 either in the pre- or postsynaptic neuron of the GF synapse. Surprisingly, expression of wild type Nrg on either side of the synapse was sufficient to restore synaptic function in all $Nrg180^{FIGQY}$ mutants. This highlights two important novel aspects of Nrg function at central synapses. First it indicates that the dynamic regulation of the Nrg-Ankyrin interaction on one side of the synapse provides molecular information that can be superimposed across the synapse and compensate for a mutant interaction on the other side. Interestingly, this trans-synaptic function of Nrg can be initiated equally well from either side of the synapse and restores both functional and morphological properties of the GF synapse. Second, because we can restore function and morphology at synapses that completely lack Nrg-Ankyrin binding on one side it indicates that Nrg can initiate the trans-synaptic signaling cascade necessary for synapse development independently of its interaction with Ankyrin. These signaling

processes could be mediated through other intracellular domains like the FERM-protein binding domain or through potential *cis*-interaction of the extracellular domain of the mutant Nrg. Candidates for such cis-signaling systems are FGF/EGF signaling or Semaphorins that have been shown to regulate synaptic connectivity and have been identified as Nrg interacting partners in *Drosophila* [23, 60-62]. Nevertheless, the general importance of the Nrg-Ankyrin interaction is highlighted by our observation that at late stages of GF development wild type Nrg in the presynaptic GF neuron rescued Nrg mutants that retained Ank2 binding capacities, but not those with severely impaired binding. Together, this indicates that Ank2 binding is essential during early phases of synapse development but modulation of this interaction is required to allow normal synapse growth and maturation. Phosphorylation of Nrg prevents either association with Ankyrins to increase mobility of Nrg or enables binding to proteins that can only bind phosphorylated Nrg. One candidate would be the microtubule binding protein Doublecortin that can specifically bind phosphorylated Neurofascin [63] but physiological relevance for this interaction in nervous system development is lacking to date.

Our complementary analysis at a peripheral and a central synapse enabled us to identify common and divergent mechanisms of Nrg function and regulation during synapse development. Both in larval motoneurons and in the Giant Fiber circuit the Ankyrin binding motif of Nrg180 does not significantly contribute to axon outgrowth or guidance. In addition, at both synapses we did not observe any requirements for the Ankyrin binding motif of Nrg167 or of the PDZ-binding motif of Nrg180, which has recently been implicated in controlling axonal outgrowth in the mushroom bodies [48]. In contrast, while constitutive Nrg-Ank2 binding ($Nrg180^{Y\text{-}F}$) is sufficient to allow development of presynaptic nerve terminals at the NMJ, it is not sufficient at the central Giant Fiber synapse suggesting that regulatory mechanisms at these synapses control the phosphorylation status of Nrg180 differently.

Our data provides new insights into how L1-family proteins contribute to nervous system development. A surprising observation from studies of vertebrate L1 family proteins was that mutations within the intracellular domain that are linked to human L1/CRASH syndrome and neuropathological diseases [30] resulted in significantly weaker phenotypes in mice compared to the complete L1 knockout [21, 35, 64, 65]. While extracellular interactions are essential for early nervous system development including neurite outgrowth and axon targeting [23], here we provide evidence that phosphorylation of the intracellular Ankyrin binding motif provides a module to fine tune synaptic connectivity without overall disruption of neuronal circuitry. Our finding that the regulation of this interaction functions equally well on either side of the synapse indicates that any activity-dependent or developmental pathway

could impinge on this system to fine tune connectivity. The expansion of the L1-type CAM family to four independent proteins in vertebrates may provide the means to cope with the diversity and complexity of synaptic connectivity in the vertebrate CNS. Indeed, while the L1CAM Ankyrin motif mutations did not affect overall organization of the nervous system, detailed analyses revealed specific impairments within particular circuits and at subsets of synapses [35, 64, 65]. The functions of the different L1-type proteins may be distinct, partly opposing or redundant as evident by an analysis of cerebellar granule cell development in L1CAM and NrCAM double mutants [36]. The coordinated phosphorylation of a subpopulation of synaptic L1 family proteins within the pre- or postsynaptic compartment may thus allow differential modulation of biophysical properties of L1 complexes to precisely control distinct aspects of synapse development. Elucidating the synaptic L1-family protein code at specific synapses and identifying their phosphorylation status during synapse development or in response to activity might uncover new mechanisms controlling synaptic plasticity in development and during learning and memory.

**Acknowledgments**

We would like to thank M. Hortsch for generous gifts of antibodies as well as the Bloomington stock center (Indiana, USA), the *Drosophila* Genomics Research center (Indiana, USA) and the Developmental Studies Hybridoma Bank (Iowa, USA) for fly stocks, Pacman constructs and antibodies. The authors would also like to thank all members of the Pielage and Godenschwege lab for helpful discussions as well as Julie Freund for excellent technical support with the GF experiments. This work was supported by a Marie Curie International Reintegration Grant and the Novartis Research foundation to J.P. and by Grant Number R01HD050725 from the National Institute of Child Health And Human Development to T.A.G. The content is solely the responsibility of the authors and does not necessarily represent the official views of the NICHD or the NIH.

**Author contributions**

E.-M. E. with the help of J.P. performed all experiments at the larval NMJ, S.R.K. with the help of J.B. and T.A.G. performed all experiments at the giant fiber synapse, E.-M. E. and E.M. with the help of R.S. generated all constructs and transgenic flies. J.P. and T.A.G designed and supervised the experiments and wrote the paper with the help of all authors.

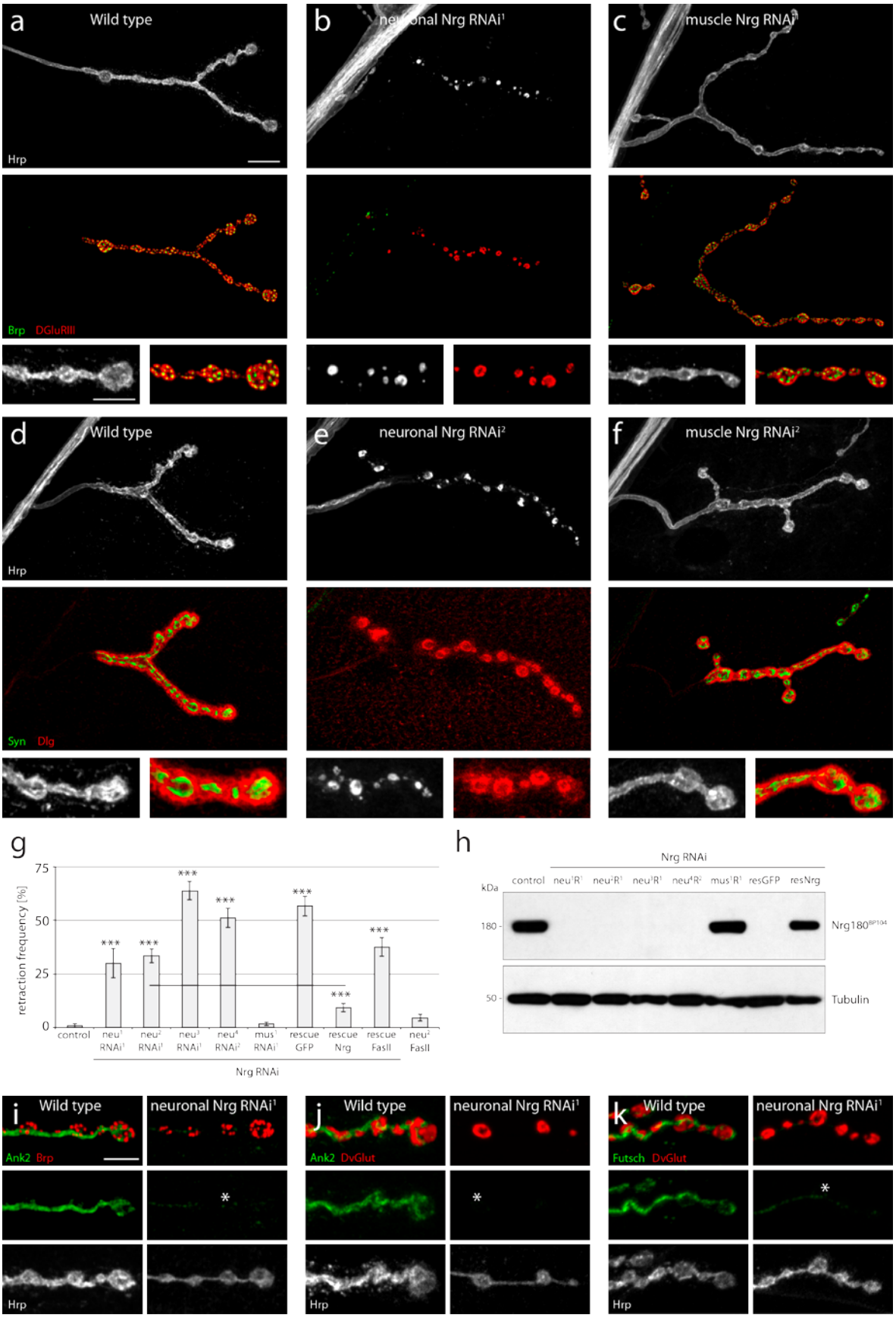


**Figure 1 - Presynaptic Nrg is essential for synapse stability.**

**(a-c)** NMJs on muscle 4 stained for the presynaptic motoneuron membrane (Hrp, white), the presynaptic active zone marker Brp (green) and postsynaptic glutamate receptors (DGluRIII, red). **(a)** A stable wild type NMJ indicated by perfect apposition of pre- and postsynaptic markers. **(b)** Knock down of presynaptic Nrg resulted in severe synaptic retraction indicated by the loss of presynaptic Brp despite the presence of postsynaptic glutamate receptors and fragments of the presynaptic membrane. Synaptic retractions caused a characteristic fusion of postsynaptic glutamate receptor clusters. (**c)** Loss of muscle Nrg did not impair synapse stability. **(d-f)** NMJs on muscle 4 stained for the presynaptic motoneuron membrane (Hrp, white), presynaptic vesicles (Syn, green) and postsynaptic Dlg (red). Identical phenotypes were observed when using an independent Nrg RNAi line and independent pre- and postsynaptic markers. Only presynaptic loss of Nrg resulted in a selective loss of synaptic vesicles, a fragmentation of the presynaptic membrane and unopposed postsynaptic bouton profiles. **(g)** Quantification of synaptic retractions in different Nrg RNAi conditions. Neuronal but not muscle specific knock down of Nrg using different Gal4 driver combinations or independent RNAi constructs resulted in a significant increase in synaptic retractions on muscle 4. The retraction frequency was significantly rescued ($P<0.001$) by co-expression of *UAS-nrg180* but not when we co-expressed either UAS-*mCD8-GFP* or UAS-*fasII*. Expression of UAS-*fasII* alone did not result in a significant increase in retractions (genotypes: neu$^{1}$ = *elav*$^{C155}$-Gal4; neu$^{2}$ = *elav*$^{C155}$-Gal4; *ok371*-Gal4; neu$^{3}$ = *elav*$^{C155}$-Gal4; UAS-*dcr2*; neu$^{4}$ = *elav*$^{C155}$-Gal4; *sca*-Gal4 UAS-*dcr2*; mus$^{1}$ = UAS-*dcr2*; *mef2*-Gal4; RNAi$^{1}$ = VDRC6688; RNAi$^{2}$ = VDRC107991; rescue indicates co-expression of UAS construct; n = 6-24 animals). **(h)** Western blot analysis of the same genotypes as in **g** probed with an antibody against Nrg180 (Nrg180$^{BP104}$). Neuronal but not muscle specific Nrg RNAi resulted in efficient knock down of Nrg180 in larval brains. Nrg180 levels could be rescued by co-expression of Nrg180 but not by co-expression of mCD8-GFP. **(i-k)** Characterization of multiple presynaptic markers in animals lacking presynaptic Nrg. **(i)** In wild type animals presynaptic Ank2 (green) and Brp (red) were present in all synaptic boutons. In the absence of Nrg Ank2 was lost prior to Brp at distal parts of an NMJ that was still stable as judged by the continuous membrane staining. **(j)** Similarly, Ank2 was lost prior to the presynaptic vesicle marker DvGlut (red) at a semi-stable NMJ. **(k)** In wild type animals the microtubule associated protein Futsch (green) and DvGlut (red) were present in all boutons. Knock down of Nrg resulted in a loss of Futsch prior to the disassembly of DvGlut at early stages of retraction. Scale bar in **a** corresponds to **a-f**, 10 µm, inset 5 µm. Scale bar in **i** corresponds to **i-k**, 5 µm. Error bars represent s.e.m.

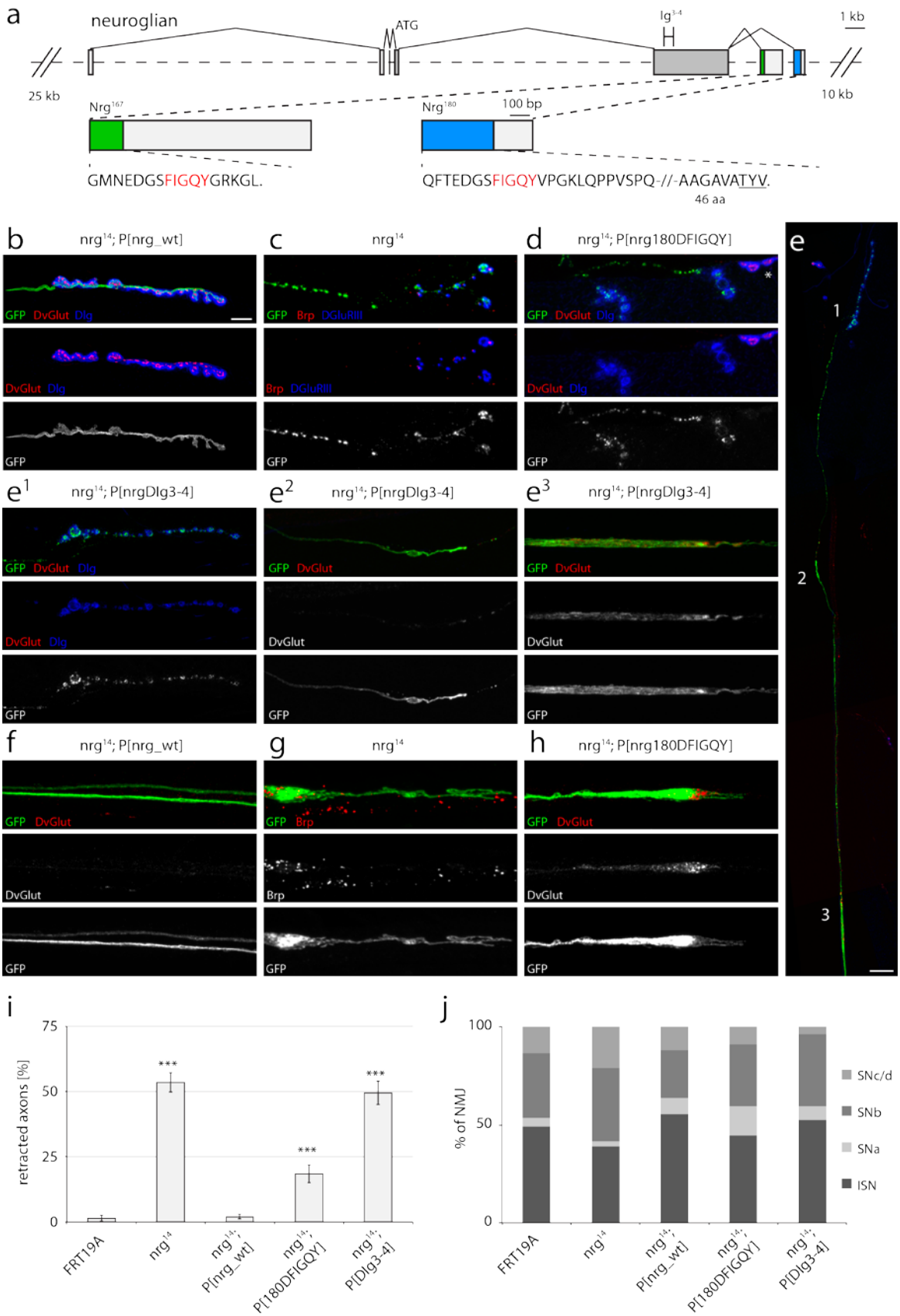
a
neuroglian
ATG
Ig3-4
1 kb
25 kb
10 kb
Nrg167
Nrg180
100 bp
GMNEDGSFIGQYGRKGL.
QFTEDGSFIGQYVPGKLQPPVSPQ-//-AAGAVATYV.
46 aa
b nrg14; P[nrg_wt]
c nrg14
d nrg14; P[nrg180DFIGQY]
e
e1 nrg14; P[nrgDlg3-4]
e2 nrg14; P[nrgDlg3-4]
e3 nrg14; P[nrgDlg3-4]
f nrg14; P[nrg_wt]
g nrg14
h nrg14; P[nrg180DFIGQY]
GFP DvGlut Dlg
GFP Brp DGluRIII
DvGlut Dlg
Brp DGluRIII
GFP
GFP DvGlut
DvGlut
Brp
1
2
3
i
retracted axons [%]
75
50
25
0
***
FRT19A
nrg14
nrg14; P[nrg_wt]
nrg14; P[180DFIGQY]
nrg14; P[Dlg3-4]
j
% of NMJ
100
50
0
SNc/d
SNb
SNa
ISN

## Figure 2 - MARCM analysis reveals unique requirements of extra- and intracellular domains of Nrg180 for synapse stability.

**(a)** Overview of the genomic locus of *nrg*. The Pacman construct spans 92 kb including the endogenous enhancer elements up- and downstream of *nrg*. The Nrg167 and Nrg180 specific exons and the relevant amino acid sequences are depicted. The position of the common Ig-domains 3 and 4 is indicated. The isoform-specific FIGQY sequences are highlighted in red and the PDZ protein-binding motif of Nrg180 isoform is underlined. **(b)** A $nrg^{14}$ MARCM clone rescued by a wild type *nrg* Pacman construct. The motoneuron clone was marked by the expression of mCD8-GFP (green). Synaptic vesicles (DvGlut, red) were found opposite postsynaptic Dlg (blue) indicating a stable NMJ. **(c)** A $nrg^{14}$ MARCM clone showing a severe retraction event. Only fragmented remnants of the membrane GFP marker were still present at a nerve terminal that almost completely lacked the presynaptic active zone marker Brp (red). Postsynaptic glutamate receptor clusters were still present and showed the characteristic fusion of neighboring clusters observed in all synaptic retractions. In addition, the axonal membrane prior to the NMJ was also fragmented. **(d)** A $nrg^{14}$ MARCM clone expressing a mutated form of Nrg180 lacking the FIGQY motif. The GFP-positive NMJ was retracted while a directly neighboring, non-marked (asterisk), NMJ remained stable. Presynaptic vesicles marked by DvGlut were absent from postsynaptic profiles marked by Dlg. The membrane marker was fragmented both at the nerve terminal and prior to the innervations. **(e)** Composite image overview of a $nrg^{14}$ MARCM clone expressing a mutated form of Nrg180 lacking the extracellular Ig3-4 domains. Three areas are shown at larger magnification in $\mathbf{e^{1\text{-}3}}$. **($\mathbf{e^1}$)** At the NMJ no presynaptic vesicles were present opposite postsynaptic Dlg. The Dlg staining was no longer interconnected and only remnants of the presynaptic membrane marker mCD8-GFP were visible indicating a complete elimination. **($\mathbf{e^2}$)** Approximately 150 µm proximal from the NMJ the axon remained intact ending in a "bulb-like" structure. Between the "bulb-like" axon ending and the NMJ only punctate staining of the membrane marker was visible. **($\mathbf{e^3}$)** At a significant distance from the "bulb" a large axonal swelling was visible that contained aggregates of the synaptic vesicle marker DvGlut. **(f)** Axonal area of a $nrg^{14}$ MARCM clone rescued by a wild type *nrg* Pacman construct. Within the axon only very low levels of the synaptic vesicle marker DvGlut are evident. **(g)** A "bulb-like" structure in a $nrg^{14}$ MARCM clone. The axon ended in a large swelling that contained increased levels of the active zone marker Brp. **(h)** A "bulb-like" structure in a $nrg^{14}$ MARCM clone expressing P[$nrg180^{\Delta FIGQY}$]. The axon ended in a large swelling that showed an aberrant accumulation of the synaptic vesicle marker DvGlut. Only remnants of the axonal marker were evident distal to this "bulb-like" structure. **(i)** Quantification of mCD8-marked axons that were not connected to target muscles ("retracted axons") in the indicated genetic background. The $nrg^{14}$ mutant phenotype was significantly rescued by the presence of a wild type *nrg* Pacman construct and partially rescued by P[$nrg180^{\Delta FIGQY}$] but not by P[$nrg180^{\Delta Ig3\text{-}4}$]. **(j)** Analysis of muscle innervation pattern of motoneuron MARCM clones that were connected to postsynaptic muscles. In all genotypes we observed normal innervation for all four major classes of motoneurons.

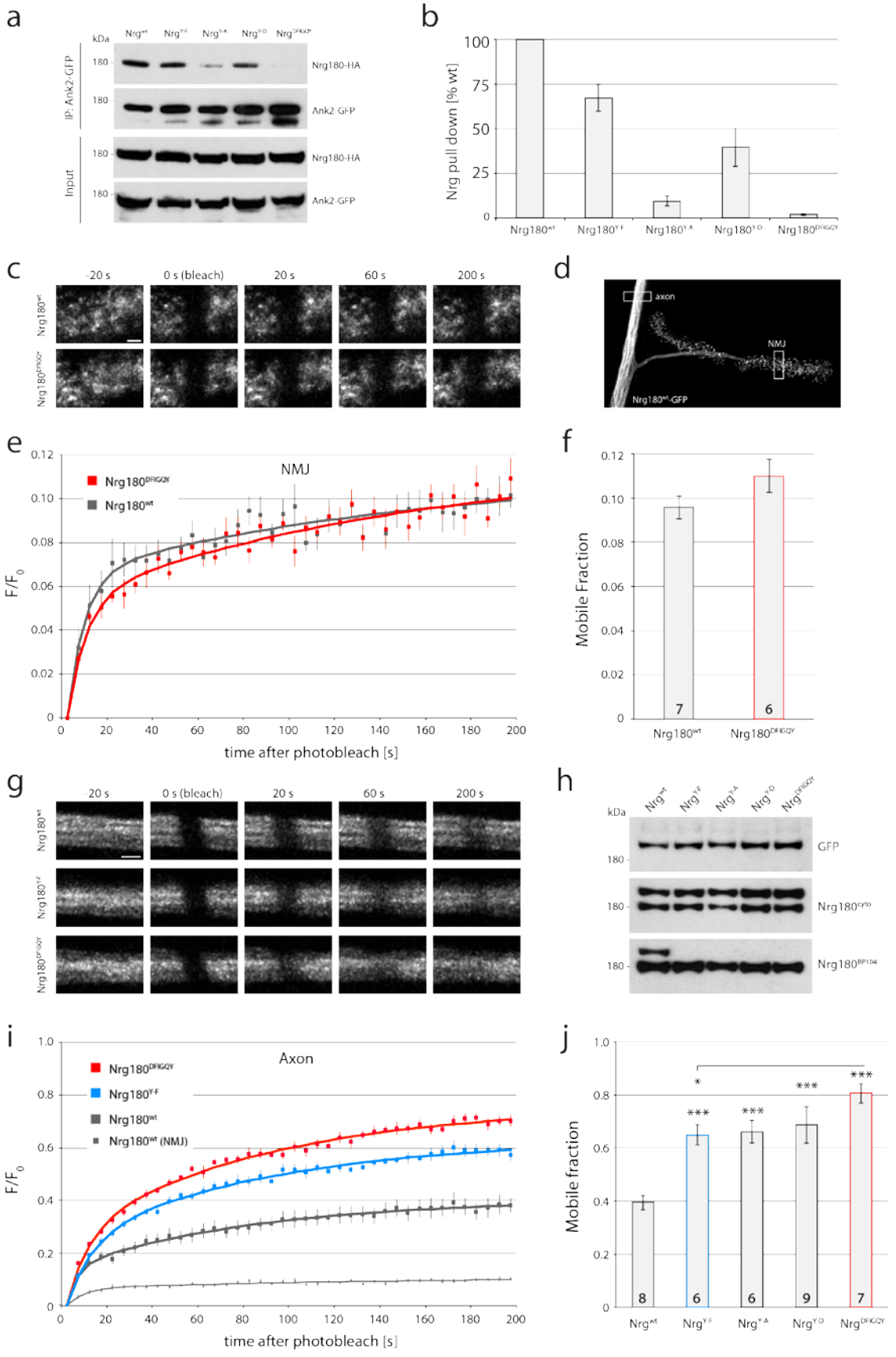
a
kDa
IP: Ank2-GFP
Input
180
Nrg180-HA
Ank2-GFP
b
Nrg pull down [% wt]
100
75
50
25
0
c
-20 s
0 s (bleach)
20 s
60 s
200 s
d
axon
NMJ
Nrg180wt-GFP
e
NMJ
F/F0
time after photobleach [s]
f
Mobile Fraction
7
6
g
h
GFP
i
Axon
F/F0
time after photobleach [s]
j
Mobile fraction
8
6
6
9
7

## Figure 3 - Mutations in the FIGQY-Ankyrin binding motif alter the Nrg-Ank2 interaction and increase Nrg mobility *in vivo*.

**(a)** Immunoprecipitation (IP) of Nrg180-HA proteins using Ank2-S-GFP. Ank2-S pulled down wild type Nrg180-HA efficiently. Mutations in the FIGQY domain differentially affected binding efficiency. Western blots show IPs and input controls. **(b)** Quantification of four independent IP experiments demonstrated reduced Ank2 binding due to the specific mutations within the FIGQY motif. **(c-j)** Fluorescence recovery after photobleaching experiments (FRAP) using GFP-tagged versions of wild type and mutant forms of Nrg180 at the NMJ. Equal levels of all GFP-tagged constructs were expressed in motoneurons (*ok371*-Gal4) as demonstrated by Western blot analysis of larval brain extracts in **h** using different Nrg180 and GFP specific antibodies. **(c)** Representative images of FRAP experiments performed at the NMJ as indicated in **d** for Nrg180 wild type and $Nrg180^{\Delta FIGQY}$. **(e, f)** Recovery curves of multiple independent FRAP experiments were fitted to a double exponential curve and used to calculate the mobile fraction of Nrg180. Nrg180 was highly immobile at the NMJ as less than 10% recover within the 200 s time frame of our experiments. We observed a slight but not significant increase in the mobile fraction when the FIGQY motif was deleted (P = 0.11). **(g)** Representative recoveries of FRAP in motoneuron axons for $Nrg180^{wt}$, $Nrg180^{Y-F}$ and $Nrg180^{\Delta FIGQY}$. **(i-j)** The recovery curves and the quantification of the mobile fraction demonstrate higher mobility of Nrg180 within axonal compartments. The mobility of Nrg180 was significantly increased when the FIGQY motif was mutated ($Nrg180^{Y-F}$). An almost 2-fold increase in mobility was observed after deletion of the Ankyrin-binding motif ($Nrg180^{\Delta FIGQY}$). The numbers in **f** and **j** represent number of independent experiments analyzed. Scale bar in **c** and **g** represents 5 µm. Error bars represent s.e.m.

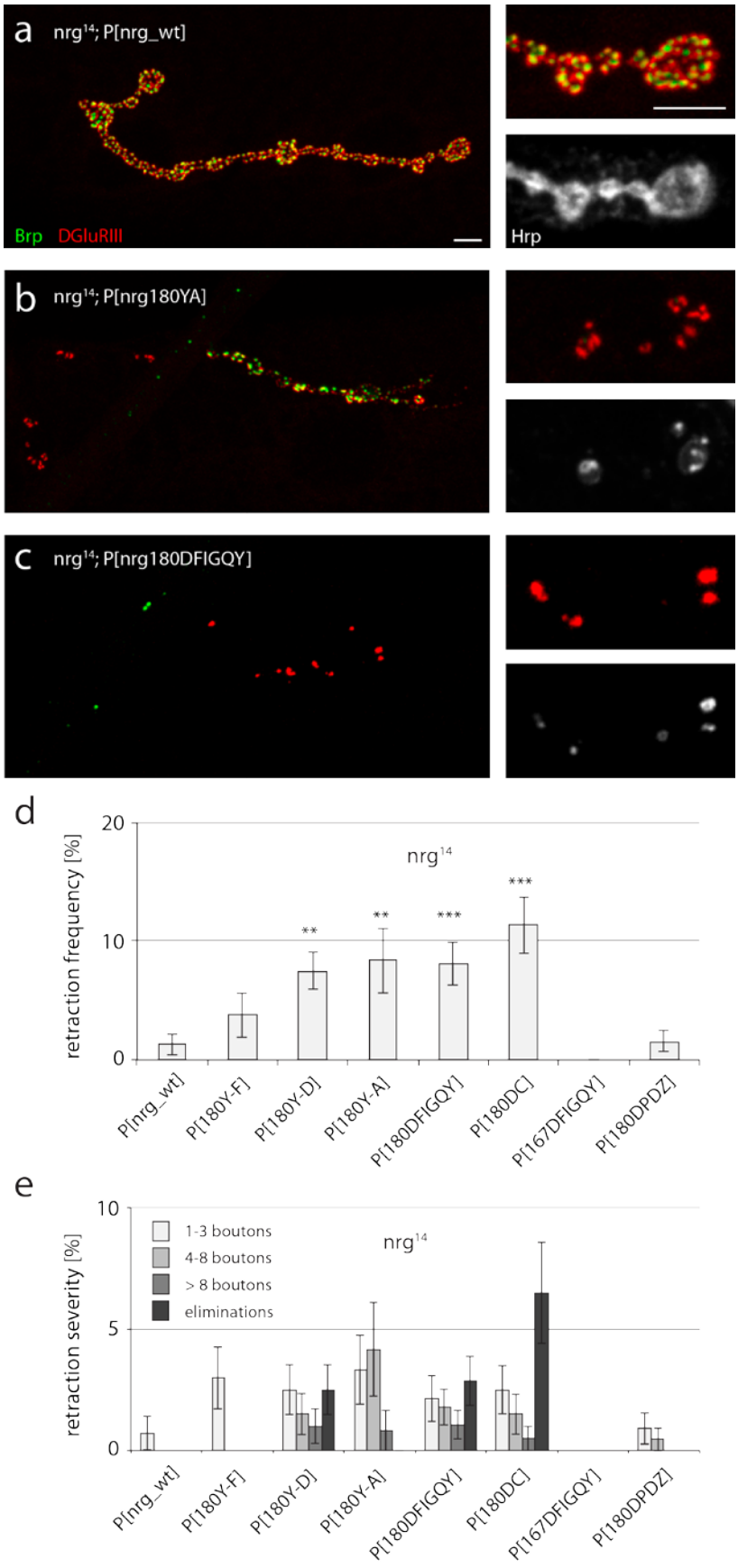


**Figure 4 - Impairment of Ank2 binding results in synaptic retractions**

**(a-c)** Analysis of synapse stability in *nrg* null mutant animals expressing different *nrg* Pacman constructs using the presynaptic marker Brp (green), postsynaptic DGluRII (red) and a marker for the presynaptic membrane (Hrp, white). **(a)** Presence of the Nrg wild type Pacman construct in $nrg^{14}$ animals resulted in wild type levels of synapse retractions. **(b)** The Y-A mutation leads to synaptic retractions **(c)** Animals lacking the Ank2 binding motif FIGQY showed significant levels of synaptic retractions including complete eliminations. **(d, e)** Quantification of retraction frequency and severity demonstrated increasing levels of synaptic retractions correlating with the gradual loss of Ank2 binding capacities. The Nrg167-FIGQY motif or the PDZ protein binding domain deletions did not show a significant increase in retraction frequency or severity (n = 12-22 animals). Asterisks indicate $P \leq 0.01$ for ** and $P \leq 0.001$ for ***. Scale bar in **a** corresponds to **a-c**, 10 µm, inset 5 µm. Error bars represent s.e.m.

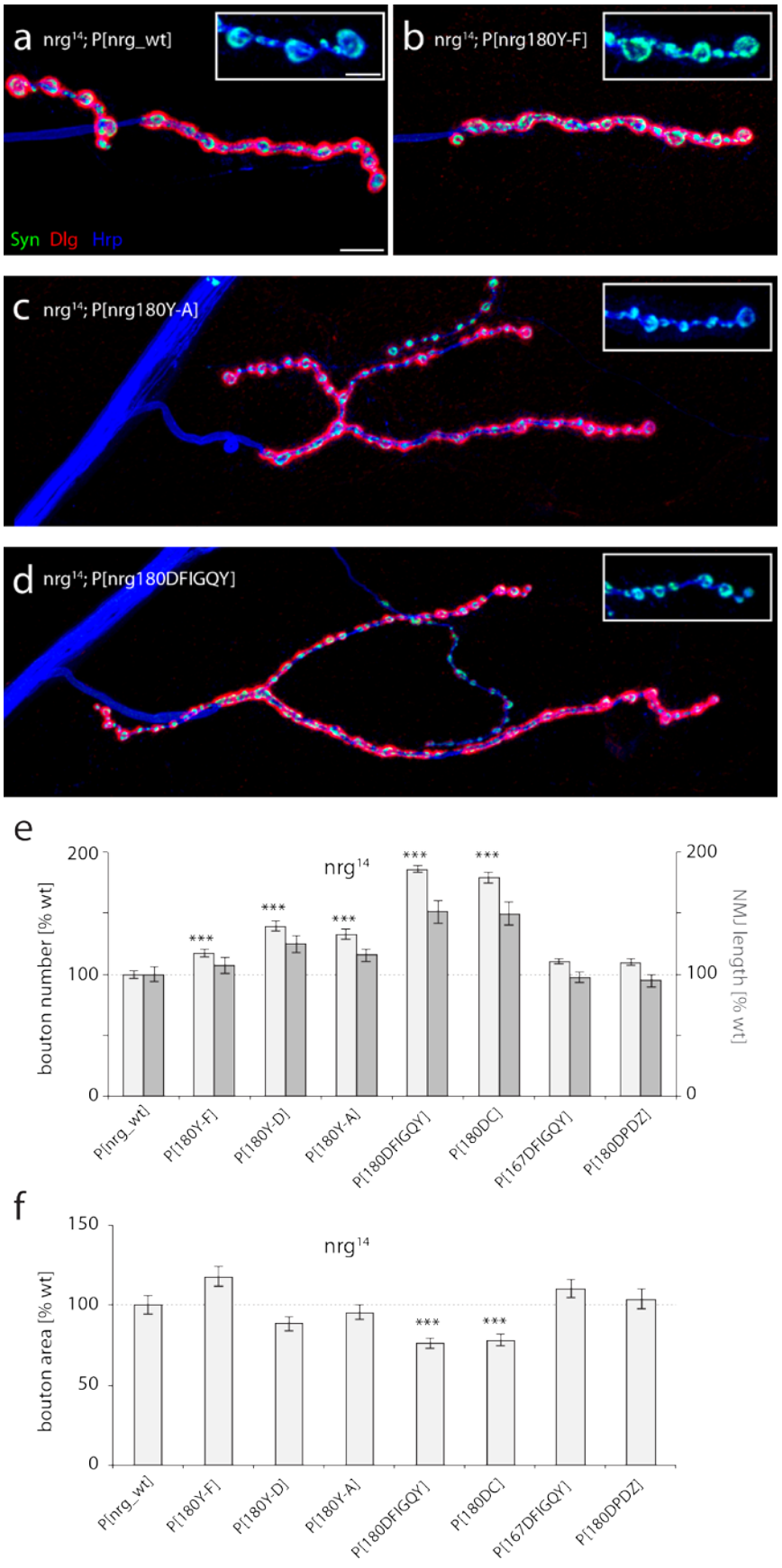


**Figure 5 - Impairment of Ank2 binding increases NMJ growth.**

Analysis of NMJ growth in *nrg*$^{14}$ mutant animals expressing different mutated *nrg* Pacman constructs using the presynaptic vesicle marker Synapsin (Syn, green), the postsynaptic marker Dlg (red) and a marker for the presynaptic membrane (Hrp, blue). **(a)** Presence of the *nrg* Pacman wild type construct resulted in wild type muscle 4 NMJs. The inset shows individual presynaptic boutons at higher magnification. **(b)** The Nrg180$^{Y\text{-}F}$ mutation resulted only in small alterations of NMJ growth. **(c)** The Nrg180$^{Y\text{-}A}$ mutation led to a significant increase in NMJ length. **(d)** Deletion of the Nrg180-FIGQY motif resulted in a significant, almost 2-fold overgrowth and a corresponding reduction in the area of individual boutons. **(e, f)** Quantification of bouton number, NMJ length and bouton area. NMJ growth defects correlated with an increasing loss of Ank2 binding capacities. No alterations were observed for mutations affecting the PDZ protein binding site or the Nrg167-FIGQY motif. Values were normalized to wild type rescue. Asterisks indicate highly significant changes ($P \leq 0.001$) for bouton number in **e** and for bouton area in **f** (n = 69-176 NMJs for bouton number, n = 20 NMJs for NMJ length and n = 10 NMJs for bouton area quantifications). Scale bar in **a** corresponds to **a-d**, 10 µm, inset 5 µm. Error bars represent s.e.m.

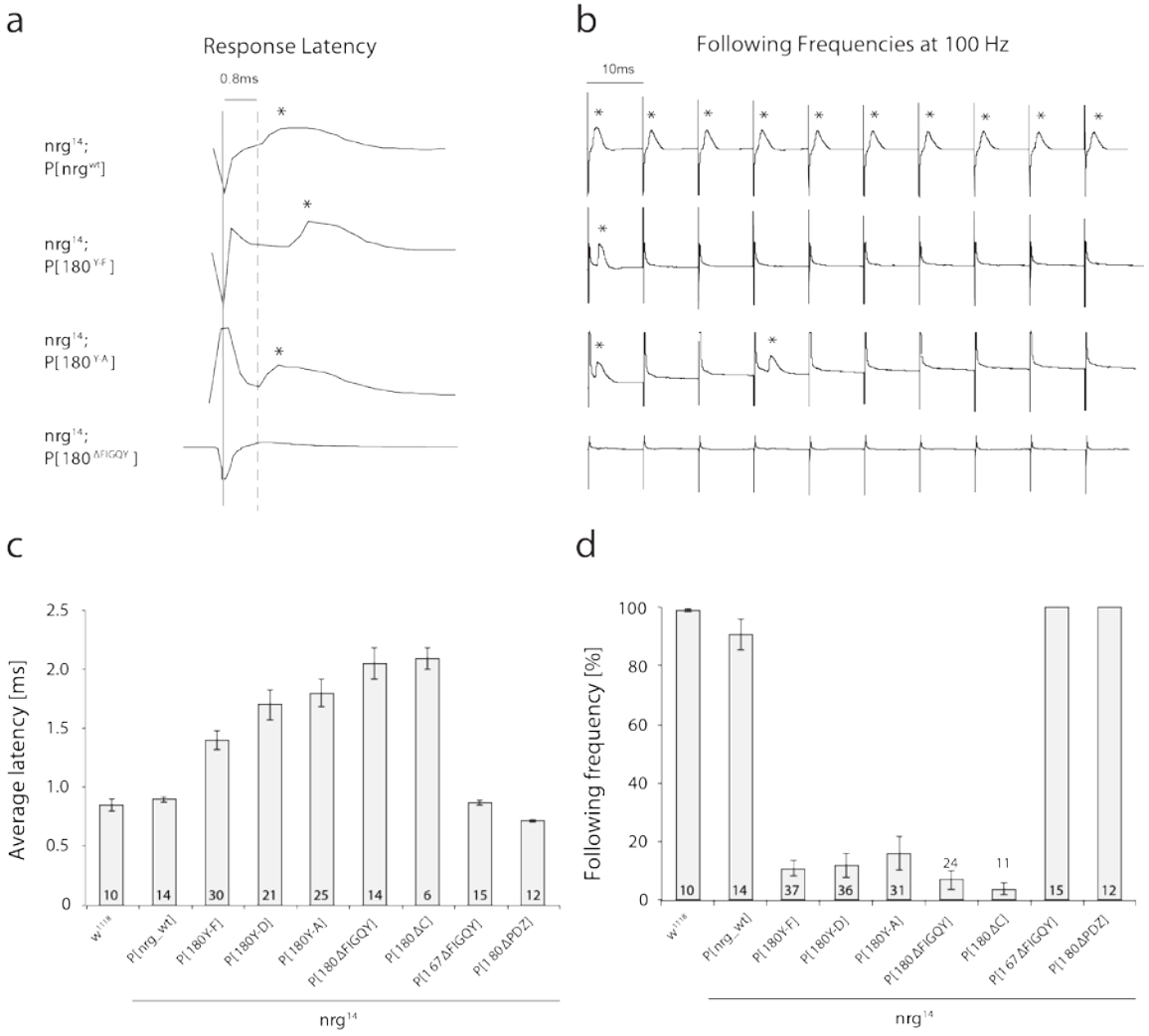


**Figure 6 - Electrophysiological phenotypes of *nrg* mutants in the giant fiber circuit. (a, b)** Sample traces of different *nrg* mutants. **(a)** TTM responses in *nrg* mutants (asterisks) upon GF stimulation in the brain (solid white line). The average response latency in wild type flies is 0.8 ms (dashed white line). Sample traces of $nrg^{14}$; P[$nrg^{wt}$], $nrg^{14}$; P[$nrg180^{Y\text{-}F}$], $nrg^{14}$; P[$nrg180^{Y\text{-}A}$] and $nrg^{14}$; P[$nrg180^{\Delta FIGQY}$] are shown. Mutations in the Nrg180-FIGQY motif led to a delay or absence of responses at the TTM. **(b)** As a measure for synaptic reliability the ability to follow stimuli at 100 Hz was determined. In contrast to $nrg^{14}$; P[$nrg^{wt}$], the GF-TTM pathway in $nrg^{14}$; P[$nrg180^{Y\text{-}F}$], $nrg^{14}$; P[$nrg180^{Y\text{-}A}$] and $nrg^{14}$; P[$nrg180^{\Delta FIGQY}$] mutants was not able to follow stimuli at 100 Hz upon GF stimulation in the brain; only rare responses were observed (asterisks). **(c, d)** Quantifications of electrophysiological phenotypes of *nrg* mutants. **(c)** Average latency of wild type and *nrg* mutants. There was no significant difference (P = 0.681, Mann-Whitney Rank Sum Test) in the average response latency between control ($w^{1118}$) and $nrg^{14}$; P[$nrg^{wt}$], $nrg^{14}$; P[$nrg167^{\Delta FIGQY}$] or $nrg^{14}$; P[$nrg180^{\Delta PDZ}$] flies. In contrast, the response latency was significantly increased in all *nrg180* mutants with a mutated FIGQY motif (Mann-Whitney Rank sum test, $P \leq 0.001$). **(d)** Average following frequencies at 100 Hz in wild type and *nrg* mutants. There was no significant difference (P = 0.841, Mann-Whitney Rank Sum Test) in the average of following frequencies at 100 Hz between control flies ($w^{1118}$) and $nrg^{14}$; P[$nrg^{wt}$], $nrg^{14}$; P[$nrg167^{\Delta FIGQY}$] and $nrg^{14}$; P[$nrg180^{\Delta FIGQY}$]. In contrast, following frequencies were significantly reduced in all *nrg180* mutants with

a missense mutation in or deletion of the FIGQY motif (Mann-Whitney Rank sum test, $P \leq 0.001$). Error bars represent s.e.m.

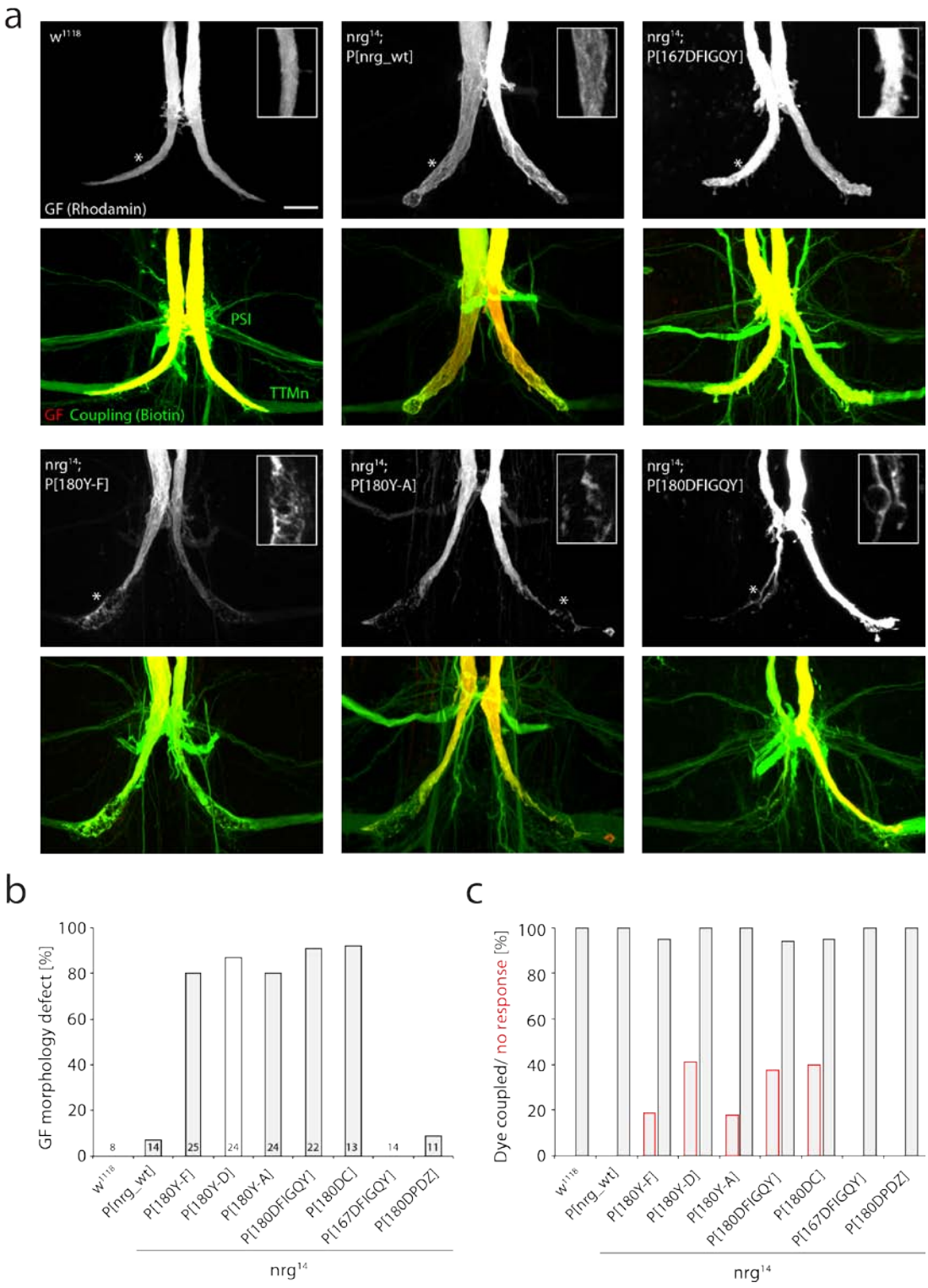


**Figure 7 - Anatomical phenotypes of the giant fiber synaptic terminals in *nrg* mutants.**

**(a)** GF synaptic terminals were visualized by injection of Rhodamine-dextran (red) into the GF. Dye-coupling of the GF to its target neurons, the Tergo Trochanteral motoneuron (TTMn) and the peripheral synapsing interneuron (PSI) via co-injection of Biotin (green) allows the detection of gap junctions between these neurons. In $w^{1118}$, $nrg^{14}$; P[$nrg^{wt}$] and $nrg^{14}$; P[$nrg167^{\Delta FIGQY}$] a normal, large GF terminal was present and we observed dye-coupling with the TTMn and the PSI. In $nrg^{14}$; P[$nrg180^{Y\text{-}F}$], $nrg^{14}$; P[$nrg180^{Y\text{-}A}$] and $nrg^{14}$; P[$nrg180^{\Delta FIGQY}$]

mutants the presynaptic terminal of the GF exhibited variable abnormal morphologies. They were thinner or swollen and contained large vacuole-like structures. However, in most cases the GF still dye-coupled with the postsynaptic target, the TTMn and the PSI. Scale bar 15 μm. **(b)** Quantification of morphological defects in $w^{1118}$ flies and *nrg* mutants. Only mutations affecting the Nrg180-FIGQY motif resulted in severe GF terminal aberrations. **(c)** Quantification of GF-to-TTMn dye-coupling (black bars) and comparison to animals with no electrophysiological responses (red bars) of the TTM with GF stimulation in the brain. A large percentage of animals expressing mutant versions of Nrg180-FIGQY proteins completely lacked electrophysiological responses despite the presence of dye-coupling in almost all animals demonstrating a severe functional defect in these animals.

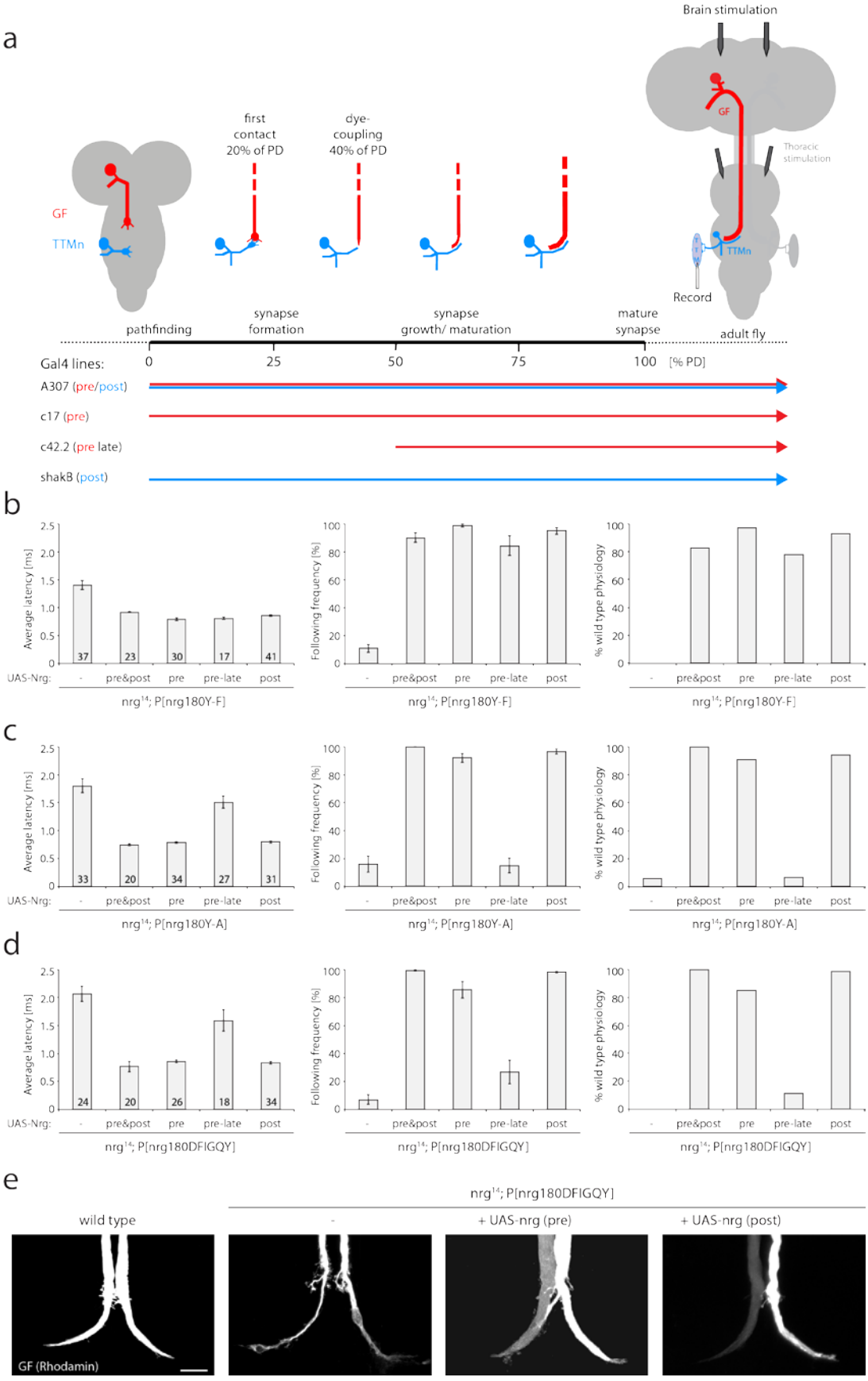


**Figure 8 - Temporal and spatial requirements of trans-synaptic Nrg signaling.**

**(a)** Schematic of GF to TTMn synapse development. First dye-coupling between the GF (red) and the TTMn (blue) can be demonstrated at 40% of pupal development [49]. Positions of stimulating and recording electrodes are indicated. Brain stimulation was used to test the GF-TTMn synapse, while thoracic stimulation bypasses the GF and allowed testing of the TTMn NMJ directly. Expression profiles of the different Gal4 lines are indicated. **(b)** Rescue of *nrg*$^{14}$; P[*nrg180*$^{Y\text{-}F}$] phenotypes using Gal4/UAS mediated expression of wild type Nrg180. Both average response latency and the ability to follow high frequency stimulation could be rescued significantly by simultaneous expression of Nrg180 pre- and postsynaptically or on either side of the synapse alone (Mann-Whitney Rank sum test, $P \leq 0.001$). Less than 20% of animals showed an electrophysiological impairment even when a late presynaptic Gal4 driver line was used for rescue (right). **(c-d)** Rescue of *nrg*$^{14}$; P[*nrg180*$^{Y\text{-}A}$] and *nrg*$^{14}$; P[*nrg180*$^{\Delta FIGQY}$] animals using cell autonomous expression of Nrg180. Simultaneous expression of Nrg180 pre- and postsynaptically or only on one side of the synapse throughout development significantly rescued the response latency (left) and following frequencies (middle) of these mutations. More than 80% of all GF-TTMn synapses showed wild type properties (right, Mann-Whitney Rank sum test, $P \leq 0.001$). In contrast to *nrg*$^{14}$;P [*nrg180*$^{Y\text{-}F}$], late expression of UAS-*nrg180* in the GF alone in *nrg*$^{14}$; P[*nrg180*$^{Y\text{-}A}$] and *nrg*$^{14}$; P[*nrg180*$^{\Delta FIGQY}$] animals did not significantly improve the average response latency (left, Mann-Whitney Rank sum test, P = 0.061 and P = 0.057, respectively) or the following frequencies (middle, Mann-Whitney Rank sum test, P = 0.9 and P = 0.081, respectively). **(e)** Presynaptic GF terminal morphology was rescued by either pre- or postsynaptic expression of Nrg180 in *nrg*$^{14}$; P[*nrg180*$^{\Delta FIGQY}$] mutant animals. Scale bar 15 μm. Error bars represent s.e.m.

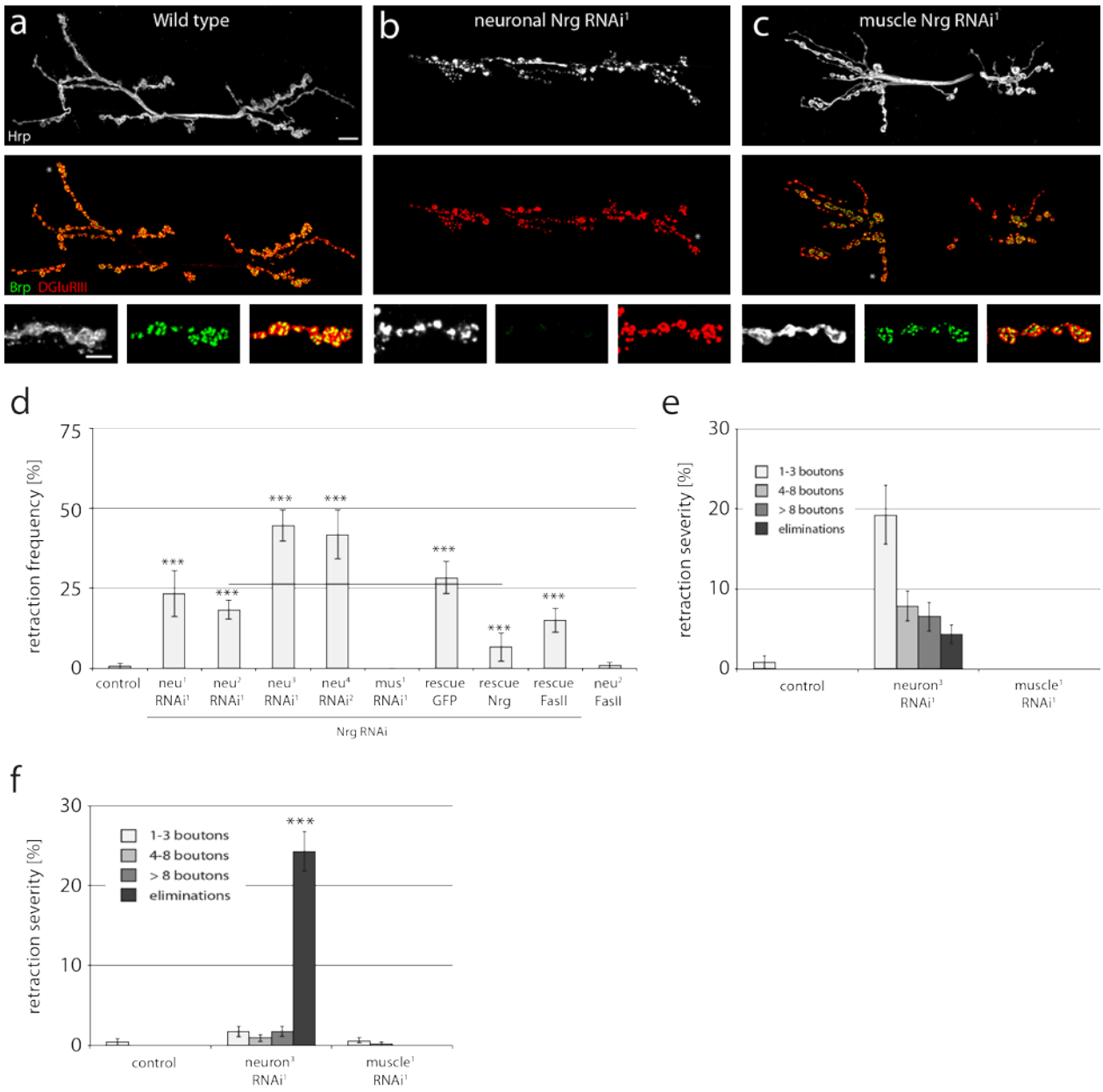


## Supplementary Figure 1 - Presynaptic Nrg is essential for synapse stability.

**(a-c)** NMJs on muscle 6/7 stained for the presynaptic motoneuron membrane (Hrp, white), the presynaptic active zone marker Brp (green) and postsynaptic glutamate receptors (DGluRIII, red). **(a)** A stable wild type NMJ indicated by perfect apposition of pre- and postsynaptic markers. **(b)** Knock down of presynaptic Nrg resulted in severe synaptic retraction indicated by a fragmented presynaptic membrane and the loss of presynaptic Brp despite the presence of postsynaptic glutamate receptors. The example shows a complete elimination of an entire NMJ at muscle 6/7. Please note the characteristic increase in postsynaptic glutamate receptor clusters at sites of retractions (inset). **(c)** Loss of muscle Nrg did not impair synapse stability. Scale bar in **a** corresponds to **a-c**, 10 µm, inset 5 µm. **(d)** Quantification of different *nrg* RNAi conditions. Neuronal but not muscle specific knock down of Nrg using different Gal4 driver combinations or independent RNAi constructs resulted in a significant increase in synaptic retractions on muscle 6/7. The retraction frequency was significantly rescued ($P \leq 0.001$) by co-expression of UAS-*nrg180* but not by co-expression of either UAS-*mCD8-GFP* or UAS-*fasII*. Expression of UAS-*fasII* alone did not result in a significant increase in retractions

(genotypes: neu$^{1}$ = *elav*$^{C155}$-Gal4; neu$^{2}$ = *elav*$^{C155}$-Gal4; *ok371*-Gal4; neu$^{3}$ = *elav*$^{C155}$-Gal4; UAS-*dcr2*; neu$^{4}$ = *elav*$^{C155}$-Gal4; *sca*-Gal4 UAS-*dcr2*; mus$^{1}$ = UAS-*dcr2*; *mef2*-Gal4; RNAi$^{1}$ = V6668; RNAi$^{2}$ = V107991; rescue indicates co-expression of the listed UAS construct; n = 6-24 animals). **(e)** Quantification of retraction severity on muscle 6/7. Only neuronal knock down of Nrg resulted in a significant increase in the severity of synapse retractions. **(f)** Quantification of retraction severity on muscle 4. Only neuronal knock down of Nrg resulted in a significant increase in the severity of synapse retractions. A very large fraction of observed retractions represent complete presynaptic eliminations. Error bars represent s.e.m.

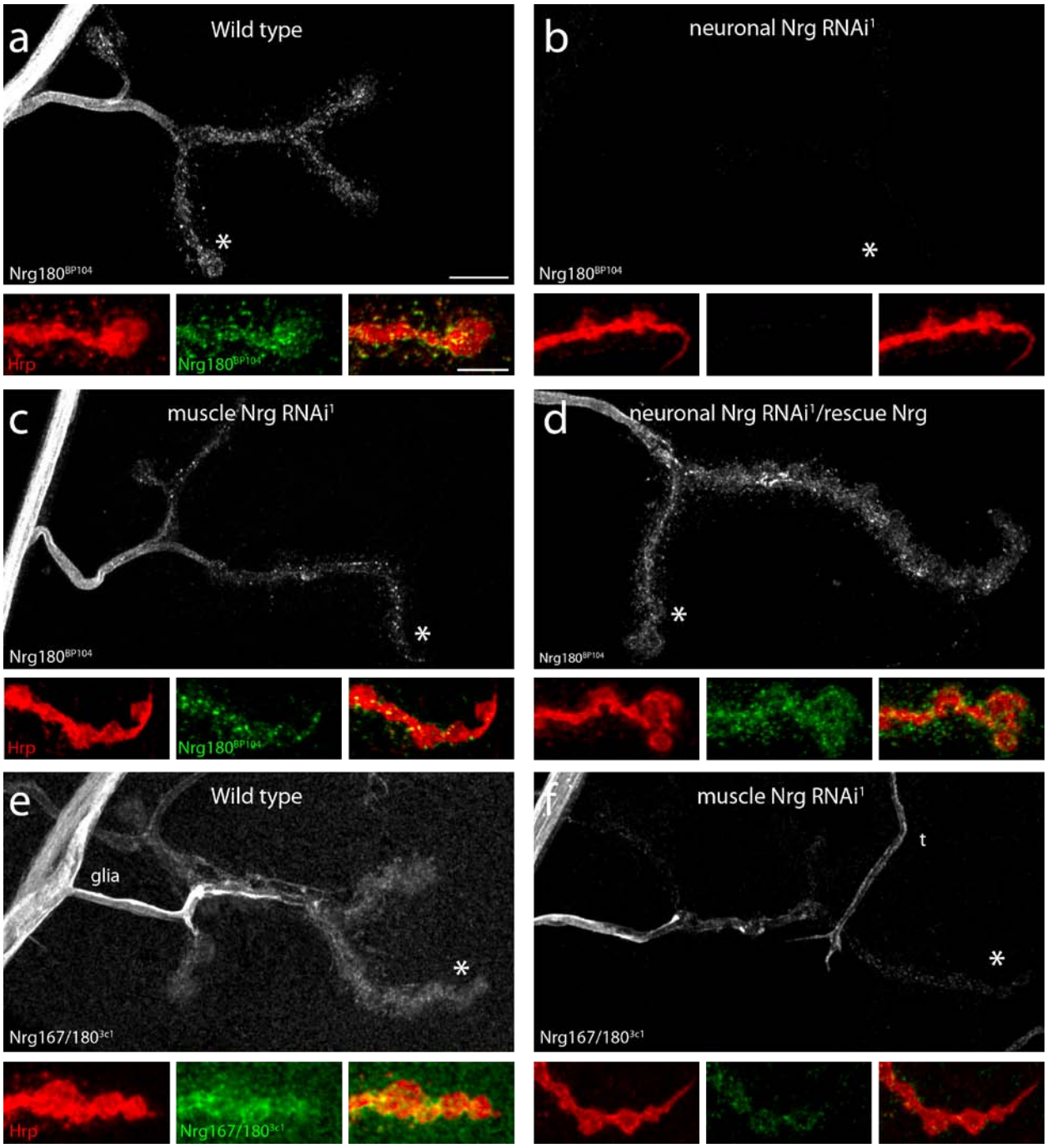


**Supplementary Figure 2 - Analysis of pre- and postsynaptic Nrg localization after specific knock down of Nrg**

**(a-d)** Muscle 4 NMJs stained with an antibody specific to the cytoplasmic tail of Nrg180 (Nrg180$^{BP104}$, white and green) and the presynaptic membrane (Hrp, red). **(a)** In wild type animals Nrg180 was present in the motoneuron axon and within the presynaptic nerve terminal marked by the membrane marker. In contrast to the uniform distribution in the axon Nrg was present in a punctate pattern at the terminal and co-localizes with Hrp at the ends of small filopodia-like membrane extensions. **(b)** Neuronally expressed Nrg RNAi resulted in an almost complete knock down of Nrg180 in the presynaptic motoneuron. **(c)** Muscle specific knock down of Nrg altered the normal distribution of Nrg180 in the presynaptic nerve terminal. **(d)** Co-expression of Nrg180 with Nrg RNAi resulted in a complete rescue of Nrg180 levels and distribution at the NMJ. **(e-f)** Muscle 4 NMJs stained with an antibody recognizing both Nrg isoforms (Nrg$^{3c1}$, white and green) and for the presynaptic membrane (Hrp, red). **(e)** In addition to neuronally expressed Nrg180 we observed Nrg167 present throughout the postsynaptic muscle and in glial cells surrounding the motoneuron axon. Nrg167 might also be present within motoneurons (due to almost complete sequence similarity to Nrg180 no specific antibody exists). **(f)** Muscle specific knock down efficiently eliminated Nrg167 expression in the muscle. Presynaptic Nrg can still be detected (asterisk). A tracheal branch expressing Nrg167 is indicated (t). Scale bar in **a** corresponds to **a-e** 10 µm, insets 5 µm.

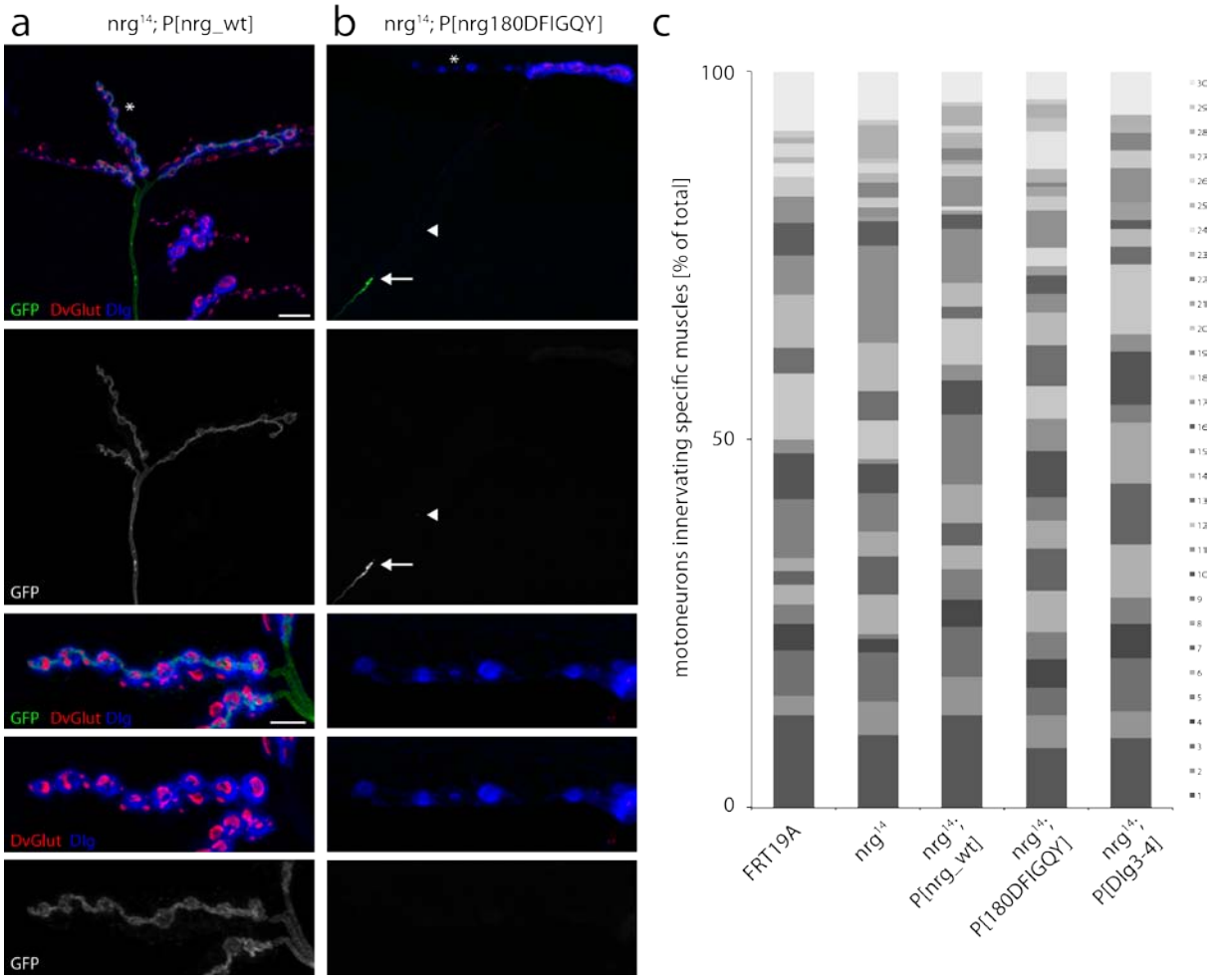


## Supplementary Figure 3 - Analysis of *nrg* MARCM clones

**(a)** A *nrg$^{14}$* MARCM clone rescued by a wild type *nrg* Pacman construct. The motoneuron clone was marked by the expression of mCD8-GFP (green). Synaptic vesicles (DvGlut, red) were found opposite postsynaptic Dlg (blue) indicating a stable NMJ (insets). Neighboring NMJs are visible that were not mutant as evident by the absence of the clonal marker. **(b)** A *nrg$^{14}$* MARCM clone expressing a mutated form of Nrg180 lacking the

FIGQY motif. A “bulb-like” structure (arrow) was present in close proximity to an NMJ that contained postsynaptic profiles marked by Dlg but no presynaptic vesicles. In contrast to the neighboring wild type NMJ the postsynaptic Dlg staining was clearly reduced and no longer formed a continuous structure (asterisk, insets). While no membrane marker remnants were visible at the eliminated NMJ we observed small GFP-puncta in between the NMJ and the retracted axon (arrowhead). **(c)** Scoring of the innervation pattern of stable NMJs of MARCM clones of indicated genotypes. In all cases we observed similar muscle innervation rates.

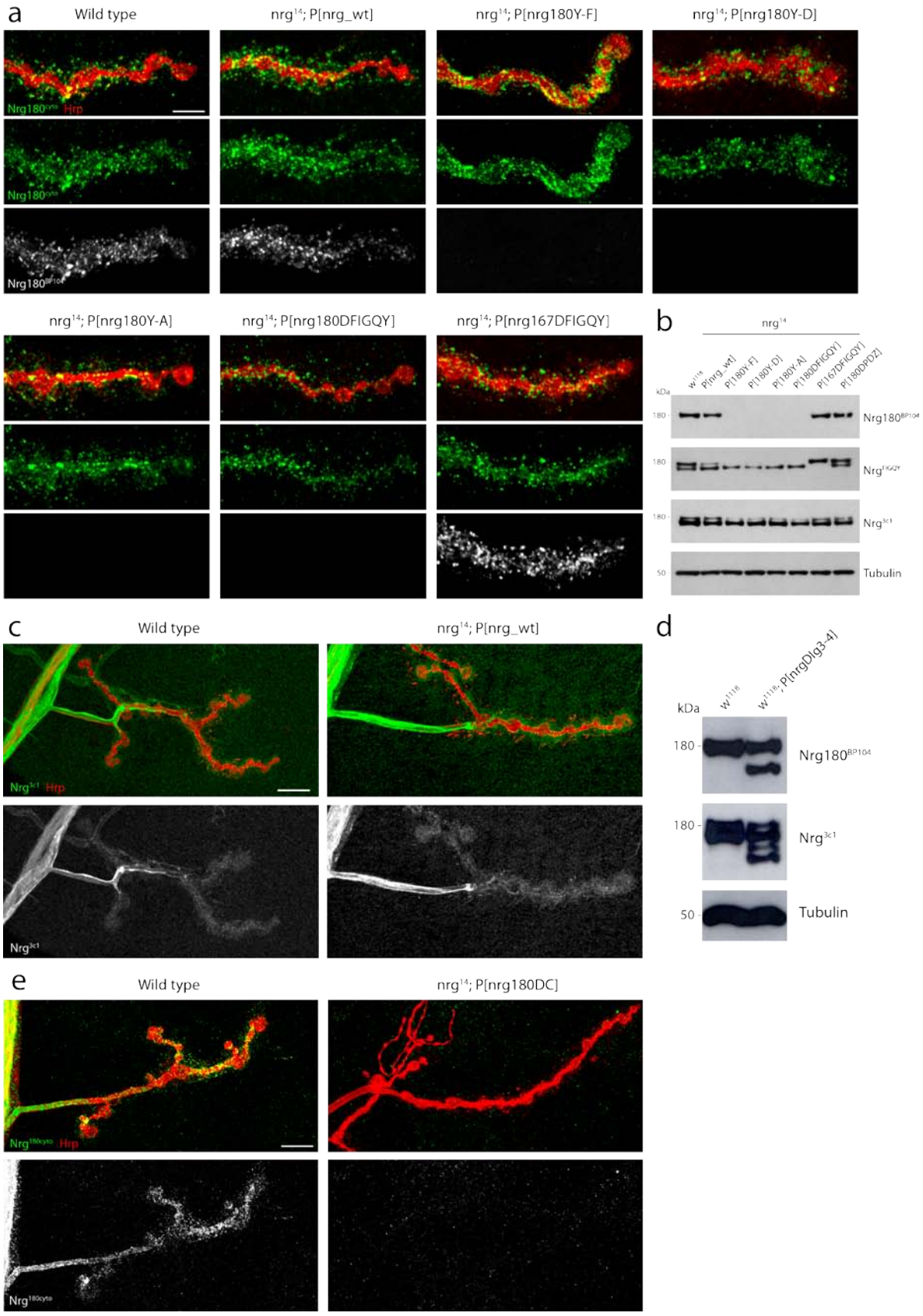


**Supplementary Figure 4 - Analysis of the expression of genomic Nrg Pacman rescue constructs.**

**(a)** Nrg180 expression of different Pacman introduced *nrg* mutations in the background of the *nrg* null mutation $nrg^{14}$. All *nrg* Pacman constructs were expressed at wild type levels at the NMJ. The cytoplasmic domain specific antibody $Nrg180^{cyto}$ (green) detected Nrg180 at the NMJ in all different mutations. In contrast, the Nrg180-FIGQY specific antibody $Nrg180^{BP104}$ (white) did not recognize FIGQY mutations of Nrg180. **(b)** Western blot analysis of larval brain extracts of all Nrg Pacman constructs in the background of the *nrg* null mutation $nrg^{14}$. Equal levels of both Nrg isoforms were detected with $Nrg^{3c1}$; $Nrg^{FIGQY}$ specifically recognizes the FIGQY motif of both Nrg isoforms thus the mutated forms were not detected in the Western blot. $Nrg180^{BP104}$ only recognized Nrg180 proteins containing a wild type FIGQY motif. **(c)** Muscle 4 NMJs stained for Nrg167 and Nrg180 ($Nrg^{3c1}$, green, white). P[$nrg^{wt}$] rescued Nrg expression and distribution of both Nrg isoforms in motoneurons, glial cells and muscles of $nrg^{14}$ mutant animals. **(d)** Western blot analysis to assay the expression of Nrg lacking Ig3-4 domains. P[$nrg^{\Delta Ig3\text{-}4}$] did not rescue the embryonic lethality associated with the $nrg^{14}$ mutation, therefore we tested if normal levels of mutated Nrg isoforms were expressed from this construct in a wild type background. Using isoform specific antibodies we could visualize equal expression levels of truncated proteins of both isoforms. **(d)** Muscle 4 NMJs stained for the $Nrg180^{cyto}$ antibody that specifically detects the C-terminal tail of Nrg180 outside the FIGQY motif. In wild type the antibody was present in a pattern similar to $Nrg180^{BP104}$ showing a punctate pattern within the presynaptic nerve terminal. We lost all antibody staining at the NMJ in $nrg^{14}$ mutant animals rescued by P[$nrg180^{\Delta C}$] demonstrating the specificity of the antibody and the specificity of the introduced mutation. Scale bar in **a** 5 µm, **c** and **e** 10 µm.

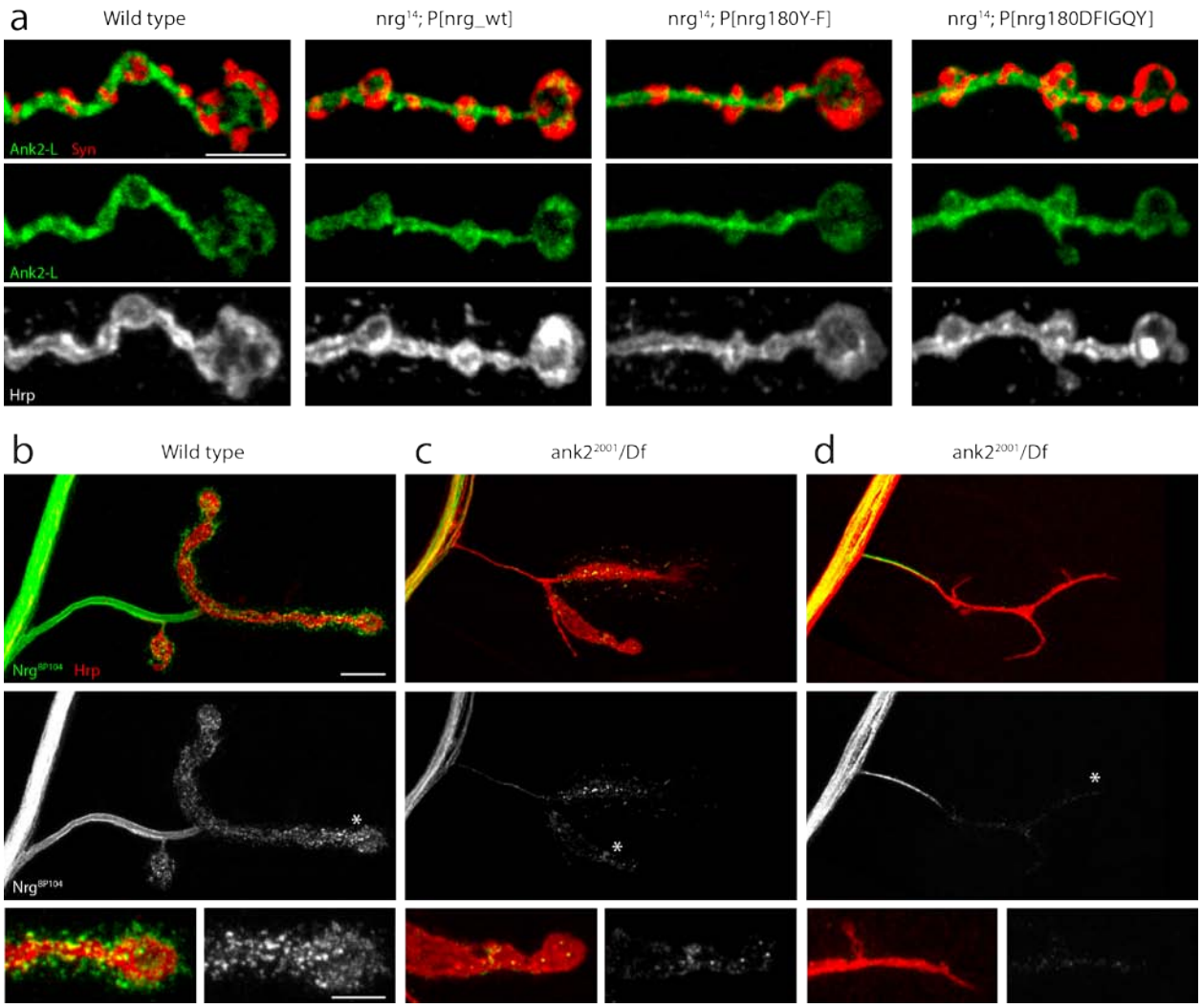


## Supplementary Figure 5 - Ank2 mutations affect presynaptic localization of Nrg180

**(a)** Analysis of Ank2-L levels and distribution in *nrg*$^{14}$ mutant animals rescued by different *nrg* Pacman constructs. We did not observe obvious changes in Ank2-L localization or levels at stable synapses in different Pacman rescued *nrg* mutants. **(b-d)** NMJs on muscle 4 stained for Nrg180 (Nrg180$^{BP104}$, green, white) and the presynaptic membrane (Hrp, red). **(b)** In wild type Nrg180 was present in a punctate pattern throughout the presynaptic nerve terminal co-localizing with the membrane marker Hrp. (**c, d)** Examples of *ank2* mutant NMJs. At semi-stable synapses that still have intact presynaptic membranes (as judged by continuous Hrp staining) we observed a partial or complete loss of Nrg180. In addition, Nrg180 levels in the axon were severely diminished. Scale bar in **a** 5 µm, **b** 10 µm.

## Methods

### Fly stocks

Flies were maintained at 25 °C on standard food. Crosses and most experiments were performed at 25 °C while RNAi assays were performed at 27 °C. The following fly strains have been used in this study: $w^{1118}$ (wild type), $nrg^{14}$ ($nrg^{1}$), $nrg^{17}$ ($nrg^{2}$), $ank2^{518}$, $\alpha$-$spec^{rg41}$, *Df(3L)RM5-2*, UAS-*mCD8-GFP*, UAS-*fasII*, $elav^{C155}$-Gal4, *ok371*-Gal4, *sca*-Gal4, *mef2*-Gal4, BG57-Gal4, UAS-*dcr2*, *ok307*-Gal4 (A307-Gal4), P(hsFLP)86E, P(hsFLP)1, P(neoFRT)19A (all Bloomington stock center); c17-Gal4, c42.2-Gal4, *shakB*-Gal4 [52]; RNAi lines were obtained from the Vienna *Drosophila* RNAi Center: Nrg RNAi line[1] (stock ID6688), Nrg RNAi line[2] (stock ID107991).

### Generation of Neuroglian UAS and P[acman] constructs

The full length Nrg180 ORF was amplified from the plasmid pMT-Neuroglian and the Nrg167 ORF from cDNA GH03573 (both obtained from the *Drosophila* Genomic Research Center, Indiana, USA). Full length ORFs were cloned into pENTR vector via TOPO cloning (Invitrogen). To obtain pUASTattB-10xUAS destination vectors suited for gateway cloning a gateway cassette with a C-terminal 3xHA or EGFP tag was introduced into the pWALIUM10-moe plasmid (TRiP collection, Harvard Medical School). Final expression constructs were generated via gateway cloning using standard procedures (Invitrogen). Deletions and point mutations were introduced into pENTR clones using the QuickChange II site-directed mutagenesis kit following the manufacturer's instructions (Agilent technologies). All constructs were verified by sequencing (FMI sequencing facility). The P[acman] clone CH321-4H20 was obtained from BACPAC Resources Center (BPRC, Oakland, California) [38] and modified using *galK* mediated recombineering [39]; NCI Frederick National Laboratory). Site-specific integration via the phi-C31 system was used to generate insertions at the $att^{P40}$-landing site for both pUAST and Pacman constructs. Primers used in this study are listed below.

### Immunohistochemistry and antibody production

Wandering third instar larvae were dissected in standard dissecting saline and fixed with Bouin's fixative for 2-3 min (Sigma-Aldrich). Primary antibodies were incubated at 4 °C overnight. Primary antibodies were used at the following dilutions: anti-Nrg180 (BP104)

1:250, anti-Bruchpilot (nc82) 1:250, anti-Futsch (22c10) 1:500, anti-Synapsin (3c11) 1:100 (all obtained from Developmental Studies Hybridoma Bank, IA); rabbit anti-Dlg 1: 30 000 (gift from V. Budnik, Worchester, MA, USA), rabbit anti-DGluRIII [12] 1: 2500; rabbit anti-DvGlut, rat anti-CD8 (Caltag Laboratories) 1:1000, anti-Nrg (3c1, gift from M. Hortsch, Ann Arbor, MI, USA) 1:500; rabbit anti-Nrg$^{FIGQY}$ (raised against the peptide: TEDGSFIGQYVPGKLQP) 1:100, rabbit anti-Nrg180$^{cyto}$ (raised against the peptide: NNSAAAHQAAPTAGGGSGAA) 1:500. Monoclonal rat anti-Ank2L 1:40 was generated against a protein fragment containing aa 3134-3728 (according to the 4083 aa isoform of Ank2-L). Rabbit Ank1-4 antibody used for IPs was generated against the Ankyrin domains 1-4. Antibodies were generated at David's Biotechnology (Regensburg, Germany)

Alexa conjugated secondary antibodies (Invitrogen) were used at 1:1000 for 2 h at RT. Directly conjugated anti-Hrp (Alexa or Cy-dyes) were used at 1:100-1000 (Jackson Immunoresearch Laboratories). Larval preparations were mounted in Prolong Gold (Invitrogen). Images were captured at room temperature using a Leica SPE confocal microscope. To process, analyze images and quantify phenotypes Adobe Photoshop, Imaris (Bitplane), Image Access (Imagic) and the open source tool FIJI/ImageJ were used.

**Quantification of phenotypes**

Synaptic retractions were quantified using presynaptic Brp and postsynaptic DGluRIII staining and counting the number of unopposed postsynaptic footprints. Complete loss of presynaptic marker Brp was considered as elimination. N indicates the number of independent animals per quantification.

Bouton area, number and NMJ length were quantified using Synapsin, Dlg and Hrp staining. Bouton area and NMJ length were quantified using the Image access software (Imagic). Hrp staining was used to visualize the bouton area and 10 A3 muscle 4 NMJs were quantified per genotype. To measure NMJ length 20 muscle 4 NMJs (segment A3 and A4, 10 each) were analyzed. Bouton number was quantified on muscle 4 in segment A2-A6 using Synapsin/Dlg staining. N indicates the number of analyzed NMJs.

**Western Blot and Immunoprecipitation**

Larval brains were dissected and transferred into 2x sample buffer (Invitrogen). 5 brains per lane were analyzed on NuPage gels (Invitrogen) according to standard procedures. Primary

antibodies were incubated overnight at 4 °C. Secondary Hrp-conjugated goat anti-mouse and goat anti-rabbit antibodies were used at 1:10 000 (Jackson Immunoresearch) for 2 h at RT. Membranes were incubated with ECL substrate (SuperSignal West Pico Kit, Thermo scientific) and developed on film (Fujifilm).

For immunoprecipitation experiments S2 cells were cotransfected with act5C-Gal4, UASAnk2-S-EGFP (Pielage at al., 2008) and UAS-Nrg-3xHA plasmids using Fugene (Roche) following manufacturer's instructions. IP`s were analyzed using mouse anti-HA (12CA5) 1:200, rabbit anti-GFP (Molecular Probes) 1:500 and rabbit anti-Ank2 (rabbit anti-Ank1-4) 1:1000 antibodies for IP and input. Quantification of Ank2 binding between mutants was performed using four independent IP experiments and Odyssey2.1 software (LI-COR).

**Fluorescence Recovery after Photobleaching (FRAP)**

Wandering third instar larvae expressing Nrg-EGFP via *ok371*-Gal4 were dissected in HL3 saline and prepared for live imaging using a magnetic pinholder device. 1-Naphthylacetyl-spermin-trihydrochloride (NSH) (100 mM; Sigma, St Louis, MO) was added to the HL3 saline to block postsynaptic glutamate receptor activation and muscle contractions, ensuring accurate image acquisition during the experiments. 6-9 motoneuron axons/NMJs from 3-4 independent experiments were photobleached in a strip spanning over the whole axon/bouton width using the Zeiss LSM700 by scanning the region for 30 iterations at 100% laser-power of the 488 nm line. 10 images were acquired before the bleach and 40 after the bleach with a time interval of 5 s.

Images from the FRAP series were corrected for animal movement with the FIJI registration plugin using the StackReg option. The fluorescence at each time point was subtracted from the background outside the axon and the minimum fluorescence in the bleached area. This value was then normalized to the fluorescence in the control region that was also subtracted from the background fluorescence outside of the axon.

The recovery curves were fit to a double exponential curve as follows:

$y = a + b*(1-\exp(-c*tx))+ d*(1-\exp(-e*tx))$

The maximum was calculated from the fitting curve ($max^{fitting}$). To calculate the real max value the following formula has been used:

$F_{max}= (F-BG_t*max^{fitting}) + F_{unbleached}$

The mobile fraction was calculated using the following formula:

$MF= (F_{max}-F_{unbleached})/ (F_{beforebleach})-F_{unbleached})$

**MARCM analysis**

The *nrg* null mutation *nrg*$^{14}$ was recombined with the P(neoFRT)19A chromosome. The stock was crossed to P(hsFLP)1, P(neoFRT)19A, tubGal80; *ok371*-Gal4, UAS-CD8-GFP; MKRS, P(hsFLP)86E. Embryos were collected for 2 h, aged for 3 h and heat shocked for 1 h at 37 °C.

**Statistical analysis**

All statistical analyses were performed using Microsoft Office Excel and an online source for unpaired student`s t-test (http://www.physics.csbsju.edu/stats/t-test.html). $P \leq 0.05$ was accepted as statistically significant ($* \leq 0.05$, $** \leq 0.01$, $*** \leq 0.001$).

**Giant fiber preparation**

Adult *Drosophila* nervous system was dissected, dye filled and fixed as previously described [50]. Young 2-5 days old flies were used for all the experiments. To visualize the morphology of giant fiber-TTMn connection either a 10mM Alexa Fluor 568 Hydrazide (Molecular Probes) in 200 mM KCl or a dye solution of 10% w/v Neurobiotin (Vector labs) and tetramethyl rhodamine-labeled dextran (Invitrogen) in 2M potassium acetate was injected into the GF axons by passing hyperpolarizing or depolarizing current respectively. Preparation of GF samples for confocal microscopy has been described previously [50]. Samples were analyzed using a Nikon C1si Fast Spectral Confocal system. Images were processed using Nikon Elements Advance Research 4.0 software.

**Electrophysiology**

Electrophysiological recordings from the giant fiber circuit were obtained as described in detail in [66]. The flies were given 10 single pulses at 30-60 mV for 0.03 ms with a 5 second interval between the stimuli and the shortest response latency of each fly was averaged. To determine the reliability of the circuit, the ability to follow frequencies at 100 Hz was determined. For this 10 trains of 10 stimuli were given at 100 Hz with an interval of 2

seconds between the trains and percent of the total responses was calculated. All the traces were recorded, stored and analyzed using pClamp 10 (Molecular Devices) software. Mann-Whitney Rank sum test was used to determine significant differences between different genotypes in average response latencies and following frequencies (Sigma Plot 11 software).

Data for Figure 1 and Figure Supplementary Figure 1

| **RNAi** | | Retraction frequency [%] | | | | | | |
|---|---|---|---|---|---|---|---|---|
| UAS | Gal4 | mu4 | p | mu6/7 | p | mu12 | mu13 | n |
| ctrl | neu$^{2}$ | 0.8 ± 0.8 | | 0.8 ± 0.8 | | 0.0 ± 0.0 | 0.0 ± 0.0 | 12 |
| RNAi$^{1}$ | neu$^{1}$ | 30.0 ± 6.8 | ≤ 0.0001 | 23.3 ± 7.1 | 0.0004 | 8.3 ± 4.0 | 20.0 ± 6.3 | 6 |
| | neu$^{2}$ | 33.4 ± 4.3 | ≤ 0.0001 | 18.3 ± 2.9 | 0.0002 | 27.5 ± 3.7 | 30.4 ± 4.5 | 24 |
| | neu$^{3}$ | 63.9 ± 3.3 | ≤ 0.0001 | 44.5 ± 4.8 | ≤ 0.0001 | 27.0 ± 3.4 | 35.7 ± 3.9 | 20 |
| | mus$^{1}$ | 1.7 ± 0.8 | ns | 0.4 ± 0.4 | ns | 0.0 ± 0.0 | 0.0 ± 0.0 | 24 |
| | | | | | | | | |
| RNAi$^{2}$ | neu$^{2}$ | 31.8 ± 5.6 | ≤ 0.0001 | 23.3 ± 5.0 | ≤ 0.0001 | 15.5 ± 2.7 | 22.7 ± 3.6 | 13 |
| | neu$^{3}$ | 38.6 ± 4.7 | ≤ 0.0001 | 21.4 ± 4.4 | ≤ 0.0001 | 18.4 ± 4.0 | 31.2 ± 4.0 | 12 |
| | neu$^{4}$ | 51.0 ± 4.5 | ≤ 0.0001 | 41.7 ± 7.5 | ≤ 0.0001 | 33.0 ± 7.0 | 48.5 ± 7.0 | 13 |
| | mus$^{1}$ | 3.8 ± 2.4 | ns | 6.1 ± 2.1 | ns | 5.3 ± 2.4 | 4.6 ± 2.4 | 13 |
| **RNAi rescue** | | | | Retraction frequency [%] | | | | |
| RNAi$^{1}$;Nrg180 | neu$^{2}$ | 9.3 ± 2.0 | 0.0002 | 5.0 ± 2.9 | 0.0014 | 0.7 ± 0.7 | 1.4 ± 1-0 | 14 |
| RNAi$^{1}$;CD8-GFP | neu$^{2}$ | 56.7 ± 4.6 | 0.0008 | 28.3 ± 4.9 | 0.074 | 35.6 ± 6.3 | 21.1 ± 4.0 | 18 |
| RNAi$^{1}$;FasII | neu$^{2}$ | 37.5 ± 4.3 | ns | 15.0 ± 3.8 | ns | 25.0 ± 6.2 | 20.0 ±7.2 | 12 |
| UAS-FasII | neu$^{2}$ | 4.4 ± 1.6 | ≤ 0.0001 | 0.9 ± 0.9 | ≤ 0.0001 | 0.9 ± 0.9 | 0.0 ± 0.0 | 11 |

**Legend**: ctrl = w$^{1118}$ x *elav*$^{C155}$-Gal4; *ok371*-Gal4, p-values$^{RNAi}$ are in comparison to ctrl, p-values$^{RNAi\ rescue}$ are in comparison to neu$^{2}$RNAi$^{1}$ (all unpaired student`s t-test). Gal4 drivers: neu$^{1}$ = *elav*$^{C155}$-Gal4, neu$^{2}$ = *elav*$^{C155}$-Gal4; *ok371*-Gal4, neu$^{3}$ = *elav*$^{C155}$-Gal4; UAS-*dcr2*, neu$^{4}$ = *elav*$^{C155}$-Gal4; *sca*-Gal4UAS-*dcr2*, mus$^{1}$ = UAS-*dcr2*; *mef2*-Gal4, n = number of animals (segments A2 to A6 were scored in each animal). Errors represent SEM.

Data for Figure 2

| Genotype | # NMJs | # affected axons | total # | % affected axons | p | n |
|---|---|---|---|---|---|---|
| FRT19A | 290 | 3 | 293 | 1.5 ± 1.0 | | 23 |
| nrg$^{14}$, FRT19A | 152 | 162 | 314 | 53.5 ± 3.7 | ≤ 0.0001 | 26 |
| nrg$^{14}$, FRT19A; P[nrg_wt] | 167 | 5 | 172 | 2.1 ± 1.0 | 0.65 | 18 |
| nrg$^{14}$, FRT19A; P[nrg180ΔFIQGY] | 209 | 46 | 255 | 18.4 ± 3.3 | 0.0005 | 22 |
| nrg$^{14}$, FRT19A; P[nrgΔIg3/4] | 78 | 69 | 147 | 49.5 ± 4.5 | ≤ 0.0001 | 21 |

**Legend**: p-values are in comparison to FRT19A (all unpaired student`s t-test), n = number of animals. % retracted axons. Errors represent SEM.

## Data for Figure 4

| Pacman mutations | amino acid sequence |
|---|---|
| P[nrg_wt] | QFTEDGS**FIGQY**VPGKLQPPVSPQ-//-AAGAVA**TYV*** |
| P[nrg180Y-F] | QFTEDGSFIGQ**F**VPGKLQPPVSPQ-//-AAGAVATYV* |
| P[nrg180Y-D] | QFTEDGSFIGQ**D**VPGKLQPPVSPQ-//-AAGAVATYV* |
| P[nrg180Y-A] | QFTEDGSFIGQ**A**VPGKLQPPVSPQ-//-AAGAVATYV* |
| P[nrg180ΔFIQGY] | QFTEDGS-----VPGKLQPPVSPQ-//-AAGAVATYV* |
| P[nrg180ΔC] | QFTEDGS(****)73* |
| P[nrg167ΔFIQGY] | GMNEDGS-----GRKGL* |
| P[nrg180ΔPDZ] | QFTEDGSFIGQYVPGKLQPPVSPQ-//-AAGAVA---* |

**Legend**: Pacman constructs are listed with the corresponding amino acid sequence with single amino acid changes (bold) and deletions (underlined). The domains are highlighted in bold in P[nrg_wt].

## Data for Figure 4

Retraction frequency [%]

| Genotype | mu4 | p | mu6/7 | mu12 | mu13 | n |
|---|---|---|---|---|---|---|
| $w^{1118}$ | 1.3 ± 0.6 | | 2.4 ± 0.8 | 0.4 ± 0.4 | 0.4 ± 0.4 | 25 |
| $nrg^{14}$/y; P[nrg_wt] | 1.3 ± 0.9 | 0.9 * | 0.7 ± 0.7 | 0.0 ± 0.0 | 0.0 ± 0.0 | 15 |
| $nrg^{14}$/y; P[nrg180Y-F] | 3.7 ± 1.8 | 0.3 | 11.0 ± 3.7 | 0.5 ± 0.5 | 2.0 ± 0.9 | 20 |
| $nrg^{14}$/y; P[nrg180Y-D] | 7.5 ± 1.6 | 0.0044 | 8.6 ± 1.8 | 5.5 ± 1.4 | 3.0 ± 1.1 | 20 |
| $nrg^{14}$/y; P[nrg180Y-A] | 8.3 ± 2.7 | 0.013 | 6.7 ± 1.9 | 1.7 ± 1.1 | 2.5 ± 1.3 | 12 |
| $nrg^{14}$/y; P[nrg180ΔFIQGY] | 8.1 ± 1.8 | 0.012 | 11.7 ± 2.2 | 7.4 ± 1.6 | 6.3 ± 1.2 | 28 |
| $nrg^{14}$/y; P[nrg180ΔC] | 11.3 ± 2.3 | 0.0015 | 11.0 ± 1.9 | 4.8 ± 1.5 | 1.4 ± 1.0 | 21 |
| $nrg^{14}$/y; P[nrg167ΔFIQGY] | 0.0 ± 0.0 | 0.0 | 3.2 ± 1.2 | 0.9 ± 0.6 | 0.9 ± 0.6 | 22 |
| $nrg^{14}$/y; P[nrg180ΔPDZ] | 1.6 ± 0.9 | 0.85 | 1.6 ± 0.9 | 0.0 ± 0.0 | 2.6 ± 1.3 | 19 |

**Legend**: p-values are in comparison to $nrg^{14}$/y; P[nrg_wt], * = p-value in comparison to $w^{1118}$ (all unpaired student`s t-test), n = number of analyzed animals (segments A2-A6 were scored in each animal). Errors represent SEM.

## Data for Figure 5

NMJ growth defects

| Genotype | NMJ length | p | Bouton area | p | Bouton no. | p | n |
|---|---|---|---|---|---|---|---|
| $w^{1118}$ | 106.9 ± 4.4 | | 6.9 ± 0.3 | | 16.6 ± 0.3 | | 123 |
| $nrg^{14}$/y; P[nrg_wt] | 103.5 ± 6.2 | | 5.7 ± 0.3 | | 15.7 ± 0.5 | | 98 |
| $nrg^{14}$/y; P[nrg180Y-F] | 110.7 ± 6.3 | 0.42 | 6.7 ± 0.3 | 0.037 | 18.5 ± 0.5 | 0.0003 | 109 |
| $nrg^{14}$/y; P[nrg180Y-D] | 128.9 ± 6.5 | 0.048 | 5.0 ± 0.2 | 0.56 | 22.0 ± 0.7 | ≤ 0.0001 | 142 |
| $nrg^{14}$/y; P[nrg180Y-A] | 119.9 ± 5.0 | 0.076 | 5.4 ± 0.3 | 0.1 | 20.9 ± 0.8 | ≤ 0.0001 | 69 |
| $nrg^{14}$/y; P[nrg180ΔFIQGY] | 156.6 ± 9.1 | ≤ 0.0001 | 4.3 ± 0.2 | 0.0002 | 29.3 ± 0.9 | ≤ 0.0001 | 112 |

| | | | | | | | |
|---|---|---|---|---|---|---|---|
| $nrg^{14}$/y; P[nrg180ΔC] | 155.1 ± 9.4 | ≤ 0.0001 | 4.4 ± 0.2 | 0.0013 | 28.2 ± 0.8 | ≤ 0.0001 | 137 |
| $nrg^{14}$/y; P[nrg167ΔFIQGY] | 100.8 ± 3.9 | 0.71 | 6.2 ± 0.3 | 0.2 | 17.4 ± 0.3 | 0.0048 | 176 |
| $nrg^{14}$/y; P[nrg180ΔPDZ] | 98.1 ± 5.2 | 0.5 | 5.9 ± 0.3 | 0.65 | 17.3 ± 0.4 | 0.016 | 115 |

**Legend**: p-values are in comparison to $nrg^{14}$/y; P[nrg_wt] (all unpaired student`s t-test), $n^{NMJ\ length}$ = 20 NMJs (segments A3 and A4,), $n^{bouton\ area}$ = 10 NMJs (segment A3), $n^{bouton\ no.}$ = number of NMJs as indicated (segments A2-A6 were scored in each animal). Errors represent SEM.

## Primer List

| *Primer* | *DNA-sequence* | |
|---|---|---|
| Nrg180-ENTR-N-term | 5`CACCATGTGGCGGCAGTCAACG | |
| Nrg180-ENTR-C-term | 5`TTAGACGTAGGTGGCCACG | |
| Nrg180-ENTR-C-term-tagged (HA, EGFP) | 5`GACGTAGGTGGCCACGGCTC | |
| Nrg180Y-F | 5`GGCTCCTTCATTGGCCAATTTGTTCCTGGAAAGCTCC | |
| Nrg180Y-D | 5`GGCTCCTTCATTGGCCAAGACGTTCCTGGAAAGCTCC | |
| Nrg180Y-A | 5`GGCTCCTTCATTGGCCAAGCTGTTCCTGGAAAGCTCC | |
| Nrg180ΔFIGQY | 5`AATTTACCGAGGATGGCTCCGTTCCTGGAAAGCTCCAACC | |
| P[nrg180Y-F] | 5`TCTTTCTAATCCCAGGACAATTTACCGAGGATGGCTCCTTCATTGG CCAATTCGTTCCTGGAAAGCTCCAACCGCCGGTTAGCCCACAGCCAC TGAACAATTC | |
| P[nrg180Y-D] | 5`TCTTTCTAATCCCAGGACAATTTACCGAGGATGGCTCCTTCATTGG CCAAGACGTTCCTGGAAAGCTCCAACCGCCGGTTAGCCCACAGCCAC TGAACAATTC | |
| P[nrg180Y-A] | 5`TCTTTCTAATCCCAGGACAATTTACCGAGGATGGCTCCTTCATTGG CCAAGCCGTTCCTGGAAAGCTCCAACCGCCGGTTAGCCCACAGCCAC TGAACAATTC | |
| P[nrg180ΔFIQGY] | 5`ATATTGTATATATCTTTCTAATCCCAGGACAATTTACCGAGGATGG CTCCGTTCCTGGAAAGCTCCAACCGCCGGTTAGCCCACAGCCACTGA ACAATTC | |
| P[nrg180ΔC] | 5`ATATTGTATATATCTTTCTAATCCCAGGACAATTTACCGAGGATGG CTCCTAAGAGGCGTGGCTGGGATTCACTTGCCCCATTGTTCTCCTGAT TTTCTA | |
| P[nrg180ΔPDZ] | 5`CCGGAGGAGCAGCTGCCAGCAATGGAGGAGCTGCAGCCGGAGCCG TGGCCCCTGTTGACAATTAATCATCGGCA | |
| P[nrg167ΔFIQGY] | 5`ACAATCACAATCAATATTAAATCGACAACGACAACCAATATCCAG GCATGAATGAAGATGGATCCGGACGCAAAGGACTTTGATTTAATTAG TAAGCAGCGCACCGCAACAGCAA | |
| P[nrgΔIg3/4] | 5`CCTCGGTGTTTCGCAGTGAATACAAGATTGGCAACAAGGTGCTCCT CGATGCTGAGCCGCCAACGATTTCCGAAGCTCCAGCAGCTGTATCCA CTGTCGA | |
| *Check and seq primer* | *Forward primer* | *Reverse primer* |

| | | |
|---|---|---|
| pENTR_nrg180wt, Y-F, Y-A, Y-D, ΔFIGQY (check mutations in FIGQY motif) | 5`AATCGGGGCGGAAAGTACG | 5`CAGGAAACAGCTATGAC |
| pENTR_nrg180wt (start and stop) | 5`TGTAAAACGACGGCCAGT | 5`CAGGAAACAGCTATGAC |
| pENTR/pUAST nrgwt, Y-F, Y-A, Y-D, ΔFIGQY (sequencing of complete ORF, primer 1-8) | 5`TGCTCTTCAAAGTGGCGC<br>5`GTTAGTGCCTCGCAGAAC<br>5`TAACTACGGTTGCAACGC<br>5`GATTCGTGAAGACCAATG<br>5`CCGAAATCGAGCACAATG<br>5`ACAATGGACGCTTCAATG<br>5`TGGATACGCGAGAATGAG<br>5`CGATACTGATTCGATGGC | 5`CCCGATCCTCCGGCAGTT<br>5`CAATGAACCATCCGGCAT<br>5`CCATCTTCATGCGTGTGA<br>5`CATTGTGAAGTTGGTGGG<br>5`GGCGTGAACGATGTATTG<br>5`CACCGTTAGCTTGGACAT<br>5`CACGTCGCAGGTGTATGT<br>5`GTGGCCGTTCCGAATTCA |
| 10xpUAST_Nrg_HA (check) | 5`AATCGGGGCGGAAAGTACG | 5`GGCATTCCACCACTGCTCCC |
| 10xpUAST_Nrg_EGFP (check) | 5`TATAAATAGAGGCGCTTCGT | 5`CAAGTCCGCCATGCCCGAAG |
| P[acman] check primer (Nrg180FIGQY mutations) | 5`AACTGACGCATTTGCCAGG | 5`GCAGACACTTAAAGCAGTT |
| P[acman] seq primer (Nrg180FIGQY mutations) | 5`CATATCATTTTGCACCGGC | 5`ACGATGCTCCACCCGATGCT |
| P[acman] check (ΔC) | 5`AACTGACGCATTTGCCAGG | 5`GCTTTAAATTCATGCGAG |
| P[acman] seq (ΔC) | 5`CATATCATTTTGCACCGGC | 5`GCAGACACTTAAAGCAGTT |
| P[acman] check (ΔPDZ) | 5`GAGGATGGCTCCTTCATTG | 5`GCTTTAAATTCATGCGAG |
| P[acman] seq (ΔPDZ) | 5`CACTGAACAATTCCGCTGC | 5`GCAGACACTTAAAGCAGTT |
| P[acman] check (Nrg167ΔFIGQY) | 5`AGCCACTTGCCGTTATAAG | 5`GGCAGTATTGATTTGCAT |
| P[acman] seq (Nrg167ΔFIGQY) | 5`GTGTTCCTTGTTATGTGT | 5`AGTCGTGGTGTTTGCACTT |
| P[acman] check (NrgΔIg3/4) | 5`CGAGCTGAATGCCTTCAAG | 5`GGAGTTAACATTCAGAATGATGG |
| P[acman] seq (NrgΔIg3/4) | 5`GATCCTGAGGGTAATCTCTG | 5`GTTATTCGATCGCTCCACTG |

## References


1. Siddiqui, T.J. & Craig, A.M. Synaptic organizing complexes. *Current opinion in neurobiology* **21**, 132-143 (2011).
2. Williams, M.E., de Wit, J. & Ghosh, A. Molecular mechanisms of synaptic specificity in developing neural circuits. *Neuron* **68**, 9-18 (2010).
3. Caroni, P., Donato, F. & Muller, D. Structural plasticity upon learning: regulation and functions. *Nature Reviews Neuroscience* **13**, 478-490 (2012).
4. Holtmaat, A. & Svoboda, K. Experience-dependent structural synaptic plasticity in the mammalian brain. *Nature Reviews Neuroscience* **10**, 647-658 (2009).

5. Xu, T., *et al.* Rapid formation and selective stabilization of synapses for enduring motor memories. *Nature* **462**, 915-919 (2009).
6. Yang, G., Pan, F. & Gan, W. Stably maintained dendritic spines are associated with lifelong memories. *Nature* **462**, 920-924 (2009).
7. Shapiro, L. & Weis, W.I. Structure and biochemistry of cadherins and catenins. *Cold Spring Harbor Perspectives in Biology* **1**, a003053 (2009).
8. Nishimura, T. & Takeichi, M. Remodeling of the adherens junctions during morphogenesis. *Current topics in developmental biology* **89**, 33-54 (2009).
9. Benson, D.L. & Huntley, G.W. Synapse adhesion: a dynamic equilibrium conferring stability and flexibility. *Current opinion in neurobiology* **22**, 397–404 (2011).
10. Brigidi, G.S. & Bamji, S.X. Cadherin-catenin adhesion complexes at the synapse. *Current opinion in neurobiology* **21**, 208-214 (2011).
11. Koch, I., *et al.* Drosophila ankyrin 2 is required for synaptic stability. *Neuron* **58**, 210-222 (2008).
12. Pielage, J., Bulat, V., Zuchero, J.B., Fetter, R.D. & Davis, G.W. Hts/Adducin controls synaptic elaboration and elimination. *Neuron* **69**, 1114-1131 (2011).
13. Pielage, J., *et al.* A presynaptic giant ankyrin stabilizes the NMJ through regulation of presynaptic microtubules and transsynaptic cell adhesion. *Neuron* **58**, 195-209 (2008).
14. Pielage, J., Fetter, R.D. & Davis, G.W. Presynaptic spectrin is essential for synapse stabilization. *Current biology : CB* **15**, 918-928 (2005).
15. Bennett, V. & Baines, A.J. Spectrin and ankyrin-based pathways: metazoan inventions for integrating cells into tissues. *Physiological reviews* **81**, 1353-1392 (2001).
16. Bednarek, E. & Caroni, P. β-Adducin Is Required for Stable Assembly of New Synapses and Improved Memory upon Environmental Enrichment. *Neuron* **69**, 1132-1146 (2011).
17. Ikeda, Y., *et al.* Spectrin mutations cause spinocerebellar ataxia type 5. *Nature Genetics* **38**, 184-190 (2006).
18. Scotland, P., Zhou, D., Benveniste, H. & Bennett, V. Nervous system defects of AnkyrinB (-/-) mice suggest functional overlap between the cell adhesion molecule L1 and 440-kD AnkyrinB in premyelinated axons. *The Journal of cell biology* **143**, 1305-1315 (1998).
19. Shapiro, L., Love, J. & Colman, D.R. Adhesion molecules in the nervous system: structural insights into function and diversity. *Annual review of neuroscience* **30**, 451-474 (2007).

20. Hortsch, M. Structural and functional evolution of the L1 family: are four adhesion molecules better than one? *Molecular and cellular neurosciences* **15**, 1-10 (2000).
21. Maness, P.F. & Schachner, M. Neural recognition molecules of the immunoglobulin superfamily: signaling transducers of axon guidance and neuronal migration. *Nature Neuroscience* **10**, 19-26 (2007).
22. Sakurai, T. The role of NrCAM in neural development and disorders--beyond a simple glue in the brain. *Molecular and cellular neurosciences* **49**, 351-363 (2012).
23. Hortsch, M., Nagaraj, K. & Godenschwege, T.A. The interaction between L1-type proteins and ankyrins--a master switch for L1-type CAM function. *Cellular & molecular biology letters* **14**, 57-69 (2009).
24. Garver, T.D., Ren, Q., Tuvia, S. & Bennett, V. Tyrosine phosphorylation at a site highly conserved in the L1 family of cell adhesion molecules abolishes ankyrin binding and increases lateral mobility of neurofascin. *The Journal of cell biology* **137**, 703-714 (1997).
25. Jenkins, S.M., *et al.* FIGQY phosphorylation defines discrete populations of L1 cell adhesion molecules at sites of cell-cell contact and in migrating neurons. *Journal of cell science* **114**, 3823-3835 (2001).
26. Tuvia, S., Garver, T.D. & Bennett, V. The phosphorylation state of the FIGQY tyrosine of neurofascin determines ankyrin-binding activity and patterns of cell segregation. *Proceedings of the National Academy of Sciences of the United States of America* **94**, 12957-12962 (1997).
27. Zhang, X., Davis, J.Q., Carpenter, S. & Bennett, V. Structural requirements for association of neurofascin with ankyrin. *The Journal of biological chemistry* **273**, 30785-30794 (1998).
28. Pocock, R., Bénard, C.Y., Shapiro, L. & Hobert, O. Functional dissection of the C. elegans cell adhesion molecule SAX-7, a homologue of human L1. *Molecular and cellular neurosciences* **37**, 56-68 (2008).
29. Wong, E.V., Cheng, G., Payne, H.R. & Lemmon, V. The cytoplasmic domain of the cell adhesion molecule L1 is not required for homophilic adhesion. *Neuroscience letters* **200**, 155-158 (1995).
30. Kenwrick, S., Watkins, A. & De Angelis, E. Neural cell recognition molecule L1: relating biological complexity to human disease mutations. *Human molecular genetics* **9**, 879-886 (2000).

31. Buttermore, E.D., *et al.* Pinceau organization in the cerebellum requires distinct functions of neurofascin in Purkinje and basket neurons during postnatal development. *Journal of Neuroscience* **32**, 4724-4742 (2012).
32. Rasband, M.N. Composition, assembly, and maintenance of excitable membrane domains in myelinated axons. *Seminars in cell & developmental biology* **22**, 178-184 (2011).
33. Zonta, B., *et al.* A critical role for Neurofascin in regulating action potential initiation through maintenance of the axon initial segment. *Neuron* **69**, 945-956 (2011).
34. Ango, F., *et al.* Ankyrin-based subcellular gradient of neurofascin, an immunoglobulin family protein, directs GABAergic innervation at purkinje axon initial segment. *Cell* **119**, 257-272 (2004).
35. Guan, H. & Maness, P.F. Perisomatic GABAergic innervation in prefrontal cortex is regulated by ankyrin interaction with the L1 cell adhesion molecule. *Cerebral cortex (New York, NY : 1991)* **20**, 2684-2693 (2010).
36. Sakurai, T., *et al.* Overlapping functions of the cell adhesion molecules Nr-CAM and L1 in cerebellar granule cell development. *The Journal of cell biology* **154**, 1259-1273 (2001).
37. Eaton, B.A., Fetter, R.D. & Davis, G.W. Dynactin is necessary for synapse stabilization. *Neuron* **34**, 729-741 (2002).
38. Venken, K.J.T., He, Y., Hoskins, R.A. & Bellen, H.J. P[acman]: a BAC transgenic platform for targeted insertion of large DNA fragments in D. melanogaster. *Science (New York, NY)* **314**, 1747-1751 (2006).
39. Warming, S., Costantino, N., Court, D.L., Jenkins, N.A. & Copeland, N.G. Simple and highly efficient BAC recombineering using galK selection. *Nucleic acids research* **33**, e36 (2005).
40. Haspel, J. & Grumet, M. The L1CAM extracellular region: a multi-domain protein with modular and cooperative binding modes. *Frontiers in bioscience : a journal and virtual library* **8**, s1210-1225 (2003).
41. Lee, T. & Luo, L. Mosaic analysis with a repressible cell marker for studies of gene function in neuronal morphogenesis. *Neuron* **22**, 451-461 (1999).
42. Hall, S.G. & Bieber, A.J. Mutations in the Drosophila neuroglian cell adhesion molecule affect motor neuron pathfinding and peripheral nervous system patterning. *Journal of neurobiology* **32**, 325-340 (1997).

43. Kristiansen, L.V., *et al.* Genetic analysis of an overlapping functional requirement for L1- and NCAM-type proteins during sensory axon guidance in Drosophila. *Molecular and cellular neurosciences* **28**, 141-152 (2005).
44. Martin, V., *et al.* The L1-type cell adhesion molecule Neuroglian is necessary for maintenance of sensory axon advance in the Drosophila embryo. *Neural Development* **3**, 10 (2008).
45. Bouley, M., *et al.* The L1-type cell adhesion molecule neuroglian influences the stability of neural ankyrin in the Drosophila embryo but not its axonal localization. *The Journal of neuroscience : the official journal of the Society for Neuroscience* **20**, 4515-4523 (2000).
46. Cavey, M., Rauzi, M., Lenne, P.-F. & Lecuit, T. A two-tiered mechanism for stabilization and immobilization of E-cadherin. *Nature* **453**, 751-756 (2008).
47. Gil, O.D., *et al.* Ankyrin binding mediates L1CAM interactions with static components of the cytoskeleton and inhibits retrograde movement of L1CAM on the cell surface. *The Journal of cell biology* **162**, 719-730 (2003).
48. Goossens, T., *et al.* The Drosophila L1CAM homolog Neuroglian signals through distinct pathways to control different aspects of mushroom body axon development. *Development (Cambridge, England)* **138**, 1595-1605 (2011).
49. Allen, M.J., Godenschwege, T.A., Tanouye, M.A. & Phelan, P. Making an escape: development and function of the Drosophila giant fibre system. *Seminars in cell & developmental biology* **17**, 31-41 (2006).
50. Boerner, J. & Godenschwege, T.A. Application for the Drosophila ventral nerve cord standard in neuronal circuit reconstruction and in-depth analysis of mutant morphology. *Journal of Neurogenetics* **24**, 158-167 (2010).
51. Godenschwege, T.A., Kristiansen, L.V., Uthaman, S.B., Hortsch, M. & Murphey, R.K. A conserved role for Drosophila Neuroglian and human L1-CAM in central-synapse formation. *Current biology : CB* **16**, 12-23 (2006).
52. Godenschwege, T.A., Hu, H., Shan-Crofts, X., Goodman, C.S. & Murphey, R.K. Bi-directional signaling by Semaphorin 1a during central synapse formation in Drosophila. *Nature Neuroscience* **5**, 1294-1301 (2002).
53. Bishop, D.L., Misgeld, T., Walsh, M.K., Gan, W.-B. & Lichtman, J.W. Axon branch removal at developing synapses by axosome shedding. *Neuron* **44**, 651-661 (2004).
54. Hoopfer, E.D., *et al.* Wlds protection distinguishes axon degeneration following injury from naturally occurring developmental pruning. *Neuron* **50**, 883-895 (2006).

55. Keller, L.C., *et al.* Glial-Derived Prodegenerative Signaling in the Drosophila Neuromuscular System. *Neuron* **72**, 760-775 (2011).
56. MacDonald, J.M., *et al.* The Drosophila cell corpse engulfment receptor Draper mediates glial clearance of severed axons. *Neuron* **50**, 869-881 (2006).
57. Schuster, C.M., Davis, G.W., Fetter, R.D. & Goodman, C.S. Genetic dissection of structural and functional components of synaptic plasticity. I. Fasciclin II controls synaptic stabilization and growth. *Neuron* **17**, 641-654 (1996).
58. Ruediger, S., *et al.* Learning-related feedforward inhibitory connectivity growth required for memory precision. *Nature* **473**, 514–518 (2011).
59. Hortsch, M., *et al.* The axonal localization of large Drosophila ankyrin2 protein isoforms is essential for neuronal functionality. *Molecular and cellular neurosciences* **20**, 43-55 (2002).
60. Godenschwege, T.A. & Murphey, R.K. Genetic interaction of Neuroglian and Semaphorin1a during guidance and synapse formation. *Journal of Neurogenetics* **23**, 147-155 (2009).
61. Terauchi, A., *et al.* Distinct FGFs promote differentiation of excitatory and inhibitory synapses. *Nature* **465**, 783-787 (2010).
62. Tran, T.S., *et al.* Secreted semaphorins control spine distribution and morphogenesis in the postnatal CNS. *Nature* **462**, 1065-1069 (2009).
63. Kizhatil, K., Wu, Y.-X., Sen, A. & Bennett, V. A new activity of doublecortin in recognition of the phospho-FIGQY tyrosine in the cytoplasmic domain of neurofascin. *Journal of Neuroscience* **22**, 7948-7958 (2002).
64. Buhusi, M., Schlatter, M.C., Demyanenko, G.P., Thresher, R. & Maness, P.F. L1 interaction with ankyrin regulates mediolateral topography in the retinocollicular projection. *Journal of Neuroscience* **28**, 177-188 (2008).
65. Nakamura, Y., Lee, S., Haddox, C.L., Weaver, E.J. & Lemmon, V.P. Role of the cytoplasmic domain of the L1 cell adhesion molecule in brain development. *The Journal of comparative neurology* **518**, 1113-1132 (2010).
66. Allen, M.J. & Godenschwege, T.A. Electrophysiological recordings from the Drosophila giant fiber system (GFS). *Cold Spring Harbor Protocols* **2010**, pdb.prot5453 (2010).

## 3.3. Additional data Neuroglian

### 3.3.1. Neuroglian controls synaptic stability

*3.3.1.1. Developmental time course of the retraction phenotype after Nrg RNAi*

A hallmark of neurodegenerative diseases is the progressive nature of the phenotype as it has been shown for example in ALS and Huntington`s disease (Boillee et al., 2006, Dion et al., 2009). To address the question if the retraction phenotype observed after *nrg* RNAi also has a progressive nature, I analyzed 2nd and early 3rd instar larvae and compared them to late 3rd instar larvae. I observed a significant increase in the number of retraction during larval development (Figure 17). Interestingly, already in 2nd instar larvae a high number of retractions including complete eliminations of muscle 4 NMJs can be observed (Figure 17 c, b).

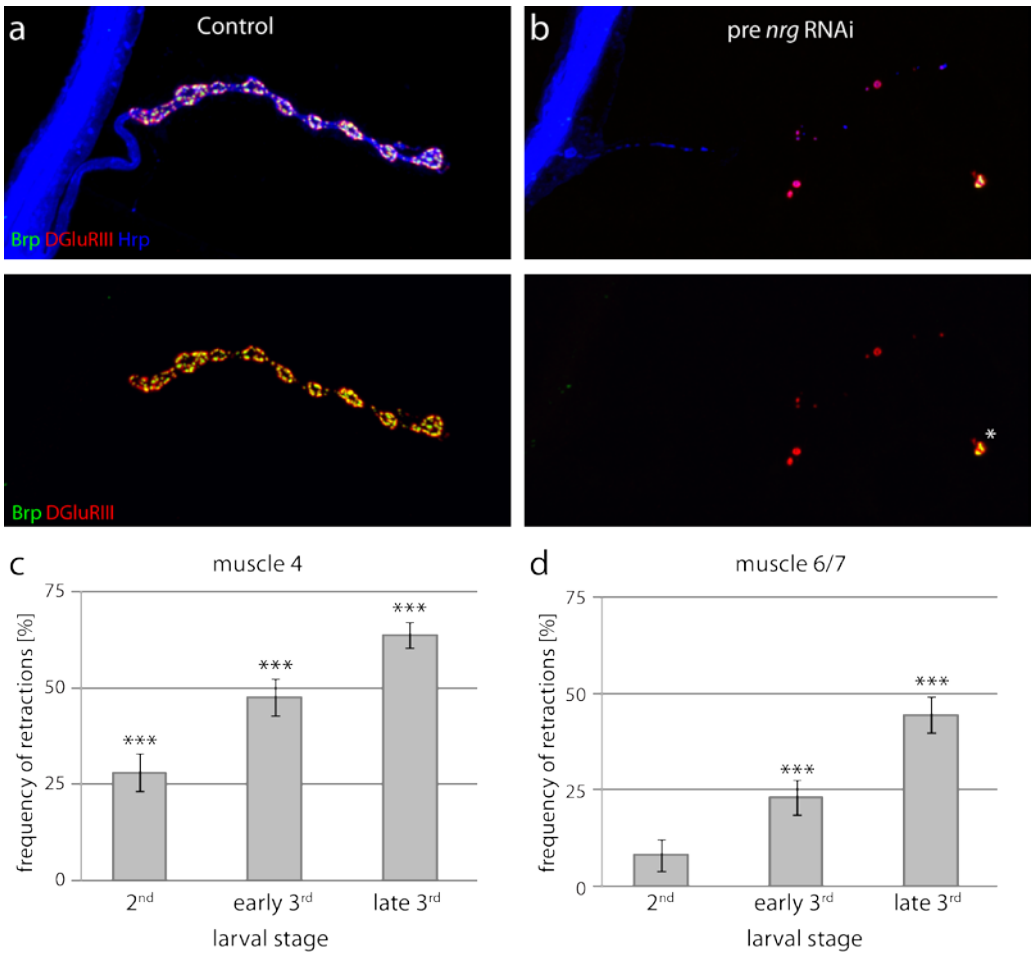


**Figure 17 - Progression of synapse instability during development after presynaptic Nrg RNAi**

**(a-b)** Muscle 4 NMJ of 2nd instar larvae stained for active zone marker Brp (green), glutamate receptors (red) and the presynaptic membrane (Hrp, blue). **(a)** An control muscle 4 NMJ with opposing pre- and postsynaptic markers and an intact presynaptic membrane (control: *elav*$^{C155}$-Gal4; UAS-*dcr2* x w$^{1118}$). **(b)** A muscle 4 NMJ after RNAi mediated knock down of Nrg. An almost complete elimination is shown. Only glutamate cluster shows opposing Brp staining but no connection to the motoneuron axon can be observed. Remnants of clustered glutamate receptors and the presynaptic membrane show that the NMJ was properly formed and became instable due to the loss of Nrg. **(c)** Quantification of retraction frequency after *nrg* RNAi using *elav*$^{C155}$-Gal4; UAS-*dcr2* on muscle 4 during development from the 2nd instar larval stage to the late 3rd instar larval stage. A progressive increase in the retraction frequency can be observed. Importantly already in 2nd instar larvae a significant number of retractions can be observed ($P \leq 0.0001$, n = 10-20 animals analyzed in segment A2-A6). **(d)** Quantification of retraction frequency after presynaptic *nrg* RNAi on muscle 6/7 during development from the 2nd instar larval stage to the late 3rd instar larval stage (Gal4 driver line: using *elav*$^{C155}$-Gal4; UAS-*dcr2*). A progressive increase in the retraction frequency can be observed. Here in the early 3rd instar larvae a significant number of retractions can be observed (n = 10-20 animals analyzed in segment A2-A6). Scale bar in **(a)** corresponds to **(a)** and **(b)**, 10µm. Error bars in **(c)** and **(d)** represent SEM.

Thus, we can conclude that Nrg is required for the maintenance of the presynaptic nerve terminal and the loss of Nrg results in a progressive loss of synapses.

### *3.3.1.2. Postsynaptic knock down of Nrg in Ank2 binding mutants results in synaptic retractions*

Next, I tried to further analyze the contribution of postsynaptic Neuroglian for the stabilization of NMJs. As discussed in the submitted manuscript, neither postsynaptic *nrg* RNAi nor the deletion of the Ankyrin binding motif of the Nrg167 isoform has an impact on synapse stability. However, by combining these two techniques, I can show here that indeed the homophilic interaction of Nrg contributes to synapse stability. I knocked down Nrg in the muscle via RNAi in the background of either *nrg*$^{14}$/y; P[*Nrgwt*] or *nrg*$^{14}$; P[*Nrg180*$^{\Delta FIGQY}$]. Only in the background of the Ank2 binding mutant I observed a significant increase in synaptic retractions in comparison both conditions alone (Figure 18). Exemplary images for muscle 4 and muscle 6/7 are shown (Figure 16 b, d). Not only the frequency of retraction but also the severity of retractions was significantly increased (Figure 16 f).

From this experiment I can conclude that homophilic interactions of Nrg between the motoneuron and the muscle indeed contribute to the synapse stabilization function of Neuroglian at the NMJ.

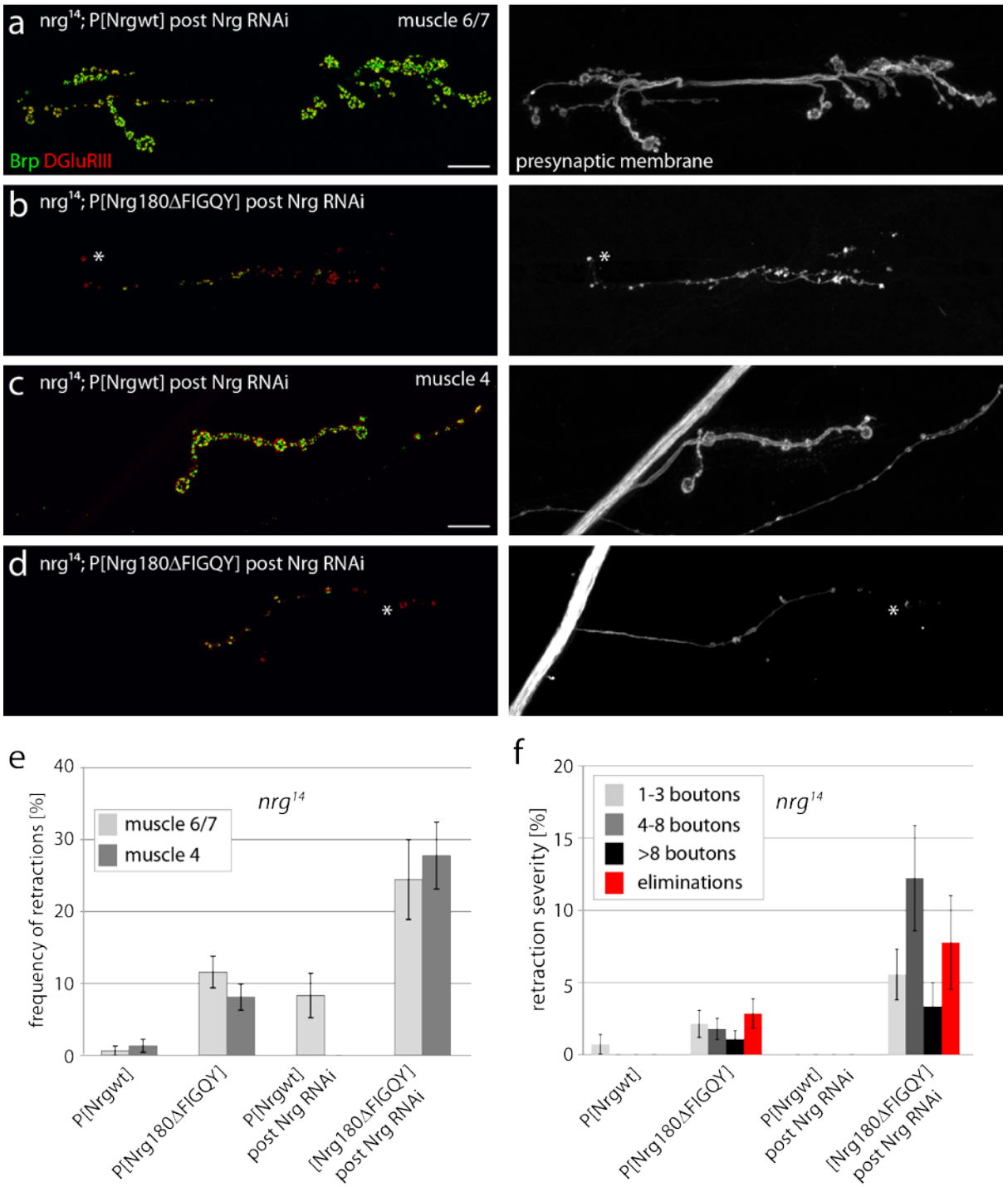


**Figure 18 - Postsynaptic knock down of Nrg in Ank2 binding mutants results in an increase in synaptic retractions**

**(a-d)** Larval muscle 6/7 and mu4 NMJ stained for presynaptic active zone marker Brp (green) and postsynaptic glutamate receptors (DGluRIII, red) as well as the presynaptic membrane (Hrp, white). **(a, c)** Larval muscle 6/7 and muscle 4 NMJs of animals that lost postsynaptic Nrg167 due to RNAi mediated knock down in the background of *nrg*$^{14}$; P[*Nrgwt*] (post Gal4 line: BG57-Gal4). Pre- and postsynaptic markers are nicely opposing each other and the membrane is intact. **(c-d)** In contrast, muscle *nrg* RNAi in the background of *nrg*$^{14}$; P[*Nrg180*$^{\Delta FIGQY}$] leads to severe synaptic retractions. **(d)** Quantification of retraction frequency on muscle 6/7 and 4. Loss of Nrg167 in the muscle leads to a significant increase ($P \leq 0.0001$ for muscle 4 and $P = 0.015$ for muscle 6/7 *nrg*$^{14}$; P[*Nrg180*$^{\Delta FIGQY}$] in

comparison to *nrg*$^{14}$; P[*Nrg180*$^{\Delta FIGQY}$]; post *Nrg* RNAi , n = 6-28). **(e)** Quantification of retraction severity based on the number of unopposed DGluRIII cluster. Scale bar in **(a)** corresponds to **(a-d)**, 10 µm, insets 5 µm. Error bars **(e)** and **(f)** represent SEM.

*3.3.1.3. Neuroglian in glial cells contributes to synapse stability at the NMJ*

Studies at the *Drosophila* larval NMJ and the vertebrate NMJ highlighted the role of glial cells during synapse maintenance and elimination (Feng et al., 2005; Keller et al., 2011). At the *Drosophila* NMJ a prodegenerative glial-derived signaling framework has been described and mutants of this signaling complex can partially suppress the retraction phenotype of *ank2* and *spec* mutants (Keller et al., 2011). Since Neuroglian is also highly expressed in glial cells, I tested the potential requirement of glial Nrg for synapse stability. Using a glial specific Gal4 line, I knocked down Nrg selectively in glial cells (Xiong et al., 1994). As shown in Figure 19, I observed a significant increase in retractions after glial knock down of Nrg (Figure 19). The phenotype was enhanced when co-expressing *dcr-2* (Figure 19 c). To analyze the potential contribution of an Nrg-Ank interaction, I also knocked down Ankyrin1 in glial cells. However, I did not observe a significant number of retractions in these animals (Figure 19 c). This construct was used in a previous study to knock down Ank1 in the muscle showing the efficiency of this particular genetic tool (Pielage et al., 2006).

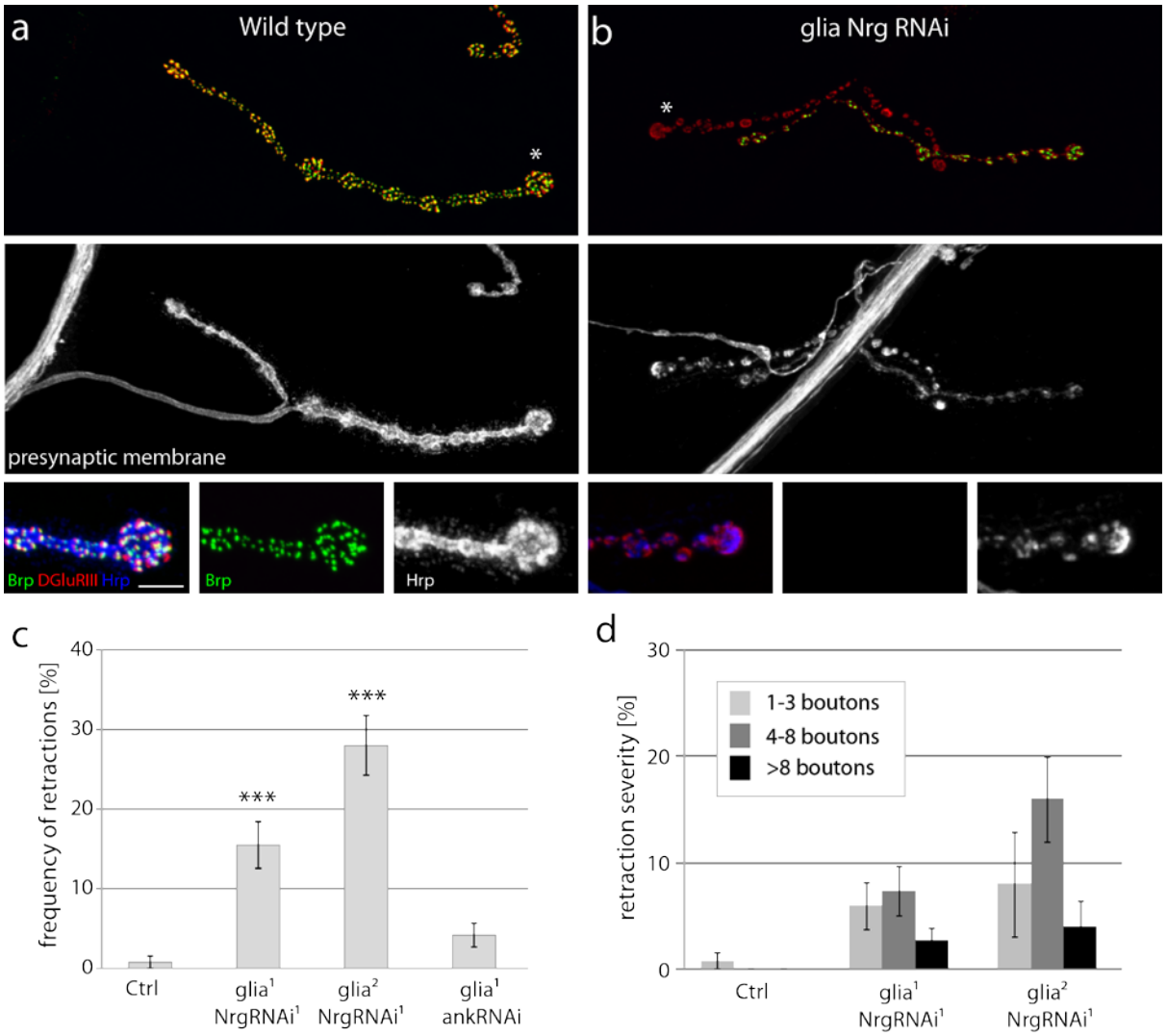


**Figure 19 - Knock down of Neuroglian in glial cells results in instable NMJ in L3 larvae**

**(a-b)** Muscle 4 NMJ stained for active zone marker Brp (green), glutamate receptors DGluRIII (red) and the presynaptic membrane (Hrp, blue, white). **(a)** A wild type muscle 4 NMJ with opposing pre- and postsynaptic markers and an intact presynaptic membrane. The asterisk indicates the area shown in the insets below. **(b)** A muscle 4 NMJ after glial *nrg* RNAi. The presynaptic marker Brp is lost completely from one NMJ terminal, the membrane is fragmented and the glutamate receptors clusters together whereas the other NMJ terminal seems to be stable. The asterisk indicates the area shown in the insets below. **(c)** Quantification of retraction frequency on muscle 4. Gal4 driver legend: glia$^{1}$= *repo*-Gal4, glia$^{2}$ = UAS-d*rc2*; *repo*-Gal4. RNAi$^{1}$ line = VDCR6688. Control: glia$^{1}$ x w$^{1118}$. The knock down of Nrg167 in glial cells leads to a significant increase in synaptic retractions which is increased upon co-expression of Dcr-2, whereas knock down of Ank1 does not impair synapse stability ($P \leq 0.0001$ for glia$^{1/2}$*Nrg* RNAi$^{1}$ in comparison to glia$^{1}$wt, P = 0.049 glia$^{1}$wt versus glia$^{1}$*ank1* RNAi, n = 5-12). d) Quantification of retraction severity based on the number of unopposed DGluRIII cluster. Scalebar in **(a)** corresponds to **(a, b)**, 10 µm, insets 5 µm. Error bars in **(c)** and **(d)** represent SEM.

These results indicate that not only presynaptic but also glial Nrg is involved in synapse stabilization and that this function is Ank1 independent. This is in accordance with the observation from the “knock-in” mutation analysis where no retractions have been observed

in *nrg*$^{14}$; P[*Nrg167*$^{\Delta FIGQY}$] animals that cannot bind Ankyrin1. In addition, it has been shown that the Gal4 line *elav*$^{C155}$ might also express Gal4 in glial cell (Berger et al., 2007; Robinow and White, 1988; Robinow and White, 1991; Yao and White, 1994), thus the loss of Nrg in glial cells might contribute to the synaptic retractions observed in the RNAi assay.

### 3.3.2. Neuroglian controls synapse growth at the NMJ

I identified the interaction between Neuroglian and Ankyrin2 as important for growth regulation as an impairment of this interaction led to an almost 2-fold increase in bouton number and NMJ length and a corresponding decrease in bouton area (chapter 3.2, submitted manuscript). Further analyses of the RNAi phenotype of *Nrg*, "knock-in" *Nrg* mutations, hypomorphic *Nrg* mutations and the overexpression of Nrg-Ank2 binding mutants in respect of NMJ growth described here confirmed these results.

*3.3.2.1 RNAi mediated loss of Neuroglian increases bouton number*

Firstly, I analyzed growth related defects after the RNAi knock down of Nrg. As shown in Figure 20, the reduction of presynaptic Nrg levels led to a significant increase in bouton number (Figure 20 c, d). In addition, a significant increase of membrane protrusions has been observed (Figure 20 b, c, e, Table 30) after both pre- and postsynaptic knock down of Nrg. This phenotype has been described recently for the actin capping molecule *hts* and further demonstrates the control of growth by *nrg* (Pielage et al., 2011). A similar number of these protrusions has been observed in the *nrg*$^{14}$; P[N*rg180*$^{\Delta FIGQY}$] animals (Table 31). This indicates that the growth defects observed after RNAi mediated knock down of Nrg are caused by the reduction of Nrg-Ank2 binding in the presynaptic motoneuron.

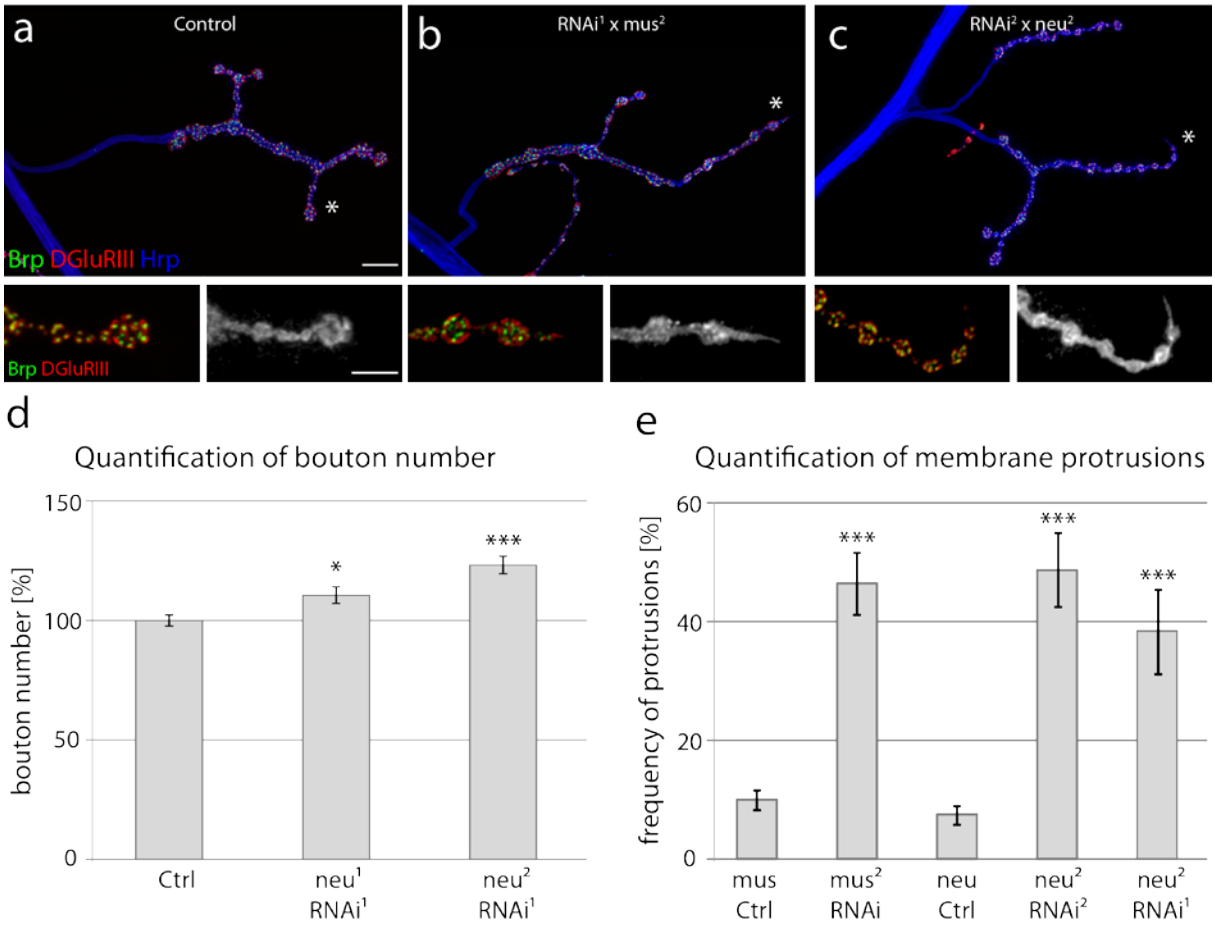


**Figure 20 - Pre- and postsynaptic knock down of Neuroglian results in growth defects**

(a-c) Muscle 4 NMJs stained for the presynaptic active marker Brp (green), postsynaptic glutamate receptors (red) and the presynaptic membrane (Hrp, blue, white). (a) A control muscle 4 NMJ with a normal size and a nicely formed terminal bouton highlighted in the insets below (asterisk). (b) A muscle 4 NMJ after postsynaptic knock down of Nrg. The NMJ terminal is normally size however shows a membrane protrusion at the terminal bouton highlighted in the inset below (asterisk). (c) A muscle 4 NMJ after presynaptic knock down of Nrg. The NMJ shows an increase in bouton number and membrane protrusion at the terminal bouton highlighted in the inset below. (d) Quantification of bouton number after presynaptic knock down of Nrg based on Synapsin/Dlg staining. A significant increase of bouton numbers can be observed for both knock down conditions ($P = 0.013$ and $\leq 0.001$ respectively, n = 50-123 NMJs segment A2-A6) (d) Quantification of protrusion frequency at still stable synapses. Both pre and postsynaptic knock down of Nrg resulted in a highly significant increase of membrane protrusions ($P \leq 0.0001$ for neu $^{2}$RNAi$^{2}$ and mus$^{2}$RNAi$^{1}$, $P = 0.0062$ for neu$^{2}$RNAi$^{1}$, n = 8-16 animals). Legend Gal4 driver lines: neu$^{1}$ = *elav*$^{C155}$-Gal4; neu$^{2}$ = *elav*$^{C155}$-Gal4; *ok371*-Gal4; mus$^{2}$ = UAS-*drc2*; *BG57*-Gal4. Legend RNAi lines: RNAi$^{1}$ = VDRC6688, RNAi$^{2}$ = VDRC107991. Scale bar in **(a)** corresponds to **(a-c)**, 10 µm, insets 5 µm. Error bars **(d)** and **(e)** represent SEM.

### *3.3.2.2. Analysis of hypomorphic Neuroglian mutants*

To further validate our RNAi and MARCM results, I analyzed hypomorphic *nrg* mutations that have been shown to be important for synapse formation and function in the adult fly, *nrg*$^{849}$ and *nrg*$^{305}$ (Boerner and Godenschwege, 2010; Godenschwege et al., 2006). I analyzed

both homozygous hypomorphic mutants and in combination with the *nrg*$^{14}$ null mutant. Both mutations showed a strong growth related phenotype with an increase in NMJ size and a decrease in the bouton area (Figure 21 c, d, Figure 22 e, g-I, Table 32). Interestingly, only the *nrg*$^{305}$ mutations showed a significant number of synaptic retractions (Figure 22 e, f). The analysis of the Nrg levels in larval brains of these mutants revealed that only in the *nrg*$^{305}$ mutation the levels of Nrg are highly reduced (compare Figure 21 b and 22 c). This is in accordance with previous studies (Godenschwege et al., 2006; Yamamoto et al., 2006). Whereas *nrg*$^{305}$ affects Nrg levels *nrg*$^{849}$ partially affects homophilic binding (Godenschwege et al., 2006; Yamamoto et al., 2006).

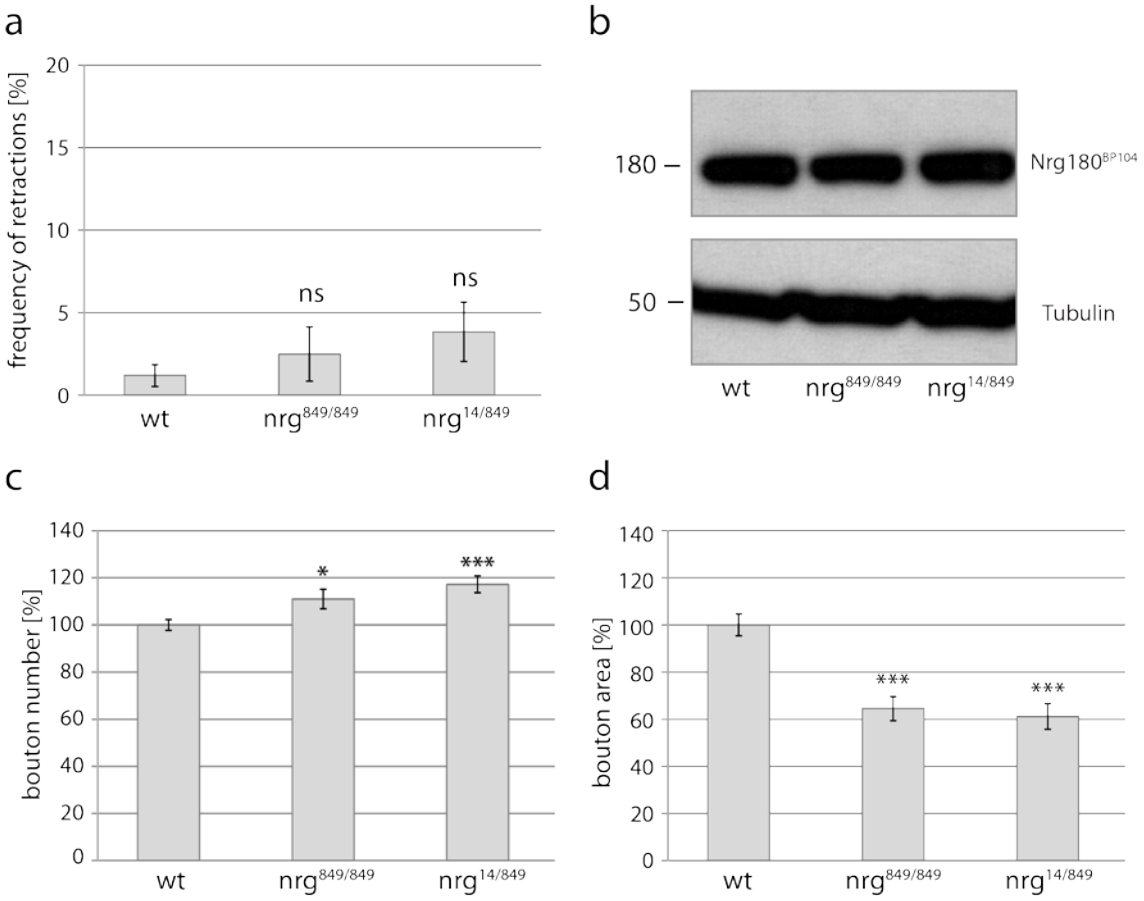


**Figure 21 - Instability and growth defects in hypomorphic *nrg*$^{849}$ mutants**

**(a)** Quantification of synaptic retractions on muscle 4. Homozygous *nrg*$^{849}$ and in combination with *nrg*$^{14}$ did not lead to a significant increase in synaptic retractions at muscle 4 (P = 0.39 and P = 0.1 respectively, n = 8-25 animals). **(b)** Western blot analysis of larval brain extracts. Wild type larval brains are compared to *nrg*$^{849}$ and *nrg*$^{14/849}$ brains for the expression level of Nrg180 using the Nrg180$^{BP104}$ antibody. Tubulin was used as a loading control. No change in Nrg180 levels has been observed for both mutant combinations. **(c, d)** Quantification of growth related phenotypes of *nrg*$^{849}$ and *nrg*$^{14/849}$ animals. Bouton number and bouton area are significant changed in these mutants

($P \leq 0.0001$ for bouton area, $P = 0.021$ and $P \leq 0.0001$ respectively for bouton number, n = 45-123 NMJs analyzed). Error bars in **(a, c, d)** represent SEM.

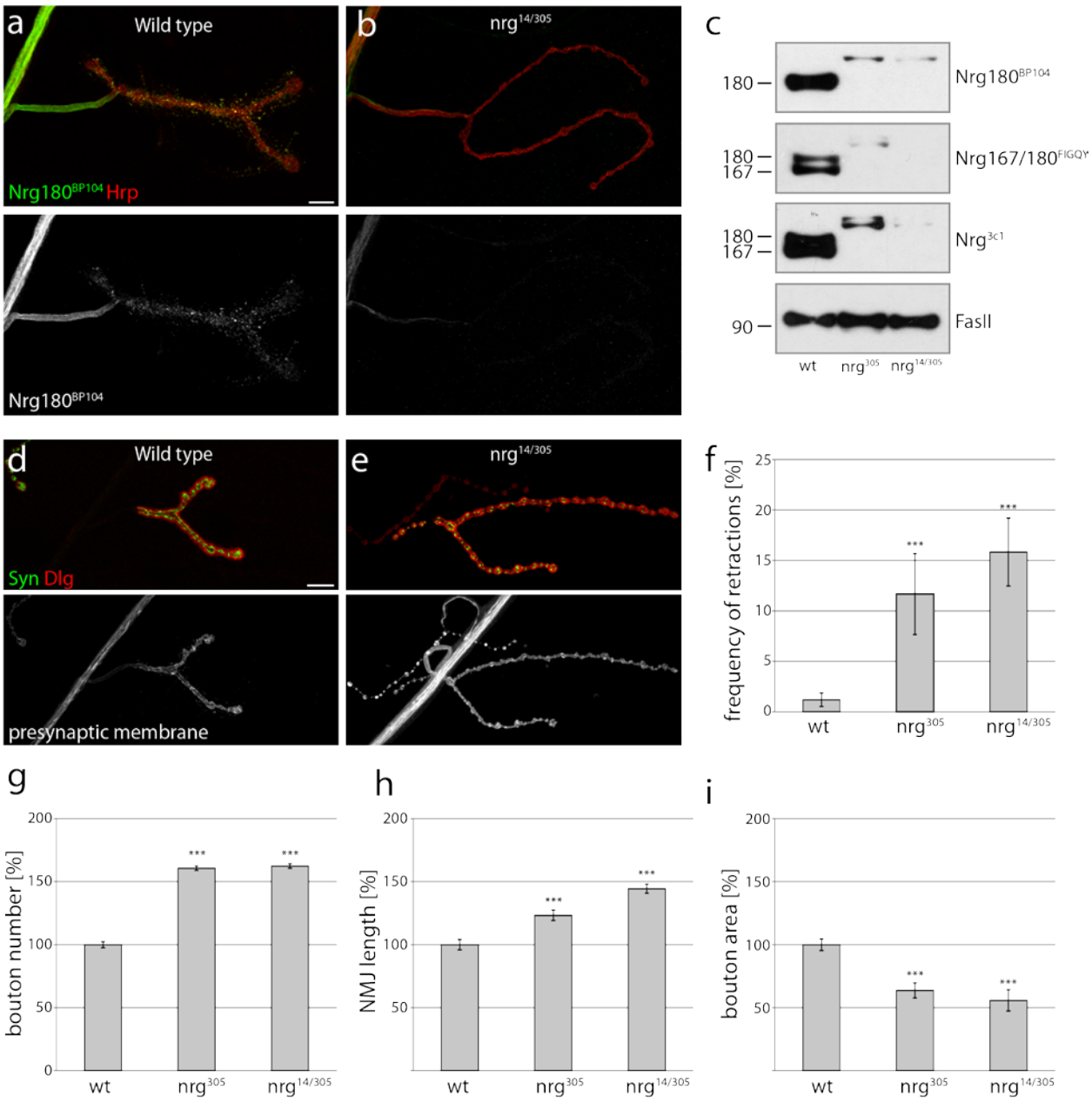


**Figure 22 - Hypomorphic Nrg mutations affect NMJ growth and stability**

**(a-c)** Analysis of Nrg protein levels in hypomorphic *nrg*$^{305}$ and *nrg*$^{305/14}$ mutant animals using immunohistochemistry and western blots. **(a)** Wild type muscle 4 NMJ stained for Nrg180 (Nrg180$^{BP104}$, green, white) and the presynaptic membrane (Hrp, red). Nrg is present throughout the presynaptic nerve terminal. **(b)** A *nrg*$^{305/14}$ mutant NMJ demonstrating a severe reduction in axonal and synaptic Nrg180 levels. **(c)** Western blots of larval brains demonstrating that the *nrg*$^{305}$ mutations equally reduces the levels of Nrg167 and Nrg180 caused by the insertion of a GFP-trap transposon in the intron upstream of the Nrg167 exon encoding the Ank2 binding motif. Blots are shown testing either only Nrg180 (Nrg180$^{BP104}$) or both isoforms (Nrg$^{FIGQY}$ and Nrg$^{3c1}$). FasII is used as a loading control. **(d, e)** Analysis of NMJ growth and stability using the presynaptic vesicle marker Synapsin

(Syn, green), postsynaptic Dlg (red) and the presynaptic membrane marker Hrp (white). **(d)** In wild type synaptic vesicles are found in apposition to the postsynaptic marker Dlg indicating a stable NMJ. **(e)** A *nrg*$^{305/14}$ mutant NMJ is shown. An overgrown type-Ib NMJ can be seen next to a retracting Type Is NMJ identified by Dlg staining that is no longer opposed by synaptic vesicles and a fragmentation of the presynaptic membrane. Scale bar in **(a)** corresponds to **(a, b, d, e)**, 10 µm, inset 5 µm. **(f)** Quantification of retraction frequencies. A highly significant increase in the number of retraction events can be observed in homozygous *nrg*$^{305}$ animals and in heterozygous *nrg*$^{305/14}$ mutant animals ($P \leq 0.001$ respectively, n = 12-13). The rate of retractions was similar to the one observed for Pacman mediated mutations of the Ank2 binding domain. **(g-i)** Quantifications of growth related phenotypes. Hypomorphic *nrg* mutations resulted in a significant increase in bouton number, NMJ length and a corresponding decrease in bouton area ($P \leq 0.0001$, n = 123 -144 for g; $P \leq 0.001$, n = 20 for h; $P \leq 0.0001$, n = 10 for i). Scale bar in **(a)** corresponds to **(a, b)**, scale bar in **(d)** corresponds to **(d, e)**, 10 µm. Error bars in **(f-j)** represent SEM.

### *3.2.2.3. Overexpression of Ank2 binding mutants impairs normal growth at the NMJ*

Finally, I tested whether overexpression of Nrg180wt or Nrg180$^{\Delta FIGQY}$ can affect NMJ development. I observed a significant increase in bouton number and NMJ length in animals overexpressing Nrg180ΔFIGQY but not Nrg180wt (Figure 23, Table 33). This demonstrates, that Nrg that cannot bind Ank2 can act as dominant negative construct disrupting NMJ growth control.

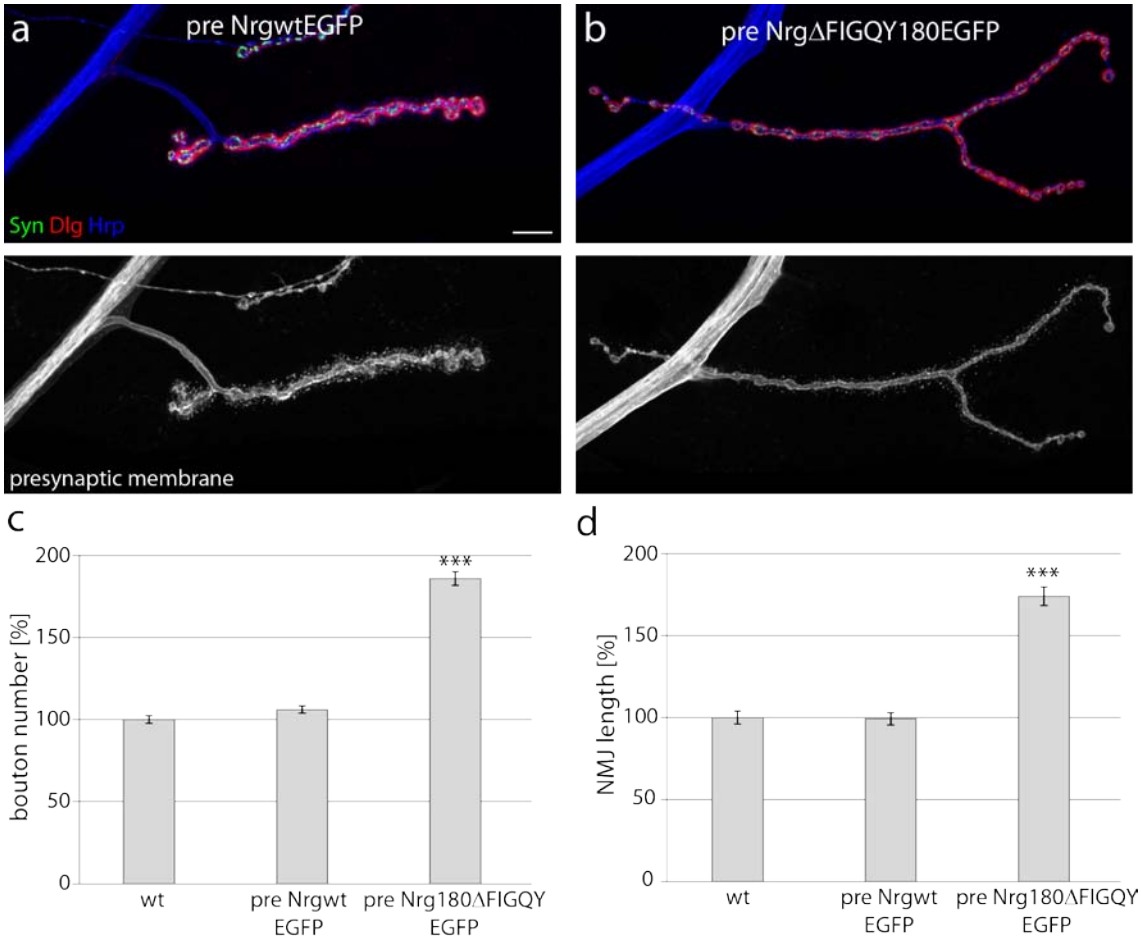

**Figure 23 - Overexpression of Nrg-Ank2 binding mutants affect NMJ growth**

**(a)** A muscle 4 NMJ overexpressing Nrg180wt protein stained for vesicle marker Synapsin (green) and postsynaptic density marker Dlg (red) as well as for the presynaptic membrane (Hrp, blue, white). This leads to normally sized NMJ. **(b)** Muscle 4 NMJ overexpressing Nrg180ΔFIGQY protein stained for Synapsin, Dlg and Hrp. An excess of protein with impaired Ank2 binding capacities led to an almost 2-fold increase in NMJ size. **(c-d)** Quantification of bouton number and NMJ length at muscle 4, an excess of Nrg180ΔFIGQY protein resulted in a significant increase in bouton number and NMJ length respectively ($P \leq 0.0001$ respectively, n = 114 -118 NMJs for bouton number, 20 NMJs for NMJ length). Scale bar in **(a)** corresponds to **(a, b)**, 10µm. Error bars in **(c)** and **(d)** represent SEM.

## 3.3.3. Genetic interactions of Neuroglian

To gain more insights into the mechanism how Nrg controls NMJ growth and stability, I performed genetic interaction experiments using mutations of genes previously identified as essential for NMJ stability and growth. Candidate genes included *ank2* as a direct interaction partner of *nrg* and *α-spec* as a stabilization protein (Garver et al., 1997; Pielage et al., 2005; Tuvia et al., 1997). Additionally, I analyzed mutants of the TGF-beta signaling pathway that regulate growth and stability at the larval NMJ (Aberle et al., 2002; Eaton and Davis, 2005; Rawson et al., 2003) and genes important for NMJ stability that are currently under investigation in the lab.

### *3.3.3.1. Neuroglian interacts genetically with ank2 and α-spectrin*

*Ank2* and *α-* and *β-Spec* are part of a molecular network underlying the cell membrane that is important for synaptic stability (Koch et al., 2008; Pielage et al., 2008; Pielage et al., 2005; Pielage et al., 2006, Figure 9). I showed that the loss of Ank2-Nrg interaction results in synaptic retractions. To analyze a potential genetic interaction of *ankyrin* and *spectrin* with *nrg* I combined the Pacman rescue assay with the classical mutations $ank2^{518}$ and $\alpha\text{-}spectrin^{rg41}$. I considered a genetic interaction if in the $nrg^{14}$/y; P[$Nrg180^{\Delta FIGQY}$] animals with the respective mutation in heterozygosity the number of retractions was more than 2-fold increase in comparison to the sum of the retraction from $nrg^{14}$; P[*Nrgwt*] and $nrg^{14}$/y; P[$Nrg180^{\Delta FIGQY}$] together (material and methods chapter 4.2.5.). Interestingly, I observed a highly significant increase in synaptic retractions for both mutations (Figure 24 c, Table 34). Thus, only the reduction of either Ank2 or α-Spec levels in $nrg^{14}$/y; P[$Nrg180^{\Delta FIGQY}$] but not in $nrg^{14}$; P[*Nrgwt*] background impaired synapse stability. Exemplary images also demonstrate the increase in retraction severity (Figure 24 a, b, d).

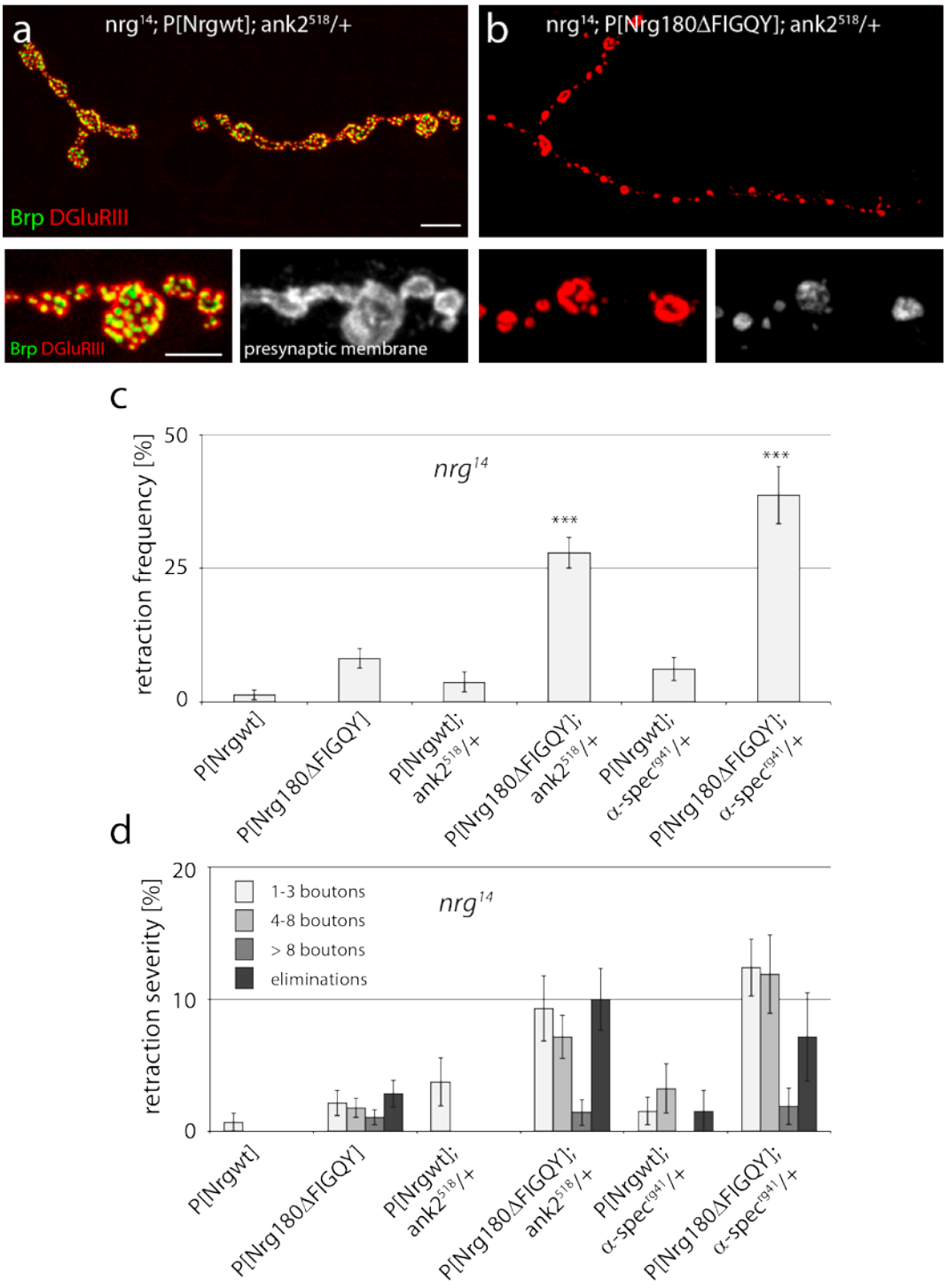


**Figure 24 - Genetic interaction of Neuroglian with Ank2 and α-Spectrin**

**(a-b)** Larval muscle 4 NMJ stained for presynaptic active zone marker Brp (green) and postsynaptic glutamate receptors (DGluRIII, red) as well as the presynaptic membrane (Hrp, white). **(a)** A *nrg*$^{14}$; P[*Nrgwt*] NMJ with reduced Ank2 levels due to the introduction of the *ank2*$^{518}$ mutation in heterozygosity. Pre- and postsynaptic markers are opposing each other and the membrane is intact (inset) indicating a stable NMJ. **(b)** A *nrg*$^{14}$; P[*Nrg180*$^{\Delta FIGQY}$] NMJ with reduced Ank2 levels due to the introduction of the *ank2*$^{518}$ mutation in heterozygosity. This NMJ is completely eliminated based on the loss of all Brp protein, the few visible highly clustered glutamate receptors and the highly fragmented membrane. **(c)** Quantification of retraction frequency. The introduction of one copy of

either the *ank2*$^{518}$ mutation or the *α-spec*$^{rg41}$ mutation in the *nrg*$^{14}$; P[*Nrg180*$^{\Delta FIGQY}$] background leads to highly significant increase in retraction number in comparison to *nrg*$^{14}$; P[*Nrg180*$^{\Delta FIGQY}$] alone ($P \leq 0.0001$, n = 8-25 animals). **(d)** Also the severity of retractions is increased based on the number of unopposed glutamate receptor cluster. Scale bar in **(a)** corresponds to **(a-b)**, 10µm, insets 5 µm. Error bars in **(c)** and **(d)** represent SEM.

These experiments further demonstrate that the Nrg-Ank2 interaction is essential for synapse stability and that impairing the interaction generates a genetic background that is highly sensitive to protein levels of other stability genes.

### *3.3.3.2. TGF-beta signaling modulates Neuroglian functions*

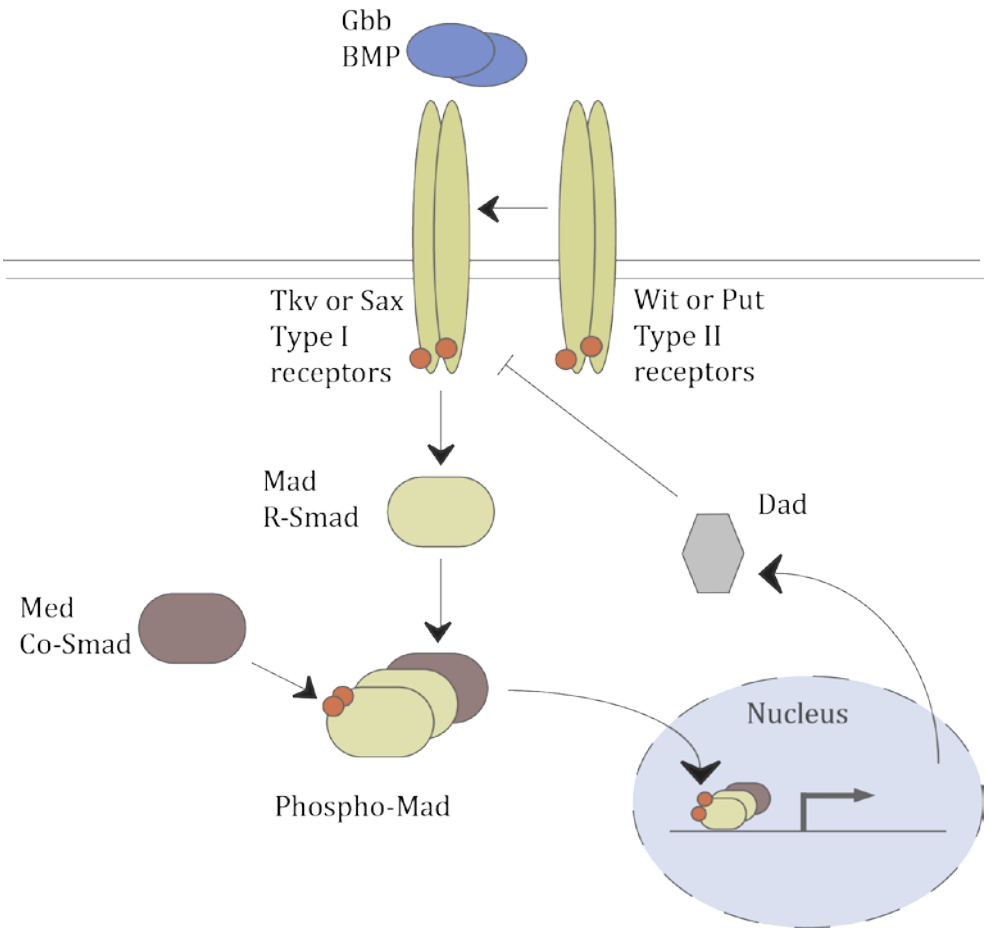


**Figure 25 - TGF-beta signaling in *Drosophila***

Retrograde TGF-beta signaling at the *Drosophila* larval NMJ controls synapse growth and stability. The BMP ligand Glass bottom boat (Gbb) is released from the muscle and binds to the tetrameric TGF-beta receptors containing type-I and type-II receptor subunits (Type I: Thickveins and Saxophone, Type II: Wishful thinking and Punt). Subsequently, the R-SMAD Mad becomes phosphorylated, binds to the Co-SMAD Med and translocates to the nucleus. Here, they act as a transcription factor controlling gene expression important for growth and stability. Negative regulators of TGF-beta signaling like Daughters against decapentaplegic (Dad) become expressed upon activation of TGF-beta signaling and inhibit further signaling.

At the *Drosophila* larval NMJ TGF-beta signaling is involved in NMJ growth regulation and mutations downregulating TGF-beta signaling have a reduced NMJ size and display synaptic retractions (Aberle et al., 2002; Eaton and Davis, 2005; Wan et al., 2000). Are TGF-beta signaling molecules potential interaction partners contributing to synaptic phenotypes observed in $nrg^{14}$/y; P[$Nrg180^{\Delta FIGQY}$] animals? To answer this question, I combined mutants of the TGF-beta signaling pathway with the Pacman assay. Here, I would like to highlight two interesting preliminary findings. Firstly, the reduction of neither the TGF-beta receptor type II Wishful thinking (Wit) nor the SMAD Mad did led to a significant increase in synaptic retractions as observed for Ank2 and α-Spec (Figure 26). In contrast the reduction of the TGF-beta receptor type I Thickveins (Tkv) did lead to a highly significant increase in synaptic retractions frequency and severity (Figure 28). Secondly, I observed a significant increase of bouton number when Wit was reduced in both $nrg^{14}$/y; P[$Nrg180^{\Delta FIGQY}$] and $nrg^{14}$; P[*Nrgwt*] animals (Figure 27). This increase in bouton number was not observed when Ank2 levels were reduced (Figure 27).

These preliminary results indicate that selective members of the TGF-beta signaling pathway contribute to the synapse stabilization and growth regulating function of Nrg. It will be interesting to see how and if other members of this pathway are involved as well.

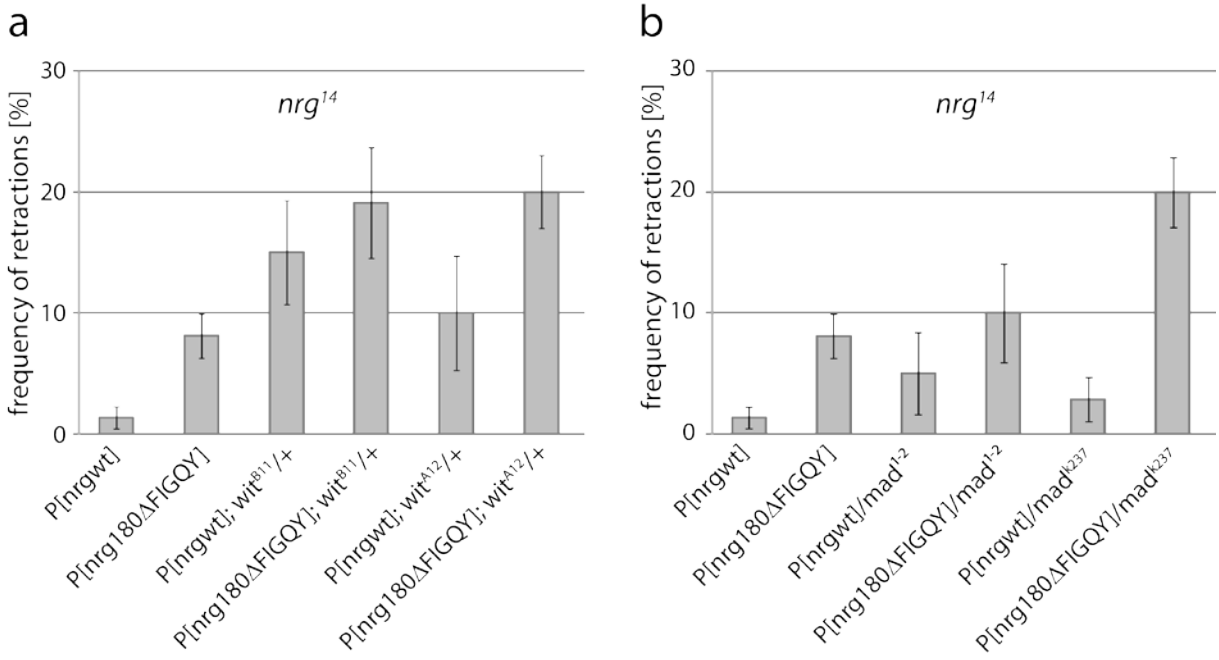


**Figure 26 - Genetic interaction of Neuroglian with Wit and Mad**

**(a)** Quantification of retraction frequency. The introduction of *wit* mutations in the Pacman rescued $nrg^{14}$ background leads to an increase in synaptic retraction for P[*Nrgwt*] and P[$Nrg180^{\Delta FIGQY}$]. There

is no significant difference between *nrg*$^{14}$; P[*Nrgwt*]; *wit*$^{mut}$ and *nrg*$^{14}$; P[*Nrg180*$^{\Delta FIGQY}$]; *wit*$^{mut}$ animals for both mutations ($P^{B11}$ = 0.57 and $P^{A12}$ = 0.84, n = 6-11). **(b)** The same result has been obtained when mad mutations (mad$^{1-2}$ and mad$^{k237}$) have been introduced into the Pacman rescue background (n= 4-15). Error bars in **(a)** and **(b)** represent SEM.

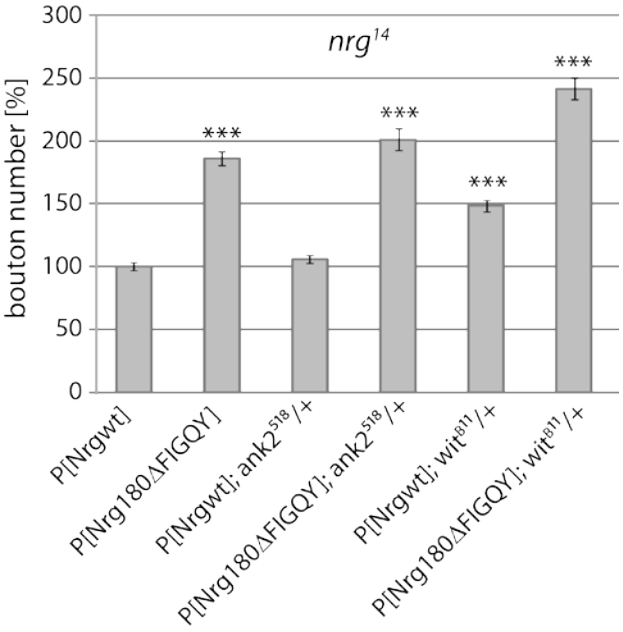


**Figure 27 - Reduction of wit signaling in Nrg pacman rescued animals influences NMJ growth**

Quantification of bouton number in *nrg*$^{14}$; P[*Nrgwt*] or *nrg*$^{14}$; P[*Nrg180*$^{\Delta FIGQY}$] animals that have reduced levels of the adaptor molecule Ank2 or the TGF-beta type II receptor Wishful thinking. The reduction of Ank2 does not have an additional influence on bouton number (P = 0.19, n = 76-98 NMJs analyzed) in comparison to the Pacman rescues. In contrast the reduction of Wit in the background of *nrg*$^{14;}$ P[*Nrgwt*] leads to an significant increase of bouton number ($P \leq 0.0001$ in comparison to *nrg*$^{14}$; P[*Nrgwt*] and *nrg*$^{14}$; P[*Nrgwt*]; *ank2*$^{518}$, n=70-98 NMJs in segment A2-A6 analyzed). In the *nrg*$^{14}$; P[*Nrg180*$^{\Delta FIGQY}$] rescue background the introduction of the *wit*$^{B11}$ mutation resulted in a significant increase of bouton number in comparison to *nrg*$^{14}$; P[*Nrg180*$^{\Delta FIGQY}$] ($P \leq 0.0001$, n = 46-122 NMJs in segment A2-A6 analyzed). Error bars represent SEM.

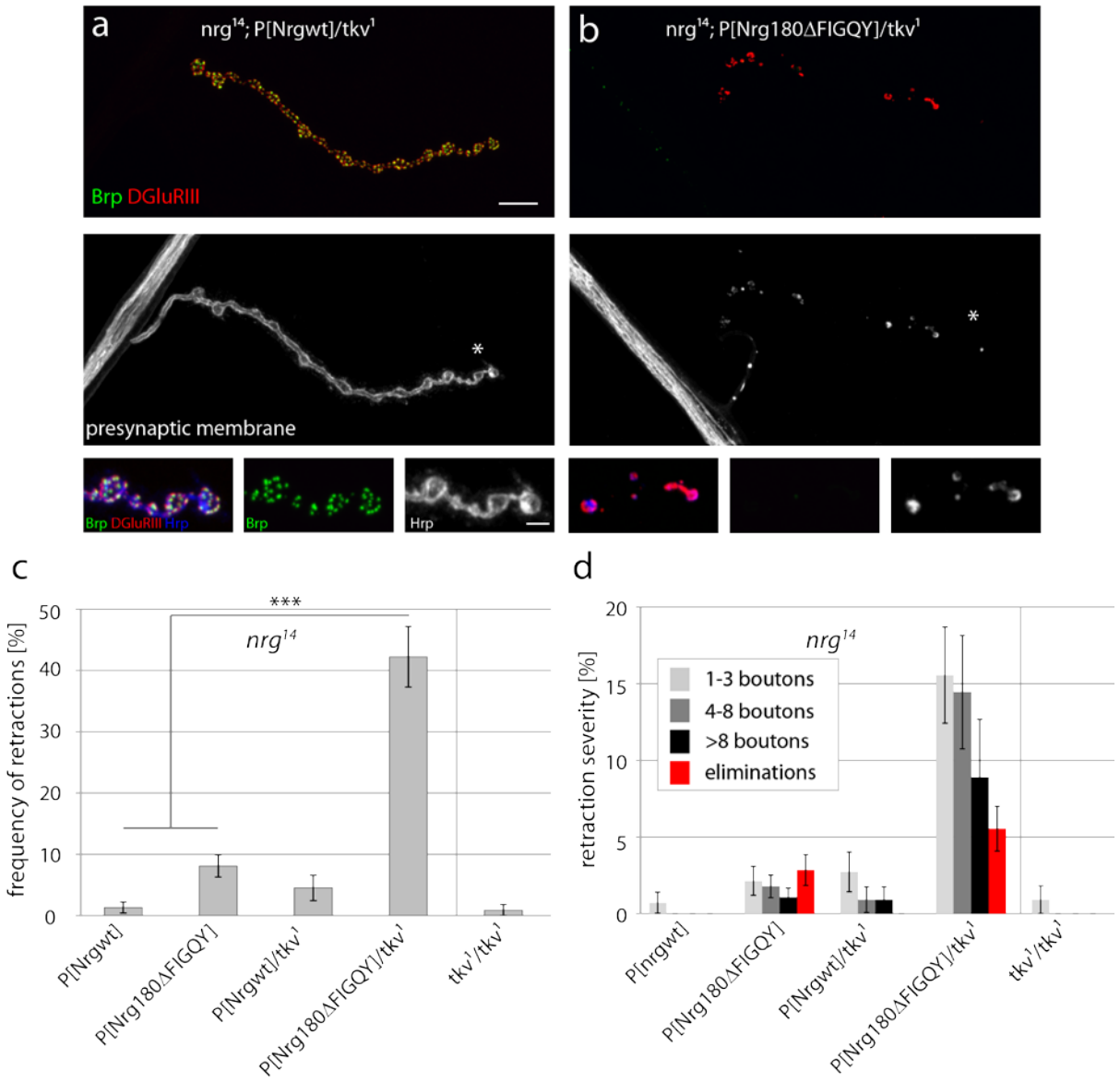


**Figure 28 - Genetic interaction between the TGF-beta receptor type I Thickveins and Neuroglian**

**(a-c)** Muscle 4 NMJ stained for presynaptic active zone marker Brp (green), postsynaptic glutamate receptors (DGluRIII, red) and the presynaptic membrane (Hrp, blue, white). **(a)** Muscle 4 NMJ of the genotype *nrg*$^{14}$; P[*Nrgwt*]/*tkv*$^{1}$. The apposition of Brp and DGluRIII as well as the intact membrane indicate a stable NMJ. The asterisk points to the area of the insets shown below. **(b)** Example of instable muscle 4 NMJ of the genotype *nrg*$^{14}$; P[*Nrg180*$^{\Delta FIGQY}$]/*tkv*$^{1}$ with a complete loss of Brp and the fragmentation of the membrane. Asterisk indicates the area shown in the insets. **(d)** Quantification of synaptic retraction frequency. Introduction of one copy of the *tkv*$^{1}$ hypomorphic mutation led to an highly significant increase in retractions ($P \leq 0.0001$, n = 9-11). The viable homozygous *tkv*$^{1}$ mutants did not display any destabilization effects (P = 0.75, n = 11-15 animals analyzed). **(e)** Quantification of the retraction severity. The number of boutons without Brp staining were counted and grouped into four categories. The percentage of these categories of all NMJs has been blotted for all genotypes in **(d)**. Also an increase in retraction frequency can be observed upon *tkv*$^{1}$ introduction into *nrg*$^{14}$; P[*Nrg180*$^{\Delta FIGQY}$]. Scale bar in **(a)** corresponds to **(a-c)**, 10µm, insets 5 µm. Error bars in **(d)** and **(e)** represent SEM.

## 3.4. The transcription unit *CG31708* encodes an Ig-domain protein important for synapse stability

### 3.4.1. CG31708 is important for synapse stability at the neuromuscular junction

In the RNAi screen I identified the Ig-domain protein CG31708. Pre- but not postsynaptic knock down of CG31708 resulted in severe synaptic retraction in 3rd instar larvae (Figure 29). The observed phenotype has some interesting characteristics which I would like to highlight here. No genetic or biochemical characterization of CG31708 has been performed so far. Since I identified CG31708 based on its retraction phenotype indicating a glue like function at the NMJ I named this gene "*uhu"* based on the famous German glue brand.

I observed two different phenotypes after presynaptic knock down of Uhu. On one hand classical retractions as described for other genes involved in NMJ maintenance (Figure 29 c) and on the other hand I observed motoneuron terminals where the presynaptic marker Brp was lost in proximal or central parts but still present in distal parts of a branch (Figure 29 b). This phenotype has never been described for other stability genes so far and might be either caused by synapse formation defects or characterizes a novel retraction mechanism. However the phenotype also shares features with classical retraction phenotypes including the aberrant clustering of glutamate receptors and the fragmentation of the presynaptic membrane (Figure 29 c). Thus the observed phenotype after *uhu* RNAi can either represent a novel retraction mechanism or combines synapse formation and stabilization defects.

In addition, the *uhu* phenotype displays motoneuron specificity. Whereas we observe a strong phenotype on muscle 6/7, 12 and 13, no retractions or formation defects can be observed on muscle 4 (Figure 29 d). So far ,all identified genes controlling synapse stability are required in all muscles and only differ in the retraction severity between muscles. *Nrg* RNAi for example displays the strongest phenotype at muscle 4 with 80% of all observed retractions being complete eliminations.

To understand the process of this special synapse destabilization/formation mechanism in more detail, I analyzed three different larval stages during larval development from 2nd instar larvae to late 3rd instar larvae. Interestingly, the retraction/formation phenotype observed and described above only develops in the last steps of larval development, since no significant increase of synaptic retractions can be observed in 2nd instar and early 3rd instar larvae

(Figure 30). In contrast, after *nrg* RNAi I observed already in 2nd instar larvae a significant number of retractions for example on muscle 4 (Figure 17 c). These observations strengthen the argument for the identification of a novel fast acting retraction mechanism.

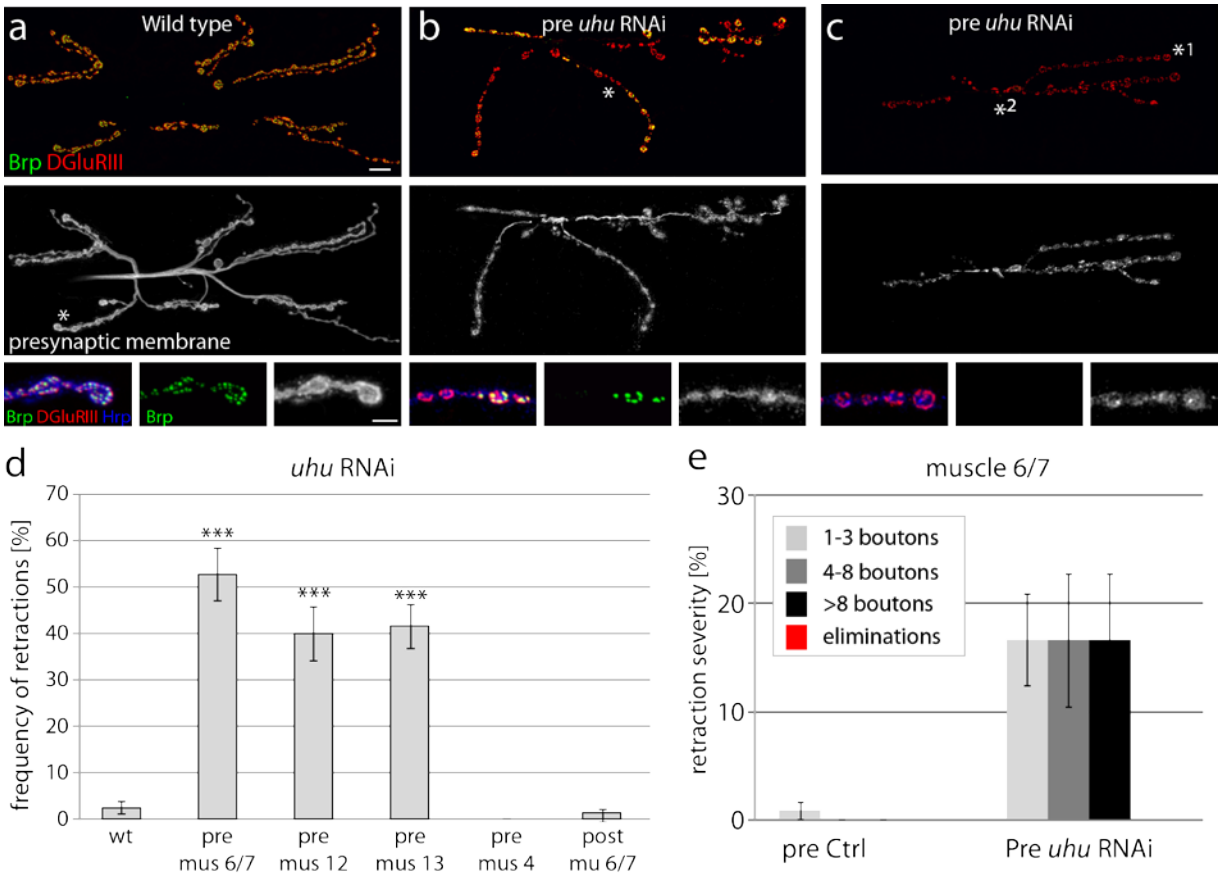


**Figure 29 - Presynaptic knock down of Uhu leads to severe synaptic retractions at a selection of NMJs**

**(a)** A wild type muscle 6/7 NMJ stained for active zone marker Brp (green) and postsynaptic glutamate receptors (DGluRIII, red). In addition the presynaptic membrane is stained using Hrp (white, blue). Pre- and postsynaptic markers are opposing each other and the membrane is continuously formed. This shows that this NMJ is stable. The asterisk indicates the region shown in the inset. **(b)** A muscle 6/7 NMJ after presynaptic *uhu* RNAi. Parts of the NMJ lost the presynaptic marker Brp and the membrane is partially fragmented. In the inset (asterisk) a part of a NMJ branch is shown where Brp was lost in proximal parts of the NMJ but still present in distal parts. **(c)** A muscle 6/7 NMJ after presynaptic *uhu* RNAi that lost the presynaptic marker Brp almost completely. $*^1$ is shown in higher magnification in the inset. $*^2$ indicates remaining Brp staining. **(d)** Quantification of retractions in ctrl (*elav*$^{C155}$-Gal4; *ok371*-Gal4 x w$^{1118}$) and after pre- and postsynaptic *uhu* RNAi. At muscle 6/7, 12 and 13 a highly significant number of retractions can be observed after presynaptic knock down ($P \leq 0.0001$, n = 6-12). In contrast, no synaptic retractions have been observed at muscle 4 and after postsynaptic knock down of Uhu. **(e)** Quantification of the retraction severity after presynaptic knock down of Uhu on muscle 6/7. The number of unopposed postsynaptic varicosities were counted and grouped into categories indicated in the legend. No complete eliminations have been observed. Gal4 driver legend: pre = *elav*$^{C155}$-Gal4; *ok371*-Gal4, post = *mef2*-Gal4. Scale bar in **(a)** corresponds to **(a-c)**, 10 µm, insets 5 µm. Error bars in **(d)** and **(e)** represent SEM.

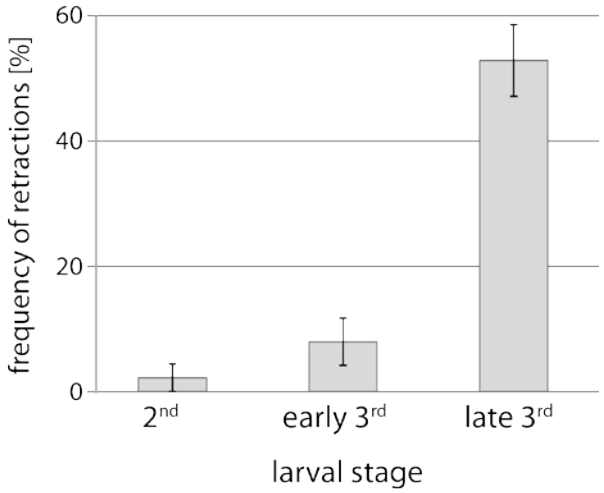


**Figure 30 - Development of retraction phenotype of Uhu during larval development on muscle 6/7**

Quantification of retraction frequency after presynaptic *uhu* RNAi during development from 2nd instar larvae to 3rd instar larvae is shown. Only in the last steps of larval development NMJs become instable. Error bars represent SEM.

In summary, the RNAi mediated knock down of Uhu showed that presynaptic Uhu is important at distinct larval NMJs and the unique features of the phenotype imply a novel mechanism of synapse disassembly. However, additional experiments have to be performed to validate this hypothesis.

### 3.4.2. Analysis of Uhu expression at the neuromuscular junction

To characterize a gene in more detail it is important to describe the expression pattern of the protein. Therefore, I generated an antibody against the last 150 amino acids of Uhu. Unfortunately, this antibody did not recognize wild type levels of Uhu either due to low levels of Uhu at the NMJ or to a low affinity of the antibody. Since we observe a phenotype after presynaptic knock down I can assume that Uhu has to be present at the NMJ. Thus, I cloned an UAS construct of Uhu and generated transgenic flies. This construct was used to overexpress Uhu either in the motoneuron or in the muscle and analyze if Uhu has the potential to localize to the NMJ. In the future it will be e.g. used for tissue-specific rescue experiments of *uhu* mutants. The presynaptic expression revealed an interesting feature of Uhu. Uhu was expressed weakly in the motoneuron axon and the nerve bundle but localized efficiently to the NMJ terminal (Figure 31 a). Within the bouton, I observed a honey-comb like structure (Figure 31 a). A similar expression pattern has been described for the Ig-domain protein FasII, which indicates that Uhu can be highly organized in subdomains of the

bouton and thus resembles features of other cell adhesion molecules. In addition, Uhu can also localize to the muscle side of the NMJ with a strong accumulation directly around the NMJ terminal and a more diffuse pattern on the muscle surface (Figure 32 b). Further analyses using co-stainings with markers for different synaptic and muscle departments are needed to characterize the expression pattern of Uhu in more detail. Importantly, no NMJ phenotype has been observed after pre- or postsynaptic overexpression of Uhu.

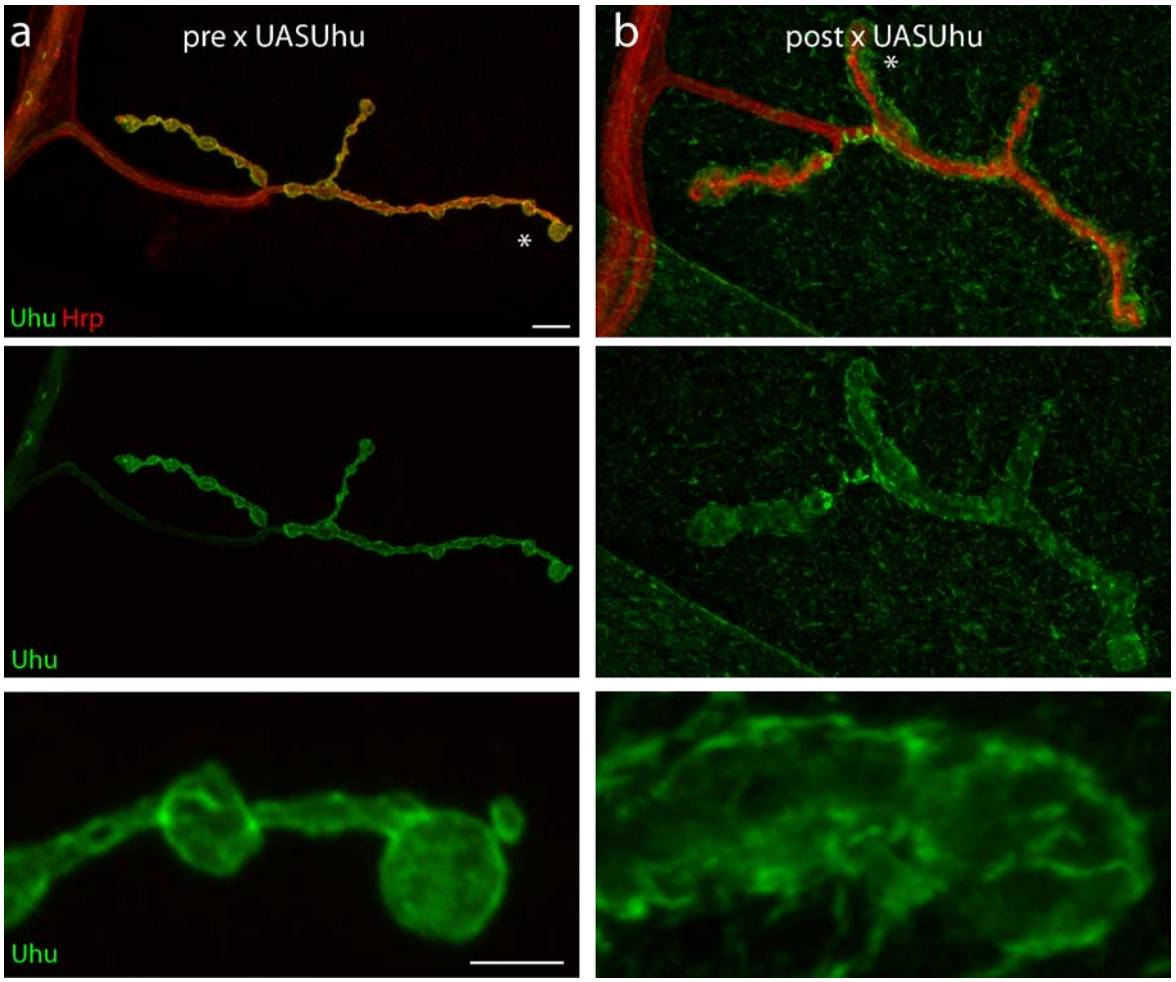


**Figure 31 - Analysis of Uhu expression in motoneurons and muscles**

**(a)** Presynaptic overexpression of Uhu using the Gal4 driver line *elav*$^{C155}$-Gal4; *ok371*-Gal4. A muscle 4 NMJ is shown which is stained for Uhu with the Uhu specific antibody (green) and the presynaptic membrane (Hrp, red). The inset shows the last boutons of a branch indicated by the asterisk. Uhu localized predominantly to the NMJ terminal and weaker to the motoneuron axon and the bypassing nerve. **(b)** Postsynaptic overexpression of Uhu using the Gal4 driver *mef2*-Gal4. A muscle 4 NMJ is shown stained with the Uhu specific antibody and Hrp to mark the presynaptic membrane. Uhu strongly accumulates in the muscle membrane directly around the NMJ terminal and was more diffusely distributed over the muscle. Scale bar in **(a)** corresponds to **(a-b)**, 10 µm, Scale bar in the insets corresponds to 5 µm.

In summary, Uhu has the potential to localize to both sides of the NMJ and might interact homophilically, however I could only identify a presynaptic function of Uhu so far.

### 3.4.3. Analysis of Uhu characteristics using bioinformatical tools

Uhu belongs to the class of Ig-like domain proteins. The Ig-domains belong to the I- and V-set family of Ig-domains as analyzed using Pfam (Punta et al., 2012). The first Ig-like domain of Uhu is classified as a V-set domain (PF07686) followed by two I-set domains (PF07679). I-set Ig domains are very common among cell adhesion molecules like NCAM, tyrosine protein kinase receptors and others. Hence, Uhu has the potential to act as a cell adhesion molecule based on the domain structure.

The RNAi mediated knock down of Uhu only affected a subset of motoneurons. Which genes are important to provide stability to the other motoneuron synapses? Is Uhu part of a molecular code controlling synapse stability at the larval NMJ? One possibility for such a code could be a number of proteins with a similar domain structure. Therefore, I analyzed the *Drosophila* genome (Flybase release 5.19) and searched for all Ig-like domain proteins with three Ig-domains. I found 27 genes that fitted this criterion. A more detailed analysis of these genes using multiple online bioinformatical tools revealed a cluster of 10 proteins with a high similarity to Uhu (Supplementary Figure 1 and 2). From these 10 proteins one displayed high similarity to Uhu based on the sequence and nature of the Ig-like domains (Supplementary Figure 1 and 2). This protein is encoded by the uncharacterized gene CG42368. The RNAi line targeting CG42368 did not give a phenotype at the larval NMJ. As this might be due to the failure to knock down CG42368 efficiently, a specific mutation has to be generated to assess potential functions at the NMJ.

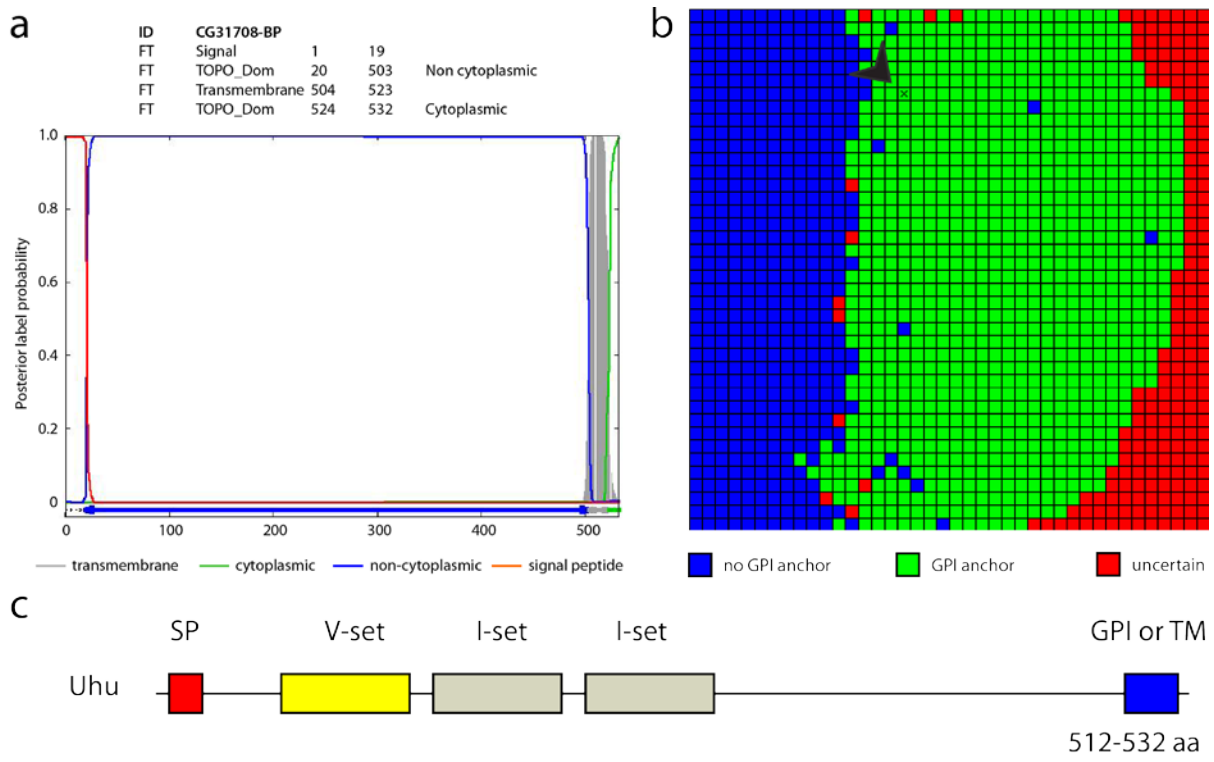


**Figure 32 - Analysis of structural characteristics of Uhu**

**(a)** The full length protein sequence of Uhu (CG31708-PB) was used to perform a Phoebius prediction. This program predicts signal peptides and transmembrane domains. The signal peptide of Uhu is predicted from amino acid 1-19 (red) and the transmembrane domain from amino acid 504-523 (grey). CG31708 has a relative short predicted cytoplasmic domain of 8 amino acids (aa 524-532, green) and a long extracellular domain from amino acid 19-503 (blue).**(b)** The full length protein sequence of Uhu (CG31708_PB) was analyzed for a potential GPI anchor using the online tool GPISOM. The program predicts a GPI anchor for Uhu as indicated by the cross in a green field of the prediction (highlighted by an arrowhead). **(c)** The predicted Uhu domain structure based on multiple bioinformatical tools: Uhu is a small protein of 512-532 amino acids depending on the isoform. A signal peptide has been identified in the very N-terminus for the localization to the endoplasmatic reticulum. One V-set Ig like domain and two I-set Ig-like domains are encoded in the *uhu* sequence. However it is unclear if Uhu has a GPI anchor or passes the membrane with a single transmembrane domain.

Next, I analyzed the structure and domains of Uhu and CG42368 in more detail (results of the other 9 genes are found in the Table 38). Using different prediction tools like Phoebius or SignalP (Kall et al., 2004; Petersen et al., 2011) I found that both Uhu and CG42368 have a signal peptide in the N-terminus region (Figure 32 a, c, Table 4). A signal peptide is often found in transmembrane, membrane-bound or secreted proteins. In contrast to the clear result concerning the signal peptide and the Ig-like domains, no final conclusion could be made about a potential transmembrane domain or a GPI-anchor (Table 4, Figure 32 c). Experiments addressing potential anchoring are required to address this question.

**Table 4 - Result of SignalP and Phoebius prediction**

| *CG number* | *SignalP* | *Phoebius* | | *GPI-SOM* |
|---|---|---|---|---|
| | Prediction | SP | TM | GPI anchor |
| CG42368-PA | Signal peptide | yes | yes/no | yes |
| CG31708-PB | Signal peptide | yes | yes | yes |

Uhu and CG42368 have been analyzed using the prediction tools SignalP, Phoebius and GPISOM. The outcome of these predictions is summarized for the presence of signal peptides (SP), transmembrane domains and GPI anchors. Both predictions agreed on the same result concerning the presence of a signal peptide. Signal peptides are about 19 amino acid long sequences at the N-terminus of proteins and are important for the localization to the endoplasmatic reticulum where posttranslational changes occur. Uhu has a predicted transmembrane domain whereas CG42368 did not give a clear result. The GPISOM prediction indicated a GPI anchor for both proteins.

What are potential homologs of Uhu in vertebrates? All 11 proteins that clustered around Uhu were blasted against the human refSeq. The best hit for all 11 proteins was an isoform of the Ig-domain protein Neurotrimin. Neurotrimin belongs to a family of GPI-anchored Ig-domain proteins called IgLONs (named after the first three identified members in rodents **L**AMP, **O**BCAM, **N**eurotrimin). In addition to Neurotrimin, opioid-binding CAM (OBCAM, named OPCML in human), Kilon (a **ki**ndred of Ig**LON**) and limbic-system associated protein (LAMP) belong to this family (Funatsu et al., 1999; Levitt, 1984; Marg et al., 1999; Pimenta et al., 1996; Schofield et al., 1989). Members of this family have been implicated in memory formation (Qiu et al., 2010), axon targeting, neurite outgrowth (Marg et al., 1999; Pimenta et al., 1995; Schafer et al., 2005) and cell adhesion (McNamee et al., 2002). For *Drosophila* the gene *lachesin* has already been proposed to be a potential homologue of the IgLON family (Strigini et al., 2006). *Lachesin* has been described as required for the formation of the blood-brain barrier and controls tracheal tube size and epithelial integrity (Llimargas et al., 2004). Interestingly, *lachesin* has been identified in the screen based on a weak retraction phenotype (Table 25) suggesting a role for this gene class in synapse stabilization.

In summary, Uhu is a novel Ig-like domain protein in *Drosophila* with a signal peptide in the very N-terminus and a potential GPI/TM domain (Figure 32 c) and represents a potential invertebrate member of the IgLON protein family required for synapse stability.

# 3. Discussion and Outlook

The aim of this study was the identification of cell adhesion molecules controlling synaptic stability and the characterization of potential underlying regulatory mechanisms. Here I will discuss and highlight results of this study not included and discussed in the submitted manuscript. These are:

(1) The ability to identify novel players in synapse stability using an RNAi-based screen.

(2) Integration of the identified candidates into a molecular network.

(3) Additional data about Neuroglian function during synapse stability and growth.

(4) The identification of the novel Ig-like domain protein Uhu.

(5) The existence of redundant mechanisms controlling synapse stability.

## 3.1. The RNAi-based screen allows the identification of novel cell adhesion molecules important for synapse development and stability

To identify novel cell adhesion molecules involved in neuronal circuit development at the *Drosophila* NMJ an unbiased RNAi screen was combined with a high resolution assay that allows the analysis of NMJs at single synapse resolution. I selected entire classes of cell adhesion molecules based on previous proposed functions during nervous system development such as synapse formation for Ig-domain proteins and LRRTMs (Biederer et al., 2002; Linhoff et al., 2009) and axon guidance for Cadherins and Semaphorins (Godenschwege and Murphey, 2009; Hummel and Zipursky, 2004; Petros et al., 2008).

The RNAi-based screening of candidates has several advantages compared to classical forward screening assays such as EMS- or P-element based screens. Firstly, the VDRC RNAi library (Dietzl et al., 2007) allows the screening of a specific subset of candidate genes of interest. Secondly, it allows spatial and temporal control of gene knock down using specific Gal4 driver lines (Brand and Perrimon, 1993), thus circumventing the early lethality caused by some mutations constraining the analysis of gene functions in later stages of development. However the technique also has some drawbacks like the potential knock down of off-targets and the limited knock down efficiency dependent on the tissue and the RNAi construct. To circumvent this problem I co-expressed a member of the RNAi pathway *dcr-2* in the nervous system which enhances the RNAi efficacy (Dietzl et al., 2007; Valakh et al., 2012).

An important question was whether the RNAi technique would allow me the identification of genes important for synapse stability at the *Drosophila* larval NMJ. To control the RNAi conditions, I tested a number of positive controls that have been previously identified as important for NMJ development and maintenance as e.g. *β-spectrin* (Pielage et al., 2005), *bruchpilot* (Fouquet et al., 2009; Kittel et al., 2006; Wagh et al., 2006), a*nkyrin2* (Koch et al., 2008; Pielage et al., 2008), *mother of decapentaplegic* (*mad*) and *medea* (*med*) (Eaton and Davis, 2005). Importantly I identified 80% of these positive controls. Most of them have been previously identified using classical mutations like *ank2*, *med* and *mad*. Thus, I can conclude that the RNAi technique is a valid assay to identify essential genes for the *Drosophila* larval NMJ. Recently a number of screens using RNAi-based knock down of candidate genes in muscles, epidermis and at the larval NMJ have been published (Lesch et al., 2010; Schnorrer et al., 2010; Valakh et al., 2012). In addition, to synapse stability defects our assay allows the characterization of other features including formation and morphology defects as I demonstrated the synaptic overgrowth induced by *highwire* RNAi (McCabe et al., 2004).

However, it has to be noted that most positive controls did not belong to the transmembrane protein class. A particular difficulty for the analysis of transmembrane proteins might be lower protein turn over compared to cytoplasmic proteins (Rasse et al., 2005; FRAP experiments in submitted manuscript). Indeed, I was not able to completely knock down FasII using different RNAi lines (data not shown).

In summary, I can conclude that the RNAi technique allows the identification of novel candidate genes important for NMJ development and stability however the knock down of cell adhesion molecules might be less efficient than the knock down of cytoplasmic proteins.

## 3.2. Candidate genes identified in the screen important for synapse stability

In the screen I identified the Ig-like domain proteins Neuroglian and CG31708 (Uhu) as novel candidate genes controlling synapse stability (chapter 3.3. and 3.4.). In addition, I identified three other genes involved in NMJ maintenance. These are the 4.1 protein Coracle, Insomniac and a so far uncharacterized LRR protein CG5195 that I will discuss in the following sections.

### 3.2.1. Coracle is important for synapse stability in the presynaptic motoneuron

I identified Coracle (Cora) as an important protein for synapse stability in the presynaptic motoneuron using two RNAi lines targeting the same DNA sequence. The protein belongs to the CAM interaction group and harbors a FERM domain which is found in a number of cytoskeleton associated proteins that interact with cell adhesion molecules (Neisch and Fehon, 2011). Importantly, the L1-type Neuroglian has a FERM binding domain in the cytoplasmic tail thus Cora could be a potential interaction partner of Nrg providing an additional link to the cytoskeleton contributing to the stabilizing function of Nrg. At the larval NMJ Cora has previously been described to control the selective anchoring of *Drosophila* glutamate receptors at the NMJ (Chen et al., 2005).

### 3.2.2. Presynaptic Insomniac controls synapse stability

Presynaptic RNAi mediated knock down of Insomniac resulted in severe synapse retractions. Inc encodes a small protein with a BTB/POZ (**B**R-C, **t**tk, **b**ab and **Po**x virus and **Z**inc finger) domain which can be found in potassium channels as well as in transcription factors. In potassium channels this domain is important for protein tetramerization acting as a protein-protein interaction domain (Bixby et al., 1999). Transcription factors with BTB/POZ domains often act as transcriptional repressors (Neisch and Fehon, 2011; Wong and Privalsky, 1998). Thus, two scenarios are possible how Inc controls synapse stability. Firstly, Inc could act as a linker protein required for the clustering of proteins like CAMs and others in subdomains of the cell membrane, which are essential for synapse stability. A similar function has been described for AnkyrinG which regulates the localization of Neurofascin and voltage-gated Na-channels to the AIS controlling the ability of the AIS to initiate action potentials (Zhou et al., 1998). Secondly, Inc could act as a transcription factor. Many transcription factors have been identified to control different aspects of larval NMJ development including growth and stability. For example the overexpression of the transcription factor FoxO leads to the destabilization of microtubules and synaptic instability (Nechipurenko and Broihier, 2012) and the SMAD transcription factor Mad has been implicated in NMJ growth regulation as well as synapse stability (Eaton and Davis, 2005; Rawson et al., 2003).

### 3.2.3. Postsynaptic CG5195 is required for synapse stability

Finally, I would like to highlight the identification of the LRR protein CG5195, which is the only candidate identified in the screen required in the postsynaptic muscle promoting synaptic stability at the larval NMJ. The retractions are accompanied by severe muscle and bouton formation defects. Importantly, other candidates in the screen showed muscle defects but no retractions. This indicates that these two phenotypes do not necessarily depend on each other. Using online bioinformatical tools I analyzed the domain structure of CG5195 in more detail. CG5195 contains 29 LRR domains that have been identified to be important for protein-protein interactions. The absence of a transmembrane domain or a GPI-anchor but the presence of a signal peptide indicates that CG5195 could be a secreted LRR protein similar to the neuronal LRR proteins Slit (Chen et al., 2001; Wong et al., 2002) and leucine-rich glioma inactivated (LGI1/4) (Owuor et al., 2009). Many LRR proteins are essential for nervous system development and function (Ko et al., 2009; Linhoff et al., 2009).

Multiple scenarios how CG5195 could control presynaptic stability from the muscle side are considerable. First of all, muscle derived CG5195 could act as a signaling activator through binding of pre- and postsynaptic receptors and a subsequent signaling cascade would control synapse stability and muscle development. A similar mechanism has been described for the *Drosophila* TGF-beta homolog Glass bottom boat (Gbb) that activates TGF-beta signaling and thereby regulates NMJ growth and stability (Eaton and Davis, 2005; McCabe et al., 2003). Secondly, the secreted protein CG5195 could interact with cell adhesion molecules on both sides of the NMJ and provide a functional linker required for synaptic stability. The secreted protein CBln1 for example interacts with both Neurexin and GluRδ2 and forms a bridge required in cerebellar granule cells and Purkinje cells during synaptogenesis in mice (Matsuda et al., 2010; Uemura et al., 2010).

## 3.3. The L1CAM homologue Neuroglian controls synapse stability and growth

In the main part of my study I focused on the L1-type CAM Neuroglian. In the RNAi screen I identified Neuroglian as key regulator of synapse stability *in vivo*. Neuroglian has the potential to interact with the adaptor molecule Ank2 in a regulated fashion (Garver et al., 1997). In a detailed analysis using biochemical, biophysical and genetic assays, I analyzed the requirement of the Nrg-Ank2 interaction for synapse development. I showed that the synapse stability of the larval neuromuscular junction depends on the extracellular Ig-domains and the intracellular Ankyrin interaction motif of Nrg. Impairment of Ankyrin binding causes an increase in Nrg mobility that correlates with increased synaptic growth and decreased stability.

Here, I would like to discuss interesting aspects of Nrg not included in the manuscript. (1) Neuroglian expressed in glial cells contributes to synapse stability at the larval neuromuscular junction. (2) Homophilic and heterophilic interactions of Nrg control synapse stability. (3) Loss of Ank2-Nrg interaction sensitizes the neuromuscular junctions for the reduction of proteins important for synapse stability. (4) The TGF-beta receptor Wit interacts genetically with Nrg during synapse growth regulation.

### 3.3.1. Glial Neuroglian contributes to synapse stability at the larval neuromuscular junction.

Glial knock down of Nrg resulted in an increase in synaptic retractions at the larval NMJ. Perineurial and subperineurial glial cells extend processes into the synaptic region of the synaptic terminal but do not cover it completely (Brink et al., 2012). Recently Keller and colleagues (2011) identified a role of glial cells during NMJ elimination at the larval NMJ (Keller et al., 2011). They postulate the existence of a prodegenerative glial derived signaling framework consisting of TNF-α and TNF-α-receptor and the downstream activation of caspases and mitochondria-dependent signaling pathways. Mutants of TNF-α and the TNF-α-receptor can ameliorate the synaptic retraction phenotype of *ank2* and s*pectrin* mutants (Keller et al., 2011). In vertebrates perisynaptic Schwann cells interact closely with the NMJ terminal and are important for proper formation and function as well as maintenance of the NMJ (Feng et al., 2005; Koirala et al., 2003).

Neuroglian has been identified as a cell adhesion molecule expressed in neurons and glial cells (Bieber et al., 1989). In the embryonic peripheral nervous system homophilic interactions between neurons and glial cells are required to establish the complex dendritic arbors of mechanosensory neurons (Yamamoto et al., 2006). This indicates that indeed the loss of homophilic Nrg interaction between motoneuron and glial cell could result in a loss of synaptic stability. An additional level of potential functional regulation provided by the L1-type CAM Neuroglian is the interaction with Ankyrins. I showed in this study that this interaction is important for the regulation of synapse stability in the presynaptic motoneuron. However in glial cells the interaction with Ank1 seems not be required for this function. Neither the deletion of the FIGQY Ankyrin binding motif of Nrg167, the only Nrg isoform present in glial cells, nor the RNAi mediated knock down of glial Ank1 impaired synapse stability. Thus, this interaction does not contribute to the glial regulation of synapse stability. However, other interaction domains like the FERM protein binding domain of Nrg167 could provide a regulatory system used in glial cells. A potential candidate to test would be the 4.1 protein Coracle that I identified in this study.

### 3.3.2. Homophilic and heterophilic interactions of Nrg contribute to synapse stability.

Neuroglian and L1CAMs have been shown to mediate homo- and heterophilic interactions through their extracellular Ig-domains and Fn-type III domains (Castellani et al., 2002; Felding-Habermann et al., 1997; Oleszewski et al., 1999; Volkmer et al., 1996; Yamamoto et al., 2006; Zhao et al., 1998). At the larval NMJ Neuroglian is expressed in motoneuron and muscles. Thus, homophilic interactions through the extracellular Ig-domains could contribute to the synapse stabilization function of Nrg. However, I showed that RNAi mediated knock down of Nrg in muscles did not impair synapse stability. From this result one can conclude that at the NMJ rather heterophilic interactions with so far unknown molecules are important. By combining the RNAi approach with the “knock-in” mutations, I could demonstrate that at least partially homophilic interactions of Nrg are involved in the control of synapse stability. Knock down of postsynaptic Nrg in animals expressing only Nrg180ΔFIGQY presynaptically ($nrg^{14}$/y; P[$Nrg180^{\Delta FIGQY}$]) resulted in a significant increase in synaptic retractions. Thus, a combination of homo- and heterophilic interactions of the extracellular domain of Nrg might be needed to promote synapse stability. It will be interesting to identify these heterophilic

interaction partners, which could include other cell adhesion molecules including receptor protein tyrosine kinases (RPTK) or ion channels.

### 3.3.3. Loss of the Ank2 Nrg interaction sensitizes the NMJ for important for genetic perturbations of proteins controlling synapse stability.

To analyze a potential genetic interaction between Nrg and members of the molecular network essential for synapse stability (Pielage et al., 2011; Pielage et al., 2008; Pielage et al., 2005; Pielage et al., 2006), I combined the "knock-in " mutations with loss-of-function mutations of *ank2*$^{518}$ and *α-spectrin*$^{rg41}$. I observed a genetic interaction in the background of the *nrg*$^{14}$; P[*Nrg180*$^{\Delta FIGQY}$], when I removed one copy of *ank2* or *α-spec*. This result provides additional evidence that Nrg acts upstream of the Ank2/Spectrin network to control synapse stability. A similar effect could be demonstrated for additional candidates including the TGF-beta receptor type I Tkv. TGF-beta signaling has been shown to influence synaptic stability (Eaton and Davis, 2005). However, two other candidates from the TGF-beta signaling pathway Wit and Mad did not result in this synergistic increase of synaptic retractions indicating a novel role of Tkv in an Nrg-dependent signaling pathway. Interestingly, both Nrg and Tkv have been implicated in MAP kinase signaling. Loss of Tkv during eye development increases MAP kinase signaling and MAP kinase signaling results in the phosphorylation of the FIGQY Ank2 binding motif of Neuroglian (Vrailas et al., 2006; Whittard et al., 2006). It will be interesting to analyze the effect of other TGF-beta signaling molecules like the SMAD Med or the other TGF-beta type I receptor Saxophone (Sax) on synapse stability in the *nrg*$^{14}$; P[*Nrg180*$^{\Delta FIGQY}$] background.

In summary, these results indicate that the deletion of the FIGQY Ank2 binding motif in the "knock-in" assay can serve as a sensitized background to screen for other candidates controlling synapse stability in a Nrg Ank2 dependent manner.

### 3.3.4. The TGF-beta receptor Wishful thinking interacts genetically with Nrg during synapse growth regulation

Mutations in TGF-beta signaling result in growth impairment of the larval NMJ (Aberle et al., 2002; Eaton and Davis, 2005; McCabe et al., 2003). In contrast, the loss of Nrg-Ank2 interaction leads to an increase in NMJ size. Using a combination of loss-of-function mutations of the TGF-beta receptor type II Wit and the Nrg Pacman "knock-in" mutations, I

aimed to analyze a potential suppression of the synaptic overgrowth in Ank2 binding mutants through the reduction of TGF-beta signaling. However, I observed the opposite phenotype: A reduction of the TGF-beta receptor type II Wit in the background of $nrg^{14}$; P[*Nrgwt*] and $nrg^{14}$; P[$Nrg180^{\Delta FIGQY}$] resulted in an further increase of bouton numbers. Importantly, the reduction of Ank2 level did not result in the same increase indicating a specific effect due to the *wit* mutation. This result could indicate first of all, that Wit is potentially part of another signaling pathway that restricts synaptic growth in contrast to the growth promoting effect of TGF-beta signaling and secondly, that this involves an FIGQY independent function of Nrg. Further experiments are required to confirm these preliminary results.

## 3.4. The potential IgLON homolog Uhu is important for synapse stability

In the RNAi screen I identified *CG31708* as an important player in synapse stability at the *Drosophila* larval NMJ. I named *CG31708* "*uhu"* to describe its role of a glue-like function between motoneuron and muscle. Uhu is essential presynaptically to control synapse stabilization. The phenotype of presynaptic knock down of Uhu has unique characteristics that I would like to discuss here in detail:

(1) In addition to synaptic retractions observed in other genotypes, I observed NMJ branches where the presynaptic marker Brp was lost in proximal parts but still present in more distal parts. This has never been described for other retraction phenotypes. Importantly, I could confirm this observation using an additional set of pre- and postsynaptic markers thereby excluding marker specific defects (data not shown). There are two possible explanations for this phenomenon: either a novel mechanism of synapse disassembly or the combination of two distinct defects of synapse formation and synapse stability.

(2) The observed phenotype developed between the early 3$^{rd}$ instar larval stage and the late 3$^{rd}$ instar larval stage. This argues for a novel, fast acting mechanisms of synapse disassembly because one would expect to observe potential synapse formation defects already in earlier larval stages. We will apply life-imaging in the future to monitor the progression of these novel types of retraction events.

(3) I demonstrated that presynaptic Uhu is controlling synapse stability only at a subset of NMJs. In contrast, Neuroglian is essential in all motoneurons to control synapse stability. This result implies the presence of a protein code of cell adhesion molecules to selectively promote synapse stability. There is no evidence for such a code for synapse stability but during other neurodevelopmental processes either multiple isoforms of the same gene as for Dscam or the expression of specific ligands binding to an receptor like for Neurexins have been described (de Wit et al., 2009; Schmucker et al., 2000; Uemura et al., 2010). Another option would be the usage of proteins with a similar domain structure that interact homo- and heterophilically. However, no other Ig-domain protein controlling synapse stability at a subset of NMJs has been identified in the screen.

A potential candidate to perform this function has been found using bioinformatical tools. CG42368 is closely related to Uhu based on the sequence and domain structure. The RNAi

knock down of CG42368 did not result in synaptic retractions. However, this can be due to inefficient knock down of CG42368 as discussed above. A possible mechanism to provide this kind of specificity is the differential expression in subsets of muscles or motoneurons. *In situ* hybridization studies would allow testing this hypothesis. Using Blast-based search for potential homologs of Uhu in vertebrates, I identified the Ig-domain IgLON family. The four members of this family (OBCAM, Kilon, LAMP and Neurotrimin) also harbor three Ig-domains in the extracellular domain and are described as GPI-linked glycoproteins (Funatsu et al., 1999). They have been implicated in a number of functions within the nervous system including neurite outgrowth, cell adhesion and memory formation (Akeel et al., 2011; Gil et al., 1998; Hashimoto et al., 2008; McNamee et al., 2002; Schafer et al., 2005). Detailed analyses of interactions within this family are available. Interestingly, they have been shown to interact homo- and heterophilic (Gil et al., 2002; Lodge et al., 2000; Marg et al., 1999; Zhukareva and Levitt, 1995). In addition, members of the IgLON family are differential expressed. This is necessary since specific homo- and heterophilic interactions are important for particular functions. For example the homophilic interactions of LAMP or Neurotrimin are important to promote neurite outgrowth whereas heterophilic interactions of Neurotrimin with other IgLON members inhibit neurite outgrowth (Gil et al., 1998).

The analysis of the subcellular localization of Uhu indicates that Uhu can localize to the NMJ pre- and postsynaptically. However, our antibody did not recognize wild type levels of Uhu. When overexpressed in motoneurons, the Uhu was predominantly detected at the NMJ and a weaker in the axon and the nerve bundles. Within the bouton, I observed a structured localization similar to the honey-comb like pattern of FasII staining (Pielage et al., 2008). This indicates that Uhu can localize to specific substructures within boutons like other CAMs. Using postsynaptic overexpression I showed that Uhu can accumulate in the muscle area that directly surrounds the NMJ. These results indicate that presynaptic Uhu potentially controls synapse stability as a homophilic cell adhesion molecules. However, I could not demonstrate a postsynaptic function for Uhu at the *Drosophila* larval NMJ. Thus, it is likely that also heterophilic interactions with so far unknown interaction partners might control Uhu dependent synaptic stabilization. For many CAMs both homo- and heterophilic interactions have been described as e.g. within the Ig-domain family (Blaess et al., 1998; Castellani et al., 2002; Sugie et al., 2010) or the Neurexins that can interact with Neuroligins and LRRTMs (de Wit et al., 2009; Ko et al., 2009; Soler-Llavina et al., 2011; Uemura et al., 2010).

Finally, Uhu seems to be required in other parts of the nervous system since the knock down of Uhu using the *elav*$^{C155}$-Gal4 line which expresses Gal4 in all postmitotic neurons (Robinow and White, 1991; Yao and White, 1994) results in sick larvae prior to the appearance of the synaptic retraction phenotype in late 3$^{rd}$ instar larvae. It will be interesting to analyze CNS requirements of Uhu in the future.

## 3.5. Redundant mechanisms to control synapse stability at the larval NMJ

In a recent publication of the embryonic neuromuscular junction Koper and colleagues (2012) demonstrated that even the knock down of entire classes of CAMs does not impair NMJ stability. Since these proteins are expressed at the NMJ the authors propose a redundant mechanism for the control of synapse maintenance (Koper et al., 2012). During early nervous system development in vertebrates a functional redundancy has been described for Neuroligin and LRRTMs (Soler-Llavina et al., 2011). Thus, redundancy is probably a common mechanism to ensure a functional nervous system controlled at multiple levels.

During my study, I obtained additional data that are in agreement this hypothesis. In my RNAi screen I identified a relatively low number of cell adhesion molecules essential for synapse stability. In fact only two of the five top candidates can act as classic cell adhesion molecules by directly connecting two neighboring neurons: the transmembrane protein L1-type CAM Neuroglian and the GPI anchored Ig-like protein Uhu. However, this could also be a result of a low knock down efficacy of some RNAi constructs as I observed an inefficient knock down of Nrg using the VDRC line 27201 (data not shown) or the low turnover of transmembrane proteins in comparison to cytoplasmic proteins (Rasse et al., 2005).

After RNAi mediated knock down of both stability genes or in the *nrg*$^{14}$ MARCM clones I still observed a high number of stable synapses indicating that other CAMs compensate the loss of Nrg and Uhu at these synapses. A potential candidate was the NCAM homolog FasII. During the outgrowth of ocellar neurons in *Drosophila* FasII can compensate for the loss of Nrg (Kristiansen et al., 2005). However, I could not confirm the same function of FasII during synapse stabilization mediated by Nrg. A potential approach to unravel such redundant CAMs could be an candidate-based interaction screen using the *nrg*$^{14}$/y; P[*Nrg180*$^{\Delta FIGQY}$] animals as a sensitized background.

# 4. Material and Methods

## 4.1. General

### 4.1.1. Fly stocks

4.1.1.1. Fly stocks used

Fly stocks used in the submitted manuscript: see method section in the submitted manuscript

Additional fly strains used in this study:

PBac{WH}*ank2*$^{f00518}$ (*ank2*$^{518}$); w$^{*}$; *ru*$^{1}$ *α-Spec*$^{rg41}$ st$^{1}$ e$^{s}$/TM6B, Tb$^{1}$ (BL31999, α-spec$^{rg41}$); *tkv*$^{1}$ (BL427); bw$^{1}$; *wit*$^{B11}$ st$^{1}$/TM6B, Tb$^{1}$ (BL5174, *wit*$^{B11}$); bw$^{1}$; *wit*$^{A12}$ st$^{1}$/TM6B, Tb$^{1}$ (BL5173, *wit*$^{A12}$), w$^{*}$; *Mad*$^{1-2}$ P{neoFRT}40A/CyO (BL7323, *mad*$^{1-2}$); y$^{1}$ w$^{67c23}$; P{lacW}*Mad*$^{k00237}$/CyO (BL10474, *mad*$^{k237}$); *nrg*$^{849}$ (BL35827); P{w[+mC]=PTT-GA}NrgG00305 (BL6844, later referred to as *nrg*$^{305}$); w[*]; P{w[+mC]=UAS-nrg[180]}28b (UAS-Nrg180, BL24169); w$^{1118}$; P{GAL4}repo/TM3, Sb$^{1}$ (BL7415, *repo*-Gal4), y$^{1}$ w$^{1118}$; PBac{y$^{+}$-attP-3B}VK00033 (BL9750, attP$^{VK33}$); y$^{1}$ v$^{1}$ P{nos-phiC31\int.NLS}X; P{CaryP}attP40 (BL25709, attP$^{40}$) (all Bloomington stock center (BL# = stock id), bold names are the nomenclature used in the study, 2$^{nd}$ chromosomal lines were rebalanced to either CyO-GFP or CyO-Wee-P, 3$^{rd}$ chromosomal lines were rebalanced to TM6B); VDRC lines used for screening are listed in the Appendix (Vienna *Drosophila* RNAi center).

4.1.1.2. Flystocks generated

The following fly strains have been generated and used in this study

**Table 5 - List of generated constructs and transgenic flies generated in this study**

| *Name* | *Integration site* | *Project* |
|---|---|---|
| pUAST-5xUAS-nrg180wt | attP$^{40}$ | Neuroglian |
| pUAST-5xUAS-nrg180Y-F | attP$^{40}$ | Neuroglian |
| pUAST-5xUAS-nrg180Y-D | attP$^{40}$ | Neuroglian |
| pUAST-5xUAS-nrg180Y-A | attP$^{40}$ | Neuroglian |
| pUAST-5xUAS-nrg180ΔFIGQY | attP$^{40}$ | Neuroglian |
| pUAST-5xUAS-nrg167ΔFIGQY | attP$^{40}$ | Neuroglian |
| pUAST-10xUAS-nrg180wt_HA | attP$^{40}$ | Neuroglian |
| pUAST-10xUAS-nrg180_GFP | attP$^{40}$ | Neuroglian |

| | | |
|---|---|---|
| pUAST-10xUAS-nrg180Y-F_GFP | attP$^{40}$ | Neuroglian |
| pUAST-10xUAS-nrg180Y-D_GFP | attP$^{40}$ | Neuroglian |
| pUAST-10xUAS-nrg180Y-A_GFP | attP$^{40}$ | Neuroglian |
| pUAST-10xUAS-nrg180ΔFIGQY_GFP | attP$^{40}$ | Neuroglian |
| 1 pUAST-10xUAS-nrg167_GFP | attP$^{40}$ | Neuroglian |
| CH321-4H20_ P[nrgwt] | attP$^{40}$ | Neuroglian |
| CH321-4H20_ P[nrg180Y-F] | attP$^{40}$ | Neuroglian |
| CH321-4H20_ P[nrg180Y-D] | attP$^{40}$ | Neuroglian |
| CH321-4H20_ P[nrg180Y-A] | attP$^{40}$ | Neuroglian |
| CH321-4H20_ P[nrg180ΔFIQGY] | attP$^{40}$ | Neuroglian |
| CH321-4H20_ P[nrg180ΔC] | attP$^{40}$ | Neuroglian |
| CH321-4H20_ P[nrg180ΔPDZ] | attP$^{40}$ | Neuroglian |
| CH321-4H20_P[nrg167ΔFIQGY] | attP$^{40}$ | Neuroglian |
| CH321-4H20_ P[nrgΔIg3/4] | attP$^{40}$ | Neuroglian |
| 5xpUASTCG31708 | attP$^{VK33}$ | Uhu |
| 5xpUASTCG31708_EGFP | attP$^{VK33}$ | Uhu |
| CH321-92N22 | attP$^{VK33}$ | Uhu |
| CH321-50F13 | attP$^{VK33}$ | Uhu |

All Neuroglian transgenes have been integrated in the att$^{P40}$ site, Uhu Pacman and pUAST constructs have been integrated into the attP$^{VK33}$ site.

## 4.1.2. Primer

### *4.1.2.1. General primer*

**Table 6 - List of general primers used in this study**

| *Primer name* | *Sequence* | *Used* |
|---|---|---|
| M13fw | 5`-TGTAAAACGACGGCCAGT | pENTR |
| M13rev | 5`-CAGGAAACAGCTATGAC | pENTR |
| Svr | 5`-GGCATTCCACCACTGCTCCC | pUAST |
| GalK ORF fw | 5`-CGTATGGGCGAGTTGATGGCG | Nrg Pacman |
| GalK ORF rev | 5`-GTGCGACAATGGGCGCATCGAG | Nrg Pacman |
| Em-7 f | 5`-GTGACAATTAATCATCGGCATAG | Nrg Pacman |
| hspfw | 5`- TATAAATAGAGGCGCTTCGT | pUAST |
| GFPrev | 5`-CTTCGGGCATGGCGGACTTG | pUAST_GFP tagged |

Primers that are not construct but vector specific and have been used for PCR based verification of constructs and sequencing

*4.1.2.2. Primer for the generation of pENTR constructs*

**Table 7 - List of primers used for the generation of pENTR clones for Neuroglian and CG31708**

| *Primer name* | *Sequence* | *Gene* |
|---|---|---|
| Nrg180-ENTR-N-term | 5`-CACCATGTGGCGGCAGTCAACG | Neuroglian |
| Nrg180-ENTR-C-term | 5`-TTAGACGTAGGTGGCCACG | Neuroglian |
| Nrg180-ENTR-C-term-tagged | 5`-GACGTAGGTGGCCACGGCTC | Neuroglian |
| CG31708pENTR fw | 5`-CACCATGTTGCCCCCGTCCTGGCATC | CG31708 |
| CG31708pENTR-C-term | 5`-TAACATAGACTTAGGCTATGG | CG31708 |
| CG31708 pENTR-C-term-tagged | 5`-ACATAGACTTAGGCTATGGCTAG | CG31708 |

*4.1.2.3. Primer for antibody production*

**Table 8 - List of primers used to generate pENTR for the antibody fragment of CG31708**

| *Primer name* | *Sequence* |
|---|---|
| CG31708 Hisfw | 5`-CACCGGCGAGGGACCAATCATACA |
| CG31708 Hisrev | 5`-CTAGTGACCCCGGGCCCCGTTGGATTCC |

Primers used for the generation of the His-tagged CG31708 construct used for antibody production in rats

*4.1.2.4. Primer for the site directed mutagenesis*

**Table 9 - List of primers used for site directed mutagenesis of Nrg constructs**

| *Primer name* | *Sequence* |
|---|---|
| Nrg180Y-F | 5`-GGCTCCTTCATTGGCCAA<u>TTT</u>GTTCCTGGAAAGCTCC |
| Nrg180Y-D: | 5`-GGCTCCTTCATTGGCCAA<u>GAC</u>GTTCCTGGAAAGCTCC |
| Nrg180Y-A: | 5`-GGCTCCTTCATTGGCCAA<u>GCT</u>GTTCCTGGAAAGCTCC |
| Nrg180ΔFIGQY: | 5`-<u>AATTTACCGAGGATGGCTCC</u>GTTCCTGGAAAGCTCCAACC |

Primers used for site-directed mutagenesis of pUAST constructs of Neuroglian. For the point mutations (Y-F, Y-A, Y-D) the three amino acids of the tyrosine where the change was introduced are underlined. For the Nrg180ΔFIGQY deletion-construct the sequence before the deletion is underlined.

### *4.1.2.5. Primer for galK insertion*

**Table 10 - List of primer used to insert galK into CH321-4H20.**

| *Primer name* | *Sequence* |
|---|---|
| 04H20-Hindge GalK fw | 5`-ACAAGATTGGCAACAAGGTGCTCCTCGATGTCAAACAGATGGGCGTTAGTcctgttgacaattaatcatcggca |
| 04H20-Hindge GalK rev | 5`-GACTGGCGACGGGAAACATATTGACGCACGGGCGGATGCTTGTTCTGCGAtcagcactgtcctgctcctt |
| 04H20-FERM GalK fw | 5`-TCATCCTCTTCATCATCATCTGCATTATCCGACGCAATCGGGGCGGAAAGcctgttgacaattaatcatcggca |
| 04H20-FERM GalK rev | 5`-TCTTCGGGATAATCCCGCCGGCCGTTGGCCAGCTCCCGATCGTGGACATCtcagcactgtcctgctcctt |
| 04H20-PDZ GalK fw | 5`-CCGGAGGAGCAGCTGCCAGCAATGGAGGAGCTGCAGCCGGAGCCGTGGCCcctgttgacaattaatcatcggca |
| 04H20-PDZ GalK rev | 5`-TAGAAAATCAGGAGAACAATGGGGCAAGTGAATCCCAGCCACGCCTCTTAtcagcactgtcctgctcctt |
| 04H20-FIGQY180 GalK fw | 5`-TCTTTCTAATCCCAGGACAATTTACCGAGGATGGCTCCTTCATTGGCCAAcctgttgacaattaatcatcggca |
| 04H20-FIGQY180 GalK fw2 | 5`-TAAAAACTAATATTGTATATATCTTTCTAATCCCAGGACAATTTACCGAGcctgttgacaattaatcatcggca |
| 04H20-FIGQY180 GalK fw3 | 5`-AATGAATCGAGAATTGTAAATAGAATAAAAACTAATATTGTATATATCTTTCTAATCCCAGGACAATTTACCGAGGATGGCTCCTTCATTGGCCAAcctgttgacaattaatcatcggca |
| 04H20-FIGQY180 GalK fw4 | 5`-CACAATTGCAATGGGGTTGTAATAGAATGAATCGAGAATTGTAAATAGAATAAAAACTAATATTGTATATATCTTTCTAATCCCAGcctgttgacaattaatcatcggca |
| 04H20-FIGQY180 GalK rev | 5`-GAATTGTTCAGTGGCTGTGGGCTAACCGGCGGTTGGAGCTTTCCAGGAACtcagcactgtcctgctcctt |
| 04H20-FIGQY167 GalK fw | 5`-TTTTTCTTTTTCCTAAACACGTAAAATAAACACAATCACAATCAATATTAAATCGACAACGACAACCAATATCCAGGCATGAATCCTGTTGACAATTAATCATCGGCA |
| 04H20-FIGQY167 GalK fw2 | 5`-AAATAAACACAATCACAATCAATATTAAATCGACAACGACAACCAATATCCAGGCATGAATGAAGATGGATCCTTTATTGGCCAACCTGTTGACAATTAATCATCGGCA |
| 04H20-FIGQY167 GalK rev | 5`-TTGCTGTTGCGGTGCGCTGCTTACTAATTAAATCAAAGTCCTTTGCGTCCtcagcactgtcctgctcctt |
| 04H20-FIGQY167 GalK rev2 | 5`-GGGGTTAAGGGCTCGGTTTCGATATTATTTTTGAGTTGCTGTTGCGGTGCGCTGCTTACTAATTAAATCAAAGTCCTTTGCGTCCtcagcactgtcctgctcctt |

The following galK constructs have been generated Hindge_galK, FERM_galK, PDZ_galK and FIGQY180_galK and FIGQY167_galK. Hindge_galK was used to generate the ΔIg3/4 construct. FERM_galK was used to generate the FERM domain deletion, PDZ_galK for the PDZ domain deletion. FIGQY180_galK was used to generate all mutations of the Ank2 binding site of the Nrg180 domain, FIGQY167_galK was used to generate the deletion of the FIGQY167 domain.

*4.1.2.6. Oligos for the generation of Pacman mutants*

**Table 11 - List of oligos used for the generation of Pacman mutants**

| *Oligo name* | *Sequence* |
|---|---|
| P[nrg180Y-F] | 5`-TCTTTCTAATCCCAGGACAATTTACCGAGGATGGCTCCTTCATTGGCCAA**TTC**GTTCCTGGAAAGCTCCAACCGCCGGTTAGCCCACAGCCACTGAACAATTC |
| P[nrg180Y-D] | 5`-TCTTTCTAATCCCAGGACAATTTACCGAGGATGGCTCCTTCATTGGCCAA**GAC**GTTCCTGGAAAGCTCCAACCGCCGGTTAGCCCACAGCCACTGAACAATTC |
| P[nrg180Y-A] | 5`-TCTTTCTAATCCCAGGACAATTTACCGAGGATGGCTCCTTCATTGGCCAA**GCC**GTTCCTGGAAAGCTCCAACCGCCGGTTAGCCCACAGCCACTGAACAATTC |
| P[nrg180ΔFIQGY] | 5`-ATATTGTATATATCTTTCTAATCCCAGGACAATTTACCGAGGATGGCTCCGTTCCTGGAAAGCTCCAACCGCCGGTTAGCCCACAGCCACTGAACAATTC |
| P[nrg180ΔC] | 5`-ATATTGTATATATCTTTCTAATCCCAGGACAATTTACCGAGGATGGCTCCTAAGAGGCGTGGCTGGGATTCACTTGCCCCATTGTTCTCCTGATTTTCTA |
| P[nrg180ΔPDZ] | 5`-CCGGAGGAGCAGCTGCCAGCAATGGAGGAGCTGCAGCCGGAGCCGTGGCCCCTGTTGACAATTAATCATCGGCA |
| P[nrg167ΔFIQGY] | 5`-ACAATCACAATCAATATTAAATCGACAACGACAACCAATATCCAGGCATGAATGAAGATGGATCCGGACGCAAAGGACTTTGATTTAATTAGTAAGCAGCGCACCGCAACAGCAA |
| P[nrgΔIg3/4] | 5`-CCTCGGTGTTTCGCAGTGAATACAAGATTGGCAACAAGGTGCTCCTCGATGCTGAGCCGCCAACGATTTCCGAAGCTCCAGCAGCTGTATCCACTGTCGA |
| P[nrgΔFERM] | 5`-TCATCCTCTTCATCATCATCTGCATTATCCGACGCAATCGGGGCGGAAAGCCTGTTGACAATTAATCATGGCA |

Oligos used for the mutagenesis via recombineering of the Neuroglian Pacman CH321-4H20. Only the forward oligos are shown, reverse oligos are complementary to the forward oligos.

*4.1.2.7. Sequencing primer*

**Table 12 - List of sequencing and check primers for the different pENTR, pUAST and Pacman constructs.**

| *Construct* | *Forward primer* | *Reverse primer* |
|---|---|---|
| pENTR_nrg180wt, Y-F, Y-A, Y-D, ΔFIGQY (check mutations in FIGQY motif) | 5`-AATCGGGGCGGAAAGTACG | 5`-CAGGAAACAGCTATGAC |
| pENTR_nrg180wt (start and stop) | 5`-TGTAAAACGACGGCCAGT | 5`-CAGGAAACAGCTATGAC |
| pENTR/pUAST nrgwt, Y-F, Y-A, Y-D, ΔFIGQY (sequencing of complete ORF, primer 1-8) | 5`-TGCTCTTCAAAGTGGCGC<br>5`-GTTAGTGCCTCGCAGAAC<br>5`-TAACTACGGTTGCAACGC<br>5`-GATTCGTGAAGACCAATG<br>5`-CCGAAATCGAGCACAATG<br>5`-ACAATGGACGCTTCAATG<br>5`-TGGATACGCGAGAATGAG<br>5`-CGATACTGATTCGATGGC | 5`-CCCGATCCTCCGGCAGTT<br>5`-CAATGAACCATCCGGCAT<br>5`-CCATCTTCATGCGTGTGA<br>5`-CATTGTGAAGTTGGTGGG<br>5`-GGCGTGAACGATGTATTG<br>5`-CACCGTTAGCTTGGACAT<br>5`-CACGTCGCAGGTGTATGT<br>5`-GTGGCCGTTCCGAATTCA |
| 10xpUAST_Nrg_HA (check) | 5`-AATCGGGGCGGAAAGTACG | 5`-GGCATTCCACCACTGCTCCC |
| 10xpUAST_Nrg_EGFP (check) | 5`-TATAAATAGAGGCGCTTCGT | 5`-CAAGTCCGCCATGCCCGAAG |
| Pacman_Hindge galK check | 5`-CGAGCTGAATGCCTTCAAG | 5`-GGAGTTAACATTCAGAATGATGG |
| Pacman_Hindge galK seq | 5`-GATCCTGAGGGTAATCTCTG | 5`-GTTATTCGATCGCTCCACTG |

| | | |
|---|---|---|
| Pacman_FERM galK check | 5`-TCCATGTACAGGATCAAGG | 5`-ACTCTAACCTGTATCGCCATC |
| Pacman_FERM galK seq | 5`-CTTTAACACGGAGAGTGCCAC | 5`-GATTTTGGGACTTACGGTTGC |
| Pacman_PDZ galK check | 5`-GAGGATGGCTCCTTCATTG | 5`-GCTTTAAATTCATGCGAG |
| Pacman_PDZ galK seq | 5`-CACTGAACAATTCCGCTGC | 5`-GCAGACACTTAAAGCAGTT |
| Pacman_FIGQY167 galK check | 5`-AGCCACTTGCCGTTATAAG | 5`-GGCAGTATTGATTTGCAT |
| Pacman_FIGQY167 galK seq | 5`-GTGTTCCTTGTTATGTGT | 5`-AGTCGTGGTGTTTGCACTT |
| Pacman_FIGQY180 galK check | 5`-AACTGACGCATTTGCCAGG | 5`-GCAGACACTTAAAGCAGTT |
| Pacman_FIGQY180 galK seq | 5`-CATATCATTTTGCACCGGC | 5`-ACGATGCTCCACCCGATGCT |
| P[acman] check (Nrg180FIGQY galK and mutations) | 5`-AACTGACGCATTTGCCAGG | 5`-GCAGACACTTAAAGCAGTT |
| P[acman] seq(Nrg180FIGQY galK and mutations) | 5`-CATATCATTTTGCACCGGC | 5`-ACGATGCTCCACCCGATGCT |
| P[acman] check (ΔC) | 5`-AACTGACGCATTTGCCAGG | 5`-GCTTTAAATTCATGCGAG |
| P[acman] seq (ΔC) | 5`-CATATCATTTTGCACCGGC | 5`-GCAGACACTTAAAGCAGTT |
| P[acman] check (ΔPDZ) | 5`-GAGGATGGCTCCTTCATTG | 5`-GCTTTAAATTCATGCGAG |
| P[acman] seq (ΔPDZ) | 5`-CACTGAACAATTCCGCTGC | 5`-GCAGACACTTAAAGCAGTT |
| P[acman] check (Nrg167ΔFIGQY) | 5`-AGCCACTTGCCGTTATAAG | 5`-GGCAGTATTGATTTGCAT |
| P[acman] seq (Nrg167ΔFIGQY) | 5`-GTGTTCCTTGTTATGTGT | 5`-AGTCGTGGTGTTTGCACTT |
| P[acman] check (NrgΔIg3/4) | 5`-CGAGCTGAATGCCTTCAAG | 5`-GGAGTTAACATTCAGAATGATGG |
| P[acman] seq (NrgΔIg3/4) | 5`- GATCCTGAGGGTAATCTCTG | 5`-GTTATTCGATCGCTCCACTG |
| pENTR/pUAST CG31701 (sequencing of complete ORF, primer 1-4) | 5`-GTTCCAAACTTCGGTGGAGC<br>5`-CCTAAACGTTGTCGTTCC<br>5`-CGAAGGTTTCAACGTCACC<br>5`-GCGATCGATTTATGCGCAGG | 5`-TTGGATTCCGCATCCGCCT<br>5`-GATGAGGCAGTGGTTGGAG<br>5`-GGTATAAGCAGCATTGGAGG<br>5`-CTGATGCGCGGATTGCGCGTG |

Forward and reverse primers PCR are listed to check the indicated constructs and to sequence vectors for final verification.

### 4.1.3. Pacman constructs generated in this study

**Table 13 - List of Nrg Pacman constructs generated in this study**

| *Pacman* | *Integration site* | *Transgenic flies* |
|---|---|---|
| CH321-4H20_ P[nrg180Y-F] | attP$^{40}$ | yes |
| CH321-4H20_ P[nrg180Y-D] | attP$^{40}$ | yes |
| CH321-4H20_ P[nrg180Y-A] | attP$^{40}$ | yes |
| CH321-4H20_ P[nrg180ΔFIQGY] | attP$^{40}$ | yes |
| CH321-4H20_ P[nrg180ΔC] | attP$^{40}$ | yes |
| CH321-4H20_ P[nrg180ΔPDZ] | attP$^{40}$ | yes |
| CH321-4H20_P[nrg167ΔFIQGY] | attP$^{40}$ | yes |
| CH321-4H20_ P[nrgΔIg3/4] | attP$^{40}$ | yes |
| CH321-4H20_ P[nrgΔFERM] | - | no |
| CH321-4H20_ P[nrg167/180ΔFIQGY] | - | no |

Pacman mutations have been generated using recombineering. All constructs have been integrated into the some genomic locus using the attP$^{40}$ landing site. No transgenic flies could be obtained from CH321-4H20_ P[nrgΔFERM] and CH321-4H20_ P[nrg167/180ΔFIQGY].

### 4.1.4. cDNAs used in this study

**Table 14 - List of the cDNA clones used in this study to generate pUAST constructs**

| *Name* | *Vector* | *Gene* |
|---|---|---|
| RE08554 | pFLC1 | CG31208 |
| pMT-neuroglian | pRMHa3 | Nrg180 |
| GH03573 | pOT2 | Nrg167 |

cDNA clones used to generate pUAST constructs of Neuroglian180 and 167 isoform and CG31708. All are obtained from the *Drosophila* Genomics Resource Center.

### 4.1.5. Vectors used in this study

**Table 15 - List of pENTR and pDEST vectors used in this study**

| *Name* | *Project used* |
|---|---|
| pENTR/D-TOPO | Uhu/Neuroglian |
| pUAST-5xUAS-rfa | Uhu/Neuroglian |
| pUAST-5xUAS-rfa-EGFP | Uhu/Neuroglian |
| pUAST-10xUAS-rfa* | Neuroglian |
| pUAST-10xUAS-rfa-EGFP* | Neuroglian |
| pUAST-10xUAS-rfa-HA* | Neuroglian |
| pDEST17 | Uhu |
| pDEST-HisMBT | Uhu |
| pDEST-periHisMBT | Uhu |

Vectors used for cloning of pENTR and pUAST constructs of Uhu and Neuroglian. * Not published vectors (submitted manuscript for details).

**Table 16 - List of P[acman] constructs used in this study**

| *Name* | *Gene of interest* |
|---|---|
| CH321-4H20 | *neuroglian* |
| CH321-92N22 | *CG31701* (*uhu*) |
| CH321-50F13 | *CG31701* (*uhu*) |

All Pacman vectors used in this study to generate transgenic flies and to generate modifications. All Pacmans have been ordered at BACPAC resources center (BPRC).

## 4.1.6. Web pages and programs

Web pages used in this study

| | |
|---|---|
| Pubmed: | http://www.ncbi.nlm.nih.gov/pubmed/ |
| Flybase: | http://flybase.org/ |
| Student t-test: | http://www.physics.csbsju.edu/stats/t-test.html |
| BLAST: | http://www.ncbi.nlm.nih.gov/blast/ |
| Bloomington: | http://flystocks.bio.indiana.edu |
| VDRC: | http://stockcenter.vdrc.at |
| Nigfly: | http://www.shigen.nig.ac.jp |
| SMART: | http://smart.embl-heidelberg.de/ |
| Expasy: | http://www.expasy.org/tools/ |
| Pacman: | http://www.pacmanfly.org/ |
| BPRC | http://bacpac.chori.org/ |
| Hybridoma Bank: | http://dshb.biology.uiowa.edu/ |
| DGRC: | https://dgrc.cgb.indiana.edu/ |
| FMI: | http://iwww.fmi.ch/ |
| Leo: | http://dict.leo.org/ |
| Google: | http://www.google.ch |
| Microsynth | http://www.microsynth.ch/ |
| Pfam | http://pfam.sanger.ac.uk/ |
| Phoebius | http://phobius.sbc.su.se/ |
| Prosite | http://prosite.expasy.org/ |
| Mobyle | hhtp://mobile.pasteur.fr |
| ProteinArchitekt | http://www.proteinarchitect.net |

Programs used in this study

**Quantifications and evaluations:**

Microsoft Office (Excel)

**Image acquisition and processing:**

Adobe Design Standard CS4 (Photoshop CS, Adobe Illustrator CS4)

ImageAccess (Imagic), Bitplane Imaris, Zeiss ZEN, FIJI (ImageJ, opensource)

**Molecular working:**

CLC Main Workbench5

**Presentations and Posters:**

Microsoft Office (Word, PowerPoint)

Adobe Design Standard CS4 (Photoshop CS, Adobe Illustrator CS4)

### 4.1.7. Media

| | |
|---|---|
| **Dissecting saline 1x (1 l, no calcium)** | 4.08 g NaCl<br>4.08 g $MgCl_2$ $6H_2O$<br>0.36 g KCl<br>1.2 g HEPES<br>0.84 g $NaHCO_3$<br>39.2 g Sucrose<br>40 ml EGTA (0.5M)<br>*Adjust to pH 7.0 with NaOH* |
| **HL3 saline (0.5 l)** | 2.04 g NaCl<br>0.186 g KCl<br>2.03 g $MgCl_2 \cdot 6H_20$<br>0.42 g $NaHCO_3$<br>0.8 g Trehalose<br>0.6 g HEPES<br>19.6 g Sucrose<br>*Dissolve in 400 ml $H_2O$ (5/4x), adjust to pH 7.2, prior to use add the following to the amount needed:*<br>20 mM $MgCl_2$<br>0.5 mM $CaCl_2$ |
| **Injection buffer (1 l)** | 1.2 g Tris<br>*Adjust to pH 8.0* |
| **PBS 10x (1 l)** | 75.97 g NaCl<br>9.94 g $Na_2HPO_4$<br>4.14 g $NaH_2PO_4$<br>*Adjust to pH 7.0 autoclave* |

| | |
|---|---|
| | *To make 10x PBT, add*<br>10 ml Triton X-100 |
| **TBS 1x (1 l)** | 2.4 g Tris<br>8.77 g NaCl<br>*Adjust tp pH 7.4, autoclave* |
| **TBST 1x (1 l)** | 1 l TBS (1x)<br>0.5 ml tween-20<br>*Mix and stir until completely dissolved* |
| **M9 medium (1 l)** | 6 g $Na_2HPO_4$<br>3 g KH2PO4<br>1 g NH4Cl<br>0.5 g NaCl<br>*autoclave* |
| **M63 medium 5x (1 l)** | 10 g $(NH_4)2SO_4$<br>68 g $KH_2PO_4$<br>2.5 mg $FeSO_4 \cdot 7H_2O$<br>*Adjust to pH 7.0* |
| **M63 minimal plates (1 l)** | 15 g agar<br>800 ml H2O<br>*Autoclave and cool down*<br>200 ml 5x M63 medium<br>1 ml $MgSO_4$-$7H_2O$<br>*Cool down to 50 °C*<br>10 ml Carbon source (galactose or 2-deoxy-galactose)<br>5 ml biotin (0.2mg/ml)<br>4.5 ml leucine (10 mg/ml)<br>*Add antibiotics and use 25 ml per plate* |
| **Lysis buffer (1 l)** | 12 g Tris, pH 7.0<br>37.2 g EDTA<br>1% SDS |
| **Standard fly food (30 l)** | 130 g Fadenagar<br>80 g USB agar<br>*Dissolve in 10 l hot water*<br>1070 g corn meal *(in 2.5 l warm water)*<br>1070 g malt<br>600 g treache *(in 1.5 l warm water)*<br>270 g soy meal *(in 2 l warm water)*<br>480 g try yeast<br>*Mix all ingredients and cook for 10 min, cool down to 72 °C*<br>64 g methyl hydroxyl benzoate *(solved in 350 ml ethanol)* |

| | |
|---|---|
| | 105 ml propionic acid |
| **Apple juice plates (2 l)** | 24 g Sucrose<br>60 g agar agar<br>*Autoclave an cool down*<br>40 ml 100% ethanol<br>20 ml 100% acetic acid |

### 4.1.8. Chemicals

All consumables and instruments used are from the following companies if not otherwise stated:

VWR (Radnor, PA, USA), Invitrogen (Paisley, UK), Agilent Technologies (Santa Clara, CA, USA), Millipore (Bedford, USA), Carl Roth GmbH (Karlsruhe, Germany), Promega (Madison, WI, USA), Roche Diagnostics GmbH (Mannheim, Germany), Fisher Scientific (Waltham, MA, USA), Leica Microsystems GmbH (Solms, Germany), Carl Zeiss AG (Jena, Germany), Bio-Rad Laboratories GmbH (Munich, Germany), Sigma-Aldrich GmbH (Steinheim, Germany), Greiner Bio-One GmbH (Frickhausen, Germany), Eppendorf (Hamburg, Germany), MBI Fermentas (Vilnius, Lithuania,) New England Biolabs (Ipswich, USA)

## 4.2. *Drosophila* Methods

### 4.2.1. *Drosophila* breeding

*Drosophila* melanogaster were kept on standard fly food at 18-27 °C. Stock collection was kept at 18 °C, working stocks at RT. Crosses to establish stocks and experiments other than RNAi experiments were carried out at 25 °C, RNAi experiments at 27 °C.

### 4.2.2. *Drosophila* genetics

Crosses were performed using different marker and balancer combinations. The most common balancers used are FM6-act-GFP for the X-chromosome, Cyo-GFP or –Wee-P for the 2$^{nd}$ chromosome and TM6B for the 3$^{rd}$ chromosome. Female virgins were crossed to males and the outcome was screened for the right genotype.

### 4.2.3. RNAi experiments at the larval NMJ

The establishment of the genome wide RNAi library allows the knock down of any gene of interested (Dietzl et al., 2007). RNAi in *Drosophila* is cell autonomous (Van Roessel et al., 2002) and can be triggered by the expression of a long double-stranded hairpin RNA (Kennerdell and Carthew, 2000; Martinek and Young, 2000). This construct is under the control of the UAS sequence and therefore can be expressed in a controlled temporal and spatial pattern via specific Gal4 driver lines. In this study virgins of the Gal4 line are crossed to males from the VDRC lines. Crosses were performed at 27°C and wandering L3 larvae were dissected.

### 4.2.4. Design of the RNAi screen

To identify novel cell adhesion molecules important for synapse development and stability I performed an unbiased RNAi screen at the *Drosophila* neuromuscular junction. Here I would like to describe the screening conditions in more detail. The Gal4 driver line *elav*$^{C155}$-Gal4; UAS-*dcr2*; BG57-Gal4 was used to knock down genes of interest pre- and postsynaptically. Virgins have been collected from this stock and crossed to males from the respective RNAi stocks from the Vienna *Drosophila* RNAi Center (VDRC). Entire classes of cell adhesion molecules important for neuronal development have been screened. A detailed list of all VDRC lines can be found in the appendix in Table 17-24. All crosses were performed at 27

°C. Wandering 3rd instar larvae were dissected and stained for the presynaptic active zone marker Brp (Bruchpilot), postsynaptic glutamate receptors (DGluRIII) and the presynaptic membrane using Hrp. Three 3rd instar larvae were analyzed for the total number of retractions and notes about muscle and morphology phenotypes like protrusions were made.

### 4.2.5. Genetic interaction experiments

To test potential interactions between Nrg and other important genes at the larval NMJ, I combined the Pacman rescue assay with classical mutations. Therefore, I crossed females of a stable stock of the Pacman rescued *Nrg* null mutation $nrg^{14}$ ($nrg^{14}$; P[*Nrgwt*] and $nrg^{14}$; P[$Nrg180^{\Delta FIGQY}$]) to males from the respective mutations. I analyzed male larvae selected based on the absence of specific balancers. A genetic interaction is considered if the retraction frequency in the $nrg^{14}$; P[$Nrg180^{\Delta FIGQY}$] background is more than double the sum of the retraction frequencies of $nrg^{14}$; P[*Nrgwt*] and $nrg^{14}$; P[$Nrg180^{\Delta FIGQY}$] including SEMs ((1.33 ± 0.91) + (8.12 ± 1.8) = 12.16 x 2 = 24.32).

### 4.2.6. Generation of FRT recombinants

$Nrg^{14}$ null mutation females were crossed to the P[FRT19A] males. Female P[FRT19A]/$nrg^{14}$ were crossed to FM6GFP males. After pre-mating for 2 days on normal food flies were put on G418 (neomycin) containing food. Because of the neomycin resistance in P[FRT19A] only FRT19A positive flies survive. The food was melted in the microwave, cooled down and 150 µl G418 (30 mg/ml stock solution) were added to 10 ml of food by stirring gently. The potential recombinant stocks were established and further selected based on the $nrg^{14}$ embryonic lethality. Loss of Nrg protein was checked using embryonic staining with $Nrg180^{BP104}$.

### 4.2.7. Generation of transgenic flies

Transgenic flies were generated either in the lab or at specialized companies (BestGene, *Drosophila* embryo injection service, Chino Hills, CA, USA). DNA was prepared using the Qiagen MIDI Kit for pUAST constructs or the Macherey-Nagel BAC100 Kit for P[acman] constructs. P[acman] constructs are injected with a concentration of 10-15 ng/10 kB. Embryos of $attP^{VK33}$ and $attP^{40}$ were used for site specific integration using Phi-C31 integrase (Bateman et al., 2006). 30 min old embryos were dechorinated using 50% bleach and aligned on tape-extract covered cover slips. After drying for 3-5 min on air, the embryos were

covered with 10S Voltalef oil to protect embryos from drying out. The DNA mix was injected using the FemtoJet devise (Eppendorf). After injection the embryos were transferred to 18 °C until hatching. The hatched larvae were transferred to food vials and kept at 25 °C until hatching. The hatched flies were crossed to second or third chromosomal balancers (IF/CyO-WeeP or TM3/TM6B respectively) and progeny was screened for $w^+$ positive flies. Transgenic stocks were established over the respective balancer.

### 4.2.8. Preparation of genomic DNA

Genomic DNA was prepared for the sequencing of transgenic Nrg Pacman flies. The following protocol was used:

- 40-50 flies were frozen at -20 °C in 100 µl lysis buffer (see list of media 2.1.7) in a 1.5 ml eppendorf tube
- Flies were homogenized using a pestle and 700 µl lysis buffer are added
- Incubate at 60 °C for 30 min and invert several times
- Add 150 µl 7.5 M KAc and incubate 30 min on ice
- Centrifuge 30 min at 10 000 rpm
- Transfer supernatant to a 1.5 ml eppendorf tube and centrifuge again
- Transfer supernatant in a new tube containing 700 µl of isopropanol
- Add 75 µl 2 M NaCl, mix gently and centrifuge at 13 000 rpm for 25 min at RT
- Discard supernatant and wash with 300 µl 70% EtOH at 13 000 rpm for 5 min at RT
- Dry pellet and resuspend in 40-100 µl RNAse-H2O (0.2 µg/ml)

### 4.2.9. Dissection of larval NMJ

$3^{rd}$ instar larvae were dissected in ice-cold standard dissecting saline (see list of Media 4.1.7.) under the stereo microscope using two forceps, a scissor (FST, Switzerland) and thin insect pins (Austerlitz, square meter 0.1 mm). The larvae were fixed ventral side up in the posterior and anterior part of the body using the insect pins. A small cut was made in the posterior part and the larvae were opened along the midline. Fatbody and organs were carefully removed to minimize the damage to the nervous system. Insect pins were used to open the larvae completely. Larvae were fixed using Bouins fixative for 2-3 min, washed in PBT and transferred to an eppendorf tube.

### 4.2.10. Immunohistochemistry at larval NMJ

See Material and Methods in the submitted manuscript

Uhu antibodies generated in this study: clones Uhu$^{59G}$ and Uhu $^{62D}$, 1:50

### 4.2.11. Immunohistochemistry of whole mount embryos

Flies were kept in cages for 2-3 days prior to embryo collection to accustom the flies to lay eggs on apple juice plates. For embryo collection depending on the age of embryos required, the embryos were aged accordingly. The following protocol was used to fix and stain embryos:

**Fixation**

- Embryos were washed from apple juice plates using PBT and collected in a mesh prepared tube
- Embryos were dechorinated for 5-6 min with 50% NaOCl and washed with $H_2O$ to remove chloride
- Embryos were transferred into a falcon tube using PBT
- PBT was removed completely and 2.25 ml Heptane and 2.25 ml PBS and 500 µl Formaldehyde (37%) (4% FA) were added
- Fixation for 20-30 min shaking at RT
- The watery phase (lower phase) was removed and 2 ml methanol were added
- Embryos were shaked intensively for 30 sec
- The upper organic phase was removed, methanol added again and shortly shaked
- Embryos are washed three times with methanol and three times with 96% ethanol

**AB staining**

- Embryos are washed 3 times 5min and 3 times 20 min with PBT at RT
- Blocking with 10% goat serum/PBS for 1 hr at RT
- Primary AB ON at 4 °C at least 15 h
- 3x short and 3x 20 min washing with PBT at RT
- Secondary AB 2 h at RT
- 3x short and 3 times 20 min washing with PBT at RT
- PBT is taken off and Vectashield H1000 was added (Vector Laboratories, inc. Burlingsame, CA 94010) as mounting medium

### 4.2.12. Mosaic analysis with repressible cell markers (MARCM)

The *Nrg* null mutation *nrg$^{14}$* was recombined with the P(neoFRT)19A chromosome. The stock was crossed to P(hsFLP)1, P(neoFRT)19A, tubGal80; *ok371*-Gal4, UAS-*CD8*-GFP;

MKRS P(hsFLP)86E four days before the experiment. At the day of the experiment two hours of egg laying at 25 °C are followed by three hours at 25 °C. The embryos are then heat shocked for one hour at 38.5 °C to induce the flipase expression and shifted to 18 °C over night to slow down development. To increase the number of clones also two flipases (hsFLP1 and hsFLP86) have been used. These two features led to a higher number of CD8-GFP positive motoneuron clones. The next day the embryos were shifted to 25 °C again and wandering female 3$^{rd}$ instar larvae were selected based on GFP positive patches in the brain and dissected as described before. Animals were stained with an rtCD8 antibody to visualize the motoneuron clones and different combinations of pre- and postsynaptic markers as stated in the experiments.

## 4.3. Molecular methods

### 4.3.1. TOPO cloning

Directional TOPO cloning was performed following the manufacturers protocol (Invitrogen). In brief, a PCR is performed with primers to produce a 5`-CACC overhang at the PCR product. The plasmid provided from the company has a 5`-GTGG overhang and a covalently bound Topoisomerase I. This ensures the right directionality of the pENTR clones. Colonies are screened using the primer m13fw and rev with the corresponding primers in the construct (Primer sequences listed in Table 6 and Table 7). After sequencing the pENTR clone is shuffled into the pUAST vector following the manufacturer protocol (Invitrogen). Obtained colonies have been checked using the SVrev primer or GFP rev primer and a corresponding forward primer within the construct (primer sequences listed in Table 6 and Table 12).

### 4.3.2. Site-directed Mutagenesis

The QuikChange Site-directed mutagenesis Kit (Statagene) was used to generate point mutations and small deletions following the manufacturer's manual. In brief, primers containing the desired mutation were designed (list of primers in Table 9) and annealed to the plasmid. Pfu-Turbo DNA polymerase is used to extend and incorporate the mutagenic primers. DpnI digests parental DNA as it is specific for methylated DNA. DNA extracted from almost all E.coli strains is methylated and therefore susceptible for DpnI digestion. The mutagenised vectors are transformed into competent cells and checked for mutations using appropriate primer-pairs (primer sequences listed in Table 12).

### 4.3.3 DNA preparation and purification

DNA of pUAST constructs of CG31708 and Neuroglian are prepared either using the Quiagen Midi Kit or the Macherey and Nagel Mini Kit according to the manufacturers' protocol in the manual. The only change to the protocols was the use of $H_2O$ instead of TE Buffer to elute the DNA. To purify fragments of digested DNA or PCR products the sample was run on an agarose gel and purified using the Gel purification kit from Quiagen using the manufacturers protocol. PCR products were also purified with the PCR-purification Kit if one clear single band could be obtained. Again $H_2O$ was used for the elution step.

### 4.3.4. Mutagenesis of P[acman] vectors using Recombineering

A modified protocol from Søren Warming was used to generate mutations in the Nrg P[acman] CH321-4H20 via recombineering. In a first step the galK cassette is inserted into the P[acman] (primer sequences used to generate the galK constructs are listed in Table 10). This galK cassette is then substituted by an oligo or PCR product with homology flanking the cassette (Oligo sequences listed in Table 11). If the galK cassette is lost the bacteria are resistant to 2-deoxy-galactose (DOG). DOG is harmless until it gets phosphorylated by the galK and turns into 2-deoxy-galactose-1-phosphate, which is toxic.

- galK primers are designed with 50 bp homology to the area flanking the target region for galK insertion.. Sequence underlined is from galK. Primers are listed in Table 10).
- fw: 5` ----50 bp---- CCTGTTGACAATTAATCATCGGCA
- rev: 5` ---- 50 bp (complementary strand) ---- TCAGCACTGTCCTGCTCCTT
- Oligos with the desired point mutations or small deletions are designed Primers are listed in Table11.
- P[acman] has been ordered from BPRC resources (vector: attB-P[acman]-$Cm^R$-BW, cells: SW102)
- The galK cassette has been amplified using the primers designed above and a proof reading polymerase. 1-2 µl DpnI are added per 25 µl reaction and incubated at 37 °C for 1 h to remove all plasmid DNA. The PCR product was purified on a gel.
- Overnight culture (5 ml with 12.5 µg/ml chloramphenicol) of SW102 with the P[acman] are inoculated and incubated at 32 °C.
- 500 µl overnight culture are diluted in 25 ml LB and incubated on 32 °C until the OD reaches 0.6 (app. 3-4 h).
- Recombination events are induced in a waterbath via heat shock at 42 °C for exactly 15 min, importantly cool down the culture immediately in a ice/waterbath slurry.
- Cultures are transferred into 15 ml falcon tubes and pelleted using 5000 rpm at 0 °C for 5 min.
- 1 ml ice-cold dd$H_2O$ is added and the pellet is gently resuspended by swirling in the ice/waterbath slurry. No pipetting and vortexing should be done at this step. 9 ml ice-cold water are added and the bacteria are pelleted again. This step is repeated twice.
- All supernatant is removed and cells are kept on ice until transformed. The following parameters are used for the transformation 25 mF, 1.75 kV and 200 ohms. After the transformation the cells are allowed to recover in 1 ml LB (15ml Falcon tube) for 1 h at 32 °C.
- After the recovery, the cells are washed twice with M9 salts: 1 ml culture is pelleted in a 2 ml eppendorf tube at 13200 rpm for 15 sec. Supernatant is removed and pellet is resuspended in M9 again. This step is repeated 3 times in total. After the last washing the cells are diluted in a series in M9 salts (1:10 and 1:100) and plated on M63 minimal plates (see above).

- Plates are incubated for 3 days at 32 °C.
- A few colonies are streaked on MacConkey + galactose + Choramphenicol indicator plates. GalK positive colonies appear to be bright red due to a pH change resulted from fermented galactose. This step is repeated in order to get a single colony.
- 5 ml LB (Chloramphenicol) are inoculated with a single bright red colony and incubated over night at 32 °C.
- The steps from above to obtain electrocompetent cells are repeated.
- The oligos designed above are thaw and annealed in vitro after the following protocol: 10 mg of each oligo are mixed with 100 µl PCR buffer. Mix is boiled for 5 min and cooled down to RT within 30 min (use PCR machine). 10 µl 3M NaAC and 250 µl EtOH are added for precipitation, the annealed oligos are pelleted via centrifugation and washed once with 70% EtOH. After air drying the pellet is resuspended in 100 µl $H_2O$. 1-3 µl oligos are used per transformation (200 ng).
- Bacteria are transformed and allowed to recover in 10 ml LB in 50 ml baffled conical flasks for 3-4 h.
- The bacteria are washed using M9 salts there dilution are made (1:10, 1:100, 1:1000). The dilutions are plated on M63 minimal plates with glycerol, leucine, biotin, DOG and Chloramphenicol
- Plates are incubated for three days at 32 °C
- Colonies are screened by PCR directly or after miniprep
- After a correct clone is isolated the DNA is transformed into EPI300 for induction of high copy numbers of the construct at 37 °C.

### 4.3.5. DNA preparation of P[acman] construct

The following protocol is used for the P[acman] miniprep:

- 5ml overnight culture was pelleted for 5 min at 5000 rpm
- Pellet is dissolved in 250 µl resuspension buffer and transferred into an eppendorf tube
- Add 250 µl lysis buffer and mix immediately by inversion
- Add 250 µl neutralization buffer and incubate after mixing for 5 min on ice
- Clear the supernatant twice by centrifugation at 13200 rpm for 5 min
- Precipitate DNA using 750 µl isopropanol, incubate 10 min on ice and centrifuge 10 min at 13 200 rpm.
- Wash once with 70% ethanol and dry on air
- Resuspend in 50 µl $H_2O$

### 4.3.6. Induction of P[acman] constructs

The EPI300 cells are special cells that can be induced to produce of a high copy number of the large Pacman constructs, which are normally on low copy number. To induce P[acman] constructs for DNA preparation in large scale the following two protocols were used.

**AutoFos induction solution**

- inocculate a preculture (5 ml) during the day (7-8 hours, until approximately saturation) in LB with appropriate antibiotic.
- Transfer 500 µl of preculture to 500 ml LB with appropriate antibiotic.
- Add 1000 µl AutoFos Induction Solution (1:500) and induce overnight shaking for 17-18 hours at 37 °C.

**CopyControl solution**

- Transfer 50 µl of preculture or single colony to 50 ml LB with appropriate antibiotic and let it shake for 17 hours overnight at 37 °C.
- Next day, add the overnight culture to 450 ml LB with appropriate antibiotic and it induce for 5 hours at 37 °C shaking by adding 100 µl CopyControl Induction Solution (1:5000)
- Transfer culture to centrifugation tube, spin for 15 min at ~5.500 rpm at 4 °C in rotor JA14 (4.600 g) and remove all LB.

Store the pellet at -80 °C overnight (recommended for at least a little while) and proceed with the protocol as stated in the manual (Nucleobond, BAC 100, Macherey-Nagel). The following option has been used during the protocol. To clarify the suspension, the suspension was filtered through a NucleoBond Folded Filter and the lysate was not centrifuged before. Pellets were dissolved directly in injection buffer (Tris-HCl, pH 8.0). To confirm DNA quality a test restriction was made before injection.

## 4.4. Biochemistry

### 4.4.1. Western Blot

Larval brains from wandering L3 larvae were dissected and transferred into 2x sample buffer (Invitrogen). 5 brains per lane were analyzed on NuPage gels (Invitrogen) according to standard procedures. Primary antibodies were incubated overnight at 4 °C. Secondary Hrp-conjugated goat anti-mouse and goat anti-rabbit antibodies were used at 1:10 000 (Jackson Immunoresearch) for 2 h at room temperature. Membranes were incubated with ECL substrate (SuperSignal West Pico Kit (Thermo scientific)) and subsequently exposed to on film (Fujifilm).

Additional (to the submitted manuscript) antibodies used in the study: rtUhu59G, rtUhu62D, 1:50 (test of expression in larval brains to test different clones of the antibody)

### 4.4.2. Generation of Antibodies

Monoclonal antibodies against Uhu were generated in the monoclonal facility of the FMI.

- A Uhu fragment (amino acid 350-500) was cloned and transferred into the pDEST17 vector for the expression of a His-tagged Uhu fragment
- A first test induction revealed that the Uhu protein fragment was not soluble and could not be made soluble using modified version of the vector pDESTHisMBT and pDESTperiHisMBT (Austin et al., 2009; Nallamsetty et al., 2005)
- The Uhu fragment was then solubilized under denaturating conditions using 5M Urea in 0.1M TrisCl pH 8.5

Induction of the protein expression:

- Add 5 ml overnight culture to 250 ml fresh LB medium (Ampicilin)
- Grow up to OD 600
- Add 1mM IPTG and induce protein expression for 3-4 h
- Harvest bacteria by centrifugation for 30 min at 4 °C with 5000rpm

Purification of the protein:

- The protein was purified using Ni-IDA columns (Protino) after the manufacturers protocol (buffers provided by the company)
- To test protein expression samples of each step were collected and analyzed using coomassie staining

- Protein was dialyzed directly with ice-cold PBS over night and samples again analyzed on a Coomassie gel
- Rats were immunized four ($2^{nd}$ time after 4 weeks, then 2 times in after another 4 weeks). An adjuvant was added to enhance the immune response the first two immunizations.

Peptide antibodies were produced at Davids Biotechnologie (Regensburg, Germany). Peptides were synthesized using Festphasensynthese. High-performance liquid chromatography (HPLC) and mass spectrometry are used for quality controls and the purity is between 70-98% for immunizations. Peptide antibodies are tested via Dot blots (protocol below) after delivery.

### 4.4.3. Dot blots

To analyze the specificity of the newly generated phospho antibodies, dot blots were performed using the following protocol:

- The top layer of paper on top of the nitrocellulose is removed. Using a pencil and ruler, grids of 1 cm by 1cm are marked on the nitrocellulose.
- The nitrocellulose membrane is placed in a petri-dish and 2-5 µl of the peptide are applied to the membrane (phosphorylated and nonphosphorylated)
- The dots are dried completely
- The membrane is blocked with 5% skim milk (made in TBST) for 1 hour.
- Then rinsed twice with TBST 1 min. each.
- Primary antibody incubation: 10 ml total, primary antibody diluted to the appropriate concentration in TBST + 1% BSA at 4 °C over night.
- Then rinsed twice with TBST 1 min. each.
- Secondary antibody incubation for 2 h at RT
- Then rinsed twice with TBST 1 min. each.
- Membrane is rinsed again with TBS + 1% Triton X-100 30 min each and then developed to film
- Nitrocellulose membrane was incubated with ECL substrate (SuperSignal West Pico Kit (Thermo scientific)) and subsequently exposed to on film (Fujifilm).

## 4.5. Microscopy

### 4.5.1. Quantification of phenotypes

Synaptic retractions were quantified using presynaptic Brp and postsynaptic DGluRIII staining by counting the number of unopposed postsynaptic footprints. The percentage of retractions was calculated and used to make the statistical analysis using the unpaired student`s t-test The classification to score the retraction severity was 1-3 bouton, 4-8 boutons, > 8 bouton and complete eliminations. Complete loss of presynaptic marker Brp was considered as elimination.

Bouton area, number and NMJ length were quantified using Synapsin (Syn), Dlg and Hrp staining. Bouton area and NMJ length were quantified using the Image access (Imagic) measurement tool. For bouton area the Hrp staining was used to visualize the bouton area and 10 A3 muscle 4 NMJ were quantified per genotype. To measure NMJ length 20 muscle 4 NMJ (segment A3 and A4, 10 each) were analyzed for the length of the NMJ (overlap of Dlg and Hrp staining). Bouton number was quantified under the microscope using a two-color filter and the 40x objective. The number of Syn/Dlg varicosities was counted per NMJ in the segments A2-A6. N is the number of NMJs scored. Numbers were normalized to wild type values.

### 4.5.2. Image acquisition

All images shown in this study are either taken at the Leica TCS SPE or the Zeiss LSM700 confocal microscope. Usually, the 63x oil objective (HCX PL APO, aperture 1.4-0.6) was used however some overgrowth phenotypes required the usage of the 40x oil objective (HCX PL APO, aperture 1.25-0.75). The images were taken with a resolution of 1024 x 2056 pixels.

### 4.5.3. Measurement of protein levels using FIJI

To analyze protein levels at the NMJ a Macro for the open source tool FIJI was generated together with Laurent Gelman from the imaging facility of the FMI. Hrp is used as the mask as is surrounds the NMJ and the axon. Only protein levels within the masking area are used for measurements. Regions of interest (ROI) were defined in the masking channel and these ROIs were used in the quantifying channel to analyze the protein level. Depending on the

genotype measurements are made in the axon bundle passing muscle 4, the motoneuron axon going to muscle 4 or at individual boutons within the NMJ terminal.

# 5. Appendix

## 5.1. Abbreviations

| | |
|---|---|
| A | alanine |
| aa | amino acid |
| AEL | after egg laying |
| AIS | axon initial segment |
| ALS | amyotrophic lateral sclerosis |
| *ank* | *ankyrin* |
| AP | action potential |
| | |
| BG | background |
| BM | bristle mechanosensory |
| bp | base pairs |
| *brp* | *bruchpilot* |
| | |
| *C. elegans* | Caenorhabditis elegans |
| CAM | cell adhesion molecule |
| cDNA | complementary DNA |
| CHL1 | close homolog of L1 |
| CNS | central nervous system |
| *cora* | *coracle* |
| CRASH | **C**orpus callosum hypoplasia, **R**etardation, **A**dducted thumbs, **S**pastic paraplegia, **H**ydrocephalus |
| | |
| D | aspartate |
| *dcr2* | *dicer-2* |
| dda | dorsal dendritic arborization |
| DGRC | *Drosophila* genome research center |
| DNA | desoxy-ribonucleic acid |
| DOG | 2-desoxy-galactose |
| Dpp | decapentaplegic |
| Dscam | Down syndrome cell adhesion molecule |
| | |
| ECL | enhanced chemi uminescence |
| EGF | epidermal growth factor |
| EGFP | enhancer green fluorescent protein |
| EGFR | epidermal growth factor receptor |
| EMS | ethyl-methanesulfonate |
| EPL | extensor pollicus longus |
| | |
| F | Fluorescence |
| F | phenylalanine |
| *fasII* | *fasciclin2* |

| | |
|---|---|
| FERM | **F** = 4.1 protein, **E** = ezrin, **R** = radixin, **M** = moesin |
| FGFR | fibroblast growth factor receptor |
| FMI | Friedrich Miescher Institute |
| Fn | Fibronectin |
| FRAP | Fluorescence recovery after photobleaching |
| | |
| *gbb* | *glass-bottom boat* |
| GF | giant fiber |
| GPI | glycosyl-phosphatidyl-inositol |
| | |
| h | hours |
| *hiw* | *highwire* |
| HPLC | high-performance liquid chromatography |
| Hrp | horse radish peroxidase |
| *hts* | *hu-li tai shao* |
| | |
| Ig | immunoglobulin |
| *inc* | *insomniac* |
| IP | immunoprecipitation |
| IP3 | inositol triphosphate |
| ISN | intersegmental nerve |
| | |
| kb | kilobase |
| kDA | kilo Dalton |
| | |
| LB | luria bertani |
| LGI | leucine-rich glioma inactivated |
| LON | **L**AMP, **O**BCAM, **N**eurotrimin |
| LRRTM | leucine rich repeat transmembrane |
| | |
| *mad* | *mother against dpp* |
| MAPK | mitogen activated protein kinase |
| MARCM | mosaic analysis with repressible cell marker |
| MASA | **M**ental retardation, **A**phasia, **S**huffling gait, **A**dducted thumbs |
| *med* | *medea* |
| MF | mobile fraction |
| min | minute |
| mus | muscle |
| | |
| NCAM | neural CAM |
| neu | neuronal |
| NgCAM | neuron-glia cell adhesion molecule |
| NGFR | neuronal growth factor receptor |
| NMJ | neuromuscular junction |

| | |
|---|---|
| NrCAM | NgCAM related CAM |
| *nrg* | *neuroglian* |
| NSH | Naphthylacetyl-spermin-trihydrochloride |
| | |
| OD | optical density |
| OP | ocelar pioneer |
| ORF | open reading frame |
| | |
| PBS | phosphate-buffered saline |
| PCR | polymerase chain reaction |
| pre | presynaptic |
| | |
| RNAi | RNA interference |
| ROI | region of interest |
| rpm | rounds per minute |
| RT | room temperature |
| | |
| *sax* | *saxophone* |
| SN | segmental nerve |
| *spec* | *spectrin* |
| SSR | sub |
| | |
| TBS | Tris-buffered saline |
| TGF | transforming growth factor |
| *tkv* | *thickveins* |
| TM | transmembrane |
| TTM | tergo-tochanteral muscle |
| | |
| UAS | upstream activating sequence |
| VDRC | Vienna *Drosophila* RNAi center |
| VNC | ventral nerve cord |
| WB | western blot |
| *wit* | *wishful thinking* |
| Y | Tyrosine |

Physical units are used according to the système international d’unités.

## 5.2. RNAi lines used for screening

### 5.2.1. Positive controls

#### Table 17 - VDRC lines of the positive controls used in the RNAi screen

| *Symbol* | *Name* | *Annotation ID* | *Transformant ID* | *Construct ID* |
|---|---|---|---|---|
| brp | bruchpilot | CG34146 | 21135 | 10046 |
| cac | cacophony | CG1522 | 5551 | 3326 |
| cpa | capping protein alpha | CG10540 | 18648 | 7009 |
| cpb | capping protein beta | CG17158 | 45668 | 9299 |
| chic | chickadee | CG9553 | 102759 | |
| ena | enabled | CG15112 | 43056 | 8910 |
| Ephrin | Ephrin | CG1862 | 105139 | |
| Gl | Glued | CG9206 | 3785 | 1455 |
| Glu-RIB | Glutamate receptor IB | CG4481 | 42891 | 3584 |
| GluRIIA | Glutamate receptor IIA | CG6992 | 101686 | 105437 |
| GluRIIB | Glutamate receptor IIB | CG7234 | 7878 | 917 |
| GluRIIC | Glutamate receptor IIC | CG4226 | 51438 | 796 |
| GluRIIE | Glutamate receptor IIE | CG31201 | 49547 | 16345 |
| hiw | highwire | CG32592 | 28163 | 14101 |
| Liprin-α | Liprin-α | CG11199 | 51707 | 7232 |
| Med | Medea | CG1775 | 19688 | 1483 |
| Mad | Mothers against dpp | CG12399 | 12635 | 4121 |
| Atpα | Na pump α subunit | CG5670 | 12330 | 3093 |
| nrv2 | nervana 2 | CG9261 | 2660 | 960 |
| ser | serrate | FlyBase Gene Report: Dmel\Ser | 27172 | 14453 |
| Syn | Synapsin | CG3985 | 46480 | 17037 |
| syt4 | synaptotagmin | CG10047 | 33317 | 2842 |
| tkv | thickveins | CG14026 | 3059 | 2549 |
| wg | wingless | CG4889 | 13351 | 5007 |
| α-Spec | α Spectrin | CG1977 | 25387/103709 | 9695/100689 |
| β-Spec | β Spectrin | CG5870 | 42053 | 11790 |

### 5.2.2. Ig-domain proteins

#### Table 18 - VDRC lines of Ig-domain proteins used in the RNAi screen

| *Symbol* | *Name* | *Annotation ID* | *Transformant ID* | *Construct ID* |
|---|---|---|---|---|
| ama | amalgam | CG2198 | 22944 | 12733 |
| beat-Ia | beaten path Ia | CG4846 | 4544 | 1386 |
| beat-Ib | beaten path Ib | CG7644 | 101662 | 105368 |
| beat-Ic | beaten path Ic | CG4838 | 45873 | 64 |
| beat-IIa | beaten path IIa | CG14334 | 18990 | 2587 |
| beat-IIb | beat-IIb | CG4135 | 17815 | 6761 |
| beat-IIIa | beat-IIIa | CG12621 | 45866 | 15037 |

| | | | | |
|---|---|---|---|---|
| beat-IIIb | beat-IIIb | CG33179 | 4784 | 2557 |
| beat-IIIc | beat-IIIc | CG15138 | 27137 | 6812 |
| beat-IV | beat-IV | CG10152 | 52413 | 16933 |
| beat-Va | beat-Va | CG10134 | 35715 | 13423 |
| Beat-Vb | Beat-Vb | CG31298 | 17832 | 6774 |
| beat-Vc | beat-Vc | CG14390 | 22736 | 12847 |
| beat-VI | beat-VI | CG14064 | 27205 | 14468 |
| boi | brother of iHog | CG32796 | 869 | 60 |
| bt | bent | CG32019 | 46252 | 14482 |
| btl | breathless | CG32134 | 27106 | 14439 |
| CG11320 | CG11320 | CG11320 | 18054 | 7268 |
| CG12484 | CG12484 | CG12484 | 25576 | 10005 |
| CG12950 | CG12950 | CG12950 | 10011 | 2880 |
| CG14141 | CG14141 | CG14141 | 43017 | 8239 |
| CG14372 | CG14372 | CG14372 | 16636 | 5643 |
| CG14521 | CG14521 | CG14521 | 104056 | 112589 |
| CG14964 | CG14964 | CG14964 | 43603 | 8498 |
| CG16857 | CG16857 | CG16857 | 24479 | 101 |
| CG17839 | CG17839 | CG17839 | 36314 | 14436 |
| CG31190 | CG31190 | CG31190 | 6685 | 74 |
| CG31431 | CG31431 | CG31431 | 1128 | 93 |
| CG31646 | CG31646 | CG31646 | 100781 | 108592 |
| CG31708 | CG31708 | CG31708 | 38261 | 6597 |
| CG31714 | CG31714 | CG31714 | 7654 | 1052 |
| CG32387 | | | 1100 | 111 |
| CG33515 | CG33515 | CG33515 | 30093 | 14652 |
| CG33543 | CG33543 | CG33543 | 17859 | 67 |
| CG34371 | - | CG34371 | 44997 | 2175 |
| CG3624 | CG3624 | CG3624 | 956 | 90 |
| CG3624 | CG3624 | CG3624 | 36304 | 14416 |
| CG4814 | | | 42353 | 15074 |
| CG6490 | CG6490 | CG6490 | 6683 | 73 |
| CG6490 | CG6490 | CG6490 | 24477 | 73 |
| CG7607 | CG7607 | CG7607 | 9208 | 3870 |
| CG8964 | CG8964 | CG8964 | 29908 | 14400 |
| cont | contactin | CG1084 | 28294/40613 | 12610 |
| dpr | defective proboscis extension response | CG13439 | 33816 | 15383 |
| dpr10 | dpr10 | CG32057 | 18919 | 6130 |
| dpr11 | dpr11 | CG33202 | 23243 | 13301 |
| dpr12 | dpr12 | CG34385 | 44740 | 15133 |
| dpr13 | dpr13 | CG33996 | 17667 | 8347 |
| dpr14 | dpr14 | CG10946 | 8005 | 2594 |
| dpr15 | dpr15 | CG10095 | 46244 | 16391 |
| dpr16 | dpr16 | CG12591 | 31986 | 7769 |
| dpr17 | dpr17 | CG31361 | 8481 | 2937 |
| dpr18 | dpr18 | CG14948 | 983 | 96 |
| dpr19 | dpr19 | CG13140 | 42789 | 1065 |

| | | | | |
|---|---|---|---|---|
| dpr2 | dpr2 | CG33507 | 29741 | 15154 |
| dpr20 | dpr20 | CG12191 | 15254 | 5971 |
| dpr3 | dpr3 | CG33516 | 25110 | 9000 |
| dpr4 | dpr4 | CG33512 | 28518 | 13088 |
| dpr6 | dpr6 | CG14162 | 41161 | 4836 |
| dpr7 | dpr7 | CG33481 | 46216 | 16254 |
| dpr8 | dpr8 | CG32600 | 39203 | 14664 |
| dpr9 | dpr9 | CG33485 | 38690 | 7773 |
| Dscam | Down syndrome cell adhesion molecule | CG17800 | 3115 | 2596 |
| ed | echinoid | CG12676 | 938 | 79 |
| elav | embryonic lethal, abnormal vision | CG4262 | 37915 | 5206 |
| Fas1 | Fasciclin 1 | CG6588 | 23015 | 12817 |
| Fas2 | Fasciclin 2 | CG3665 | 8392 | 2579 |
| Fas3 | Fasciclin 3 | CG5803 | 42231 | 14367 |
| fra | frazzled | CG8581 | 6557 | 68 |
| fred | friend of echinoid | CG31774 | 33298 | 2574 |
| hbs | hibris | CG7449 | 9471 | 70 |
| hig | hikaru genki | CG2040 | 13266 | 5279 |
| htl | heartless | CG7223 | 27180 | 14457 |
| iHog | interference Hedgehog | CG9211 | 29897 | 14317 |
| ImpL2 | Ecdysone-inducible gene L2 | CG15009 | 30930 | 6004 |
| kek1 | kekkon-1 | CG12283 | 36252 | 14381 |
| kek2 | kekkon-2 | CG4977 | 42449 | 9 |
| kek5 | kekkon5 | CG12199 | 1401 | 36 |
| kek6 | kek6 | CG1804 | 19184 | 8810 |
| kirre | kin of irre | CG3653 | 27227 | 14476 |
| klg | klingon | CG6669 | 36162 | 14314 |
| Lac | Lachesin | CG12369 | 35524 | 12649 |
| lea | leak/Robo2 | CG5481 | 11823 | 109 |
| Nrg | Neuroglian | CG1634 | 6688 | 82 |
| nrm | neuromusculin | CG8779 | 979 | 94 |
| Nrx-IV | Neurexin IV | CG6827 | 8353 | 2436 |
| Ppn | Papilin | CG33103 | 16523 | 6325 |
| PQBP-1 | Poly-glutamine tract binding protein 1 | CG31369 | 28752 | 13399 |
| Pxn | Peroxidasin | CG12002 | 15276 | 5987 |
| robo | roundabout | CG13521 | 47921 | 14414 |
| robo3 | robo3 | CG5423 | 44702 | 14351 |
| Ror | Ror | CG4926 | 935 | 40 |
| rst | roughest | CG4125 | 951 | 86 |
| sdk | sidekick | CG5227 | 9437 | 2553 |
| sev | sevenless | CG18085 | 49924 | 3307 |
| side | sidestep | CG31062 | 1283 | 321 |
| sls | sallimus | CG1915 | 47301 | 9680 |
| sns | sticks and stones | CG33141 | 877 | 65 |

| | | | | |
|---|---|---|---|---|
| tutl | turtle | CG15427 | 3064 | 2558 |
| unc-5 | unc-5 | CG8166 | 8138 | 3510 |
| vn | vein | CG10491 | 50358 | |
| wrapper | wrapper | CG10382 | 101567 | |
| | | CG13992 | 2642 | |
| | CG15744 | | 4800 | |
| | | CG13532 | 12848 | |
| | | CG5597 | 12875 | |
| | | | | |
| | | CG13672 | 23488 | |
| | | CG33274 | 25365 | |
| | | CG30171 | 29412 | |
| | | CG13134 | 29729 | |
| | | CG34353 | 29845 | |
| | | CG31619 | 33102 | |
| | | CG5699 | 34517 | |
| | | CG31970 | 37842 | |
| | | CG15630 | 37843 | |
| | | CG34114 | 38809 | |
| | | CG15354 | 40821 | |
| | | CG16974 | 42226 | |
| | | CG34391 | 42353 | |
| | CG8434 | lambik | 43898 | |
| | CG11136 | tartan/caps -like | 44991 | 14419 |
| | | CG14583 | 49553 | |
| | | CG15312 | 101286 | |
| | | CG31369 | 102322 | |
| | | CG13020 | 104044 | |

## 5.2.3. LRR-proteins

### Table 19 - VDRC lines of LRR-domain proteins used in the RNAi screen

| *Symbol* | *Name* | *Annotation ID* | *Transformant ID* | *Construct ID* |
|---|---|---|---|---|
| caps | capricious | CG11282 | 3046 | 2530 |
| | CG10148 | | 44841 | |
| | CG10255 | | 18600 | |
| | CG10307 | | 27150 | |
| | CG11099 | | 9272 | |
| | CG11136 | tartan/caps -like | 44991 | 14419 |
| | CG11280 | tartan | 5242 | 2450 |
| | CG11807 | | 38564 | |
| | CG11910 | | 14737 | |
| | CG13125 | | 17123 | |
| | CG13487 | | 44532 | |
| | CG13708 | | 17690 | |
| | CG14185 | | 32097 | |
| | CG14351 | tartan/caps -like | 36220 | 14353 |

| | | | | |
|---|---|---|---|---|
| | CG14662 | | 8472 | |
| | CG14762 | | 31014 | |
| | CG1484 | | 39528 | |
| | CG14995 | | 12725 | |
| | CG1504 | | 18513 | |
| | CG15151 | rdo | 107213 | |
| | CG15658 | | 3040 | 2509 |
| CG15744 | CG15744 | CG15744 | 1096 | |
| | CG17319 | | 8384 | 2518 |
| | CG17335 | CG1644 | 32691 | |
| | CG17667 | | 36144 | 14305 |
| | CG18024 | | 16588 | |
| | CG18095 | | 886 | 1 |
| | CG18249 | | 3816 | 2519 |
| | CG18480 | | 1071 | 26 |
| | CG3040 | | 19219 | |
| | CG3095 | | 14524 | |
| | CG31076 | | 28776 | |
| | CG31635 | | 33979 | |
| | CG32085 | | 34053 | |
| | CG32372 | | 18977 | |
| | CG32687 | | 20819 | |
| | CG3408 | | 36306 | 14429 |
| | CG3413 | | 37209 | |
| | CG3494 | | 24760 | |
| | CG3980 | | 34773 | |
| | CG4054 | | 1702 | |
| | CG4781 | | 7605 | 2215 |
| | CG4950 | | 9931 | 1664 |
| | CG5096 | | 27060 | 14378 |
| | CG5195 | | 31044 | |
| | CG5407 | | 27410 | |
| | CG5490 | toll precursor | 100078 | |
| | CG5528 | Toll-9 | 36308 | 14431 |
| | CG5784 | | 49386 | |
| | CG5810 | | 44988 | |
| | CG5819 | | 27076 | 14412 |
| | CG5820 | Gp150 | 900 | 10 |
| | CG5851 | | 42051 | |
| | CG5888 | | 12413 | |
| | CG6098 | | 27567 | |
| | CG6590/32055 | | 6335 | |
| | CG6860 | | 7306 | |
| | CG6890 | Toll, Tak1 | 9431 | 2510 |
| | CG7121 | Tehoa, Toll-5 | 17903 | 2534 |
| | CG7250 | Toll-6 | 27102 | 14438 |
| | CG7457 | | 26740 | |
| | CG7503 | | 17898 | |

| | | | | |
|---|---|---|---|---|
| | CG7509 | | 51584 | |
| | CG7702 | connectin like | 1059 | 21 |
| | CG7800 | | 6673 | 2520 |
| | CG7896 | tartan/caps -like | 36343 | 14469 |
| | CG8272 | | 24262 | |
| | CG8561 | | 44361 | |
| | CG8595 | Toll-7 | 24473 | 16 |
| | CG8930 | | 904 | |
| | CG9031 | | 42188 | |
| | CG9044 | | 42193 | |
| lbk | lambik | CG8434 | 4319 | 71 |

## 5.2.4. Cadherins

### Table 20 - VDRC lines of all Cadherins used in the RNAi screen

| *Symbol* | *Name* | *Annotation ID* | *Transformant ID* | *Construct ID* |
|---|---|---|---|---|
| | CG1744 | | 108053 | |
| stan | starry night | CG11895 | 1665 | 607 |
| shg | shotgun | CG3722 | 27081 | 14421 |
| Ret | Ret oncogene | CG14396 | 843 | 45 |
| lbm | late bloomer | CG2374 | 7937 | 1843 |
| ft | fat | CG3352 | 9396 | 881 |
| fat2 | fat2 | CG7794 | 35275 | 12286 |
| ds | dachsous | CG17941 | 4312 | 2646 |
| CG4655 | CG4655 | CG4655 | 26587 | 11388 |
| Cad74A | Cad74A | CG6445 | 36320 | 14440 |
| Cad86C | Cad86C | CG4509 | 3744 | 158 |
| Cad87A | Cad87A | CG6977 | 8578 | 3637 |
| Cad87A | | | 49325 | 17452 |
| Cad88C | Cad88C | CG3389 | 36164 | 14315 |
| Cad89D | Cad89D | CG14900 | 36331 | 14455 |
| Cad99C | Cad99C | CG31009 | 3733 | 151 |
| CadN | Cadherin-N | CG7100 | 1092 | 161 |
| CadN2 | CadN2 | CG7527 | 36166 | 14316 |
| cals | calsyntenin-1 | CG11059 | 36348 | 14484 |

## 5.2.5. Integrins

### Table 21 - VDRC lines of all Integrins used in the RNAi screen

| *Symbol* | *Name* | *Annotation ID* | *Transformant ID* | *Construct ID* |
|---|---|---|---|---|
| if | inflated/aPS2 | CG9623 | 44885 | 1175 |
| mew | multiple edematous wings | CG1771 | 44890 | 1230 |
| mew/aPS1 | multiple edematous wings | CG1771 | 5671 | 1230 |

| | | | | |
|---|---|---|---|---|
| mys | myospheroid | CG1560 | 29619 | 15002 |
| scb | scab | CG8095 | 4891 | 2006 |
| αPS4 | αPS4 | CG16827 | 37172 | 2007 |
| αPS5 | αPS5 | CG5372 | 6646 | 2181 |
| βInt-ν | $\beta^{v}$ integrin | CG1762 | 893 | 7 |

## 5.2.6. Laminins

### Table 22 - VDRC lines of all Laminins used in the RNAi screen

| *Symbol* | *Name* | *Annotation ID* | *Transformant ID* | *Construct ID* |
|---|---|---|---|---|
| crb | crumbs | CG6383 | 39177 | 14463 |
| drpr | draper | CG2086 | 27086 | 14423 |
| LanA | Laminin A | CG10236 | 18873 | 6022 |
| LanB1 | Laminin B1 | CG7123 | 23119 | 13179 |
| LanB2 | Laminin B2 | CG3322 | 42559 | 2394 |
| NetB | Netrin-B | CG10521 | - | 3356 |
| Nrx-1 | Neurexin-1 | CG7050 | 36328 | 14451 |
| trol | terribly reduced optic lobes | CG33950 | 22642 | 12341 |
| wb | wing blister | CG15288 | 3141 | 1560 |

## 5.2.7. Semaphorins

### Table 23 - VDRC lines of all Semaphorins used in the RNAi screen

| *Symbol* | *Name* | *Annotation ID* | *Transformant ID* | *Construct ID* |
|---|---|---|---|---|
| Sema-1a | Sema-1a | CG18405 | 36148 | 14307 |
| Sema-1b | Sema-1b | CG6446 | 107233 | 104666 |
| Sema-2a | Sema-2a | CG4700 | 15810 | 5476 |
| Sema-5c | Semaphorin-5c | CG5661 | 9429 | 2501 |
| plexA | plexin A | CG11081 | 4740 | 2499 |
| plexB | plexin B | CG17245 | 8382 | 2500 |
| dsd | distracted | CG5634 | 1106 | 135 |
| CG7166 | CG7166 | CG7166 | 27116 | 14443 |
| CG7466 | CG7466 | CG7466 | 42462 | 138 |
| CG33960 | CG33960 | CG33960 | 48056 | 16812 |

## 5.2.8. Cell adhesion molecule interaction proteins

### Table 24 - VDRC lines of all CAM interaction proteins used in the RNAi screen

| *Symbol* | *Name* | *Annotation ID* | *Transformant ID* | *Construct ID* |
|---|---|---|---|---|
| 18w | 18 wheeler | CG8869 | 963 | 17 |
| arm | armadillo | CG11579 | 7767 | 1372 |
| baz | bazooka | CG5055 | 2914 | 1384 |
| boss | bride of sevenless | CG8285 | 4365 | 292 |

| | | | | |
|---|---|---|---|---|
| cno | canoe | CG2534 | 7769 | 1395 |
| CG18146 | CG18146 | CG18146 | 3120 | 2622 |
| CG32810 | CG32810 | CG32810 | 18225 | 7621 |
| CG7422 | CG7422 | CG7422 | 27997 | 12232 |
| CG8942 | CG8942 | CG8942 | 40747 | 14386 |
| cora | coracle | CG11949 | 9788 | 1405 |
| crq | croquemort | CG4280 | 45883 | 784 |
| Csp | Cysteine string protein | CG6395 | 34167 | 10571 |
| Dl | Delta | CG3619 | 3720 | 146 |
| dlg1 | discs large 1 | CG1725 | 2612 | 855 |
| dsh | dishevelled | CG18361 | 101525 | 108967 |
| Dg | Dystroglycan | CG18250 | 107029 | 100828 |
| eag | ether a go-go | CG10952 | 9127 | 3363 |
| fas | faint sausage | CG17716 | 42236 | 14405 |
| fz | frizzled | CG17697 | 43075 | 4614 |
| fz2 | frizzled 2 | CG9739 | 26928 | 13804 |
| fz3 | frizzled 3 | CG16785 | 30214 | 3174 |
| fz4 | frizzled 4 | CG4626 | 5451 | 3269 |
| Gli | Gliotactin | CG3903 | 37116 | 1735 |
| Glt | Glutactin | CG9280 | 15429 | 5017 |
| Glu-RI | Glutamate receptor I | CG8442 | 44438 | 3582 |
| grk | gurken | CG17610 | 3121 | 2624 |
| in | inturned | CG16993 | 26133 | 10892 |
| Nrt | Neurotactin | CG9704 | 8495 | 3597 |
| N | Notch | CG3936 | 27229 | 14477 |
| ppk12 | pickpocket 12 | CG10972 | 105131 | 101805 |
| Psn | Presenilin | CG18803 | 43083 | 4624 |
| santa-maria | scavenger receptor acting in neural tissue and majority of rhodopsin is absent | CG12789 | 33153 | 969 |
| scrib | scribbled | CG5462 | 27424 | 11663 |
| shakB | shaking B | CG34358 | 24578 | 7794 |
| shi | shibire | CG18102 | 3799 | 1529 |
| sli | slit | CG8355 | 38233 | 5822 |
| syt | synaptotagmin | CG3139 | 8875 | 842 |
| sdc | syndecan | CG10497 | 13322 | 4545 |
| Ten-a | Tenascin accessory | CG32659 | 8322 | 3330 |
| Ten-m | Tenascin major | CG5723 | 51173 | 3620 |
| trp | transient receptor potential | CG7875 | 1365 | 372 |

## 5.3. Supplementary Figures and data summaries

### 5.2.1. Supplementary data of the RNAi screen

**Table 25 - Top10 Hits of the RNAI screen based on the number of retractions**

| *ranking* | *VDRC line* | *name* | *# of retraction/ 3 animals* | *Small retraction/ big retractions* | *Class of proteins* |
|---|---|---|---|---|---|
| 1 | 107991 | nrg | 62 | 24/38 | Ig-domain |
| 2 | 38261* | CG31708 | - | - | Ig-domain |
| 3 | 18225 | inc | 60 | 47/13 | CAM interaction |
| 4 | 9788 | cora | 42 | 26/16 | CAM interaction |
| 5 | 31044 | CG5536 | 37 | 25/12 | LRR |
| 6 | 23243 | CG33202 | 30 | 24/6 | Ig-domain |
| 7 | 35275 | CG7794 | 25 | 17/8 | LRR |
| 8 | 107450 | lac | 23 | 17/6 | Ig-domain |
| 9 | 9787 | cora | 23 | 13/10 | CAM interaction |
| 10 | 27424 | scrib | 23 | 20/3 | CAM interaction |

Ranking of the Top10 hits based on the number of retractions (* lethal after pre- and postsynaptic knock down thus not analyzed during the screen). The name of the gene is included if the gene is characterized otherwise the CG number is shown. The symbol is used instead of the full name (*nrg= neuroglian, inc = insomniac, cora = coracle, lac = lachesin, scrib = scribbled)*. All muscles of three animals have been analyzed for synaptic retractions. This number was then separated in two categories of small (1-3 boutons) and big (4 or more boutons) retractions as. The numbers indicate the number of small and big retractions observed in three animals (all muscles analyzed). The last column indicates the class of CAMs to which the hit belongs based on Table 3.

### 5.3.1. Supplementary data of Neuroglian

#### *5.3.1.1. Supplementary data of retraction*

**Table 26 - Quantification of retractions during development**

*Retraction frequency [%]*

| UAS | stage | Gal4 | mu 4 | mu 6/7 | mu 12 | mu 13 | n |
|---|---|---|---|---|---|---|---|
| RNAi[1] | L2 | ed/neu[3] | 28.00 ± 4.90 | 8.00 ± 4.16 | 7.00 ± 3.35 | 8.00 ± 3.27 | 10 |
| | earlyL3 | ed/neu[3] | 48.46 ± 4.78 | 23.07 ± 4.58 | 17.69 ± 5.21 | 22.31 ± 5.45 | 13 |
| | L3 | ed/neu[3] | 63.85 ± 3.32 | 44.5 ± 4.78 | 27.0 ± 3.41 | 35.65 ± 3.86 | 20 |

**Legend:** RNAi[1] = VDRC6688**,** Gal4 drivers: neu[2] = *elav*$^{C155}$-Gal4; UAS-*dcr2*, n = numbers of analyzed animals, numbers represent values ± SEM.

## Table 27 - Quantification of retractions after postsynaptic RNAi in Pacman background

| Genotype | mu4 | mu6/7 | mu12 | mu13 | n |
|---|---|---|---|---|---|
| *nrg*$^{14}$/y; P[*Nrgwt*] | 1.33 ± 0.91 | 0.67 ± 0.67 | 0.0 ± 0.00 | 0.0 ± 0.00 | 15 |
| *nrg*$^{14}$/y; P[*Nrg180ΔFIQGY*] | 8.12 ± 1.81 | 11.70 ± 2.20 | 7.41 ± 1.60 | 6.25 ± 1.22 | 28 |
| *nrg*$^{14}$/y; P[*Nrgwt*] mus$^{3}$ RNAi$^{2}$ | 0.0 ± 0.0 | 8.33 ± 3.07 | 0.0 ± 0.00 | 0.0 ± 0.00 | 6 |
| *nrg*$^{14}$/y; P[*Nrg180ΔFIQGY*] mus$^{3}$ RNAi$^{2}$ | 27.78 ± 4.65 | 24.44 ± 5.56 | 36.67 ± 5.27 | 10.00 ± 2.89 | 9 |

**Legend:** P value is in comparison to *nrg*$^{14}$/y; P[*Nrgwt*] (unpaired student`s t-test), RNAi$^{2}$ = VDRC107991, n = number of analyzed animals, numbers represent values ± SEM.

## Table 28 - Quantification of Nrg glial RNAi

| *UAS* | *Gal4* | *mu4* | *mu6/7* | *mu12* | *mu13* | *n* |
|---|---|---|---|---|---|---|
| ctrl | repo | 0.77 ± 0.77 | 0.00 ± 0.00 | 0.77 ± 0.77 | 0.77 ± 0.77 | 13 |
| Nrg RNAi$^{1}$ | repo | 15.22 ± 3.06 | 2.67 ± 1.53 | 1.33 ± 0.91 | 15.48 ± 2.93 | 15 |
| Nrg RNAi$^{1}$ | dcr2; repo | 28 ± 3.74 | 6.00 ± 4.00 | 6.00 ± 4.00 | 0.00 ± 0.00 | 5 |
| Ank$^{1}$ RNAi | repo | 4.17 ± 1.49 | 6.66 ± 2.84 | 2.5 ± 1.79 | 0.83 ± 0.83 | 12 |

**Legend:** ctrl = w$^{1118}$ x *repo*-Gal4, RNAi$^{1}$ = VDRC6688, P values are in comparison to the ctrl (all unpaired student`s t-test), n = number of analyzed animals, numbers represent values ± SEM.

### *5.3.1.2. Supplementary data of growth related phenotypes*

## Table 29 - Quantification of growth defects after Nrg RNAi

| *UAS* | *Gal4* | *Bouton number* | *P* | *n* |
|---|---|---|---|---|
| Ctrl | | 16.6 ± 0.38 | | 123 |
| RNAi$^{1}$ | e/neu1 | 18.36 ± 0.57 | 0.013 | 50 |
| RNAi$^{1}$ | eo/neu2 | 20.45 ± 0.60 | ≤ 0.0001 | 75 |

**Legend:** ctrl=w1118, P values are in comparison to the ctrl (all unpaired student`s t-test). Gal4 drivers: neu$^{1}$= *elav*$^{C155}$-Gal4, neu$^{2}$=*elav*$^{C155}$-Gal4; *ok371*-Gal4, RNAi$^{1}$ = VDCR line 6688, n= number of analyzed muscle 4 NMJ, numbers represent values ± SEM.

## Table 30 - Quantification of protrusions in Nrg RNAi animals

| *UAS* | *Gal4* | *% mu 4 NMJ with protrusions* | *P* | *# of protrusions/NMJ* | *P* | *n* |
|---|---|---|---|---|---|---|
| ctrl | eo/neu$^{2}$ | 7.5 ± 1.64 | | 0.075 ± 0.03 | | 8 |
| RNAi$^{1}$ | eo/neu$^{2}$ | 38.39 ± 7.09 | 0.0062 | 0.42 ± 0.06 | ≤0.0001 | 16 |
| RNAi$^{2}$ | eo/neu$^{2}$ | 48.63 ± 6.23 | ≤0.0001 | 0.62 ± 0.07 | ≤0.0001 | 14 |
| ctrl | dB/mus$^{2}$ | 10 ± 1.74 | | 0.1 ± 0.03 | | 12 |
| RNAi$^{1}$ | dB/mus$^{2}$ | 46.36 ± 5.27 | ≤0.0001 | 0.65 ± 0.08 | ≤0.0001 | 11 |

**Legend:** ctrl=w$^{1118}$ x *elav*$^{C155}$-Gal4; *ok371*-Gal4 or UAS-*drc2*; *BG57*-Gal4, P values are in comparison to the ctrl (all unpaired student`s t-test). Gal4 drivers: neu$^{2}$ = *elav*$^{C155}$-Gal4; *ok371*-Gal4, mus$^{2}$ = UAS-*dcr2*; BG57-Gal4, n = number of analyzed animals, only stable NMJs were included, numbers represent values ± SEM.

## Table 31 - Quantification of protrusions in Pacman rescued animals

| *Pacman* | *% mu 4 NMJ with protrusions* | *P* | *n* |
|---|---|---|---|
| *nrg*$^{14}$/y; P[*Nrgwt*] | 7.78 ± 3.64 | | 9 |
| *nrg*$^{14}$/y; P[*Nrg180*$^{\Delta FIQGY}$] | 37.64 ± 6.10 | 0.0009 | 11 |

**Legend:** P value is in comparison to *nrg*$^{14}$/y; P[*Nrgwt*] (unpaired student`s t-test), n = number of analyzed animals, numbers represent values ± SEM.

## Table 32 - Quantification of Nrg hypomorphic mutations

*Retraction frequency [%]*

| *Genotype* | *mu4* | *p* | *mu6/7* | *mu12* | *mu13* | *n* |
|---|---|---|---|---|---|---|
| w$^{1118}$ | 1.3 ± 0.66 | | 2.4 ± 0.87 | 0.4 ± 0.4 | 0.4 ± 0.4 | 25 |
| *nrg*$^{849/849}$ | 2.5 ± 1.64 | 0.39 | 3.75 ± 2.63 | 0 ± 0 | 1.25 ± 1.25 | 8 |
| *nrg*$^{14/849}$ | 3.85 ± 1.85 | 0.1 | 3.85 ± 1.40 | 0 ± 0 | 1.54 ± 1.04 | 13 |
| *nrg*$^{305/305}$ | 9.23 ± 2.39 | 0.0002 | 12.31 ± 2.57 | 3.08 ± 1.33 | 6.15 ± 1.8 | 13 |
| *nrg*$^{305/14}$ | 15.83 ± 3.36 | ≤ 0.0001 | 20 ± 3.26 | 4.17 ± 1.93 | 2.5 ± 1.80 | 12 |

*Growth defects (real numbers)*

| *Genotype* | *NMJ length (n=20)* | *p* | *bouton area (n=10)* | *p* | *bouton number* | *p* | *n* |
|---|---|---|---|---|---|---|---|
| w$^{1118}$ | 106.93 ± 4.36 | | 6.95 ± 0.32 | | 16.6 ± 0.38 | | 123 |
| *nrg*$^{849/849}$ | 99.72± 5.28 | 0.3 | 4.48 ± 0.23 | ≤ 0.0001 | 18.42 ± 0.77 | 0.021 | |
| *nrg*$^{14/849}$ | 112.33 ± 6.36 | 0.48 | 4.25 ± 0.23 | ≤ 0.0001 | 19.46 ± 0.69 | ≤ 0.0001 | |
| *nrg*$^{305/305}$ | 131.85 ± 6.67 | 0.0034 | 4.43 ± 0.17 | ≤ 0.0001 | 26.67 ± 0.71 | ≤ 0.0001 | 146 |
| *nrg*$^{305/14}$ | 154.24 ± 8.03 | ≤ 0.0001 | 3.88 ± 0.18 | ≤ 0.0001 | 26.95 ± 0.77 | ≤ 0.0001 | 144 |

**Legend:** P values are in comparison to w$^{1118}$ (all unpaired student`s t-test), n$^{retractions}$ = number of animals (segments A2-A6 were scored in each animal), n$^{boutonnumber}$ = number of NMJ (segments A2-A6 were scored in each animal), n$^{NMJlength}$ = number of NMJ (segments A3 and A4, 10 each), n$^{boutonarea}$ = number of NMJ (segment A3), numbers represent values ± SEM.

## Table 33 - Quantification of growth after Nrg overexpression

| *UAS* | *Gal4* | *Bouton number* | *p* | *n* |
|---|---|---|---|---|
| Ctrl | | 16.6 ± 0.38 | | 123 |
| UASnrg180wt_EGFP | *ok371* | 17.06 ± 0.38 | 0.061 | 118 |
| UASnrg180ΔFIGQY_EGFP | *ok371* | 30.89 ± 0.69 | ≤ 0.0001 | 114 |

**Legend:** ctrl = $w^{1118}$ x *ok371*-Gal4, P values are in comparison to ctrl (all unpaired student`s t-test). n = number of NMJs analyzes (segment A2-A6 were scored for each animal). Numbers represent values ± SEM.

### *5.3.1.3. Supplementary data of genetic interaction experiments*

## Table 34 - Quantification of retractions in genetic interaction experiments with Ank2 and α-Spectrin

*Retraction frequency [%]*

| Genotype | mu 4 | P | mu 6/7 | mu 12 | mu 13 | n |
|---|---|---|---|---|---|---|
| $w^{1118}$ | 1.30 ± 0.66 | | 2.40 ± 0.87 | 0.4 ± 0.4 | 0.40 ± 0.40 | 25 |
| *nrg*$^{14}$/y; P[*Nrgwt*]/+ | 1.33 ± 0.91 | 0.9 * | 0.67 ± 0.67 | 0.00 ± 0.00 | 0.00 ± 0.00 | 15 |
| *nrg*$^{14}$/y; P[*Nrg180ΔFIQGY*] | 8.12 ± 1.81 | 0.012 | 11.70 ± 2.20 | 7.41 ± 1.60 | 6.25 ± 1.22 | 28 |
| *nrg*$^{14}$/y; P[*Nrgwt*]/+; *ank2*$^{518}$/+ | 3.75 ± 1.83 | 0.2 | 5.00 ± 2.67 | 1.25 ± 1.25 | 3.75 ± 1.83 | 8 |
| *nrg*$^{14}$/y; P[*Nrg180ΔFIQGY*]/+; *ank2*$^{518}$/+ | 27.86 ± 2.81 | ≤ 0.0001 | 27.86 ± 4.71 | 16.43 ± 3.41 | 17.86 ± 4.22 | 14 |
| *nrg*$^{14}$/y; P[*Nrgwt*]/+; *α-spec*$^{rg41}$/+ | 6.15 ± 2.13 | 0.038 | 10.77 ± 3.83 | 1.54 ± 1.54 | 5.38 ± 2.43 | 13 |
| *nrg*$^{14}$/y; P[*Nrg180ΔFIQGY*] /+; *α-spec*$^{rg41}$/+ | 33.33 ± 4.60 | ≤ 0.0001 | 30.48 ± 4.39 | 15.24 ± 2.98 | 8.75 ± 2.10 | 21 |

**Legend:** p value is in comparison to *nrg*$^{14}$/y; P[*Nrgwt*] p* = in comparison to $w^{1118}$ (unpaired student`s t-test), n = number of analyzed animals, numbers represent values ± SEM.

## Table 35 - Quantification of retraction in genetic interaction experiments

| *Genotype* | *mu 4* | *mu 6/7* | *mu 12* | *mu 13* | *n* |
|---|---|---|---|---|---|
| $w^{1118}$ | 1.30 ± 0.66 | 2.40 ± 0.87 | 0.4 ± 0.4 | 0.40 ± 0.40 | 25 |
| *nrg*$^{14}$/y; P[*Nrgwt*] | 1.33 ± 0.91 | 0.67 ± 0.67 | 0.0 ± 0.0 | 0.0 ± 0.0 | 15 |
| *nrg*$^{14}$/y; P[*Nrg180ΔFIQGY*] | 8.12 ± 1.81 | 11.70 ± 2.20 | 7.41 ± 1.60 | 6.25 ± 1.22 | 28 |
| *nrg*$^{14}$/y; P[*Nrgwt*]/+; wit$^{B11}$/+ | 15.0 ± 4.28 | 20.00 ± 8.56 | 11.67 ± 6.54 | 6.67 ± 3.33 | 6 |
| *nrg*$^{14}$/y; P[*Nrg180ΔFIQGY*] /+; wit$^{B11}$/+ | 19.10 ± 4.56 | 17.27 ± 3.59 | 12.72 ± 3.83 | 10.0 ± 3.30 | 11 |
| *nrg*$^{14}$/y; P[*Nrgwt*]/+; wit$^{A12}$/+ | 10.0 ± 4.71 | 9.00 ± 3.59 | 7.00 ± 2.60 | 3.00 ± 2.13 | 10 |
| *nrg*$^{14}$/y; P[*Nrg180ΔFIQGY*] /+; wit$^{A12}$/+ | 20.0 ± 3.05 | 22.73 ± 5.83 | 14.54 ± 3.40 | 5.45 ± 2.07 | 11 |
| *nrg*$^{14}$/y; P[*Nrgwt]*/mad$^{1-2}$ | 5.0 ± 3.42 | 7.0 ± 2.13 | 0.0 ± 0.0 | 4.22 ± 1.33 | 10 |
| *nrg*$^{14}$/y; P[*Nrg180ΔFIQGY*]/mad$^{1-2}$ | 10.0 ± 4.08 | 15.0 ± 6.46 | 2.5 ± 2.5 | 5.00 ± 2.89 | 4 |

| | | | | | |
|---|---|---|---|---|---|
| *nrg*$^{14}$/y; P[*Nrgwt]*/mad$^{k237}$ | 2.85 ± 1.84 | 4.29 ± 2.02 | 0.00 ± 0.00 | 7.14 ± 2.86 | 7 |
| *nrg*$^{14}$/y; P[*Nrg180ΔFIQGY*]/mad $^{k237}$ | 20.0 ± 2.89 | 26.67 ± 5.00 | 24.44 ± 4.12 | 6.67 ± 2.36 | 9 |
| *nrg*$^{14}$/y; P[*Nrgwt*]/*tkv*$^{1}$ | 4.45 ± 2.07 | 4.45 ± 3.11 | 0.91 ± 0.91 | 0.91 ± 0.91 | 11 |
| *nrg*$^{14}$/y; P[*Nrg180ΔFIQGY*]/*tkv*$^{1}$ | 42.22 ± 4.94 | 43.33 ± 4.71 | 30.00 ± 5.00 | 27.78 ± 3.64 | 9 |
| *Genotype* | *mu 4* | *mu 6/7* | *mu 12* | *mu 13* | *n* |
| *tkv*$^{1}$/*tkv*$^{1}$ | 0.9 ± 0.9 | 1.81 ± 1.81 | 0.0 ± 0.0 | 0.0 ± 0.0 | 11 |
| *wit*$^{B11}$/+ | 2.5 ± 1.64 | 8.75 ± 2.95 | 0.0 ± 0.0 | 1.25 ± 1.25 | 8 |
| *wit*$^{A12}$/+ | 4.0 ± 2.21 | 7.0 ± 3.0 | 1.0 ± 1.0 | 0.0 ± 0.0 | 10 |
| *nrg*$^{14}$/+ | 5.87 ± 2.08 | 8.57 ± 3.4 | 0.0 ± 0.00 | 2.86 ± 1.84 | 7 |

**Legend:** n = number of analyzed animals, numbers represent values ± SEM.

## Table 36 - Quantification of bouton number in genetic interaction experiments

| *Genotype* | *Bouton number* | *P* | *n* |
|---|---|---|---|
| w$^{1118}$ | 16.6 ± 0.38 | | 123 |
| *nrg*$^{14}$/y; P[*Nrgwt*] | 15.74 ± 0.50 | 0.17* | 98 |
| *nrg*$^{14}$/y; P[*Nrg180ΔFIQGY*] | 29.30 ± 0.90 | ≤ 0.0001 | 112 |
| *nrg*$^{14}$/y; P[*Nrgwt*]/+; a*nk2*$^{518}$/+ | 16.68 0.49 | 0.19 | 76 |
| *nrg*$^{14}$/y; P[*Nrg180ΔFIQGY*]/+; *ank2*$^{518}$/+ | 31.68 1.38 | 0.14** | 56 |
| *nrg*$^{14}$/y; P[*Nrgwt*]/+; *wit*$^{B11}$/+ | 23.37 ± 0.73 | ≤ 0.0001 | 70 |
| *nrg*$^{14}$/y; P[*Nrg180ΔFIQGY*] /+; *wit*$^{B11}$/+ | 38.04 ± 1.38 | ≤ 0.0001** | 46 |

**Legend:** P values are in comparison to *nrg*$^{14}$/y; P[*Nrgwt*] , P* = in comparison to w$^{1118}$ , P** = in comparison to *nrg*$^{14}$/y; P[*Nrg180*$^{ΔFIGQY}$] (all unpaired student`s t-test), n = number of analyzed NMJs (segment A2-A6 were scored per animal), numbers represent values ± SEM.

### *5.3.1.4. Supplemental data to Uhu*

## Table 37 - Quantification of retractions after *uhu* RNAi

*Retraction frequency [%]*

| *VDRC* | *stage* | *Gal4* | *mu 4* | *mu 6/7* | *mu 12* | *mu 13* | *n* |
|---|---|---|---|---|---|---|---|
| 38261 | L2 | eo/neu$^{2}$ | 1.11 ± 1.11 | 2.22 ± 2.22 | 1.11 ± 1.11 | 0.0 ± 0.00 | 9 |
| 38261 | early L3 | eo/neu$^{2}$ | 0.0 ± 0.0 | 8.0 ± 3.74 | 6.0 ± 2.45 | 2.0 ± 2.0 | 5 |
| 38261 | L3 | eo/neu$^{2}$ | 0.0 ± 0.0 | 52.83 ± 5.72 | 40.0 ± 5.77 | 41.67 ± 4.77 | 6 |

**Legend:** VDRC38261 targets CG31708, Gal4 driver line = neu$^{2}$ = *elav*$^{C155}$-Gal4; *ok371*-Gal4, n = number of analyzed animals (segment A2-A6 were scored per animal), numbers represent values ± SEM.

## Table 38 - Summary of SignalP and Phoebius prediction

| *CG number* | *SignalP* | *Phoebius* | |
|---|---|---|---|
| | Prediction | Signal peptide | Transmembrane |
| CG14010-PA | Non-secretory protein | no | yes |
| CG11320-PB | Signal peptide | yes | no |
| CG14521-PA | Signal peptide | yes | yes/no |
| CG31646-PA | Signal anchor | yes/no | yes/no |
| CG32791-PA | Signal peptide | yes | yes/no |
| CG40378-PA | Non-secretory protein | no | no |
| CG34391-PC | Non-secretory protein | no | no |
| CG42343-PC | Non-secretory protein | no | yes |

Result of the SignalP and Phoebius prediction of 9 genes with three Ig-like domains and the highest similarity to CG31708 and CG42368 are summarized for the presence of signal peptides, signal anchors and transmembrane domains. Signal peptides are about 19 amino acid long sequences at the N-terminus of proteins and are important for the localization to the endoplasmatic reticulum. A signal anchor indicates a single pass transmembrane protein. If the protein has neither a signal peptide nor a signal anchor it is predicted to be a non secretory protein.

## 5.3.2. Supplementary Figures

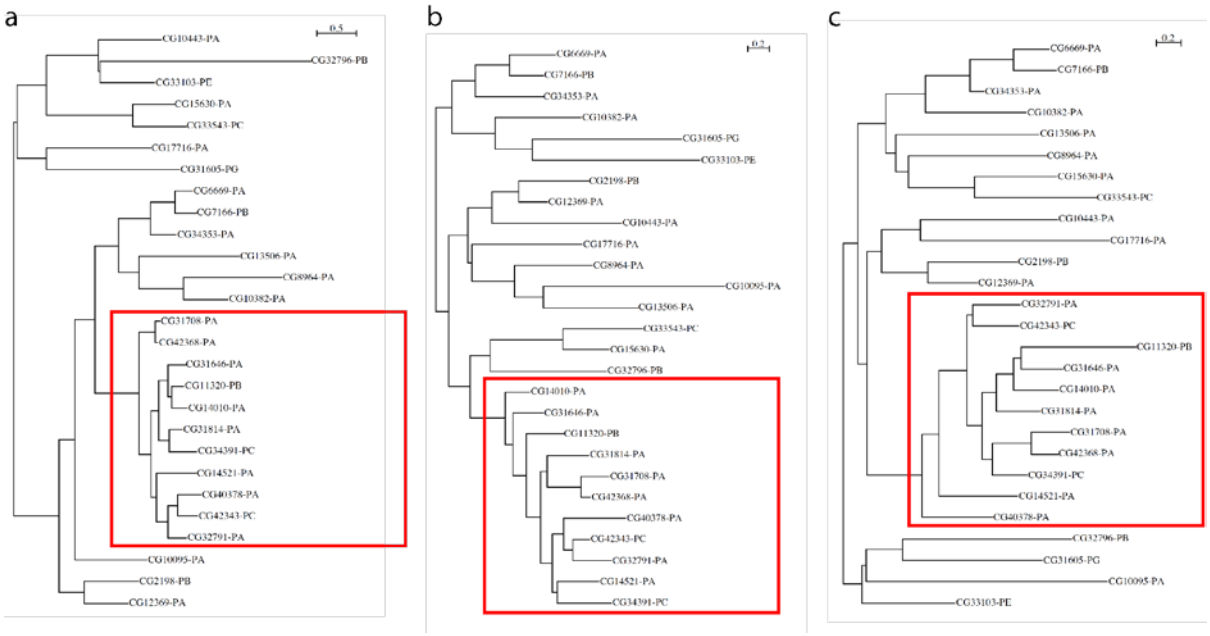


**Supplementary Figure 33 - Phylogentic trees of the Ig-domains of Drosophila proteins harboring three Ig-domains**

Analysis of all *Drosophila* proteins with exactly 3 Ig-like domains using ClustalW followed by PHYML (www. mobyle.pasteur): the Ig-like domains were analyzed separately and phylogentic trees have been generated based on the result **(a)** The result of the1$^{st}$ Ig-domain. **(b)** The result of the 2$^{nd}$ Ig-domain. **(c)** The result of the 3$^{rd}$ Ig-domain. The red boxes indicate the cluster of 10 genes around CG31708 (Uhu). CG42368 is always the closest relative to Uhu. The Scalebar represents the branch length and is relative to the number of changes within the sequence.

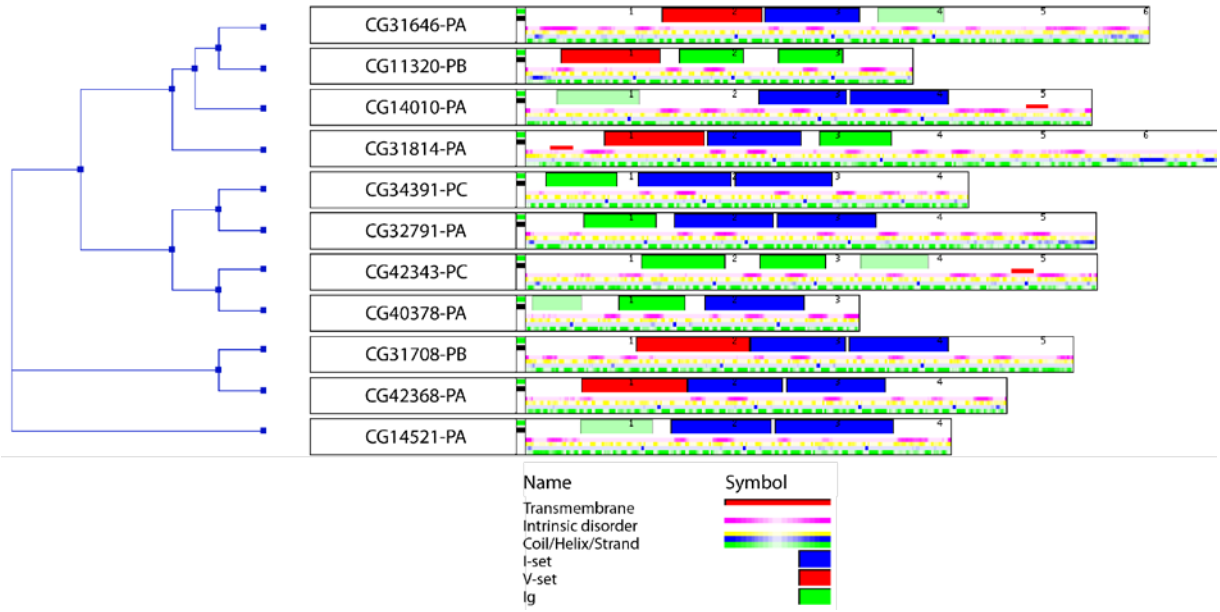


**Supplementary Figure 34 - result of the ProteinArchitect analysis for CG31708 and the 10 closest relatives**

The protein sequences of Uhu and its closest relatives were analyzed using the online tool ProteinArchitekt (http://www.proteinarchitect.net). This program compares protein sequences on multiple levels and gives a representative visualization of the relationship between these sequences. This analysis showed that Uhu and CG42368 are closely related and have the same order and types of Ig-like domains. None of the other proteins showed this order of Ig-like domains.

## 5.4. Index of Figures

## 5.5. Index of Tables

# 6. References

.Aberle, H., A.P. Haghighi, R.D. Fetter, B.D. McCabe, T.R. Magalhaes, and C.S. Goodman. 2002. wishful thinking encodes a BMP type II receptor that regulates synaptic growth in Drosophila. *Neuron*. 33:545-558.

Akeel, M., C.J. McNamee, S. Youssef, and D. Moss. 2011. DIgLONs inhibit initiation of neurite outgrowth from forebrain neurons via an IgLON-containing receptor complex. *Brain Res*. 1374:27-35.

Amores, A., A. Force, Y.L. Yan, L. Joly, C. Amemiya, A. Fritz, R.K. Ho, J. Langeland, V. Prince, Y.L. Wang, M. Westerfield, M. Ekker, and J.H. Postlethwait. 1998. Zebrafish hox clusters and vertebrate genome evolution. *Science*. 282:1711-1714.

Ango, F., G. di Cristo, H. Higashiyama, V. Bennett, P. Wu, and Z.J. Huang. 2004. Ankyrin-based subcellular gradient of neurofascin, an immunoglobulin family protein, directs GABAergic innervation at purkinje axon initial segment. *Cell*. 119:257-272.

Appel, F., J. Holm, J.F. Conscience, and M. Schachner. 1993. Several extracellular domains of the neural cell adhesion molecule L1 are involved in neurite outgrowth and cell body adhesion. *J Neurosci*. 13:4764-4775.

Arikkath, J., and L.F. Reichardt. 2008. Cadherins and catenins at synapses: roles in synaptogenesis and synaptic plasticity. *Trends Neurosci*. 31:487-494.

Arnaout, M.A., B. Mahalingam, and J.P. Xiong. 2005. Integrin structure, allostery, and bidirectional signaling. *Annu Rev Cell Dev Biol*. 21:381-410.

Austin, B.P., S. Nallamsetty, and D.S. Waugh. 2009. Hexahistidine-tagged maltose-binding protein as a fusion partner for the production of soluble recombinant proteins in Escherichia coli. *Methods Mol Biol*. 498:157-172.

Barbin, G., M.S. Aigrot, P. Charles, A. Foucher, M. Grumet, M. Schachner, B. Zalc, and C. Lubetzki. 2004. Axonal cell-adhesion molecule L1 in CNS myelination. *Neuron Glia Biol*. 1:65-72.

Bateman, J.R., A.M. Lee, and C.T. Wu. 2006. Site-specific transformation of Drosophila via phiC31 integrase-mediated cassette exchange. *Genetics*. 173:769-777.

Becker, C.G., B.C. Lieberoth, F. Morellini, J. Feldner, T. Becker, and M. Schachner. 2004. L1.1 is involved in spinal cord regeneration in adult zebrafish. *J Neurosci*. 24:7837-7842.

Bednarek, E., and P. Caroni. 2011. beta-Adducin is required for stable assembly of new synapses and improved memory upon environmental enrichment. *Neuron*. 69:1132-1146.

Bennett, V., and P.J. Stenbuck. 1980. Association between ankyrin and the cytoplasmic domain of band 3 isolated from the human erythrocyte membrane. *J Biol Chem*. 255:6424-6432.

Benson, D.L., and G.W. Huntley. 2012. Synapse adhesion: a dynamic equilibrium conferring stability and flexibility. *Curr Opin Neurobiol*. 22:397-404.

Berger, C., S. Renner, K. Luer, and G.M. Technau. 2007. The commonly used marker ELAV is transiently expressed in neuroblasts and glial cells in the Drosophila embryonic CNS. *Dev Dyn*. 236:3562-3568.

Bieber, A.J., P.M. Snow, M. Hortsch, N.H. Patel, J.R. Jacobs, Z.R. Traquina, J. Schilling, and C.S. Goodman. 1989. Drosophila neuroglian: a member of the immunoglobulin superfamily with extensive homology to the vertebrate neural adhesion molecule L1. *Cell*. 59:447-460.

Biederer, T., Y. Sara, M. Mozhayeva, D. Atasoy, X. Liu, E.T. Kavalali, and T.C. Sudhof. 2002. SynCAM, a synaptic adhesion molecule that drives synapse assembly. *Science*. 297:1525-1531.

Bixby, K.A., M.H. Nanao, N.V. Shen, A. Kreusch, H. Bellamy, P.J. Pfaffinger, and S. Choe. 1999. Zn2+-binding and molecular determinants of tetramerization in voltage-gated K+ channels. *Nat Struct Biol*. 6:38-43.

Blaess, S., R.A. Kammerer, and H. Hall. 1998. Structural analysis of the sixth immunoglobulin-like domain of mouse neural cell adhesion molecule L1 and its interactions with alpha(v)beta3, alpha(IIb)beta3, and alpha5beta1 integrins. *J Neurochem*. 71:2615-2625.

Boerner, J., and T.A. Godenschwege. 2010. Application for the Drosophila ventral nerve cord standard in neuronal circuit reconstruction and in-depth analysis of mutant morphology. *J Neurogenet*. 24:158-167.

Boillee, S., C. Vande Velde, and D.W. Cleveland. 2006. ALS: a disease of motor neurons and their nonneuronal neighbors. *Neuron*. 52:39-59.

Boulin, T., R. Pocock, and O. Hobert. 2006. A novel Eph receptor-interacting IgSF protein provides C. elegans motoneurons with midline guidepost function. *Curr Biol*. 16:1871-1883.

Brand, A.H., and N. Perrimon. 1993. Targeted gene expression as a means of altering cell fates and generating dominant phenotypes. *Development*. 118:401-415.

Brink, D.L., M. Gilbert, X. Xie, L. Petley-Ragan, and V.J. Auld. 2012. Glial processes at the Drosophila larval neuromuscular junction match synaptic growth. *PLoS One*. 7:e37876.

Bucher, D., and J.M. Goaillard. 2011. Beyond faithful conduction: short-term dynamics, neuromodulation, and long-term regulation of spike propagation in the axon. *Prog Neurobiol*. 94:307-346.

Castellani, V., E. De Angelis, S. Kenwrick, and G. Rougon. 2002. Cis and trans interactions of L1 with neuropilin-1 control axonal responses to semaphorin 3A. *Embo J*. 21:6348-6357.

Chavis, P., and G. Westbrook. 2001. Integrins mediate functional pre- and postsynaptic maturation at a hippocampal synapse. *Nature*. 411:317-321.

Chen, J.H., L. Wen, S. Dupuis, J.Y. Wu, and Y. Rao. 2001. The N-terminal leucine-rich regions in Slit are sufficient to repel olfactory bulb axons and subventricular zone neurons. *J Neurosci*. 21:1548-1556.

Chen, K., C. Merino, S.J. Sigrist, and D.E. Featherstone. 2005. The 4.1 protein coracle mediates subunit-selective anchoring of Drosophila glutamate receptors to the postsynaptic actin cytoskeleton. *J Neurosci*. 25:6667-6675.

Chen, S.Y., and H.J. Cheng. 2009. Functions of axon guidance molecules in synapse formation. *Curr Opin Neurobiol*. 19:471-478.

Cheng, L., K. Itoh, and V. Lemmon. 2005a. L1-mediated branching is regulated by two ezrin-radixin-moesin (ERM)-binding sites, the RSLE region and a novel juxtamembrane ERM-binding region. *J Neurosci*. 25:395-403.

Cheng, L., S. Lemmon, and V. Lemmon. 2005b. RanBPM is an L1-interacting protein that regulates L1-mediated mitogen-activated protein kinase activation. *J Neurochem*. 94:1102-1110.

Craig, A.M., and Y. Kang. 2007. Neurexin-neuroligin signaling in synapse development. *Curr Opin Neurobiol*. 17:43-52.

Crossin, K.L., and L.A. Krushel. 2000. Cellular signaling by neural cell adhesion molecules of the immunoglobulin superfamily. *Dev Dyn*. 218:260-279.

Cunha, S.R., N. Bhasin, and P.J. Mohler. 2007. Targeting and stability of Na/Ca exchanger 1 in cardiomyocytes requires direct interaction with the membrane adaptor ankyrin-B. *J Biol Chem*. 282:4875-4883.

Cunha, S.R., S. Le Scouarnec, J.J. Schott, and P.J. Mohler. 2008. Exon organization and novel alternative splicing of the human ANK2 gene: implications for cardiac function and human cardiac disease. *J Mol Cell Cardiol*. 45:724-734.

Cunha, S.R., and P.J. Mohler. 2009. Ankyrin protein networks in membrane formation and stabilization. *J Cell Mol Med*. 13:4364-4376.

Dahme, M., U. Bartsch, R. Martini, B. Anliker, M. Schachner, and N. Mantei. 1997. Disruption of the mouse L1 gene leads to malformations of the nervous system. *Nat Genet*. 17:346-349.

Dalva, M.B., A.C. McClelland, and M.S. Kayser. 2007. Cell adhesion molecules: signalling functions at the synapse. *Nat Rev Neurosci*. 8:206-220.

Davis, J.Q., and V. Bennett. 1984. Brain ankyrin. A membrane-associated protein with binding sites for spectrin, tubulin, and the cytoplasmic domain of the erythrocyte anion channel. *J Biol Chem*. 259:13550-13559.

Davis, J.Q., and V. Bennett. 1994. Ankyrin binding activity shared by the neurofascin/L1/NrCAM family of nervous system cell adhesion molecules. *J Biol Chem*. 269:27163-27166.

De Angelis, E., J. MacFarlane, J.S. Du, G. Yeo, R. Hicks, F.G. Rathjen, S. Kenwrick, and T. Brummendorf. 1999. Pathological missense mutations of neural cell adhesion molecule L1 affect homophilic and heterophilic binding activities. *Embo J*. 18:4744-4753.

De Angelis, E., A. Watkins, M. Schafer, T. Brummendorf, and S. Kenwrick. 2002. Disease-associated mutations in L1 CAM interfere with ligand interactions and cell-surface expression. *Hum Mol Genet*. 11:1-12.

de Wit, J., W. Hong, L. Luo, and A. Ghosh. 2011. Role of leucine-rich repeat proteins in the development and function of neural circuits. *Annu Rev Cell Dev Biol*. 27:697-729.

de Wit, J., E. Sylwestrak, M.L. O'Sullivan, S. Otto, K. Tiglio, J.N. Savas, J.R. Yates, 3rd, D. Comoletti, P. Taylor, and A. Ghosh. 2009. LRRTM2 interacts with Neurexin1 and regulates excitatory synapse formation. *Neuron*. 64:799-806.

Demyanenko, G.P., A.Y. Tsai, and P.F. Maness. 1999. Abnormalities in neuronal process extension, hippocampal development, and the ventricular system of L1 knockout mice. *J Neurosci*. 19:4907-4920.

Dickson, T.C., C.D. Mintz, D.L. Benson, and S.R. Salton. 2002. Functional binding interaction identified between the axonal CAM L1 and members of the ERM family. *J Cell Biol*. 157:1105-1112.

Dietzl, G., D. Chen, F. Schnorrer, K.C. Su, Y. Barinova, M. Fellner, B. Gasser, K. Kinsey, S. Oppel, S. Scheiblauer, A. Couto, V. Marra, K. Keleman, and B.J. Dickson. 2007. A genome-wide transgenic RNAi library for conditional gene inactivation in Drosophila. *Nature*. 448:151-156.

Dion, P.A., H. Daoud, and G.A. Rouleau. 2009. Genetics of motor neuron disorders: new insights into pathogenic mechanisms. *Nat Rev Genet*. 10:769-782.

Eaton, B.A., and G.W. Davis. 2005. LIM Kinase1 controls synaptic stability downstream of the type II BMP receptor. *Neuron*. 47:695-708.

Eaton, B.A., R.D. Fetter, and G.W. Davis. 2002. Dynactin is necessary for synapse stabilization. *Neuron*. 34:729-741.

Faulkner, R.L., L.K. Low, and H.J. Cheng. 2007. Axon pruning in the developing vertebrate hippocampus. *Dev Neurosci*. 29:6-13.

Felding-Habermann, B., S. Silletti, F. Mei, C.H. Siu, P.M. Yip, P.C. Brooks, D.A. Cheresh, T.E. O'Toole, M.H. Ginsberg, and A.M. Montgomery. 1997. A single immunoglobulin-like domain of the human neural cell adhesion molecule L1 supports adhesion by multiple vascular and platelet integrins. *J Cell Biol*. 139:1567-1581.

Feng, Z., S. Koirala, and C.P. Ko. 2005. Synapse-glia interactions at the vertebrate neuromuscular junction. *Neuroscientist*. 11:503-513.

Forni, J.J., S. Romani, P. Doherty, and G. Tear. 2004. Neuroglian and FasciclinII can promote neurite outgrowth via the FGF receptor Heartless. *Mol Cell Neurosci*. 26:282-291.

Fouquet, W., D. Owald, C. Wichmann, S. Mertel, H. Depner, M. Dyba, S. Hallermann, R.J. Kittel, S. Eimer, and S.J. Sigrist. 2009. Maturation of active zone assembly by Drosophila Bruchpilot. *J Cell Biol*. 186:129-145.

Fransen, E., V. Lemmon, G. Van Camp, L. Vits, P. Coucke, and P.J. Willems. 1995. CRASH syndrome: clinical spectrum of corpus callosum hypoplasia, retardation, adducted thumbs, spastic paraparesis and hydrocephalus due to mutations in one single gene, L1. *Eur J Hum Genet*. 3:273-284.

Fransen, E., G. Van Camp, L. Vits, and P.J. Willems. 1997. L1-associated diseases: clinical geneticists divide, molecular geneticists unite. *Hum Mol Genet*. 6:1625-1632.

Funatsu, N., S. Miyata, H. Kumanogoh, M. Shigeta, K. Hamada, Y. Endo, Y. Sokawa, and S. Maekawa. 1999. Characterization of a novel rat brain glycosylphosphatidylinositol-anchored protein (Kilon), a member of the IgLON cell adhesion molecule family. *J Biol Chem*. 274:8224-8230.

Garcia-Alonso, L., S. Romani, and F. Jimenez. 2000. The EGF and FGF receptors mediate neuroglian function to control growth cone decisions during sensory axon guidance in Drosophila. *Neuron*. 28:741-752.

Garver, T.D., Q. Ren, S. Tuvia, and V. Bennett. 1997. Tyrosine phosphorylation at a site highly conserved in the L1 family of cell adhesion molecules abolishes ankyrin binding and increases lateral mobility of neurofascin. *J Cell Biol*. 137:703-714.

Gil, O.D., T. Sakurai, A.E. Bradley, M.Y. Fink, M.R. Cassella, J.A. Kuo, and D.P. Felsenfeld. 2003. Ankyrin binding mediates L1CAM interactions with static components of the cytoskeleton and inhibits retrograde movement of L1CAM on the cell surface. *J Cell Biol*. 162:719-730.

Gil, O.D., G. Zanazzi, A.F. Struyk, and J.L. Salzer. 1998. Neurotrimin mediates bifunctional effects on neurite outgrowth via homophilic and heterophilic interactions. *J Neurosci*. 18:9312-9325.

Gil, O.D., L. Zhang, S. Chen, Y.Q. Ren, A. Pimenta, G. Zanazzi, D. Hillman, P. Levitt, and J.L. Salzer. 2002. Complementary expression and heterophilic interactions between IgLON family members neurotrimin and LAMP. *J Neurobiol*. 51:190-204.

Godenschwege, T.A., L.V. Kristiansen, S.B. Uthaman, M. Hortsch, and R.K. Murphey. 2006. A conserved role for Drosophila Neuroglian and human L1-CAM in central-synapse formation. *Curr Biol*. 16:12-23.

Godenschwege, T.A., and R.K. Murphey. 2009. Genetic interaction of Neuroglian and Semaphorin1a during guidance and synapse formation. *J Neurogenet*. 23:147-155.

Goossens, T., Y.Y. Kang, G. Wuytens, P. Zimmermann, Z. Callaerts-Vegh, G. Pollarolo, R. Islam, M. Hortsch, and P. Callaerts. 2011. The Drosophila L1CAM homolog Neuroglian signals through distinct pathways to control different aspects of mushroom body axon development. *Development*. 138:1595-1605.

Grotewiel, M.S., C.D. Beck, K.H. Wu, X.R. Zhu, and R.L. Davis. 1998. Integrin-mediated short-term memory in Drosophila. *Nature*. 391:455-460.

Haas, M.A., J.C. Vickers, and T.C. Dickson. 2004. Binding partners L1 cell adhesion molecule and the ezrin-radixin-moesin (ERM) proteins are involved in development and the regenerative response to injury of hippocampal and cortical neurons. *Eur J Neurosci*. 20:1436-1444.

Hall, S.G., and A.J. Bieber. 1997. Mutations in the Drosophila neuroglian cell adhesion molecule affect motor neuron pathfinding and peripheral nervous system patterning. *J Neurobiol*. 32:325-340.

Hashimoto, T., M. Yamada, S. Maekawa, T. Nakashima, and S. Miyata. 2008. IgLON cell adhesion molecule Kilon is a crucial modulator for synapse number in hippocampal neurons. *Brain Res*. 1224:1-11.

Haspel, J., and M. Grumet. 2003. The L1CAM extracellular region: a multi-domain protein with modular and cooperative binding modes. *Front Biosci*. 8:s1210-1225.

Hassel, B., F.G. Rathjen, and H. Volkmer. 1997. Organization of the neurofascin gene and analysis of developmentally regulated alternative splicing. *J Biol Chem*. 272:28742-28749.

Hattori, D., S.S. Millard, W.M. Wojtowicz, and S.L. Zipursky. 2008. Dscam-mediated cell recognition regulates neural circuit formation. *Annu Rev Cell Dev Biol*. 24:597-620.

Helmbacher, F., S. Schneider-Maunoury, P. Topilko, L. Tiret, and P. Charnay. 2000. Targeting of the EphA4 tyrosine kinase receptor affects dorsal/ventral pathfinding of limb motor axons. *Development*. 127:3313-3324.

Henderson, R.H., Z. Li, M.M. Abd El Aziz, D.S. Mackay, M.A. Eljinini, M. Zeidan, A.T. Moore, S.S. Bhattacharya, and A.R. Webster. 2010. Biallelic mutation of protocadherin-21 (PCDH21) causes retinal degeneration in humans. *Mol Vis*. 16:46-52.

Herron, L.R., M. Hill, F. Davey, and F.J. Gunn-Moore. 2009. The intracellular interactions of the L1 family of cell adhesion molecules. *Biochem J*. 419:519-531.

Hillenbrand, R., M. Molthagen, D. Montag, and M. Schachner. 1999. The close homologue of the neural adhesion molecule L1 (CHL1): patterns of expression and promotion of neurite outgrowth by heterophilic interactions. *Eur J Neurosci*. 11:813-826.

Hopitzan, A.A., A.J. Baines, M.A. Ludosky, M. Recouvreur, and E. Kordeli. 2005. Ankyrin-G in skeletal muscle: tissue-specific alternative splicing contributes to the complexity of the sarcolemmal cytoskeleton. *Exp Cell Res*. 309:86-98.

Hortsch, M. 2000. Structural and functional evolution of the L1 family: are four adhesion molecules better than one? *Mol Cell Neurosci*. 15:1-10.

Hortsch, M., A.J. Bieber, N.H. Patel, and C.S. Goodman. 1990. Differential splicing generates a nervous system-specific form of Drosophila neuroglian. *Neuron*. 4:697-709.

Hortsch, M., K. Nagaraj, and T.A. Godenschwege. 2009. The interaction between L1-type proteins and ankyrins--a master switch for L1-type CAM function. *Cell Mol Biol Lett*. 14:57-69.

Hummel, T., M.L. Vasconcelos, J.C. Clemens, Y. Fishilevich, L.B. Vosshall, and S.L. Zipursky. 2003. Axonal targeting of olfactory receptor neurons in Drosophila is controlled by Dscam. *Neuron*. 37:221-231.

Hummel, T., and S.L. Zipursky. 2004. Afferent induction of olfactory glomeruli requires N-cadherin. *Neuron*. 42:77-88.

Humphries, M.J., P.A. McEwan, S.J. Barton, P.A. Buckley, J. Bella, and A.P. Mould. 2003. Integrin structure: heady advances in ligand binding, but activation still makes the knees wobble. *Trends Biochem Sci*. 28:313-320.

Islam, R., L.V. Kristiansen, S. Romani, L. Garcia-Alonso, and M. Hortsch. 2004. Activation of EGF receptor kinase by L1-mediated homophilic cell interactions. *Mol Biol Cell*. 15:2003-2012.

Islam, R., S.Y. Wei, W.H. Chiu, M. Hortsch, and J.C. Hsu. 2003. Neuroglian activates Echinoid to antagonize the Drosophila EGF receptor signaling pathway. *Development*. 130:2051-2059.

Jan, L.Y., and Y.N. Jan. 1976a. L-glutamate as an excitatory transmitter at the Drosophila larval neuromuscular junction. *J Physiol*. 262:215-236.

Jan, L.Y., and Y.N. Jan. 1976b. Properties of the larval neuromuscular junction in Drosophila melanogaster. *J Physiol*. 262:189-214.

Jenkins, S.M., and V. Bennett. 2001. Ankyrin-G coordinates assembly of the spectrin-based membrane skeleton, voltage-gated sodium channels, and L1 CAMs at Purkinje neuron initial segments. *J Cell Biol*. 155:739-746.

Kall, L., A. Krogh, and E.L. Sonnhammer. 2004. A combined transmembrane topology and signal peptide prediction method. *J Mol Biol*. 338:1027-1036.

Kamiguchi, H., K.E. Long, M. Pendergast, A.W. Schaefer, I. Rapoport, T. Kirchhausen, and V. Lemmon. 1998. The neural cell adhesion molecule L1 interacts with the AP-2 adaptor and is endocytosed via the clathrin-mediated pathway. *J Neurosci*. 18:5311-5321.

Kantor, D.B., and A.L. Kolodkin. 2003. Curbing the excesses of youth: molecular insights into axonal pruning. *Neuron*. 38:849-852.

Keller, L.C., L. Cheng, C.J. Locke, M. Muller, R.D. Fetter, and G.W. Davis. 2011. Glial-derived prodegenerative signaling in the Drosophila neuromuscular system. *Neuron*. 72:760-775.

Kennerdell, J.R., and R.W. Carthew. 2000. Heritable gene silencing in Drosophila using double-stranded RNA. *Nat Biotechnol*. 18:896-898.

King, R.C., D. Mohler, S.F. Riley, P.D. Storto, and P.S. Nicolazzo. 1986. Complementation between alleles at the ovarian tumor locus of Drosophila melanogaster. *Dev Genet*. 7:1-20.

Kittel, R.J., C. Wichmann, T.M. Rasse, W. Fouquet, M. Schmidt, A. Schmid, D.A. Wagh, C. Pawlu, R.R. Kellner, K.I. Willig, S.W. Hell, E. Buchner, M. Heckmann, and S.J. Sigrist. 2006. Bruchpilot promotes active zone assembly, Ca2+ channel clustering, and vesicle release. *Science*. 312:1051-1054.

Kizhatil, K., Y.X. Wu, A. Sen, and V. Bennett. 2002. A new activity of doublecortin in recognition of the phospho-FIGQY tyrosine in the cytoplasmic domain of neurofascin. *J Neurosci*. 22:7948-7958.

Ko, J., M.V. Fuccillo, R.C. Malenka, and T.C. Sudhof. 2009. LRRTM2 functions as a neurexin ligand in promoting excitatory synapse formation. *Neuron*. 64:791-798.

Koch, I., H. Schwarz, D. Beuchle, B. Goellner, M. Langegger, and H. Aberle. 2008. Drosophila ankyrin 2 is required for synaptic stability. *Neuron*. 58:210-222.

Koirala, S., L.V. Reddy, and C.P. Ko. 2003. Roles of glial cells in the formation, function, and maintenance of the neuromuscular junction. *J Neurocytol*. 32:987-1002.

Kolodkin, A.L., D.J. Matthes, and C.S. Goodman. 1993. The semaphorin genes encode a family of transmembrane and secreted growth cone guidance molecules. *Cell*. 75:1389-1399.

Koper, A., A. Schenck, and A. Prokop. 2012. Analysis of adhesion molecules and basement membrane contributions to synaptic adhesion at the Drosophila embryonic NMJ. *PLoS One*. 7:e36339.

Koroll, M., F.G. Rathjen, and H. Volkmer. 2001. The neural cell recognition molecule neurofascin interacts with syntenin-1 but not with syntenin-2, both of which reveal self-associating activity. *J Biol Chem*. 276:10646-10654.

Kriebel, M., J. Wuchter, S. Trinks, and H. Volkmer. 2012. Neurofascin: a switch between neuronal plasticity and stability. *Int J Biochem Cell Biol*. 44:694-697.

Kristiansen, L.V., E. Velasquez, S. Romani, S. Baars, V. Berezin, E. Bock, M. Hortsch, and L. Garcia-Alonso. 2005. Genetic analysis of an overlapping functional requirement

for L1- and NCAM-type proteins during sensory axon guidance in Drosophila. *Mol Cell Neurosci*. 28:141-152.

Kunz, S., M. Spirig, C. Ginsburg, A. Buchstaller, P. Berger, R. Lanz, C. Rader, L. Vogt, B. Kunz, and P. Sonderegger. 1998. Neurite fasciculation mediated by complexes of axonin-1 and Ng cell adhesion molecule. *J Cell Biol*. 143:1673-1690.

Landgraf, M., V. Jeffrey, M. Fujioka, J.B. Jaynes, and M. Bate. 2003. Embryonic origins of a motor system: motor dendrites form a myotopic map in Drosophila. *PLoS Biol*. 1:E41.

Lee, T., and L. Luo. 2001. Mosaic analysis with a repressible cell marker (MARCM) for Drosophila neural development. *Trends Neurosci*. 24:251-254.

Lefebvre, J.L., Y. Zhang, M. Meister, X. Wang, and J.R. Sanes. 2008. gamma-Protocadherins regulate neuronal survival but are dispensable for circuit formation in retina. *Development*. 135:4141-4151.

Lefevre, G. 1981. The distribution of randomly recovered X-ray-induced sex-linked genetic effects in Drosophila melanogaster. *Genetics*. 99:461-480.

Lesch, C., J. Jo, Y. Wu, G.S. Fish, and M.J. Galko. 2010. A targeted UAS-RNAi screen in Drosophila larvae identifies wound closure genes regulating distinct cellular processes. *Genetics*. 186:943-957.

Levitt, P. 1984. A monoclonal antibody to limbic system neurons. *Science*. 223:299-301.

Linhoff, M.W., J. Lauren, R.M. Cassidy, F.A. Dobie, H. Takahashi, H.B. Nygaard, M.S. Airaksinen, S.M. Strittmatter, and A.M. Craig. 2009. An unbiased expression screen for synaptogenic proteins identifies the LRRTM protein family as synaptic organizers. *Neuron*. 61:734-749.

Llimargas, M., M. Strigini, M. Katidou, D. Karagogeos, and J. Casanova. 2004. Lachesin is a component of a septate junction-based mechanism that controls tube size and epithelial integrity in the Drosophila tracheal system. *Development*. 131:181-190.

Lodge, A.P., M.R. Howard, C.J. McNamee, and D.J. Moss. 2000. Co-localisation, heterophilic interactions and regulated expression of IgLON family proteins in the chick nervous system. *Brain Res Mol Brain Res*. 82:84-94.

Low, L.K., and H.J. Cheng. 2005. A little nip and tuck: axon refinement during development and axonal injury. *Curr Opin Neurobiol*. 15:549-556.

Lowe, J.S., O. Palygin, N. Bhasin, T.J. Hund, P.A. Boyden, E. Shibata, M.E. Anderson, and P.J. Mohler. 2008. Voltage-gated Nav channel targeting in the heart requires an ankyrin-G dependent cellular pathway. *J Cell Biol*. 180:173-186.

Lu, B., K.H. Wang, and A. Nose. 2009. Molecular mechanisms underlying neural circuit formation. *Curr Opin Neurobiol*. 19:162-167.

Luo, L., and D.D. O'Leary. 2005. Axon retraction and degeneration in development and disease. *Annu Rev Neurosci*. 28:127-156.

Luo, L., and J.G. Flanagan. 2007. Development of continuous and discrete neural maps. *Neuron*. 56:284-300.

Maness, P.F., and M. Schachner. 2007. Neural recognition molecules of the immunoglobulin superfamily: signaling transducers of axon guidance and neuronal migration. *Nat Neurosci*. 10:19-26.

Marg, A., P. Sirim, F. Spaltmann, A. Plagge, G. Kauselmann, F. Buck, F.G. Rathjen, and T. Brummendorf. 1999. Neurotractin, a novel neurite outgrowth-promoting Ig-like protein that interacts with CEPU-1 and LAMP. *J Cell Biol*. 145:865-876.

Marquardt, T., R. Shirasaki, S. Ghosh, S.E. Andrews, N. Carter, T. Hunter, and S.L. Pfaff. 2005. Coexpressed EphA receptors and ephrin-A ligands mediate opposing actions on growth cone navigation from distinct membrane domains. *Cell*. 121:127-139.

Martinek, S., and M.W. Young. 2000. Specific genetic interference with behavioral rhythms in Drosophila by expression of inverted repeats. *Genetics*. 156:1717-1725.

Matsuda, K., E. Miura, T. Miyazaki, W. Kakegawa, K. Emi, S. Narumi, Y. Fukazawa, A. Ito-Ishida, T. Kondo, R. Shigemoto, M. Watanabe, and M. Yuzaki. 2010. Cbln1 is a ligand for an orphan glutamate receptor delta2, a bidirectional synapse organizer. *Science*. 328:363-368.

McCabe, B.D., S. Hom, H. Aberle, R.D. Fetter, G. Marques, T.E. Haerry, H. Wan, M.B. O'Connor, C.S. Goodman, and A.P. Haghighi. 2004. Highwire regulates presynaptic BMP signaling essential for synaptic growth. *Neuron*. 41:891-905.

McCabe, B.D., G. Marques, A.P. Haghighi, R.D. Fetter, M.L. Crotty, T.E. Haerry, C.S. Goodman, and M.B. O'Connor. 2003. The BMP homolog Gbb provides a retrograde signal that regulates synaptic growth at the Drosophila neuromuscular junction. *Neuron*. 39:241-254.

McGeachie, A.B., L.A. Cingolani, and Y. Goda. 2011. Stabilising influence: integrins in regulation of synaptic plasticity. *Neurosci Res*. 70:24-29.

McNamee, C.J., J.E. Reed, M.R. Howard, A.P. Lodge, and D.J. Moss. 2002. Promotion of neuronal cell adhesion by members of the IgLON family occurs in the absence of either support or modification of neurite outgrowth. *J Neurochem*. 80:941-948.

Michaely, P., and V. Bennett. 1993. The membrane-binding domain of ankyrin contains four independently folded subdomains, each comprised of six ankyrin repeats. *J Biol Chem*. 268:22703-22709.

Michaely, P., and V. Bennett. 1995a. The ANK repeats of erythrocyte ankyrin form two distinct but cooperative binding sites for the erythrocyte anion exchanger. *J Biol Chem*. 270:22050-22057.

Michaely, P., and V. Bennett. 1995b. Mechanism for binding site diversity on ankyrin. Comparison of binding sites on ankyrin for neurofascin and the Cl-/HCO3- anion exchanger. *J Biol Chem*. 270:31298-31302.

Millard, S.S., J.J. Flanagan, K.S. Pappu, W. Wu, and S.L. Zipursky. 2007. Dscam2 mediates axonal tiling in the Drosophila visual system. *Nature*. 447:720-724.

Mohler, P.J., J.Q. Davis, and V. Bennett. 2005. Ankyrin-B coordinates the Na/K ATPase, Na/Ca exchanger, and InsP3 receptor in a cardiac T-tubule/SR microdomain. *PLoS Biol*. 3:e423.

Mohler, P.J., W. Yoon, and V. Bennett. 2004. Ankyrin-B targets beta2-spectrin to an intracellular compartment in neonatal cardiomyocytes. *J Biol Chem*. 279:40185-40193.

Montgomery, A.M., J.C. Becker, C.H. Siu, V.P. Lemmon, D.A. Cheresh, J.D. Pancook, X. Zhao, and R.A. Reisfeld. 1996. Human neural cell adhesion molecule L1 and rat homologue NILE are ligands for integrin alpha v beta 3. *J Cell Biol*. 132:475-485.

Nagaraj, K., L.V. Kristiansen, A. Skrzynski, C. Castiella, L. Garcia-Alonso, and M. Hortsch. 2009. Pathogenic human L1-CAM mutations reduce the adhesion-dependent activation of EGFR. *Hum Mol Genet*. 18:3822-3831.

Nakamura, Y., S. Lee, C.L. Haddox, E.J. Weaver, and V.P. Lemmon. 2010. Role of the cytoplasmic domain of the L1 cell adhesion molecule in brain development. *J Comp Neurol*. 518:1113-1132.

Nallamsetty, S., B.P. Austin, K.J. Penrose, and D.S. Waugh. 2005. Gateway vectors for the production of combinatorially-tagged His6-MBP fusion proteins in the cytoplasm and periplasm of Escherichia coli. *Protein Sci*. 14:2964-2971.

Nechipurenko, I.V., and H.T. Broihier. 2012. FoxO limits microtubule stability and is itself negatively regulated by microtubule disruption. *J Cell Biol*. 196:345-362.

Neisch, A.L., and R.G. Fehon. 2011. Ezrin, Radixin and Moesin: key regulators of membrane-cortex interactions and signaling. *Curr Opin Cell Biol*. 23:377-382.

Nelson, W.J., and P.J. Veshnock. 1987. Ankyrin binding to (Na+ + K+)ATPase and implications for the organization of membrane domains in polarized cells. *Nature*. 328:533-536.

Nishimune, H., C. Bernreuther, P. Carroll, S. Chen, M. Schachner, and C.E. Henderson. 2005. Neural adhesion molecules L1 and CHL1 are survival factors for motoneurons. *J Neurosci Res*. 80:593-599.

Ohyama, K., K. Tan-Takeuchi, M. Kutsche, M. Schachner, K. Uyemura, and K. Kawamura. 2004. Neural cell adhesion molecule L1 is required for fasciculation and routing of thalamocortical fibres and corticothalamic fibres. *Neurosci Res*. 48:471-475.

Oleszewski, M., S. Beer, S. Katich, C. Geiger, Y. Zeller, U. Rauch, and P. Altevogt. 1999. Integrin and neurocan binding to L1 involves distinct Ig domains. *J Biol Chem*. 274:24602-24610.

Owald, D., and S.J. Sigrist. 2009. Assembling the presynaptic active zone. *Curr Opin Neurobiol*. 19:311-318.

Owald, D., O. Khorramshahi, V.K. Gupta, D. Banovic, H. Depner, W. Fouquet, C. Wichmann, S. Mertel, S. Eimer, E. Reynolds, M. Holt, H. Aberle, and S.J. Sigrist. 2012. Cooperation of Syd-1 with Neurexin synchronizes pre- with postsynaptic assembly. *Nat Neurosci*.

Owuor, K., N.Y. Harel, D.J. Englot, F. Hisama, H. Blumenfeld, and S.M. Strittmatter. 2009. LGI1-associated epilepsy through altered ADAM23-dependent neuronal morphology. *Mol Cell Neurosci*. 42:448-457.

Pebusque, M.J., F. Coulier, D. Birnbaum, and P. Pontarotti. 1998. Ancient large-scale genome duplications: phylogenetic and linkage analyses shed light on chordate genome evolution. *Mol Biol Evol*. 15:1145-1159.

Petersen, T.N., S. Brunak, G. von Heijne, and H. Nielsen. 2011. SignalP 4.0: discriminating signal peptides from transmembrane regions. *Nat Methods*. 8:785-786.

Petros, T.J., A. Rebsam, and C.A. Mason. 2008. Retinal axon growth at the optic chiasm: to cross or not to cross. *Annu Rev Neurosci*. 31:295-315.

Piccione, M., F. Matina, M. Fichera, M. Lo Giudice, G. Damiani, M.C. Jakil, and G. Corsello. 2010. A novel L1CAM mutation in a fetus detected by prenatal diagnosis. *Eur J Pediatr*. 169:415-419.

Pielage, J., V. Bulat, J.B. Zuchero, R.D. Fetter, and G.W. Davis. 2011. Hts/Adducin controls synaptic elaboration and elimination. *Neuron*. 69:1114-1131.

Pielage, J., L. Cheng, R.D. Fetter, P.M. Carlton, J.W. Sedat, and G.W. Davis. 2008. A presynaptic giant ankyrin stabilizes the NMJ through regulation of presynaptic microtubules and transsynaptic cell adhesion. *Neuron*. 58:195-209.

Pielage, J., R.D. Fetter, and G.W. Davis. 2005. Presynaptic spectrin is essential for synapse stabilization. *Curr Biol*. 15:918-928.

Pielage, J., R.D. Fetter, and G.W. Davis. 2006. A postsynaptic spectrin scaffold defines active zone size, spacing, and efficacy at the Drosophila neuromuscular junction. *J Cell Biol*. 175:491-503.

Pimenta, A.F., I. Fischer, and P. Levitt. 1996. cDNA cloning and structural analysis of the human limbic-system-associated membrane protein (LAMP). *Gene*. 170:189-195.

Pimenta, A.F., V. Zhukareva, M.F. Barbe, B.S. Reinoso, C. Grimley, W. Henzel, I. Fischer, and P. Levitt. 1995. The limbic system-associated membrane protein is an Ig superfamily member that mediates selective neuronal growth and axon targeting. *Neuron*. 15:287-297.

Pocock, R., C.Y. Benard, L. Shapiro, and O. Hobert. 2008. Functional dissection of the C. elegans cell adhesion molecule SAX-7, a homologue of human L1. *Mol Cell Neurosci*. 37:56-68.

Pollerberg, G.E., K. Burridge, K.E. Krebs, S.R. Goodman, and M. Schachner. 1987. The 180-kD component of the neural cell adhesion molecule N-CAM is involved in cell-cell contacts and cytoskeleton-membrane interactions. *Cell Tissue Res*. 250:227-236.

Pratte, M., G. Rougon, M. Schachner, and M. Jamon. 2003. Mice deficient for the close homologue of the neural adhesion cell L1 (CHL1) display alterations in emotional reactivity and motor coordination. *Behav Brain Res*. 147:31-39.

Punta, M., P.C. Coggill, R.Y. Eberhardt, J. Mistry, J. Tate, C. Boursnell, N. Pang, K. Forslund, G. Ceric, J. Clements, A. Heger, L. Holm, E.L. Sonnhammer, S.R. Eddy, A. Bateman, and R.D. Finn. 2012. The Pfam protein families database. *Nucleic Acids Res*. 40:D290-301.

Qiu, S., D.L. Champagne, M. Peters, E.H. Catania, E.J. Weeber, P. Levitt, and A.F. Pimenta. 2010. Loss of limbic system-associated membrane protein leads to reduced hippocampal mineralocorticoid receptor expression, impaired synaptic plasticity, and spatial memory deficit. *Biol Psychiatry*. 68:197-204.

Ramser, E.M., G. Wolters, G. Dityateva, A. Dityatev, M. Schachner, and T. Tilling. 2010. The 14-3-3zeta protein binds to the cell adhesion molecule L1, promotes L1 phosphorylation by CKII and influences L1-dependent neurite outgrowth. *PLoS One*. 5:e13462.

Raper, J.A. 2000. Semaphorins and their receptors in vertebrates and invertebrates. *Curr Opin Neurobiol*. 10:88-94.

Rasse, T.M., W. Fouquet, A. Schmid, R.J. Kittel, S. Mertel, C.B. Sigrist, M. Schmidt, A. Guzman, C. Merino, G. Qin, C. Quentin, F.F. Madeo, M. Heckmann, and S.J. Sigrist. 2005. Glutamate receptor dynamics organizing synapse formation in vivo. *Nat Neurosci*. 8:898-905.

Rawson, J.M., M. Lee, E.L. Kennedy, and S.B. Selleck. 2003. Drosophila neuromuscular synapse assembly and function require the TGF-beta type I receptor saxophone and the transcription factor Mad. *J Neurobiol*. 55:134-150.

Reid, R.A., and J.J. Hemperly. 1992. Variants of human L1 cell adhesion molecule arise through alternate splicing of RNA. *J Mol Neurosci*. 3:127-135.

Reiff, D.F., P.R. Thiel, and C.M. Schuster. 2002. Differential regulation of active zone density during long-term strengthening of Drosophila neuromuscular junctions. *J Neurosci*. 22:9399-9409.

Robinow, S., and K. White. 1988. The locus elav of Drosophila melanogaster is expressed in neurons at all developmental stages. *Dev Biol*. 126:294-303.

Robinow, S., and K. White. 1991. Characterization and spatial distribution of the ELAV protein during Drosophila melanogaster development. *J Neurobiol*. 22:443-461.

Rosenthal, A., M. Jouet, and S. Kenwrick. 1992. Aberrant splicing of neural cell adhesion molecule L1 mRNA in a family with X-linked hydrocephalus. *Nat Genet*. 2:107-112.

Ruediger, S., C. Vittori, E. Bednarek, C. Genoud, P. Strata, B. Sacchetti, and P. Caroni. 2011. Learning-related feedforward inhibitory connectivity growth required for memory precision. *Nature*. 473:514-518

Sasakura, H., H. Inada, A. Kuhara, E. Fusaoka, D. Takemoto, K. Takeuchi, and I. Mori. 2005. Maintenance of neuronal positions in organized ganglia by SAX-7, a Caenorhabditis elegans homologue of L1. *Embo J*. 24:1477-1488.

Schafer, M., A.U. Brauer, N.E. Savaskan, F.G. Rathjen, and T. Brummendorf. 2005. Neurotractin/kilon promotes neurite outgrowth and is expressed on reactive astrocytes after entorhinal cortex lesion. *Mol Cell Neurosci*. 29:580-590.

Scheiffele, P., J. Fan, J. Choih, R. Fetter, and T. Serafini. 2000. Neuroligin expressed in nonneuronal cells triggers presynaptic development in contacting axons. *Cell*. 101:657-669.

Schmid, R.S., and P.F. Maness. 2008. L1 and NCAM adhesion molecules as signaling coreceptors in neuronal migration and process outgrowth. *Curr Opin Neurobiol*. 18:245-250.

Schmucker, D., J.C. Clemens, H. Shu, C.A. Worby, J. Xiao, M. Muda, J.E. Dixon, and S.L. Zipursky. 2000. Drosophila Dscam is an axon guidance receptor exhibiting extraordinary molecular diversity. *Cell*. 101:671-684.

Schnorrer, F., C. Schonbauer, C.C. Langer, G. Dietzl, M. Novatchkova, K. Schernhuber, M. Fellner, A. Azaryan, M. Radolf, A. Stark, K. Keleman, and B.J. Dickson. 2010. Systematic genetic analysis of muscle morphogenesis and function in Drosophila. *Nature*. 464:287-291.

Schofield, P.R., K.C. McFarland, J.S. Hayflick, J.N. Wilcox, T.M. Cho, S. Roy, N.M. Lee, H.H. Loh, and P.H. Seeburg. 1989. Molecular characterization of a new immunoglobulin superfamily protein with potential roles in opioid binding and cell contact. *Embo J*. 8:489-495.

Schuster, C.M., G.W. Davis, R.D. Fetter, and C.S. Goodman. 1996a. Genetic dissection of structural and functional components of synaptic plasticity. I. Fasciclin II controls synaptic stabilization and growth. *Neuron*. 17:641-654.

Schuster, C.M., G.W. Davis, R.D. Fetter, and C.S. Goodman. 1996b. Genetic dissection of structural and functional components of synaptic plasticity. II. Fasciclin II controls presynaptic structural plasticity. *Neuron*. 17:655-667.

Schwarting, G.A., and T.R. Henion. 2011. Regulation and function of axon guidance and adhesion molecules during olfactory map formation. *J Cell Biochem*. 112:2663-2671.

Scotland, P., D. Zhou, H. Benveniste, and V. Bennett. 1998. Nervous system defects of AnkyrinB (-/-) mice suggest functional overlap between the cell adhesion molecule L1 and 440-kD AnkyrinB in premyelinated axons. *J Cell Biol*. 143:1305-1315.

Shapiro, L., J. Love, and D.R. Colman. 2007. Adhesion molecules in the nervous system: structural insights into function and diversity. *Annu Rev Neurosci*. 30:451-474.

Shapiro, L., and W.I. Weis. 2009. Structure and biochemistry of cadherins and catenins. *Cold Spring Harb Perspect Biol*. 1:a003053.

Shimada, T., M. Toriyama, K. Uemura, H. Kamiguchi, T. Sugiura, N. Watanabe, and N. Inagaki. 2008. Shootin1 interacts with actin retrograde flow and L1-CAM to promote axon outgrowth. *J Cell Biol*. 181:817-829.

Siddiqui, T.J., and A.M. Craig. 2011. Synaptic organizing complexes. *Curr Opin Neurobiol*. 21:132-143.

Silan, F., I. Ozdemir, and W. Lissens. 2005. A novel L1CAM mutation with L1 spectrum disorders. *Prenat Diagn*. 25:57-59.

Silletti, S., F. Mei, D. Sheppard, and A.M. Montgomery. 2000. Plasmin-sensitive dibasic sequences in the third fibronectin-like domain of L1-cell adhesion molecule (CAM) facilitate homomultimerization and concomitant integrin recruitment. *J Cell Biol*. 149:1485-1502.

Soler-Llavina, G.J., M.V. Fuccillo, J. Ko, T.C. Sudhof, and R.C. Malenka. 2011. The neurexin ligands, neuroligins and leucine-rich repeat transmembrane proteins, perform convergent and divergent synaptic functions in vivo. *Proc Natl Acad Sci U S A*. 108:16502-16509.

Stan, A., K.N. Pielarski, T. Brigadski, N. Wittenmayer, O. Fedorchenko, A. Gohla, V. Lessmann, T. Dresbach, and K. Gottmann. 2010. Essential cooperation of N-cadherin and neuroligin-1 in the transsynaptic control of vesicle accumulation. *Proc Natl Acad Sci U S A*. 107:11116-11121.

Stavropoulos, N., and M.W. Young. 2011. insomniac and Cullin-3 regulate sleep and wakefulness in Drosophila. *Neuron*. 72:964-976.

Strigini, M., R. Cantera, X. Morin, M.J. Bastiani, M. Bate, and D. Karagogeos. 2006. The IgLON protein Lachesin is required for the blood-brain barrier in Drosophila. *Mol Cell Neurosci*. 32:91-101.

Sugie, A., D. Umetsu, T. Yasugi, K.F. Fischbach, and T. Tabata. 2010. Recognition of pre- and postsynaptic neurons via nephrin/NEPH1 homologs is a basis for the formation of the Drosophila retinotopic map. *Development*. 137:3303-3313.

Tanaka, H., W. Shan, G.R. Phillips, K. Arndt, O. Bozdagi, L. Shapiro, G.W. Huntley, D.L. Benson, and D.R. Colman. 2000. Molecular modification of N-cadherin in response to synaptic activity. *Neuron*. 25:93-107.

Thomas, U., and S.J. Sigrist. 2012. Glutamate receptors in synaptic assembly and plasticity: case studies on fly NMJs. *Adv Exp Med Biol*. 970:3-28.

Triana-Baltzer, G.B., Z. Liu, and D.K. Berg. 2006. Pre- and postsynaptic actions of L1-CAM in nicotinic pathways. *Mol Cell Neurosci*. 33:214-226.

Tuvia, S., T.D. Garver, and V. Bennett. 1997. The phosphorylation state of the FIGQY tyrosine of neurofascin determines ankyrin-binding activity and patterns of cell segregation. *Proc Natl Acad Sci U S A*. 94:12957-12962.

Uemura, T., S.J. Lee, M. Yasumura, T. Takeuchi, T. Yoshida, M. Ra, R. Taguchi, K. Sakimura, and M. Mishina. 2010. Trans-synaptic interaction of GluRdelta2 and Neurexin through Cbln1 mediates synapse formation in the cerebellum. *Cell*. 141:1068-1079.

Valakh, V., S.A. Naylor, D.S. Berns, and A. DiAntonio. 2012. A large-scale RNAi screen identifies functional classes of genes shaping synaptic development and maintenance. *Dev Biol*. 366:163-171.

van Oort, R.J., J. Altamirano, W.J. Lederer, and X.H. Wehrens. 2008. Alternative splicing: a key mechanism for ankyrin-B functional diversity? *J Mol Cell Cardiol*. 45:709-711.

Van Roessel, P., N.M. Hayward, C.S. Barros, and A.H. Brand. 2002. Two-color GFP imaging demonstrates cell-autonomy of GAL4-driven RNA interference in Drosophila. *Genesis*. 34:170-173.

Vitriol, E.A., and J.Q. Zheng. 2012. Growth cone travel in space and time: the cellular ensemble of cytoskeleton, adhesion, and membrane. *Neuron*. 73:1068-1081.

Volkmer, H., R. Leuschner, U. Zacharias, and F.G. Rathjen. 1996. Neurofascin induces neurites by heterophilic interactions with axonal NrCAM while NrCAM requires F11 on the axonal surface to extend neurites. *J Cell Biol*. 135:1059-1069.

Vrailas, A.D., D.R. Marenda, S.E. Cook, M.A. Powers, J.A. Lorenzen, L.A. Perkins, and K. Moses. 2006. smoothened and thickveins regulate Moleskin/Importin 7-mediated MAP kinase signaling in the developing Drosophila eye. *Development*. 133:1485-1494.

Wagh, D.A., T.M. Rasse, E. Asan, A. Hofbauer, I. Schwenkert, H. Durrbeck, S. Buchner, M.C. Dabauvalle, M. Schmidt, G. Qin, C. Wichmann, R. Kittel, S.J. Sigrist, and E. Buchner. 2006. Bruchpilot, a protein with homology to ELKS/CAST, is required for structural integrity and function of synaptic active zones in Drosophila. *Neuron*. 49:833-844.

Wan, H.I., A. DiAntonio, R.D. Fetter, K. Bergstrom, R. Strauss, and C.S. Goodman. 2000. Highwire regulates synaptic growth in Drosophila. *Neuron*. 26:313-329.

Wang, X., J.A. Weiner, S. Levi, A.M. Craig, A. Bradley, and J.R. Sanes. 2002. Gamma protocadherins are required for survival of spinal interneurons. *Neuron*. 36:843-854.

Wei, J., M. Hortsch, and S. Goode. 2004. Neuroglian stabilizes epithelial structure during Drosophila oogenesis. *Dev Dyn*. 230:800-808.

Whittard, J.D., T. Sakurai, M.R. Cassella, M. Gazdoiu, and D.P. Felsenfeld. 2006. MAP kinase pathway-dependent phosphorylation of the L1-CAM ankyrin binding site regulates neuronal growth. *Mol Biol Cell*. 17:2696-2706.

Wiencken-Barger, A.E., J. Mavity-Hudson, U. Bartsch, M. Schachner, and V.A. Casagrande. 2004. The role of L1 in axon pathfinding and fasciculation. *Cereb Cortex*. 14:121-131.

Williams, M.J. 2009. The Drosophila cell adhesion molecule Neuroglian regulates Lissencephaly-1 localisation in circulating immunosurveillance cells. *BMC Immunol*. 10:17.

Wong, C.W., and M.L. Privalsky. 1998. Components of the SMRT corepressor complex exhibit distinctive interactions with the POZ domain oncoproteins PLZF, PLZF-RARalpha, and BCL-6. *J Biol Chem*. 273:27695-27702.

Wong, E.V., A.W. Schaefer, G. Landreth, and V. Lemmon. 1996a. Casein kinase II phosphorylates the neural cell adhesion molecule L1. *J Neurochem*. 66:779-786.

Wong, E.V., A.W. Schaefer, G. Landreth, and V. Lemmon. 1996b. Involvement of p90rsk in neurite outgrowth mediated by the cell adhesion molecule L1. *J Biol Chem*. 271:18217-18223.

Wong, K., H.T. Park, J.Y. Wu, and Y. Rao. 2002. Slit proteins: molecular guidance cues for cells ranging from neurons to leukocytes. *Curr Opin Genet Dev*. 12:583-591.

Xiong, W.C., H. Okano, N.H. Patel, J.A. Blendy, and C. Montell. 1994. repo encodes a glial-specific homeo domain protein required in the Drosophila nervous system. *Genes Dev*. 8:981-994.

Yamamoto, M., R. Ueda, K. Takahashi, K. Saigo, and T. Uemura. 2006. Control of axonal sprouting and dendrite branching by the Nrg-Ank complex at the neuron-glia interface. *Curr Biol*. 16:1678-1683.

Yamasaki, M., P. Thompson, and V. Lemmon. 1997. CRASH syndrome: mutations in L1CAM correlate with severity of the disease. *Neuropediatrics*. 28:175-178.

Yao, K.M., and K. White. 1994. Neural specificity of elav expression: defining a Drosophila promoter for directing expression to the nervous system. *J Neurochem*. 63:41-51.

Yip, P.M., X. Zhao, A.M. Montgomery, and C.H. Siu. 1998. The Arg-Gly-Asp motif in the cell adhesion molecule L1 promotes neurite outgrowth via interaction with the alphavbeta3 integrin. *Mol Biol Cell*. 9:277-290.

Zhang, X., and V. Bennett. 1998. Restriction of 480/270-kD ankyrin G to axon proximal segments requires multiple ankyrin G-specific domains. *J Cell Biol*. 142:1571-1581.

Zhao, G., and M. Hortsch. 1998. The analysis of genomic structures in the L1 family of cell adhesion molecules provides no evidence for exon shuffling events after the separation of arthropod and chordate lineages. *Gene*. 215:47-55.

Zhao, X., and C.H. Siu. 1995. Colocalization of the homophilic binding site and the neuritogenic activity of the cell adhesion molecule L1 to its second Ig-like domain. *J Biol Chem*. 270:29413-29421.

Zhao, X., P.M. Yip, and C.H. Siu. 1998. Identification of a homophilic binding site in immunoglobulin-like domain 2 of the cell adhesion molecule L1. *J Neurochem*. 71:960-971.

Zhou, D., C.S. Birkenmeier, M.W. Williams, J.J. Sharp, J.E. Barker, and R.J. Bloch. 1997. Small, membrane-bound, alternatively spliced forms of ankyrin 1 associated with the sarcoplasmic reticulum of mammalian skeletal muscle. *J Cell Biol*. 136:621-631.

Zhou, D., S. Lambert, P.L. Malen, S. Carpenter, L.M. Boland, and V. Bennett. 1998. AnkyrinG is required for clustering of voltage-gated Na channels at axon initial segments and for normal action potential firing. *J Cell Biol*. 143:1295-1304.

Zhukareva, V., and P. Levitt. 1995. The limbic system-associated membrane protein (LAMP) selectively mediates interactions with specific central neuron populations. *Development*. 121:1161-1172.

# Acknowledgment

"There's real poetry in the real world. Science is the poetry of reality."

Richard Dawkins

This work was performed in the laboratory of Dr. Jan Pielage at the Friedrich Miescher Institute in Basel. I am deeply grateful to Jan for his continuous support and open door during the last 4 ½ years of exciting and challenging *Drosophila* research. He gave me the opportunity to be his first PhD student and I really enjoyed it. Thank you very much!

I would like to thank my thesis committee for their support and advice during my PhD thesis, especially Prof. Heinrich Reichert who serves as the Koreferent.

A special thank goes to Eliza Moreno for her help in difficult cloning times, for the hours of embryo injections and the immunoprecipitation experiments, Raiko Stephan for vectors and help with the transgenic animals and the whole Pielage lab for a nice atmosphere and discussions in and outside the lab.

For their contributions to the submitted manuscript I would like to thank our collaborators Prof. Tanja A. Godenschwege and Sirisha Kudumala.

I`m grateful to Julia, Raiko, Ingrid and Claudius for critical comments on the thesis manuscript: First what are Genes and *proteins* and second commas who needs commas?

I also would like to thank the whole imaging facility especially Laurent for his help and support especially during the FRAP experiments, the monoclonal facility for the Uhu antibody, the bioinformatic facility and especially Hans for his help with *uhu* and friends and the IT for continuous support.

A big thank you goes to all the present and former FMI members who made the PhD a memorable time in my life.

An dieser Stelle möchte ich ganz besonders meiner Familie danken, die mich durch ihre Unterstützung und bedingungslose Liebe während meines Studiums und der Doktorarbeit gestärkt haben.

Zum Schluss möchte ich mich bei Ralph danken, der mich durch seine Liebe, Geduld und diverse Kühlschrankfüllungen in den letzten Jahren unterstützt hat.